Seismic Analysis and Design of Confined Masonry Buildings

by

Bonisha Borah

DEPARTMENT OF CIVIL ENGINEERING
INDIAN INSTITUTE OF TECHNOLOGY GUWAHATI
GUWAHATI-781039, INDIA

November 2021

SEISMIC ANALYSIS AND DESIGN OF CONFINED MASONRY BUILDINGS

A Thesis Submitted
in Partial Fulfilment of the Requirements
for the Degree of

DOCTOR OF PHILOSOPHY

by

Bonisha Borah

DEPARTMENT OF CIVIL ENGINEERING
INDIAN INSTITUTE OF TECHNOLOGY GUWAHATI
GUWAHATI-781039, INDIA

November 2021

CERTIFICATE

It is certified that the work contained in this thesis titled "*Seismic Analysis and Design of Confined Masonry Buildings*" by **Ms. Bonisha Borah** bearing roll no. 156104002 has been carried out under our supervision and submitted to Indian Institute of Technology Guwahati to award the degree of **Doctor of Philosophy**. This work has not been submitted elsewhere for a degree to the best of our knowledge and belief.

Dr. Hemant B. Kaushik
Professor
Department of Civil Engineering
Indian Institute of Technology Guwahati
Guwahati-781039, Assam, India

Dr. Vaibhav Singhal
Assistant Professor
Department of Civil & Environmental Engineering
Indian Institute of Technology Patna
Patna-801103, Bihar, India

22 November 2021
IIT Guwahati

ABSTRACT

Confined masonry (CM) building system has been in use in several earthquake-prone countries, for example, several countries in Latin America and Mediterranean Europe, because confinement of the masonry walls with nominal tie-elements has been found to be very effective in their superior performance during past earthquakes. CM has also emerged over the last few decades as a popular, cost-effective alternative to seismically vulnerable unreinforced masonry (URM) buildings and improperly constructed and non-ductile reinforced concrete (RC) frame buildings with masonry infills in many developing countries. The uniqueness of CM building lies in its simple construction methodology, good wall-to-frame connections and load transfer mechanism, and full utilization of material strength that contribute to their earthquake safety and make the construction system economic. Though this building system has exhibited good performance in the past seismic events, there is a huge scope of studying its engineering behavior because of significant variation in materials used, lack of research on understanding the complex composite mechanism, and lack of development efforts in building sectors. Therefore, the primary objective of the present study was to investigate the behavior of CM walls under gravity and lateral loading and develop simple methodologies for their seismic analysis and design.

In the present study, three CM walls of different aspect ratios (from slender wall to squat wall) were designed based on present international practice and corresponding half-scale specimens were tested under quasi-static cyclic loading. The test results highlighted the important role of aspect ratio of wall, especially on the initiation of shear or flexural cracking in different members. The tie-columns of the squat wall suffered major damage quite early. This necessitates a need of proper guidelines for the design of tie-columns as well as masonry walls of CM buildings considering the influence of important parameters. Most of the available seismic design codes for CM are still under development with several gap areas remaining to be addressed. As a step towards filling this gap, the design values of shear and flexural strengths of CM walls tested in the present and several past experimental studies were estimated using all the existing codes of CM by considering all the associated safety factors. A comparative design versus actual lateral strength assessment was carried out to compare the global safety margins obtained from different codes. It was observed that some codes provide considerable global safety margins, whereas some do not, even after considering all the recommended safety factors. These inconsistencies raise questions on the effectiveness of the existing guidelines for the safe and economical design of CM buildings.

A comparative study with some preliminary models was carried out to develop a simplified numerical model for CM walls by realistically simulating the axial forces in tie-columns and tie-beam deflection under the action of gravity loads. A new macro-model "V-D strut model" was finally developed for the analysis of CM walls under the action of both gravity and seismic loads. Due care was taken to simulate not only the initial stiffness and strength of CM walls but also to characterize their failure modes in a simplified way using the *effective shear strength* of masonry estimated by carrying out a parametric finite element study. Effectiveness of the V-D strut model in predicting the lateral strength of CM walls was validated using several CM walls tested previously. The developed analysis method using V-D strut model was found to be extremely simple and effective to use.

Estimation of lateral strength, as well as complete backbone profile of CM walls under lateral loading, is necessary for seismic performance-based design of CM structures. Existing formulations were utilized to estimate the lateral stiffness, strength, and deformability at different performance levels of several CM specimens tested in past as well as in the present study. The experimentally obtained backbone curve parameters were compared with those estimated analytically from different formulations to evaluate their effectiveness. Based on these observations, proposals were made for a generalized analytical backbone curve model of CM walls that may be used for performance-based seismic analysis and design. Further, the available literature does not provide an estimation of design forces in individual members of CM walls. Thus, an extensive parametric finite element study was carried out considering the influence of several important parameters, and based on the results a methodology was finally developed for relative distribution of shear forces in tie-columns and masonry walls of CM walls under the action of lateral loading.

ACKNOWLEDGEMENT

Rome was not built in a day, and neither is research occasioned by an individual. So, at the end of my PhD journey, I am obligated to thank everyone who has laid bricks for my work. Their contributions are indelible and ineffable. I feel fortunate for this opportunity to pen down a few words of gratitude for all those responsible who made my thesis worthy of submission. Although I feel no words of gratitude will suffice to justify their efforts.

Firstly, I extend my deep and sincere gratitude to my supervisor Prof. Hemant B. Kaushik and co-supervisor Dr. Vaibhav Singhal. They have encouraged, guided, and supported me throughout my PhD journey. To accomplish a PhD work, one needs to win many small battles; they have aided me to find, and in many cases to fabricate the key to overcoming every stumbling block of my research work. I highly regard their support and wisdom pearled suggestions. The experience of working under them has burnished my knowledge and technical know-how. I am grateful to Prof. Hemant B. Kaushik in especial, who showed immense patience, care, and understanding. He allowed me the room to work in my way, whilst also enlightening me through regular interactions. It encouraged me to venture into different avenues during my research with the least fear of failure.

I, also, advance my gratitude to the members of my Doctoral Committee, who have reviewed my work and provided valuable suggestions and comments. With utmost sincerity, I offer my thanks to Prof. Sajal Kanti Deb, Dr. Sandip Das, and Prof. Uday Shanker Dixit. Their valued suggestions, comments, and intriguing discussions steeled me to aspire for continuous improvements in my work. I extend my thanks to all my teachers who have imparted me knowledge on various subjects. The technical and non-technical staff (Er. Sanjeet Kumar, Mr. Manoj Saw, and Mr. Milan Saw) at Structural Engineering Laboratory, IIT Patna have helped me immensely during the experiments; I thank their bejeweled inputs and earnest assistance. I am grateful to Mr. Akshay Gupta, PhD student at IIT Patna, for introducing me to the laboratory test setup of IIT Patna besides aiding with the experiments. I also acknowledge with profound thankfulness the research grant (ECR/2018/000489) provided by the Department of Science and Technology to conduct this research work and the financial assistance provided by the Ministry of Human Resource Development (MHRD), Government of India.

I am extremely grateful to my friend Mr. Sanil Naik, who befriended and supported me during and after his master's journey at IIT Guwahati. The various technical insights and valued ideas shared by him have always reinforced my quest for learning. I owe my juniors, Mr. Saurabh Kumar Sarma, and Mr. Anubhab Mukherjee, for lending me their helping hands during the last phase of my thesis work. The time we spent together during different work and projects related visits will be cherished.

I consider myself blessed to have been environed with the most amazing group of friends and colleagues throughout my PhD life. Pallab, Kasturi, Lavish, Pranjal, and Subhadip had commenced and co-traveled the PhD journey with me. They have been supportive, caring, and comforting and I cannot thank them enough for that. My humble thanks extend to Dr. Snehal Kaushik: the personal love and care she showered upon me will be forever treasured. I highly regard my seniors Dr. Biswajit Chand, Dr. Nishant Sharma, and Dr. Thainswemong Choudhury: their encouraging words have always illuminated my way through eclipses. My hostel mates (Harsha, Krishna, Jyotirekha, Dipsikha, Mamata, Prajna, Seema, Prinza, Monjusha, Tori, and Elina) have made my hostel life worth relishing. The light-hearted moments I shared with them helped me brush aside my fatigue and upkeep my work tempo. I would like to acknowledge everyone who made my stay at IITG and IITP pleasant and memorable. A special appreciation goes to my childhood friend Mr. Sourabh Jyoti Borah for sticking by my side through the good times and the hard.

Last but not the least, I extend my grateful prayer to my parents and my brother. Their immense patience and iron support kept me moving through this journey. I miss the presence of my father Late Bibek Borah. He awaited with enthusiasm to witness the fructification of my efforts; I wish he had been there to embrace me at the finishing line. I will be forever indebted to my mother Mrs. Monimala Borah; the foundation of my life is constructed with her unappreciated sacrifices and divine blessings. She canopied me from all other worries which allowed me to maintain my focus.

The journey to PhD has been rather thorned and constant uphill. But, the accompaniments I received throughout made it a worthwhile and joyous learning experience. An experience that has molded me irreversibly for the better. An experience I so highly regarded that the prospect of it nearing to end leaves me sullen and teary-eyed. With these words, I would like to pull down the curtains of my PhD life and thank everyone again with the deepest sincerity.

Bonisha Borah

TABLE OF CONTENTS

LIST OF TABLES

List of Figures

List of Symbols

α_s	Reduction of normalized shear strength per unit of $\rho_h f_y$ for estimation of V_{wr}
β	Support condition factor for estimation of $K_{i,p}$
δ	Lateral drift of CM wall
θ	Angle between the diagonal strut centerline and the horizontal axis
$\delta_{cr,p}$	Empirically predicted lateral drift corresponding to $V_{cr,p}$
$\delta_{cr,e}$	Lateral drift obtained from experimental data corresponding to $V_{cr,e}$
δ_0	Lateral drift of CM wall at the end of first cycle of loading
δ_{cr}	Lateral drift of CM wall corresponding to V_{cr}
δ_u	Lateral drift of CM wall corresponding to V_u
δ_m	Lateral drift of CM wall corresponding to V_m
$\delta_{m,e}$	Experimentally obtained lateral drift corresponding to $V_{m,e}$
$\delta_{m,p}$	Empirically predicted lateral drift corresponding to $V_{m,p}$
$\delta_{m,FE}$	Lateral drift corresponding to $V_{m,FE}$ obtained from FE analysis
δ_r	Lateral drift of CM wall corresponding to V_r
$\delta_{u,p}$	Empirically predicted lateral drift corresponding to $V_{u,p}$
$\delta_{u,e}$	Experimentally obtained lateral drift corresponding to $V_{u,e}$
ζ	Equivalent viscous damping ratio
Δ_{cr}	Deformation corresponding to V_{cr}
Δ_m	Deformation corresponding to V_m
Δ_r	Deformation corresponding to V_r
Δ_u	Deformation corresponding to V_u
$\Delta_{u,bl}$	Ultimate deformation corresponding to $0.9V_{m,e}$ of the bilinear idealized curve
Δ_e	Elastic deformation corresponding to $0.9V_{m,e}$ of the bilinear idealized curve
Δ	Deflection of tie-beam under gravity loading
η	Efficiency factor for horizontal reinforcement in masonry
η_c	Constrained correction coefficient of wall: 1.0 in general situation; 1.1 if constructional column spacing < 3 m
η_s	Partial efficiency factor for horizontal reinforcement in masonry depending on f'_m
μ	Displacement ductility factor
ξ_c	Participation service factor of the central constructional column: 0.5 if one column is arranged in the centre, 0.4 if more than one column is arranged
ρ_h	Represents the horizontal reinforcing steel in the wall
ρ_l	Percentage of longitudinal rebars in each tie-column ($100\times A_{sl}/tb_t$)
ρ_t	Percentage of transverse rebars in each tie-column ($100\times A_{st}/sb_t$)
σ	Compressive stress (overburden pressure) on CM wall
Υ_m	Partial factor for materials, including uncertainties about geometry and modeling

$a,b,c,d,$ e,p,q	Constants used to consider influence of different parameters in generalized equations
A	Cross-sectional area of wall including area of tie-columns
AF	Axial forces in tie-columns
AR	Aspect Ratio = H_w/L_w
A_c	Cross-sectional area of concrete in tie-column
A_{cc}	Total cross-sectional area of middle constructional column
A_d	Cross-sectional area considered in design codes
A_{gn}	Ratio of net area to gross area of masonry
A_{sh}	Area of horizontal reinforcing steel placed at a spacing s_h
A_{sl}	Total area of longitudinal reinforcing steel placed in each end tie-column
A_{slc}	Total area of longitudinal reinforcement in constructional column
A_{st}	Total area of transverse reinforcement in each tie columns
A_w	Cross-sectional area of wall excluding tie-columns
b_t	Width of a tie-column
C_{cr}	Reduction factors used to reduce V_m to V_{cr}
C_{sr}	Reduction factors used to reduce V_m to V_u
C_{sd}	Strength degradation factor $=V/V_{max}$
c_v	Coefficient of variation of diagonal compressive strength of walls specimens (≥ 0.2)
d_{bl}	Diameter of longitudinal bars in tie-columns
d_{sc}	distance between centroid of tensile steel and extreme compression fiber
d_s	distance between centroids of reinforcement placed at both ends of a wall
E_c	Modulus of elasticity of concrete
E_{dc}	Cumulative energy dissipation
E_m	Modulus of elasticity of masonry
E_s	Modulus of elasticity of steel
E_{bm}	Enhanced modulus of elasticity of concrete in tie-beam
f_b	Compressive strength of brick units
f_c	Mean compressive strength of concrete cubes
f_j	Compressive strength of mortar cubes
f'_m	Uniaxial compressive strength of masonry prism
f'_{md}	Design compressive strength of masonry
f_{AR}	Factor allowing for the effects of wall aspect ratio
f_{ck}	Characteristic compressive strength of concrete cubes at 28 days
f_{tc}	Tensile strength of concrete
f_{ss}	Effective shear strength of masonry used in V-D strut model
F_{ss}	Limiting axial capacity of diagonal strut in STM
F_E	Reduction factor allowing for the effects of slenderness and eccentricity of loading
F_M	Strength modification factor for flexure
F_P	Strength reduction factor for axial load
F_S	Strength modification factor for shear

f_{tcc}	Tensile strength of concrete in the constructional column
f_y	Mean yield strength of reinforcement in tie-column
f_{yh}	Yield stress of horizontal reinforcing steel or welded wire mesh
f_{yl}	Yield strength of longitudinal rebar in tie-elements
f_{yt}	Yield strength of transverse rebar in tie-elements
f_{ylc}	Yield strength of longitudinal rebar in the constructional column
G_c	Shear modulus of concrete
G_m	Shear modulus of masonry
H	Height of CM wall including depth of tie-beam
H_w	Height of CM wall excluding tie-beam
H_s/H	Height of a particular section in terms of total height of CM wall
I	Moment of inertia of wall section
I_c	Moment of inertia of tie-column section
I_d	Damage index for empirical prediction of degraded stiffness
K	Stiffness enhancement factor of tie-beam in V-D strut model
K_i	Initial lateral stiffness
$K_{i,e}$	Initial lateral stiffness from experimental data
$K_{i,p}$	Empirically predicted initial lateral stiffness
K_c	Cyclic stiffness of CM wall
K_{c0}	Initial cyclic stiffness of CM wall
K_{dp}	Empirically predicted degraded stiffness
L	Length of CM wall including width of tie-columns
L_i/L_p	Confinement factor defined as the ratio of total centerline length of internal confining elements to centerline length of confining elements at perimeter of the wall
L_w	Length of CM wall excluding tie-columns
L_c	Centerline length of CM wall
L_d	Length of the diagonal strut
l_p	Plastic hinge length
M	Moment at the base of the wall
M_{des}	In-plane design flexural strength of confined masonry wall
M_p	Contribution of compressive stress on wall to M_{des}
M_{sl}	Contribution of longitudinal steel of tie-columns to M_{des}
$M/(V_bL)$	Shear span ratio
m	modular ratio, i.e., the ratio of modulus of elasticity of concrete (E_c) to modulus of elasticity of masonry (E_m)
n	Number of tie-columns
n_r	Number of longitudinal rebars in one tie-column
n_i	Number of intermediate tie-columns
P	Total axial load acting on the wall, without multiplying by the load factor
P_D	Design axial strength on wall
P_m	Contribution of vertical compressive resistances of masonry wall to P_D

P_{tc}	Contribution of resistance of tie-columns, including the contribution from concrete and longitudinal steel to P_D
SD	Standard Deviation
s	Spacing of transverse reinforcement in tie-columns
s_h	Spacing of horizontal steel in wall or horizontal wires of welded wire mesh
t	Wall thickness
t_e	Effective thickness of wall used in codes
V	Lateral load acting on CM wall
V_b	Shear force at the base of the wall
V_{cr}	Lateral load at cracking of wall
$V_{cr,p}$	Empirically predicted lateral load at cracking of wall
$V_{cr,e}$	Experimentally obtained lateral load at cracking of wall
V_u	Ultimate lateral load at 20% strength degradation
$V_{u,e}$	Experimentally obtained ultimate lateral load at 20% strength degradation
$V_{u,p}$	Empirically predicted ultimate lateral load at 20% strength degradation
V_r	Residual lateral load
V_{des}	Design shear strength of CM wall
V'_{des}	Equivalent design shear strength of CM wall obtained as M_{des}/L
v_m	Mean shear strength of masonry from diagonal compression tests
v_{m0}	Mean initial shear strength of masonry obtained from triplet tests
v_{m5}-v_{m1}	Maximum and minimum values of experimentally obtained diagonal compressive strength of five wallette specimens
V_{mas}	Contribution of masonry wall to design shear strength
V_m	Lateral strength
$V_{m,p}$	Empirically predicted lateral strength
$V_{m,e}$	Experimentally obtained lateral strength
$V_{m,FE}$	Lateral strength obtained from FE analysis
$V_{m,VD}$	Lateral strength obtained from V-D strut analysis
v_{md}	Design shear strength of masonry from diagonal compression tests
v_{mk0}	Characteristic initial shear strength of masonry under zero compressive stress due to shear sliding
V_{tc}	Contribution of tie-columns to design shear strength
V_{wr}	Contribution of horizontal reinforcement in CM wall to design shear strength
V_w/V	Contribution of masonry wall in terms of total lateral load
V_{tc}/V	Contribution of tie-column in terms of total lateral load
w_{vs}	Width of vertical strut
w_{ds}	Width of diagonal strut

Chapter 1
INTRODUCTION

CONTENTS

1.1 OVERVIEW

In the quest for safe and affordable housing, numerous building typologies have emerged in the past in different parts of the world. While safety is a function of the quality of materials, workmanship, building configuration, and adherence to the construction and design guidelines among other measurable and non-measurable parameters, cost primarily depends upon the extent to which locally available materials and labor are used in the construction. In some seismically active regions, especially those in the under-developed and developing countries, the relationship between safety and affordability becomes more complex as cost starts playing a major role in housing construction. Such eccentric focus on reducing the cost of construction leads to poorer construction of housing typologies, even of those for which design and construction guidelines are readily available, e.g., unreinforced masonry (URM) buildings and reinforced concrete (RC) frame buildings. This *pursuit* of affordability at the cost of safety has clearly increased the seismic risk in some seismically active regions as observed during several past earthquakes (Jain et al. 2002, Murty et al. 2006a, Kaushik and Jain 2007, Kaushik and Dasgupta 2013, Joshi and Kaushik 2017, Rai et al. 2017, Brzev and

Mitra 2018, Furtado et al. 2021). A large number of URM and RC buildings, have suffered severe damages and collapse during past earthquakes as shown in Fig. 1.1, and strengthening of reparable URM buildings using variety of techniques is a common practice after every earthquake (Corradi et al. 2002, Borri et al. 2013, Borri et al. 2019, Choudhury and Kaushik 2021). Many reasons can be attributed to such unacceptable performance of some of these most common housing typologies, one of the primary reasons being adoption of cost-cutting measures by ignoring seismic features and using poor quality materials and workmanship.

Figure 1.1: Performance of URM and RC buildings in past earthquakes: (a) collapse of a 3-story URM building at Bhaktapur, Nepal (2015 earthquake), (b) out-of-plane collapse of several walls of a 4-story URM building in Dolakha, Nepal (2015 earthquake), (c) pan-cake type failure of intermediate stories of an RC building in Gangtok, Sikkim (2011 earthquake), and (d) poor performance of recently constructed RC building in Imphal, Manipur (2016 earthquake).

Masonry has been the most commonly used construction material in the world, and confined masonry (CM) has been recognized as one of the safe and affordable housing typologies in many countries. CM originated in Italy as a reconstruction technique of the collapsed URM buildings after the 1908 Messina earthquake having magnitude 7.2 (Brzev 2007). Thereafter, its practice expanded to several other countries or regions of high seismic risk (mainly Latin American countries). Confined masonry is an improved masonry structural system, where gravity as well as lateral loads are primarily resisted by the load-bearing masonry walls that are confined by lightly reinforced tie-columns and tie-beams. In CM system, the masonry walls are first constructed, and then reinforced concrete columns and beams (tie-elements) are cast-in-place around the boundaries of each wall and by enclosing the openings (Fig. 1.2). Though these tie-elements are smaller in size and are lightly reinforced compared to normal RC columns and beams, they improve the flexural as well as shear behavior of masonry by developing confining effects on masonry. Toothed edges (an arrangement of bricks alternately projecting at the end of a wall to permit bonding while pouring concrete in tie-columns as shown in Fig. 1.2) or joint reinforcement (anchorage) can also be used to improve the bonding between masonry wall and RC tie-elements and to delay undesirable cracking and separation at the interface under loading. Thus, under the action of lateral seismic loads, CM walls have significantly higher strength and deformability in comparison to URM walls and even poorly constructed non-ductile masonry infilled RC frame buildings, reflecting better seismic performance. Further, though the finished form of CM buildings is similar to masonry infilled RC frame buildings, CM requires minimal engineering intervention in all stages of construction as the RC tie-elements are not designed as moment-resisting frames. The construction provides economic advantages as instead of the RC confining frame, it utilizes the full masonry strength in the main load-bearing element (Marques and Lourenço 2014, Jain et al. 2014).

Over the years, engineered CM buildings around the world have performed reasonably well during past earthquakes (Figs. 1.3a, 1.3b). Naturally, CM has been embraced as an affordable and resilient seismic solution for low-rise buildings in many countries. Some of these buildings suffered severe damages because of absence of tie-columns around the openings (Fig. 1.3c). The buildings with inadequate size and spacing of tie-columns, weaker masonry, and that constructed with poor workmanship also suffered varying degrees of damages in past earthquakes (EERI 2007, and Galvis et al. 2017).

(b) (c)

Figure 1.2: Typical confined masonry building: (a) key components of a typical confined masonry building, (b) a single-story confined masonry building with tie-columns, tie-beams, lintel bands, and sill bands (Schacher and Hart (2015), and (c) construction sequence of a masonry wall along with the tie-columns (Jain et al. 2015).

Such damage in CM buildings usually took place at the first story level (Fig. 1.3d) and represented two major failure modes related to shear and flexure (Brzev 2007, Meli et al. 2011, Marques and Lourenço 2019). These failure modes are controlled by several parameters, such as wall aspect ratio, reinforcement percentage in tie-columns, overburden pressure, material strength, etc. The observed damages in CM buildings can be prevented or reduced by providing sufficient confinement to the openings in the walls and by using good quality materials and improved workmanship. This can be achieved by developing analytical and numerical models that can incorporate realistic loading conditions and that can be used to estimate the design forces in elements of CM walls. Consideration of variation in important parameters related to material, loading, geometry, and detailing is equally important while developing analytical or empirical models and design guidelines for CM buildings.

(a) (b) (c) (d)

Figure 1.3: Performance of CM buildings during past earthquakes: (a) Severely damaged RC building adjacent to undamaged CM building in 2008 Wenchuan, China earthquake (Wang 2008), (b) Undamaged six-story CM building adjacent to collapsed URM building in 2007 Pisco, Peru earthquake (Brzev and Mitra 2018), (c) Absence of RC tie-columns in walls with openings resulted in damage to CM building in the 2010 Chile earthquake (Brzev and Mitra 2018), and (d) damaged to the ground floor of a medium-rise CM apartment buildings in the 2010 Maule, Chile, earthquake (Brzev and Mitra 2018).

1.2 Motivation of the Study

With the increasing use of confined masonry buildings in different parts of the world, it has been realized that additional methods are required for their seismic analysis and design as the existing methods may not be sufficient to cater to the present needs due to the reasons discussed in the following. Huge variation in not only the material properties of masonry, but also the types of masonry used in CM buildings, intensifies the necessity of developing generalized analytical and numerical models for seismic analysis of these buildings. Though some methods have already been developed for analysis of CM walls, a numerical model that can realistically simulate the gravity as well as lateral load response of CM walls is not yet fully developed. The existing analytical methods are too simplistic for a complex system such as confined masonry. Some of the existing methods may not be used for nonlinear analysis (e.g., strut and tie method), while some cannot simulate the interaction between masonry and concrete elements under gravity and lateral loads (e.g., wide column method). Finite element simulation models can be used for both nonlinear analysis and simulating the masonry-concrete interaction, but their effectiveness in estimating the design forces in tie-members or masonry walls has not been validated.

Backbone models have been developed in the past for estimation of lateral load carrying capacity, stiffness, and deformability of CM walls. The mathematical formulations have been developed using the past experimental data obtained from limited studies in only a few countries. Considering the huge variations in material properties and construction methodologies in different regions, it is important that more such formulations are developed for different conditions so that generalized backbone curve model (lateral load – deformation envelopes) for CM walls can be developed. These backbone curve models can be very useful in estimating the initial stiffness, lateral strength, and deformability of CM walls while designing for seismic forces.

Several guidelines and design codes have been developed over the years in different countries to provide basic design details on CM and promote its construction practice; however, they convey a large dispersion in rules and many gaps. Moreover, most of the design codes and guidelines provide prescriptive methods of design using some common thumb rules. Design guidelines need to be further developed to reduce the dependence on limited guidelines and design codes developed by a few countries. Further, there is a need to assess the effectiveness of the design guidelines and provisions of different codes in ensuring the seismic safety of

CM buildings, especially in the context of those countries in which very weak and soft bricks are commonly used. The distribution of design seismic forces to masonry walls and tie-columns of CM buildings is also not clearly discussed in the existing literature.

The above-mentioned issues form the basis of motivation of the present study in which experimental, analytical, and numerical investigations are systematically carried out to recommend possible solutions to the identified problems related to the seismic analysis and design of confined masonry buildings.

1.3 OBJECTIVES OF THE STUDY

Though CM buildings started as an informal construction practice, their lateral load behavior has been found to be significantly better than the URM buildings as well as poorly constructed non-ductile masonry infilled RC frame buildings. As a result, CM buildings have attracted considerable interest in the research field particularly in order to further improve their analysis and design methodologies and understand the influence of some important parameters on their seismic behavior. Some analysis and design guidelines have been developed in the past for CM buildings; however, most of these guidelines are based on some thumb rules and simplified assumptions, and are primarily applicable for only one to two-story buildings. Therefore, systematic research is required to be carried out for developing numerical and analytical methods for seismic analysis of CM walls. Similarly, an engineered design approach is essentially required to be developed for CM walls instead of a prescriptive approach, which is commonly used in many countries. Based on these points, the primary objectives of the study are framed below:

- Understanding the influence of aspect ratio on the lateral load behavior of confined masonry walls by carrying out an experimental study. The experimental data will also be used in developing and validating the numerical and analytical models for CM walls.
- Development of a simple numerical model for nonlinear lateral load analysis of confined masonry buildings considering the influence of the important parameters, including that of the gravity loads.
- Assessing the effectiveness of the existing design codes and guidelines to safely design the CM walls.

- Use of existing analytical prediction model and experimental data, including that obtained in the present study, and develop analytical model or formulations for the estimation of lateral strength, stiffness, and deformability of CM walls. The developed formulations will be used in the development of generalized backbone curve model for CM walls that can be used by design engineers for the seismic analysis and design of CM buildings.
- Estimation of the design forces in different members of CM walls by finite element simulation that can be used to analyze CM walls under the action of gravity and lateral loads.

These objectives will be fulfilled by carrying out systematic experimental, numerical, and analytical studies on CM walls. The final goal is to recommend simple numerical and analytical models for seismic analysis of CM walls using which different elements of CM walls can be formally designed. Several intermediate objectives, as discussed above, will be achieved in order to accomplish the final goal.

1.4 Organization of the Thesis

The experimental, analytical, and numerical research work accomplished in the thesis are reported in eight chapters of the thesis. These chapters cover five major contributions arising from the thesis as identified in the objectives of the study. Each chapter first introduces the subject matter to the reader and ends with a summary of discussion with sufficient links to the subsequent chapters. In the first chapter, the research topic is first introduced followed by a brief discussion on the motivation of the study and finally the objectives of the study are identified. The existing literature on lateral load behavior of CM walls, their performance in past earthquakes in comparison to URM buildings and some other building typologies, past experimentally observed behavior, and existing analytical models for analysis of CM walls are covered in Chapter 2.

Chapter 3 provides complete details on the methodology used, test setup, and results obtained in the experimental study carried out on three half-scale specimens of CM walls. The cyclic lateral load behavior of CM walls having different aspect ratios are discussed with the help of hysteresis curves, stiffness degradation curves, and energy dissipation curves. Damage progression and failure modes observed in all the specimens are compared for understanding the influence of aspect ratio on lateral load response of CM walls. A simple numerical model, described as “V-D Strut Model”, for seismic analysis of CM walls is developed in the fourth chapter. The applicability of the developed model in nonlinear seismic analysis of CM walls is highlighted. It is shown that the V-D strut model is able to consider the influence of the gravity loads as well as several other parameters in the lateral load analysis. The simple numerical model is validated with past studies and it is observed to be highly effective in predicting the lateral load response of CM walls.

In Chapter 5, the existing design guidelines are assessed for understanding their effectiveness in safely estimating the design forces on CM walls by comparing their estimation with a large number of past experimental and analytical results. It is shown that most of the existing guidelines cannot be used as generalized methods for seismic design of CM walls. Generalized backbone curve models in the form of tri-linear force-deformation curves are developed for CM walls in Chapter 6. The formulations are developed based on the experimental data obtained in the present study and several past studies, along with the data reported in the past analytical studies. It is shown that the developed backbone model can be easily used for initial design and assessment of CM walls.

Chapter 7 utilizes the experimental data, analytical formulations, and detailed finite element models of CM walls for extracting the forces developed in different elements of CM walls. The estimation provides an in-depth understanding of the influence of tie-columns on the lateral load behavior of CM walls in great detail for developing design guidelines for tie-columns and masonry walls. Finally, the study is summarized in the last chapter wherein the major contributions are reported and conclusions are drawn. Limitations of the study and the scope of potential research work on confined masonry are also discussed.

Chapter 2
REVIEW OF LITERATURE

CONTENTS

2.1 OVERVIEW

Confined masonry (CM), a typical affordable housing solution for several seismically-prone countries, has steadily boosted its popularity as an alternative construction technique across different parts of the world. This housing system has huge variations, in terms of the properties of materials used for construction, detailing of tie-elements, construction practices, etc., across different regions. Several experimental and numerical studies have been carried out in the past to understand the behavior of CM buildings. In this chapter, relevant literature has been reviewed to develop a basic understanding of the subject. First, the performance of CM buildings in past earthquakes reported by several research teams is discussed, and possible failure modes are shortlisted to understand the general behavior of CM buildings. Different experimental investigations of CM buildings are reviewed and the influence of important parameters on lateral load response of CM are highlighted. Numerical models developed in the past for simulating the lateral load behavior of CM buildings are also reviewed. This is followed by a discussion on the existing design methods for CM buildings. Finally, based on the review of the past literature, gap areas in the state-of-the-art are identified and the objectives of the present study are formulated.

2.2 Past Performance

The direction of ground shaking is often at an angle to the walls in a structure, and so the earthquake excitation can be divided into components in line with the principal building axes. Thus, the walls of a building are usually classified as in-plane and out-of-plane walls (Figure 2.1). The walls oriented parallel to the direction of shaking are called in-plane walls, and the walls perpendicular to in-plane walls are defined as out-of-plane (OOP) walls. Walls have to be able to act in the in-plane and out-of-plane direction at the same time. Several reports of the past earthquakes have identified the OOP collapse of URM and masonry infill walls of RC frames as one of the predominant modes of failure (Figure 1.1). In the infilled RC frames due to construction difficulties, loose-fitting of masonry beneath the concrete beam are quite common, which resulted in the OOP collapse of these panels during the past earthquakes. The OOP failure of URM walls, is in fact, one of the most common failure modes of URM buildings in all the major earthquakes as discussed in this chapter. However, a superior integration between the masonry and adjacent RC tie-elements is naturally developed in CM walls because of the unique construction sequences. Thus, it will be interesting to review the performance and vulnerability of CM buildings in past earthquakes, especially in the OOP direction, compared to URM or infilled RC frame buildings.

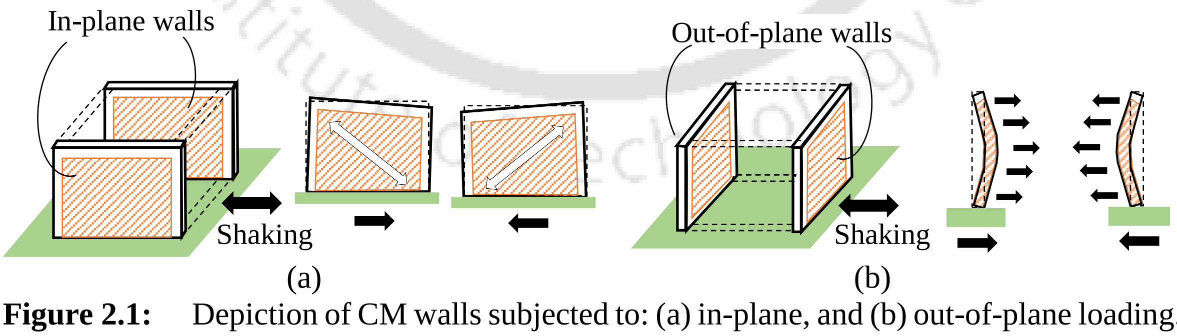

Figure 2.1: Depiction of CM walls subjected to: (a) in-plane, and (b) out-of-plane loading.

The first use of CM construction was reported in the reconstruction of buildings destroyed by the 1908 Messina, Italy earthquake of magnitude 7.2. After that, its practice started in Chile, Colombia, and Mexico in 1930s and 1940s, and subsequently, this building type was accepted in several countries of high seismic risk because of its satisfactory performance in the past earthquakes (Moroni et al. 2002, Murty et al. 2006b, Brzev 2007, Brzev et al. 2008, Meli et al. 2011). Table 2.1 includes some countries where CM buildings have been used for housing construction and the history of remarkable earthquakes experienced by them (Yang and Jian 1988, Schultz 1994, Jimenez et al. 1999, Asfura and Flores 1999, EERI 1999, 2001, Hashemi et al. 2003, Moroni et al. 2004, Meisl et al. 2006, Alcocer and Klingner 2006, Boen 2005, Bilek et al. 2007, Brzev 2007, Brzev et al. 2010, Galvis et al. 2020).

Table 2.1: Performance of CM buildings in past notable earthquakes.

	Year	Location	Magnitude	Remarks
Chile	1939	Chillán	7.8	Significantly better performance than URM. Around 50% of inspected CM sustained no damage, whereas around 60% of URM either partially or entirely collapsed.
	1985	Llolleo	7.8	Majority of CM buildings survived the earthquake. Damage was mainly due to inadequate tie-columns in salient locations.
	2010	Maule	8.8	A few CM buildings damaged mainly due to inadequate material quality, design and detailing, and geotechnical issues.
Mexico	1985	Guerrero-Michoacán	8.0	Low- to medium-rise (up to 4 and 5 stories high) CM buildings performed very well; even better than RC buildings.
	1999	Tehuacan	6.5	Significantly better performance than URM. A few 2-story CM houses damaged due to inadequate wall strength and poor construction quality.
	2003	Tecomán	7.6	Significantly better performance than URM. The observed damage was mainly due to the inadequate numbers and arrangement of tie-columns.
	2017	Mexico City	7.1	Around 11% collapse buildings were CM construction, and damage were due to irregularities, improper design.
Peru	1970	Chimbote	7.8	CM performed well. Poor performance in some buildings due to poor soil conditions and inadequate wall-to-floor connection
	2007	Pisco	8.0	CM performed very well. Buildings with irregularities and inadequate detailing showed poor performance.
Colombia	1983	Popayan	5.5	Significantly better performance than URM. Some minor damages were observed in window piers.
	1999	El Quindio	6.2	In some CM houses, shear cracks and OOP failure of masonry wall observed due to inadequate wall-to-tie connections.
Iran	1990 2003	Manjil Bam	7.6 6.6	Single-storey CM houses with timber roofs in the rural parts performance well
El Salvador	2001	Offshore El Salvador	7.7	Very few CM houses damaged beyond repair. The damage was mainly associated with in-plane shear or OOP failures.
China	1976	Tangshan	8.2	Excellent performance of CM buildings
Indonesia	2004	Great Sumatra	9.0	Damage to CM observed mainly in the tsunami due to poor construction practices
	2005	Northern Sumatra	8.7	Most CM buildings survived without collapse; cracking in walls were observed in some cases
	2007	Bengkulu	8.4	Some damage due to inadequate wall-to-tie connections, poor workmanship, excessive openings, and slender walls

In these countries, CM has been used both in the form of non-engineered and engineered residential construction, and its applications range from single-story houses to six-story apartment buildings. Clearly, the past earthquake performance of CM buildings has been very satisfactory compared to other types of construction, such as unreinforced masonry (URM) (e.g. 1939 Chile; 1999 Tehuacán, Mexico; 2003 Bam, Iran; 2003 Tecomán, Mexico; 2007 Pisco, Peru; 2011 Christchurch, New Zealand; 2015 Nepal; 2021 Haiti earthquakes, etc.) and masonry infilled reinforced concrete (RC) frame buildings (e.g. 1985 Guerrero-Michoacán, Mexico; 2001 Bhuj, India; 2004 Sumatra, Indonesia; 2008 Sichuan, China; 2010 Haiti; 2011 Sikkim, India; 2015 Nepal; 2016 Imphal, India earthquakes, etc.).

In general, commonly adopted housing typologies, like, adobe, URM, and even non-engineered infilled RC frame buildings have performed quite poorly in many seismic events that occurred worldwide; on the other hand, CM buildings have shown acceptable seismic resistance. Figs. 1.3(a), 1.3(b), and 2.2 show some examples of the superior performance of CM construction under different earthquakes. Interestingly, a large number of adjacent URM buildings as well as RC frame buildings suffered severe damages in some of these earthquakes. Amid the devastation, CM buildings were found to have performed really well; for example, in the town of Santa Cruz Analquito after 2001 El Salvador earthquake and Banda Aceh after 2004 Sumatra, Indonesia, earthquake (Fig. 2.2). Most low-rise dwellings did not experience any damage in past earthquakes with even minor design flaws; however, a few CM buildings suffered severe damage, especially high-rise buildings in the lower-most story. Figs. 1.3(c), 1.3(d), and 2.3 show some examples of the poor performance of CM construction under different earthquakes.

(a) (b)

Figure 2.2: Excellent performance of CM in: (a) 2001 El Salvador Earthquake (Brzev 2007), and (b) 2004 Sumatra, Indonesia, earthquake (Boen, 2005).

(a) (b)

Figure 2.3: Poor performance of CM in: (a) 2017 Mexico City earthquake (Galvis et al. 2020), and (b) 2007 Pisco, Peru earthquake (EERI 2007).

As reported in different literature, the damages in CM buildings during these earthquakes were mainly observed in some buildings with common design and construction flaws, such as - inadequate tie-columns at wall intersections and around the openings, poor material quality, insufficient anchorage of reinforcement in the tie-elements, insufficient detailing of RC tie-columns, torsional problems arising due to irregularities, poor diaphragm connections, etc. Further, the predominant failures modes in CM buildings are due to shear, and not due to flexure. Different possible failure modes of CM structures are discussed in detail in the next section.

2.3 General Behavior

Structural resistance of CM walls is a result of composite action of the masonry wall and adjacent RC confining elements – tie-columns and tie-beams along with a combination of plinth bands, sill bands, lintel bands and roof slab (Tomaževič and Klemenc 1997a, Brzev 2007, Meli et al. 2011, Iyer et al. 2012, Bourzam et al. 2008a, b, 2013). In confined masonry buildings, the concrete is cast in place after the construction of masonry walls resulting in an integral composite action of the RC and the masonry elements that in turn improves their interface-connection. Masonry walls are the primary load-resisting members in a CM building under the action of gravity as well as lateral earthquake loading as shown in Fig. 2.4. Under incremental cyclic lateral loading, compressive diagonal struts are developed in masonry walls at right angles to the tensile stresses. As masonry is very weak in tension, cracks develop in the masonry walls when the stress demand exceeds the capacity; and depending on the relative strength of mortar joints, brick mortar interface, and brick units, the diagonal shear cracks either follow the path of bed and head joints (stepped) or through the bricks. The primary role of RC tie-elements is to confine masonry walls to improve their lateral stability and integrity for enhanced lateral deformation capacity and better connectivity with the other walls and floor diaphragms. The tie-columns resist a major portion of all the loads acting on CM walls after the masonry walls suffer severe damage (Meli et al. 2011). These RC confining members act in tension and/or compression, depending on the direction of lateral forces and magnitude of gravity loads (Brzev 2007, Meli et al. 2011, Schacher and Hart 2015). Under the combined effect of axial load and bending moment, a portion of CM wall goes in tension as shown in Fig. 2.5 (Meli et al. 2011). It is assumed that the masonry and concrete are not able to resist tension, and the tensile stresses are resisted by the longitudinal reinforcement in tie-columns. Conversely, the compression stresses are resisted by concrete, masonry, and longitudinal reinforcement in tie-columns.

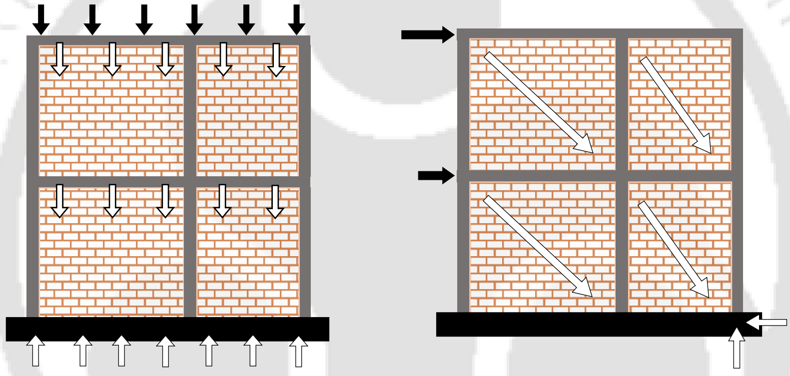

Figure 2.4: Flow of loads in CM walls: (a) vertical forces, (b) lateral forces.

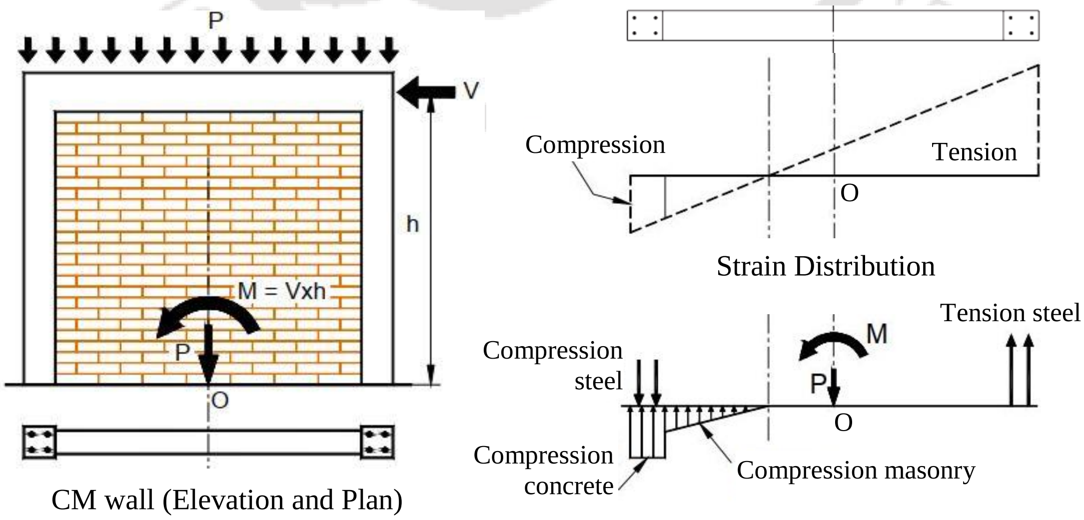

Figure 2.5: A typical CM wall subjected to combined axial and bending loads: strain, and internal force distributions (Meli et al. 2011).

The various potential failure modes of CM buildings that have been identified in the past earthquake damage reports and research studies are - in-plane failure, overturning or OOP failure, diaphragm failure, connection failure, and non-structural failure as shown in Fig. 2.6 (Matthews et al. 2007, Brzev 2007). The in-plane seismic effects are more critical in the ground story (Tomaževič and Klemenc 1997b, Brzev 2007); whereas, OOP effects are more prominent at the upper stories of the building (Tomaževič 1999) as shown in Fig. 2.7. OOP lateral loading creates bending, and shear stresses in the wall, and because of the low tensile strength of masonry, cracks may appear in walls leading to possible collapse by overturning. Depending upon the distance between the vertical lateral supports in comparison to the distance between the horizontal lateral supports, OOP failure can be vertical or horizontal (Matthews et al. 2007). The OOP displacement response also depends on wall geometric parameters, diaphragm flexibility, and their connection with adjacent confining elements. As the confining frame and masonry wall share good bonding, it exerts thrust on the beams and columns and forms an effective arching mechanism. Therefore, the OOP failure mode is not catastrophic in the case of CM buildings in comparison to URM and infilled RC frame structure (Brzev 2007, Tu et al. 2010, Singhal and Rai 2014, 2016). Among all the failure modes, the in-plane failure mode is the most critical as it is along the primary lateral load transfer path for CM walls.

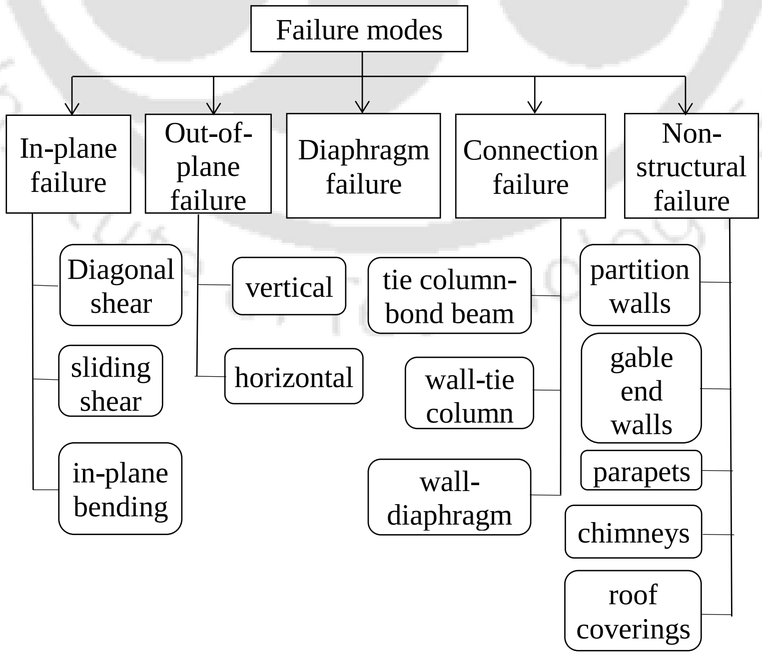

Figure 2.6: Different failure modes of CM buildings.

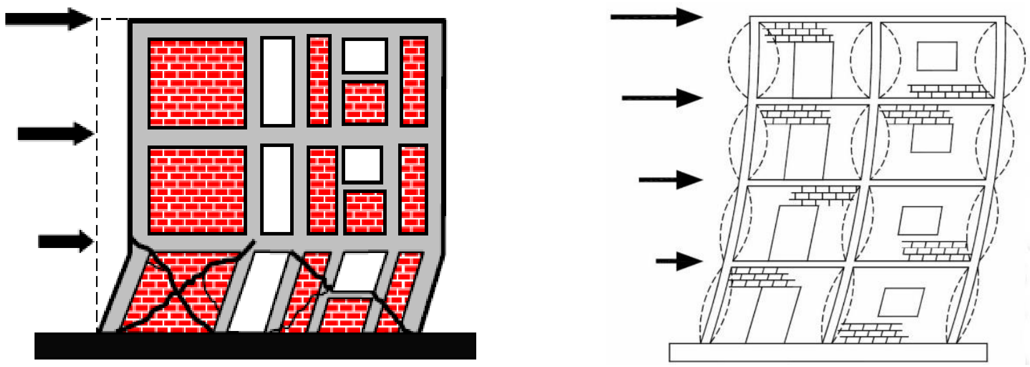

Figure 2.7: Critical seismic effects in CM buildings: (a) in-plane effects at the ground floor (Tomaževič and Klemenc 1997b, Brzev 2007), and (b) OOP effects at the upper floors (Tomaževič 1999).

Two major in-plane failure modes of CM walls subjected to lateral loading are those related to shear and flexural failure. Fig. 2.8 shows all possible in-plane failure modes in masonry wall and ties in a typical CM wall under lateral loading. For the tie-columns, shear cracks at the ends, flexural cracks along the height, concrete crushing in the ends due to compression, and yielding of rebars at the end due to tension were observed in the past (Varela-Rivera et al. 2019, Yekrangnia et al. 2021). These different failure modes of CM wall depend on geometric parameters (aspect ratio and slenderness ratio), loadings and boundary conditions.

Shear-induced in-plane damages, in the form of bed joint sliding, diagonal compression/strut action, diagonal-tension (shear cracks emanating from masonry wall and propagating towards the tie-columns), are frequently observed in CM structures (Meli et al. 2011, Dhanasekar and Haider 2011, Gavilán et al. 2015, Brzev and Mitra 2018, Marques and Lourenço 2019). The typical well-developed diagonal crack in walls is observed in CM buildings with light frames, i.e., small cross-sections of tie-columns with less percentage of steel, which is the usual case. For strong frames, when the relative stiffness of RC frame is significant compared to masonry wall (or the tie-elements have larger sections), the behavior of a CM wall may be similar to an RC frame with masonry infill (Meli et al. 2011). In such cases, masonry wall fails through complex mechanisms involving diagonal cracking, bed joint sliding, and toe-crushing (Dhanasekar and Haider 2011).

On the other hand, very few flexure-induced in-plane damages are observed in the form of horizontal tensile cracks in the lower courses of masonry and tie-columns at the tension end of the wall, crushing of bricks as well as concrete in the compression zone, and yielding of rebars in tie-columns (Zabala et al. 2004, Varela-Rivera et al. 2019). Walls with a higher aspect ratio (slender walls) or higher moment-to-shear ratio are susceptible to in-plane flexural damages. As flexural failure is ductile than brittle shear failure, it is generally considered as a desirable failure mode. However, it certainly is a matter of practical design requirements and architectural planning. When the wall is very short in comparison to the height (i.e., high AR) which is common in piers between openings, has a low overburden load, or lower percentage of reinforcement in the tie-columns (not enough flexural strength), the possibility of flexural failure occurrence increases under seismic loading. Flexural failure is not a typically observed failure mode in CM structure; however, a mixed shear-flexural failure is more likely to occur (Marques and Lourenço 2019).

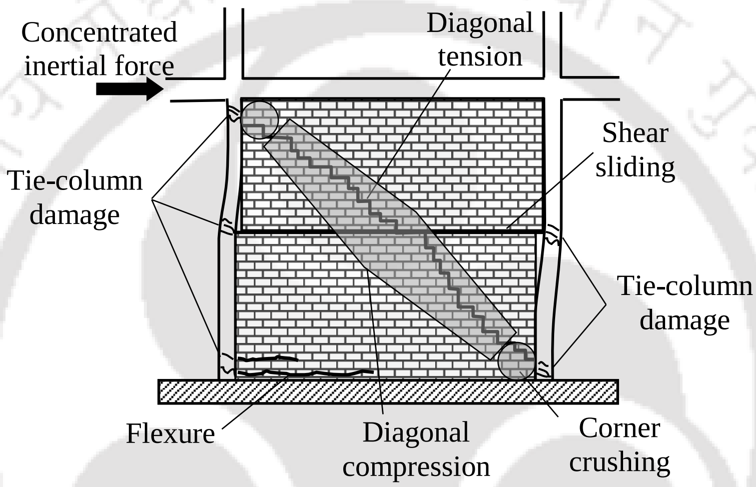

Figure 2.8: Schematic of different in-plane failure modes for CM walls.

2.4 Experimental Behaviour

During the last few decades, interest of research community in CM buildings has increased due to their excellent performance in past earthquakes. Several experimental efforts have been undertaken to characterize their seismic behavior. In various quasi-static cyclic to shake table tests conducted on CM walls, the main goal was to characterize the performance of this construction system when subjected to gravity and lateral loadings. The quasi-static lateral loads are applied cyclically using servo-controlled hydraulic actuator at low frequency to understand the cyclic behavior of structures during earthquakes and to observe their failure modes. Such controlled tests are important to get an insight into the performance of structures at varying lateral drift levels. On the other hand, the dynamic loads applied through the shake table provide details related to dynamic behavior of structures required for the design. Though experimental studies have been carried out on individual CM walls or models under different loading conditions (gravity, in-plane as well as out-of-plane), most seismic research studies are based on experimental testing of walls subjected to lateral in-plane loading.

2.4.1 Experimental Study for Evaluating the Influence of Important Parameters

The summary of experimental studies conducted to understand the in-plane behavior of CM walls in the past three decades is presented by Meli et al. (2011). Initially in a CM wall, the masonry wall resists the effect of lateral earthquake loads while the confining elements do not play any role other than keeping the masonry wall stable and intact. Once the cracking takes place in masonry units or mortar joint, the panel becomes less effective in transferring the forces. If the lateral displacement continues to increase, the masonry panel typically begins to lose strength, and at this stage, the vertical reinforcement in tie-columns becomes engaged in resisting tensile and compressive stresses. Thus, even if the lateral loads on the wall exceed its capacity, because of the confining effects provided by the tie-elements, the walls will stay intact and continue to deform until the lateral loads lessen. In this way, the CM wall has significantly higher strength and considerably higher deformation capacity than URM walls, and thus their collapse is prevented. The increasing lateral deformations cause further damage to the masonry wall and tie-columns. In many cases, ultimate failure occurs when the tie columns completely fail in shear by the extension of diagonal shear failure of the wall. The out-of-plane behavior of CM walls has also been studied experimentally by a few researcher teams, where the CM walls were either subjected to monotonically increasing uniform static pressure using airbags (Varela-Rivera et al. 2011, Varela-Rivera et al. 2012, Moreno-Herrera et al. 2015, and Navarrete-Macias et al. 2016) or subjected to out-of-plane dynamic loads (Tu et al. 2010, Singhal and Rai 2014). The behavior of a CM building depends on several parameters, such as material properties, overburden pressure, geometric characteristics, number and spacing of tie-columns, reinforcement detailing of tie-columns, openings, number of stories, etc. As the present study is concerned about the in-plane behavior of CM walls, different experimental investigations are reviewed below to understand the influence of these parameters on only the in-plane behavior of CM buildings.

2.4.1.1 Influence of type of masonry

Masonry wall in CM consists of two primary materials, masonry units such as bricks, blocks, etc., and mortar, which can be cement or lime-based with sand, soil, and water. Depending upon the availability of materials, different types of unit and mortar combinations are adopted. Different experimental studies have shown that the load resistance of CM walls strongly depends on the strength of the masonry units and the quality of construction. Shaking table tests on CM walls were conducted by Iiba et al. (1996) considering several variables: masonry units (Mexican or Japanese masonry unit), wall reinforcement, and tie-column reinforcement. The test results showed that the CM wall constructed with Japanese unit (36 MPa) provided around 1.5 times higher lateral strength than that with the Mexican units (5 MPa) because of the higher compressive strength of the unit. CM walls built using low-strength hollow concrete blocks are generally more prone to brittle failures compared to the walls built using solid concrete or clay units (Meli et al. 2011). Influence of different types of masonry units and different opening sizes in walls was studied by Decanini et al. (1985) by testing eight CM wall specimens. The tests were performed by applying cycles of lateral displacements at the wall head; however, no vertical load was applied. The test results showed that the walls made of solid clay bricks attained 50% more strength against ultimate cracking than against initial cracking. On the other hand, the walls made of hollow clay bricks attained only 20% more strength against ultimate cracking than against initial cracking. Similarly, sixteen full-scale CM specimens were tested by Yáñez et al. (2004) considering four types of CM walls (one solid and three with different percentages of opening: two specimens for each pattern), with two types of masonry unit – concrete masonry unit and hollow clay brick unit. Horizontal cyclic load was applied along the axis of the top beam using an actuator. There was no vertical load applied. The test results showed that all specimens failed in shear. The CM walls made with hollow clay brick units provided significantly higher lateral strength and energy dissipation capacity in comparison to the walls made with concrete masonry units; however, degradation of strength and stiffness was more in the former specimens.

2.4.1.2 Influence of overburden load

Overburden load is an influencing parameter on the lateral strength of CM wall. The resistance offered against sliding is developed by friction and adhesion between bricks and mortar. As frictional resistance is directly related to normal stress applied, the overburden load improves lateral capacity and energy dissipation characteristics of CM wall as observed in the test results of Yoshimura et al. (2000) and Varela-Rivera et al. (2019). In order to investigate the effect of vertical axial loads, wall reinforcement, and applied lateral forces on seismic behavior of CM walls, eighteen different half-scaled wall specimens of aspect ratio around 0.84, made of hollow concrete blocks, were tested by Yoshimura et al. (2000) under constant compression or tension vertical axial load, and cyclically applied lateral loads. Test results showed that the ultimate lateral shear strength increases in proportion to the applied vertical axial load. Again, six full-scale CM specimens made of hollow clay bricks, with reduced amount of longitudinal steel reinforcement in tie-columns to induce flexural failure, were tested by Varela-Rivera et al. (2019) where the variable parameters were: aspect ratio (three specimens with AR > 1), and overburden load (corresponds to two, four, and six story building). As shown in Fig. 2.9a, as the axial compressive stress increased, the flexural strength increased, and the drift ratios and displacement ductility decreased for walls with same aspect ratio.

2.4.1.3 Influence of aspect ratio

An important geometric parameter of CM wall is the aspect ratio (AR), here it is defined as the ratio of the height of CM wall excluding tie-beam to the length of the CM wall excluding the end tie-columns, which mostly controls the failure mode of a CM wall. Seven solid CM walls (5 single-bay, 2 multi-bay) with varying aspect ratios from slender to squat were tested by Gavilán et al. (2015). For the single-bay walls, lateral load was applied through a double-acting hydraulic actuator; vertical load was exerted by means of two actuators. The vertical load was applied so that wall flexural deformations were permitted. For multi-bay walls, axial load was applied through vertical ties and the lateral load by two hydraulic actuators. Test results showed that all the walls failed in shear, and as AR decreases, the lateral strength increases, whereas the drift corresponding to ultimate load decreases (Fig. 2.9b). Panels of squat walls with intermediate tie-columns behave as a single structure; i.e., they do not behave like panels of isolated walls with the same aspect ratio. Again, in the study of Varela-Rivera et al. (2019) with slender CM walls as mentioned earlier, the wall behavior was characterized by yielding of the longitudinal reinforcement followed by vertical and diagonal cracks in the masonry panel. The failure of the walls was assumed to be a pure flexural failure with crushing of concrete in tie-columns. Test results showed that the flexural strength of the CM wall increased, whereas the drift ratio decreased, as the aspect ratio of wall decreased.

2.4.1.4 Influence of number and spacing of tie-columns

After the initial diagonal crack in masonry, when lateral load increases the cracks get propagated to the tie-columns leading to shear concentration at the ends of the tie column. Therefore, the number and spacing of tie-columns are important parameters in CM wall design. The effect of the number and spacing of confining-columns in the seismic behavior of four full-scaled CM walls made of hollow concrete blocks was evaluated experimentally by Marinilli and Castilla (2004).

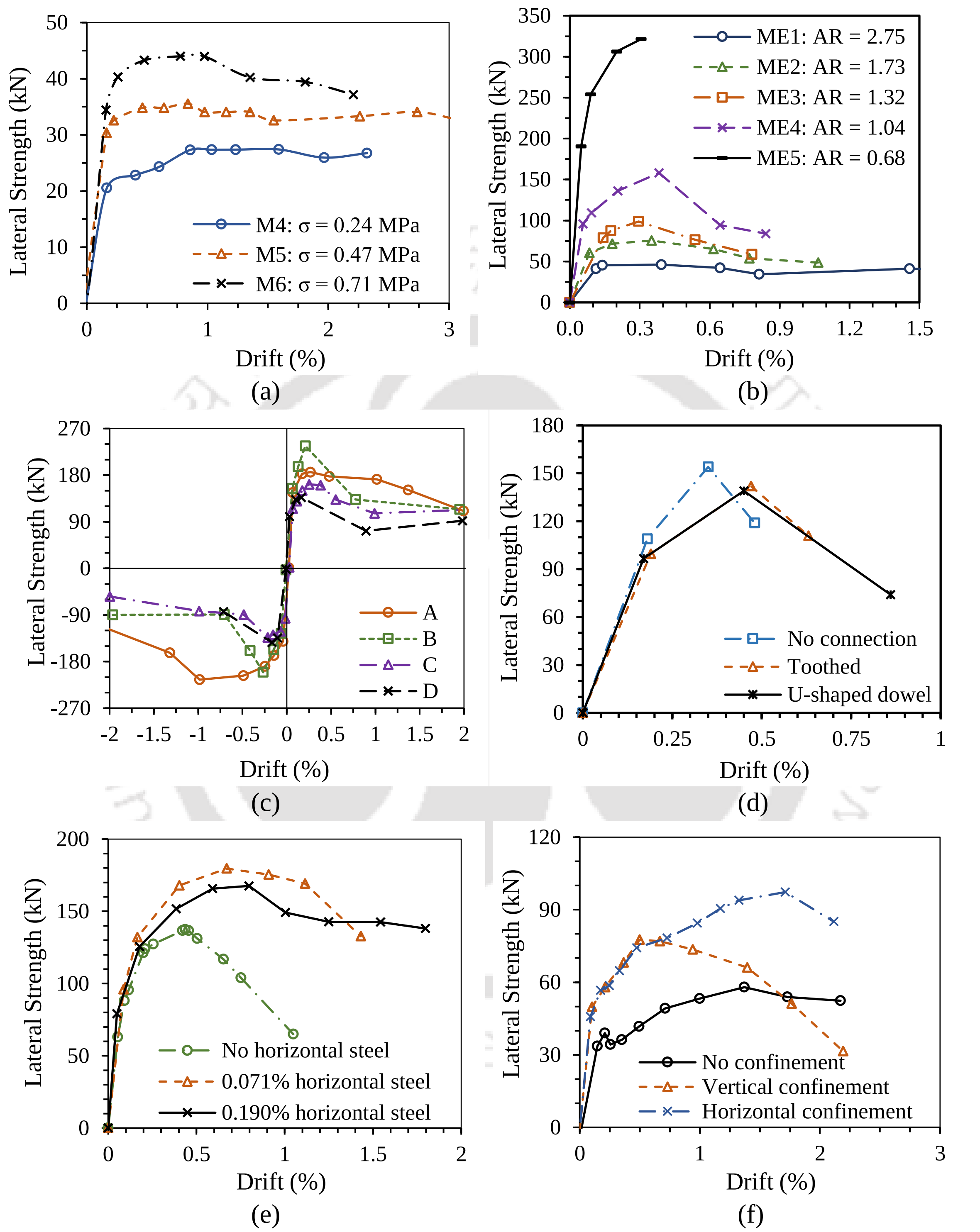

Figure 2.9: Influence of different parameters on lateral load behavior of confined masonry walls: (a) overburden pressure (Varela-Rivera et al. 2019), (b) aspect ratio (Gavilán et al. 2015), (c) tie-column reinforcement (Kato et al. 1992), (d) wall to tie-column interface (Matošević et al. 2015), (e) horizontal reinforcement in masonry walls (Aguilar et al. 1996), and (f) confinement around openings (Singhal and Rai 2016).

The first specimen consisted of one panel and two confining-columns. The second specimen consisted of two panels and three equally spaced confining-columns. The third specimen also consisted of two panels, but the central confining-column was located at one-third of the specimen length. Finally, the fourth specimen contained three panels and four equally spaced confining-columns. Each of the walls was tested against reversed cyclic lateral loads applied at the top of the wall. Based on the results obtained, it can be said that the presence of more confining-columns at a smaller spacing seems to spread the cracking along the masonry panels more uniformly, thus improving the damage distribution. Further, the inclusion of confining columns was found to enhance the strength of the walls.

2.4.1.5 Influence of reinforcement in tie-columns

Even though the role of confining element is to confine masonry wall to avoid premature failure, certain minimum reinforcement is required to avoid sudden failure of members. Four different sets of reinforcement detailing in the tie-columns of half-scaled CM wall, made of Japanese brick and with aspect ratio around 1.5, were studied by Kato et al. (1992). The first set composed of high longitudinal reinforcement ratio (3.8%) and high shear reinforcement ratio (1.28%), second set consisted of high axial (3.8%) and poor shear (0.3%) reinforcement ratio, third set had poor axial (0.99%) and high shear (1.28%) reinforcement ratio, and the fourth set had poor axial (0.99%) and poor shear (0.3%) reinforcement ratio combinations. Under the constant axial and lateral cyclic loading, it was observed that around four times increase in tie-columns' axial reinforcement percentage resulted in 1.5 times increase in the lateral capacity. In addition, the lateral drift at peak lateral strength increased by 1.4 times and rose up to 2.7 times with four times increase in tie-columns' shear reinforcement percentage. Thus, sufficient axial reinforcement in tie-columns can improve load-carrying capacity of CM wall. Also, sufficient shear reinforcement is required in the tie-columns to improve the concrete confinement to delay the shear failure.

The effect of axial reinforcement percentage in tie-columns (2% and 0.5%) on the behavior of CM wall was also studied by Iiba et al. (1996) under shake table testing as mentioned earlier. The test found that the steel bars at the bottom end of tie-column fractured in the CM walls having little reinforcement in tie-columns. Due to overturning moment of the concrete mass, repeated compressive and tensile forces are developed in the tie-columns. The fracture of bars resulted in the uplifting of the CM walls. Again, in order to investigate the possibility for simplifying the reinforcing detailing in the typical RC confining columns, Yoshimura et al. (1996) tested half-scaled CM walls with and without horizontal reinforcement and with two different number of rebars in the tie-columns - four bars and one bar. For the second set of specimens, spiral hoops were used for transverse reinforcement. Constant gravity load was applied, and the tests were conducted under cyclic lateral loads applied by a double-acting hydraulic jack. Though the difference in lateral strength was not significant in the two types of CM walls, the failure pattern was different. In the first type, diagonal cracks formed in the masonry wall propagated into top and bottom of both tie-columns, and passed through the bottom tie-columns and through the beam-to-column connection at the top of each tie-column. However, in the second type (one bar in tie-columns), most of the cracks in the masonry wall concentrated along the horizontal bottom joint of masonry wall. As the result, bottom-half of both columns damaged severely.

Another experimental study was conducted by Quiroz et al. (2017), where four full-scale CM walls (aspect ratio was around one) with different axial reinforcement ratios of the confining elements were studied under cycling loading. In all the walls, four longitudinal bars were used in both tie-columns and tie-beam; however, the diameter of bar varies – two specimens of the first group were studied considering the variation in tie-beam's reinforcement ratio (9.5 mm or 12.7 mm bars in tie-beam, and 12.7 mm bars in tie-columns for both specimens); the other two specimens of the second group were studied considering the variation in the reinforcement ratio of the tie-columns (9.5 mm or 12.7 mm bars in tie-columns, and 9.5 mm bars in tie-beam for both specimens). In both groups, the transverse reinforcement of the confining elements was kept constant. Gravity as well as lateral cyclic loads were applied during the tests, and the test results confirmed a slight reduction in the maximum strength and lateral stiffness when the lower reinforcement ratios for the tie-beam and tie-columns were used in the confining elements (Fig. 2.9c).

2.4.1.6 Influence of wall to tie-column connection

Sufficient bonding between masonry walls and RC tie-elements is important for satisfactory earthquake performance and for delaying undesirable cracking and separation at the wall-to-tie-column interface. Four full-scale CM walls (aspect ratio around one) were studied by Wijaya et al. (2011) under four different wall-to-tie connections – one with common practice (no connection), short anchorage in second, zigzag toothed connection in third, and continuous anchorage in fourth. The tests were conducted by applying in-plane quasi-static cyclic lateral loads and there was no vertical loading. The study showed that the additional short anchor slightly improves the lateral strength of the wall. The zigzag toothed connection did not improve the lateral load capacity; in fact, this specimen had the lowest capacity. CM wall with continuous anchorage had the highest lateral load capacity due to strong confinement. However, the lateral drift capacity at different limit states was significantly higher in the wall with zigzag toothed connection, followed by continuous anchorage and short anchorage. Singhal and Rai (2014) tested three half-scale two-bay CM wall specimens with different densities of toothed connections (no toothing, coarse toothing, and fine toothing) under successive applications of in-plane (quasi-static cyclic) and OOP (dynamic) loading. In order to simulate gravity loads on the masonry panels, a vertical pre-compression force of 0.10 MPa was applied over the wall specimen with the help of a flexible wire rope arrangement. From the tests, it was concluded that the increased density of toothing did not have a significant effect on OOP behaviour at the initial stages; however, it did cause significant improvement in post-peak behavior under in-plane loads (Fig. 2.9d). The specimen with a high density of toothing showed larger ductility and reduced strength degradation compared to the other schemes. Also, the toothing density had a significant effect on controlling the OOP displacement at a higher in-plane drift level (1.0% to 1.75% drift).

Another comparison study was performed by Matošević et al. (2015) to study the in-plane response of nine CM walls (of aspect ratio around 1.3) at 1:1.5 scale with different connection details - toothed connection, U-shaped dowel connection, and no connection (three CM walls for each). Under the combined action of gravity and lateral cyclic loads, all CM walls behaved as composite structures up to a drift level of about 0.2 %, until which the structures remained practically elastic. After that drift level, the influence of the connection type on the inelastic wall behavior was significant. Also, the test results showed that the connection details did not influence the initial stiffness or the maximum lateral resistance significantly, but they did improve the nonlinear wall behavior and hysteretic energy dissipation. Wall with toothed or U-shaped dowel connectors exhibited more ductile behavior compared to the one with no connection (Fig. 2.9d).

2.4.1.7 Influence of wall reinforcement

The seismic response of CM walls can be improved by placing horizontal wall reinforcement within the mortar joints, though it is not a much popular choice in many regions. Several experimental studies have been carried out in the past to study the influence of the wall reinforcement on lateral load response of CM walls (Yoshimura et al. 1996, 2000, 2004a, Kumazawa and Ohkubo 2000, Zabala et al. 2004, Gouveia and Lourenço 2007, Medeiros et al. 2013, Cruz et al. 2019). With the provision of horizontal wall reinforcement, the process of crack initiation and propagation gets delayed as reinforcement helps in resisting shear-induced tensile stresses, in addition to improved lateral load, deformation (Fig. 2.9e), energy dissipation capacity, and more uniform distribution of inclined cracking in walls under lateral loading.

2.4.1.8 Influence of openings in walls

Unconfined opening in a wall usually has negative effects on capacity when subjected to seismic loads. Under the action of lateral loading, stress concentration is observed at the corners of openings causing shear cracks, which makes the panel unstable and leads to failure (Basha et al. 2020, Furtado et al. 2021). The deficiencies due to openings can be overcome by the provision of confining elements around the openings in a CM wall. Different studies suggest different locations and arrangements of confining elements around openings in a CM wall (Aguilar et al. 1996, Yáñez et al. 2004, Kuroki et al. 2010, 2012, Singhal and Rai 2016). It has been observed in these studies that the negative influence of openings on the lateral strength of CM walls can be compensated if sufficient confinement is provided around the openings by means of tie-members. In some studies, the openings had no RC confining elements around their borders, but horizontal and vertical reinforcing bars were placed around the openings (Yáñez et al. 2004). From different experiment studies, it can be concluded that the provision of continuous sill and lintel beam improves the behavior of CM walls with opening (Fig. 2.9f). Two popular confining schemes studied in the past are: (1) continuous tie-columns along the whole wall height (vertical confinement) and discontinuous tie-beams at the top and bottom of opening; and (2) continuous sill and lintel beams along the whole wall length (horizontal confinement) and discontinuous tie-columns on both sides of opening. It was found that though the lateral strength of CM walls in both cases is almost the same, the later system is more ductile as the beam divides the wall into smaller panels with low aspect ratio ensuring well distributed diagonal shear cracks throughout the wall.

2.4.1.9 Influence of number of stories

Literature related to the influence of number of stories on the behavior of confined masonry buildings are very limited. The seismic behaviour of a 1: 2.5 scaled three-story CM structure - two parallel perimetric walls connected by RC slabs, which was made of clay brick masonry (6 MPa prism strength) and designed as per the Peruvian code, was studied by San Bartolomé et al. (1992) by carrying out tests under the action of earthquake loads using a shaking table. In addition, horizontal reinforcement was added in the first-story in a small ratio. Similarly, pseudo dynamic tests were also carried out by Scaletti et al. (1992) to investigate the behavior of one full-scale and one half-scale clay brick (10.8 MPa prism strength) CM building – two-story one-bay specimens with two parallel walls connected by stiff horizontal slabs, based on Peruvian standard. Again, two 1: 5 scaled models of a three-story CM building (with 1.27 MPa prism strength), which conform to the requirements of Eurocode 8 for simple buildings, were tested by Tomaževič and Klemence (1997b) on a shaking-table by subjecting them to a series of simulated seismic ground motions with increased intensity of shaking in each successive test run. Similarly, Tomaževič et al. (2004), Alcocer et al. (2004), Flores et al. (2017), Alcocer and Casas (2021) also studied scaled specimens of one to three storeyed CM buildings with different configurations. In all these tests, the ultimate damage, causing collapse, was mostly concentrated in the lower-most story as also observed during the past earthquakes.

2.4.2 Comparison with Other Structural Systems

The in-plane performance of CM walls in comparison to URM or infilled RC frame walls has been studied by some researchers. Nine specimens were tested by Yoshimura and Kikuchi (1995) to compare the behavior of CM wall with unreinforced masonry wall, and with RC ductile moment-resisting frame having the same cross-sectional details as that of the CM specimen. As the CM wall specimen showed higher strength and ductility than the URM and infilled RC frame specimens, it was concluded that CM construction is an excellent structural system.

Three specimens of each confined and plain masonry walls with a height-to-length ratio equal to 1.5, made at 1:5 scale were tested by Tomaževič and Klemenc (1997a) under the application of constant vertical load (approximately 22% of the masonry compression strength) and programmed pattern of cyclically acting horizontal displacements. From their study, it was observed that by confining the wall with RC tie-columns, lateral resistance of a URM wall is improved by more than 1.5 times and deformation capacity by almost five times in addition to enhancing the energy dissipation capacity by six to seven times as shown in Fig. 2.10a.

Further, to investigate the effective seismic strengthening methods for masonry walls in developing countries, twenty-eight URM and CM walls of aspect ratio around 0.77 were constructed and tested by Yoshimura et al. (2004b). The specimens consisted of 2D and 3D walls with or without wall reinforcing bars or U-shaped connecting bars, which were tested under repeated lateral force (lateral load application point considered was at a height of 0.67 or 1.1 times the height of the wall measured from the top of the foundation beam), and constant axial stress (0.48 MPa or 0.84 MPa). Based on the observations of test results, it can be concluded that CM wall system with connecting bars at the vertical wall-to-wall connections as well as the horizontal wall reinforcing bars developed reasonably higher ultimate lateral strength with the increase of vertical axial load and showed better ductility as compared to the conventional URM specimens. As an example, Fig. 2.10(b) shows the lateral load-versus-story drift plot for 2D URM and CM wall specimens (with and without dowel bars) without wall horizontal reinforcement under the axial stress of 0.48 MPa and inflection point of 0.67 times the height of wall. As shown in the figure, CM specimen with or without U-shaped connecting bar showed better performance than the URM wall in terms of lateral load-carrying capacity and ductility.

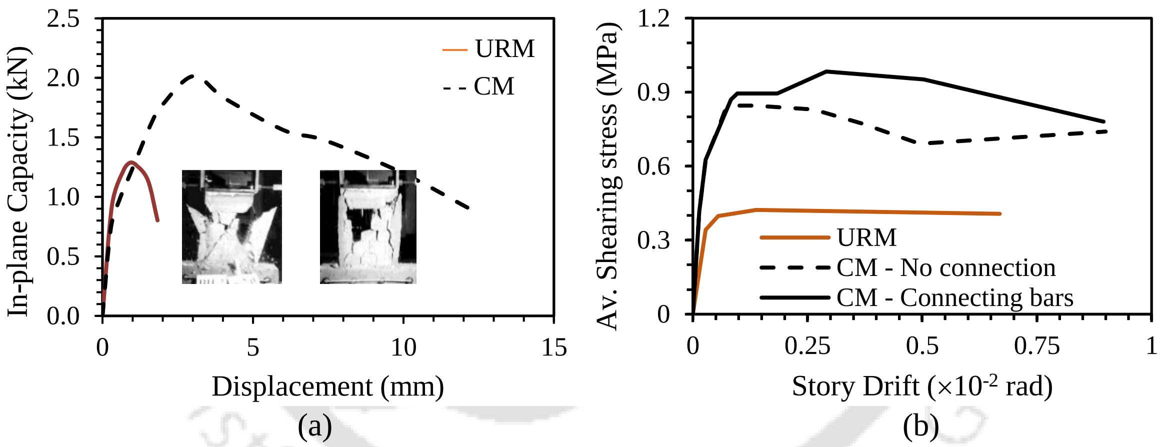

Figure 2.10. Comparison of the in-plane response of CM and URM walls tested by: (a) Tomaževič and Klemenc (1997a), and (b) Yoshimura et al. (2004b).

In another study, sixteen walls comprising of URM and CM with aspect ratio around one, made of lightweight concrete blocks, at 1:2 scale, were tested for constant vertical (about 30% of the masonry strength) and horizontal cyclic load (Goveia and Lourenço 2007). Nine URM wall configurations consisted of: four walls without bed joint reinforcement with unfilled mortar in vertical joints, three walls without bed joint reinforcement with filled mortar in vertical joints, and two walls with light bed joint reinforcement with unfilled vertical joints. Similarly, seven CM wall configurations consisted of: two walls with unfilled vertical joints without bed joint reinforcement, and three walls with unfilled vertical joints with light bed joint reinforcement anchored in the masonry only, and two walls with unfilled vertical joints with light bed joint reinforcement anchored to the RC tie-columns. The pre-compression load and the horizontal cyclic load was applied to the specimen, and it was observed that by confining the masonry wall with RC tie-elements, the lateral capacity of standard URM walls can be improved by 1.17 times and deformation capacity by 1.43 times in comparison to the CM walls in which bed joint reinforcement were not provided. Whereas, with bed joint reinforcement in the CM walls, the lateral capacity of CM walls was increased by about 1.22 times and deformation capacity by 1.43 times of the similar URM walls.

The out-of-plane behavior of CM walls has been examined by a few researchers either under the application of dynamic loads (such as shake-table generated ground motions) or by applying uniformly distributed surface pressure on walls using airbags. Seismic performance of CM walls in comparison with that of a typical masonry infilled RC frames was studied by Singhal and Rai (2014 and 2016) considering the successive applications of quasi-static cyclic in-plane loading and out-of-plane dynamic loading on shake table. It was observed that the CM walls with or without toothing exhibited improved in-plane and out-of-plane responses in comparison to the infilled RC frames (Fig. 2.11).

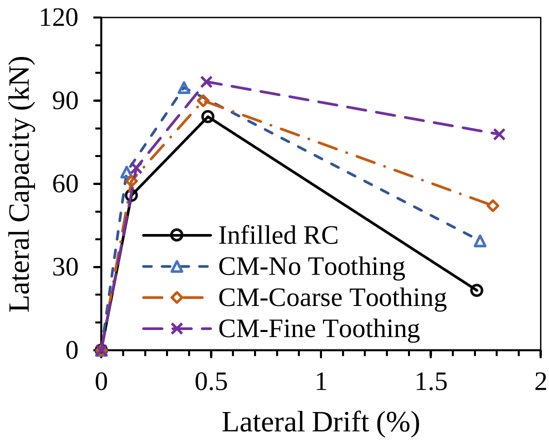

Figure 2.11: Comparison of the in-plane responses of CM walls of different densities of toothing with infilled RC frame under successive applications of in-plane and out-of-plane loading (Singhal and Rai 2014).

Further, shaking table tests were carried out on full-scale single-story CM building by Tu et al. (2010) to investigate the out-of-plane behavior of CM walls having different thicknesses in comparison with masonry infilled RC frames (Fig. 2.12). The test results suggested that CM walls can sustain significant OOP loads without severe damage. The composite action between the wall and confining frames prevented the masonry panels from falling out of the frame and helped to reduce the influence of inertia forces caused by their self-weight. On the contrary, infill panels separated from the boundary frame and collapsed due to the OOP inertia forces.

(a) (b)

Figure 2.12: The final state of full-scale specimens tested by Tu et al. (2010) and comparison with the OOP response: (a) minor cracks at the top and base of CM wall, and (b) collapse of masonry infilled RC frame.

2.5 NUMERICAL MODELING AND ANALYSIS METHODS

Though CM building typology started after the 1908 Messina, Italy earthquake; its engineering behavior has been established at a slow rate, and continues today. This is due to huge variation in materials and construction methodologies resulting in a limited understanding of the complex composite behavior under different loading conditions. Limited studies have attempted some numerical modeling strategies for the analysis of CM buildings. Considering the similarity in the behavior of CM walls with other building types, such as masonry infilled RC frame buildings and URM buildings, different analytical modeling techniques have been developed for the analysis of CM walls over the years. An overview of different numerical and analytical modeling techniques that have been adopted in the past studies to simulate and analyse confined masonry systems has been provided by Lang et al. (2014). The modelling strategies, as summarized in Fig. 2.13, have different degrees of refinement and precision to capture the failure modes and predict the lateral load behavior of CM walls. The practical applicability of realistic and reliable FE models is very limited, especially for large structures, as they are computationally intensive, complex, and require a large number of input parameters that are not available easily. In simplified 2D line element models, the elements of the building are modeled either as two-noded beam-column elements or as four-noded shell elements. Various popular simplified models developed in past literature are: wide-column model (WCM), strut-and-tie model (STM), equivalent strut/shell model (ESM).

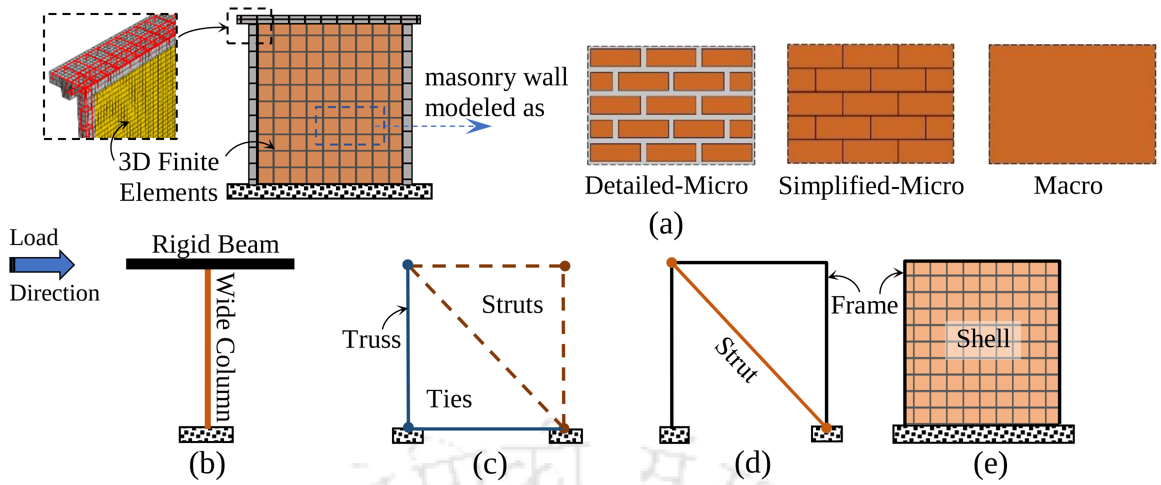

Figure 2.13: Schematic of 3D and 2D modeling strategies for CM wall: (a) FEM, (b) WCM, (c) STM, (d) ESM-strut, and (e) ESM-shell.

2.5.1 Finite Element Model (FEM)

The finite element (FE) method is a universally accepted structural analysis method, which provides the opportunity to study the structure more thoroughly (Fig. 2.13a). FE analysis of masonry structures can be performed at micro or macro level (Lourenço et al. 1995, Asteris et al. 2014, Bolhassani et al. 2015). Micro-modeling approaches are mostly suited for small structural elements in order to closely represent the heterogeneous states of masonry using the properties of each constituent and interface. The micro modeling has also been done using a simplified approach in which bricks are expanded up to half of the mortar thickness in vertical and horizontal directions, and the mortar is clamped into mortar interface. Macro-modeling approaches are also commonly adopted to represent the global structural behavior, where the distinction between the individual units and the joints is not made, and the material parameters are obtained from the masonry tests under homogeneous states of stress. Both modeling approaches have been widely used by researchers to predict the behavior of masonry walls. Smoljanović et al. (2017) used a very detailed micro modeling approach to simulate the behavior of CM walls. The RC and masonry elements were discretized with linear elastic triangular elements. The material non-linearity, including fracture and fragmentation of discrete elements, was considered through contact elements which were smeared between these discrete finite elements. The interface between masonry elements was modeled considering cracking of joint in tension and sliding along bed joints of masonry using the coulomb dry friction model. Amouzadeh Tabrizi and Soltani (2017) also used a micro modeling approach to simulate masonry walls in which masonry blocks were simulated with continuum model and potential cracks were smeared in the developed model.

The masonry joint interfaces were modeled considering shear sliding and opening of joints. Using this approach, the crack propagation and yielding of reinforcement bars were precisely predicted in the analysis.

Okail et al. (2004), Tripathy and Singhal (2019), and Yacila et al. (2019) developed a FE macro model to simulate the behavior of CM walls by following a slightly different approach. Continuum elements were adopted to model masonry panel and RC elements. The interfaces were modeled using traction separation law with *hard contact* in the normal direction and the frictional properties were assigned using Mohr-Coulomb failure criteria in the tangential direction. Medeiros et al. (2013) also used a similar approach, where masonry and RC elements were defined by the smeared crack model. Another change was adopted in the FE simulation by Eshghi and Pourazin (2009) who developed a 2D macro model for CM wall, in which plasticity-based material models were used along with Coulomb friction model with tension cut-off mode for the interface zone between the confining elements and the masonry panel. Janaraj and Dhanasekar (2014) described the calibration of a macro modeling method for unconfined and confined masonry panels tested under diagonal compression. In this study, the hollow and the grouted masonry were defined using smeared properties, which successfully predicted the failure modes, shear strength, and deformation characteristics of CM walls.

2.5.2 Wide Column Model (WCM)

Wide Column Model (WCM) for CM walls was mainly developed using the concept of Equivalent Frame model of URM buildings (Kappos et al. 2002, Lagomarsino et al. 2013), where, the wall is modeled as a one-dimensional two-noded centerline beam-column element (*wide column*), as shown in Fig. 2.13b, with transformed section properties accounting for composite action of masonry and RC tie-columns. Thus, the width of tie-columns is transformed to equivalent masonry width so that the equivalent area of the wide column section (A_{wc}) is equal to:

$$A_{wc} = A_w + 2mA_c \tag{2.1}$$

where, A_w and A_c are the cross-sectional area of masonry wall and RC tie-column, respectively, and m is the modular ratio, i.e., the ratio of modulus of elasticity of concrete (E_c) to modulus of elasticity of masonry (E_m). Tie-beam is modeled using a two-noded beam-column element and the axial rigidity provided by the masonry wall below the tie-beams is simulated by modeling the tie-beam as rigid having an infinite stiffness because the connectivity between the tie-beam and the wide-column is realized through only a node. Two types of beam sections are used in walls with openings: rigid and flexible (Rangwani and Brzev 2017). WCM has been recognized as a viable model (NTC-M 2004) as this technique provides the opportunity for the structural analysis of CM structure with commercial computer programs. Application of WCM for CM wall was demonstrated by Terán-Gilmore et al. (2009) by analyzing a three-story building where nonlinearity (axial lumped hinge) was defined near the bottom of each wide-columns using shear force-deformation relationship from a past backbone curve model of CM wall. Further, Ranjbaran et al. (2012), Ahmad et al. (2012), and Rangwani and Brzev (2017) also demonstrated the applicability of WCM in analysis of CM structures. However, selection of a reliable existing backbone model for the shear hinge definition in WCM for the CM wall is a difficult task. Further, the hypothesis of monolithic behavior assumed in WCM does not provide the opportunity to study the individual behavior of tie-columns and complex force transmission in different elements under loading. In fact, the concept of monolithic behavior of masonry wall and tie-columns is mainly valid to represent the elastic response at the initial stage.

2.5.3 Strut-and-Tie Model (STM)

Strut-and-Tie Model (STM) was originally developed as a hand calculation procedure for the analysis and design of shear critical structures and D (disturbed) regions in concrete structures. In STM, based on experience and intuition, internal load paths are drawn through the structure in the form of trusses; i.e., compressive stress fields (represented by struts) are interconnected by tensile stress fields (represented by ties) and design member force resultants are computed using static equilibrium, provided the STM is statically determinate (Schlaich et al. 1987, Wight and MacGregor 2005). Considering the wall-type structures as analogous to very deep beams, where the entire wall represents the D region as per St. Venant's Principle, many past studies adopted STM. The STM analysis for CM wall subjected to lateral loading, i.e., pin-jointed structural truss connected by both tension and compression members (Fig. 1c) is suggested in the past literature (Brzev 2007, Brzev and Gavilán 2013, 2016, Ghaisas et al. 2017, Singhal 2014, and Tripathi and Singhal 2019), and also in the Mexican code (NTC-M 2004) for the design of CM walls; however, no guidelines are provided on the development of STM for walls with openings. Horizontal component of diagonal strut force is used to determine the shear capacity of masonry wall. Whereas, the calculated axial forces in tie are used to find the required amount of reinforcement in tie-members.

Brzev and Gavilán (2013 and 2016) showed the application of STM through a four-story two-bay CM wall, where one bay comprises of wall with opening in each story. The strut action of the walls with opening was disregarded in the study and the structure was analyzed for the given story shear forces. Ghaisas et al. (2017) showed that the orientation of strut elements is influenced by the openings and panel configurations, but the suggested configurations were not validated further for their ability to predict lateral capacity as well as load distribution in different members. Singhal (2014) and Tripathy and Singhal (2019) used the strut-and-tie analysis of CM wall from the principal stress resultants obtained from FE analysis and subsequently estimated its lateral load-carrying capacity. The axial forces in ties evaluated by assuming the yielding of longitudinal reinforcement in tie-columns, i.e., $f_{yl}A_{sl}$, where A_{sl} is the total area of longitudinal reinforcing steel placed in a tie-column and f_{yl} is the yield strength of the rebar. Tripathy and Singhal (2019) proposed an empirical formula for the limiting axial capacity (F_{ss}) of diagonal strut in STM as:

$$F_{ss} = F_1\left(\sqrt{f'_m}A_w\right) \tag{2.2}$$

where,

$$F_1 = C_1\left(\frac{1}{\lambda}\right)\left(\frac{H}{L}\right) + C_2 \tag{2.3}$$

$$\lambda = H\left(\frac{E_m t \sin 2\theta}{4E_c I_c H}\right)^{0.25} \tag{2.4}$$

Here, for $H/L > 1$, $C_1 = 2.23$ and $C_2 = 0.1$; for $H/L \leq 1$, $C_1 = 2.65$ and $C_2 = 0.08$; f'_m is the compressive strength of masonry prism; H is the height of CM wall including the depth of tie-beam; L is the length of CM wall including the width of tie-columns; t is the wall thickness; I_c is the moment of inertia of tie-column section; θ is the angle between the strut centerline and the horizontal axis. Axial force in the diagonal strut is calculated using the method of joint considering yielding of longitudinal reinforcement in tie-columns (i.e., $f_{yl}A_{sl}$ /sinθ). If the force exceeds the limiting capacity (F_{ss}), then the axial force in strut is set to F_{ss} and the horizontal component of the force is treated as the lateral capacity of the wall. Rankawat et al. (2021) proposed a modified version of STM for CM walls such that it can be implemented in commercial software, and the method was renamed as Equivalent Truss Model. Using the relationship between lateral stiffness of wall and axial stiffness of diagonal strut, the study suggested the width of the diagonal strut in STM as:

$$w_{ds} = \frac{K_i L_d^3}{t E_m L_c^2} \tag{2.5}$$

where, L_d is the length of the diagonal strut, L_c is the centerline length of CM wall in STM, K_i is the initial stiffness of wall that can be obtained from past developed formulations. Further, applicability of the model in nonlinear analysis was demonstrated on a three-story building, where the nonlinearity was defined only in the diagonal strut in stress-strain terms using the available backbone model of CM wall. Thus, selection of a reliable existing backbone model for the axial hinge definition in diagonal strut is important here. The method may be effective in predicting the lateral strength of CM walls, however, it cannot predict the failure of tie-columns as no nonlinearity is considered for the tie-members.

2.5.4 Equivalent Strut/Shell Model (ESM)

Equivalent strut model is a commonly used and globally accepted model for modeling masonry infilled RC frame buildings, whose gravity load behavior as well as the lateral load behavior is quite different from the CM wall buildings (Kaushik et al. 2009, Rodrigues et al. 2010). A diagonal strut with end moments released at both ends is used to define the lateral resistance of the infill panel in RC frames. This method was originally proposed by Polyakov (1956) to estimate the lateral stiffness of masonry infilled RC frames and is a basis of several other models developed in the following years. Holms (1961) proposed a single strut model with the width of strut as one-third of the diagonal length of the panel. However, later it was found that this model overestimates the actual stiffness of infilled frame. Therefore, based on different experimental and analytical observations, the effective width was defined through different empirical formulations. A commonly adopted generalized form of the effective width has been one-fourth of the diagonal length of infill frames (Paulay and Priestley 1992). It has been argued that a single strut cannot precisely simulate the complex interaction between masonry panel and RC frame, and thus, multi strut models, which can provide a limited simulation of the contact between masonry panel and RC frame, were also utilized in some past literature (Kaushik et al. 2009).

Researchers have also attempted to use equivalent strut model for CM walls (Fig. 1d); however, their applicability is limited because these studies considered failure modes in CM walls similar to that considered in masonry infilled frames. Kaushik and Sanganee (2010) estimated a strut width reduction factor for ESM if it is to be used in case of CM walls. But their study was limited to calibrating only the lateral stiffness of CM walls with the past experimental studies. Torrisi et al. (2012) and Torrisi and Crisafulli (2017) developed a 12-node masonry panel element model, which internally includes 6 diagonal struts for nonlinear analysis of infilled RC frames and CM walls considering similar behavior for masonry infilled RC frames and CM walls. Likewise, masonry walls have also been modeled as four-noded shell elements in between the centerline beam-column elements of the RC frame (Fig. 1e) in some past studies. Kaushik and Sanganee (2010), Ghaisas et al. (2017), Chakra-Varthy and Basu (2021), have carried out linear analysis of CM walls by modeling masonry walls using linear shell elements. However, shell model is not capable of simulating nonlinear responses.

2.5.5 Backbone Curve Model

In addition to the numerical models, analytical backbone curve models for lateral load analysis (strength, stiffness, and deformability) of CM walls were also developed in the past using the results of past experimental studies (Flores and Alcocer 1996, Tomaževič and Klemenc 1997a, Marinilli and Castilla 2006, Bourzam et al. 2008a, 2008b, Riahi et al. 2009, Marques and Lourenço 2013, Gavilán et al. 2015, Singhal and Rai 2016, Yekrangnia et al. 2017, Marques and Lourenço 2019). However, the existing models are either highly influenced by the methods originally developed for unreinforced and reinforced masonry walls or based on the limited number of laboratory tests. The existing prediction models may not work well with CM practiced in different places. Thus, they should be studied further for understanding their effectiveness in estimating the strength, stiffness, and deformability of different CM walls tested in different regions of the world.

2.6 Design Methods

The development of standard codes and guidelines for the structural design and construction of buildings is a major concern to protect public safety and welfare as they relate to the adequate performance (i.e., safety and serviceability) of the buildings. Several guidelines have been developed over the years to provide basic details on CM and promote its construction practice (Blondet 2005, Schacher 2009, Boen and associates 2009, Totten 2010, Meli et al. 2011, Arya et al. 2014, Schacher and Hart 2015, Carlevaro and Roux-Fouillet 2015, Brzev et al. 2019). In some countries standard codes have been adopted to design and construct CM buildings, such as - Mexico (NTC-M 2017), Peru (NT E.070 2019), Chile (NCh2123 2003), Argentina (INPRES-CIRSOC 103 2018), Colombia (NSR-98 2010), Costa Rica (CSCR 2002), Europe (CEN 2005), and China (GB 50003 2011). Moreover, the recent revision of Indian code IS 4326 (BIS 2013) contains some construction provisions for CM and along with that a separate building code for CM practice is under development (BIS

2021). In some other countries (e.g., Indonesia, Pakistan, Haiti, Switzerland, Venezuela, etc.), CM construction has been practiced with basic construction guidelines without formal building codes. In all the available codes and guidelines, some basic concepts for the seismic design of a CM building are common. For example, the building configuration, i.e., size and shape, determines the way of seismic force distribution within the structure. Generally irregular configurations are avoided for their undesirable stress concentration and torsion. Symmetrical arrangement of mass and balanced stiffness against either direction is necessary to keep torsion within a manageable range.

Seismic design of structures highly depends on their characteristic force-deformation relationship, which is defined as a function of three most important design parameters - strength, stiffness and deformability or ductility. For adequate seismic performance, strength and deformation capacities of a structure must be greater than the demand imposed by a design earthquake. The available guidelines provide requirements regarding different aspects of a CM building, such as the maximum height of walls, maximum slenderness ratio (height to thickness), minimum thickness of wall, minimum wall aspect ratio (height to length), location, spacing, minimum dimension, and reinforcement detailing of tie-elements, foundation rules, etc. Fig. 2.14 summarizes these requirements in a typical confined masonry house relative to the limiting dimensions according to Meli et al. (2011).

Though the basic design concepts of CM buildings are similar, the available design codes and guidelines show large differences, especially in those requirements related to the detailing of tie elements, dimensions of masonry wall and tie-columns, as well as different material and other safety factors (Meli et al. 2011, Marques and Lourenço 2019). For acceptable seismic performance, various country codes suggest 100 mm to 200 mm tie-columns with 4 bars of longitudinal reinforcement and 6 mm diameter ties in confining elements. However, the bar diameter for longitudinal reinforcement varies; some country codes, like Chile and Colombia suggest 10 mm; and some other country codes like China, Argentina, and Eurocode suggest different bar diameters ranging from 5 to 12 mm (Meli et al. 2011). Most of the guidelines were mainly developed based on simple thumb rules and they are non-conclusive on methods to be adopted in design and detailing of different elements in a typical CM building instead of prescriptive approaches. Most of these guidelines are still under development with several gap areas remaining to be addressed.

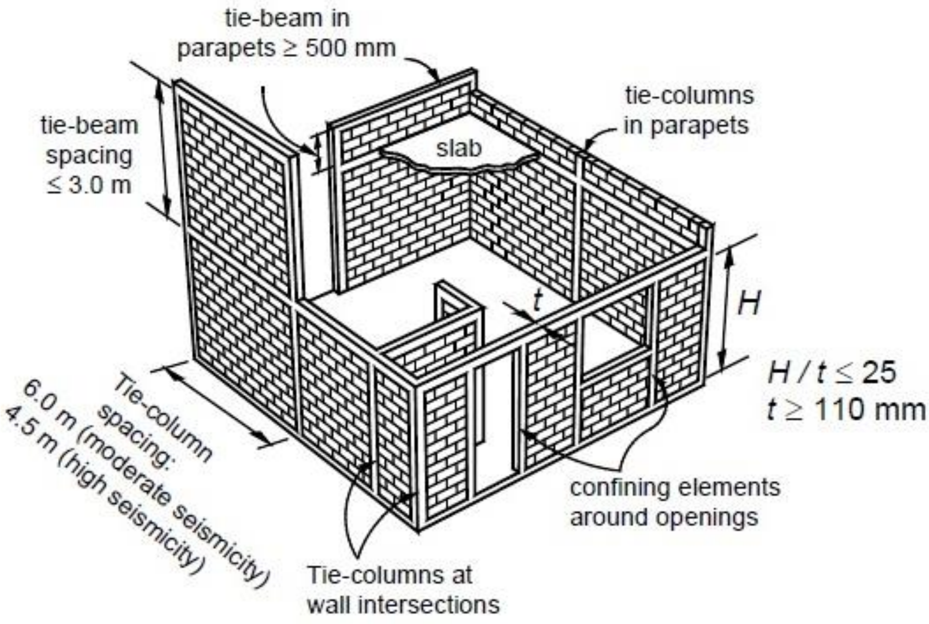

(a)

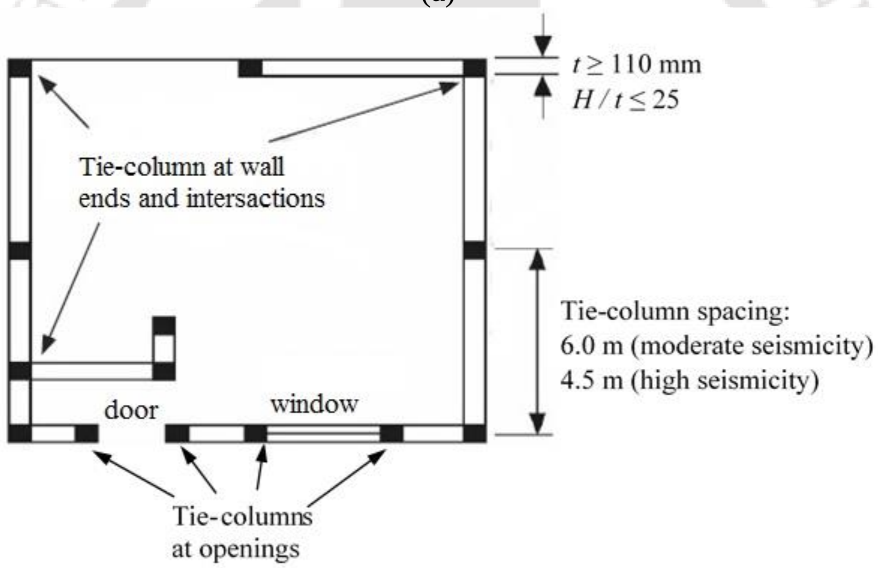

(b)

Figure 2.14: Key recommendations for non-engineered CM buildings: (a) Elevation, and (b) Plan (Meli et al. 2011).

2.7 Gap Areas

Past literature shows that significant work has been carried out on CM structures in different parts of the world, especially in Latin American countries with high seismicity. Different researchers have identified the possible failure modes of CM structures through experimental investigations and experience gained in past earthquakes. Further, several past experimental studies on CM walls with the influence of different parameters related to material, geometry, and loading provide knowledge concerning the structural behavior of CM walls. Some numerical and analytical modeling techniques have been suggested for the analysis of CM structures. In addition, some construction and design rules have been established for safe and adequate performance. Still, there are significant gaps in the state-of-the-art, especially in experimental testing, analysis methods, and seismic design. A review of past studies shows that additional experimental and analytical research is required to develop generalized analytical modeling techniques and design methodologies for CM walls. Thus, further research studies should be undertaken in the following areas:

1. Aspect ratio, though not widely studied, controls failure modes, initial stiffness, and strength of CM walls. The experimental studies are limited and not sufficient to get sufficient understanding of the influence of AR on the behavior of CM, particularly in the global context when the material and construction methodology have huge variations.
2. The modeling techniques for analysis of CM building available in the literature, such as finite element model, wide-column model, strut-and-tie model, and equivalent strut/shell model, have limited applications. A simple numerical model that can realistically simulate the gravity as well as lateral load response of CM walls is not yet fully developed.
3. Several guidelines and design codes have been developed over the years in different countries to provide basic details on CM and promote its construction practice; however, they convey a large dispersion in rules and many gaps. Thus, there is a need to assess the effectiveness of the design guidelines and provisions of different codes in ensuring the seismic safety of CM buildings, especially in the context of those countries in which available masonry is quite weak and soft.
4. Performance-based seismic design methodology requires a complete backbone profile (lateral load – displacement relationship) to be known; therefore, existing models for the prediction of lateral stiffness, strength, and deformability at different performance levels of CM walls should be assessed.
5. Significant variation in size and detailing of tie-elements is observed in the literature. More study is required to determine how the tie-columns behave (yielding of rebar, damage pattern) due to the change in aspect ratio. The distribution of design lateral forces to masonry walls and tie-columns is also not clearly discussed in the existing literature.

Chapter 3
EXPERIMENTAL EVALUATION OF LATERAL LOAD BEHAVIOR

CONTENTS

3.1 OVERVIEW

Seismic behavior of confined masonry (CM) buildings has been a subject of experimental studies for many years. Past earthquake damage reports emerging from various parts of the world and research studies conducted in different countries have contributed to the comprehensive understanding of the seismic behavior of CM buildings in terms of their damage patterns and failure modes. From different investigations, the general failure modes of CM structures are mostly categorized into those corresponding to the in-plane failures, out-of-plane failures, diaphragm failures, failures of connections between different members of confined masonry buildings, and non-structural failures (Matthews et al. 2007). The in-plane failure mode is more critical in case of CM as it is along the primary lateral load transfer path. On the other hand, unlike unreinforced masonry (URM) and infilled reinforced concrete

(RC) frame structures, overturning or out-of-plane failure mode is not catastrophic in case of CM buildings because the confining frame and masonry wall share good bonding (Tu et al. 2010, Singhal et al. 2014).

Most of the studies carried out in the past have shown that shear failure in the form of bed joint sliding or diagonal shear cracks from center of the masonry wall to the tie-columns is the most common type of failure in CM structures under in-plane lateral loading (Meli et al. 2011). In some limited studies, flexure-induced damages in the form of horizontal cracks in the lower courses of wall, yielding of rebars in tie-columns, or out-of-plane failure of masonry wall were observed (Zabala et al. 2004, Varela-Rivera et al. 2019). The failure modes are controlled by several parameters related to geometry, materials, and loading. Among all these parameters, aspect ratio of CM wall, i.e., height to length ratio of masonry panel, mainly controls the failure mode. The walls with a low aspect ratio (length of the wall is larger than the height) mainly fail in shear mode; however, the walls with a large aspect ratio (length of wall is much less than the height) are more susceptible to flexural mode of failure due to excessive bending. Some studies have been conducted on CM walls for understanding the influence of aspect ratio on lateral load performance (e.g., Gavilán et al. 2015, Varela-Rivera et al. 2019). Number of such studies is limited, and hence, not sufficient to get a comprehensive understanding of the subject particularly in the global context when the material properties and construction methodology have huge variations. Moreover, the available studies are limited to comparison of the lateral load response in terms of backbone profile, deformation characteristics, energy dissipation, etc., whereas the behavior of tie-columns (yielding of rebar, damage pattern) due to the change in aspect ratio is not studied significantly. In the present work, lateral load behavior of half-scale CM wall specimens, designed as per international standards, was investigated by carrying out quasi-static cyclic tests, and effect of aspect ratio on the failure mode of CM wall components – masonry wall and tie-columns, was examined in detail. The results of the experimental study will be utilized in later chapters of the thesis in (i) development of finite element and simplified numerical models for lateral load analysis of confined masonry walls, (ii) assessing the effectiveness of the recommendations of design codes and past studies in estimating the lateral load response (strength, stiffness, and lateral drift) of confined masonry walls, and (iii) development of a design methodology for members (tie-columns as well as masonry walls) of confined masonry buildings.

3.2 Description of Test Specimens

The prototype represented an exterior ground floor wall of a two-story CM building with a room size of 4.5 m × 3.5 m. In absence of an established design code for CM buildings in India, the Mexican masonry code (NTC-M 2017) was followed for design and detailing of the walls. The study intended to consider at least one slender CM wall, one wall with an intermediate aspect ratio, and one relatively squat wall, so that representative behavior of all three cases can be studied. Therefore, three aspect ratios (AR), defined as the ratio of the height of the CM wall excluding tie-beam (H_w) to the length of the CM wall excluding tie-columns (L_w), were considered as 2.0, 1.5, and 1.0, though the code permits CM walls up to AR 0.75. In India, the compressive strength of available bricks is generally low, therefore, the usual practice is to construct one-brick thick walls, which was also followed for the test specimens. Thus, the thickness of all the prototype walls was taken as one brick thick (i.e., t = 250 mm) ensuring that the slenderness ratio (H_w /t) is less than the limit of 30. The size of the prototype tie-elements considered was 250 mm × 250 mm as their minimum dimension is generally taken equal to the actual thickness of the masonry wall. Height (H_w) of the confined masonry walls was considered as 3 m based on general practice and the length (L_w) of the walls was taken as 1.5 m (for AR = 2.0), 2 m (for AR = 1.5), and 3 m (for AR = 1.0) by following the rules for maximum allowable spacing criterion between the two tie-columns recommended in the guideline ($\leq 1.5H_w$ or 4 m, whichever is lesser). Based on the concrete compressive strength (min 15 MPa), yield strength of rebars, and wall thickness, reinforcement in tie-members was decided to satisfy the minimum reinforcement requirement of the code. Considering the Indian practice scenario, no wall reinforcement was considered.

The model CM walls were designed for laboratory testing as per similitude relations considering a geometric half-scaling factor in the prototype walls (including the brick units). For a reliable correlation study with the prototype, the scale factors for length, force, area, moment, shear, volume were obtained as 0.5, 0.25, 0.125, 0.125, 0.25, and 0.125, respectively using similitude relations. The geometric properties and reinforcement detailing of the half-scale test specimens are shown in Fig. 3.1. RC tie-members in all the half-scale specimens had a cross-section of 125 mm × 125 mm in which 4 deformed bars of 6 mm diameter were provided as longitudinal reinforcement and 3 mm diameter stirrups (smooth bars) were provided as transverse reinforcement with 100 mm center-to-center spacing in the mid-span that was reduced to 40 mm at the ends over a length of 250 mm.

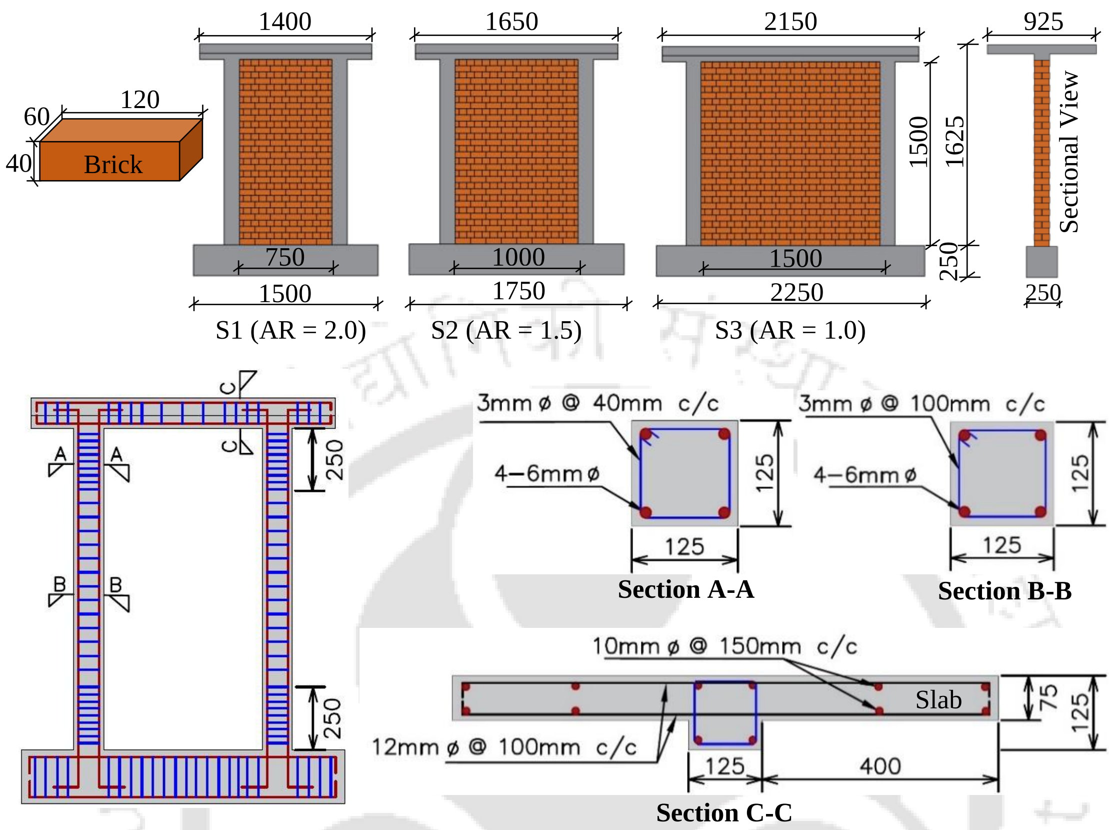

Note: All dimensions in millimeters (mm) except where mentioned otherwise. ϕ represents diameter of bar

Figure 3.1: Geometric and reinforcement detailing in specimens S1, S2, and S3.

3.3 Material Characterization

Material properties were evaluated using relevant standards by conducting tests on masonry and its constituents, concrete, and reinforcing bars (Table 3.1). Masonry is a non-homogenous, anisotropic material composed of two different materials - bricks and mortar. Different tests carried out for determining the material properties of masonry are shown in Fig. 3.2. The compressive strength of brick units (f_b) was determined by testing brick units under uniaxial compression in accordance with ASTM C67-13 (ASTM 2013a) and IS 3495 (BIS 1992). The average f_b of the burnt clay bricks was found to be 15.41 MPa [COV 10%]. The mortar used had a volume ratio of 1:1:6 of lime, cement and sand. The water-binder ratio was maintained as 0.75 to obtain a workable mix. The compressive strength of mortar cubes (f_j) was determined by testing 50-mm cube specimens under uniaxial compression in accordance with ASTM C109/C109M-13 (ASTM 2013b), and IS 2250 (BIS 1995). The average f_j was found to be 7.92 MPa [COV 8.8%]. Clearly, the bricks are significantly stronger than the mortar used. Five-bricks high masonry prisms with an average height of 220 mm were constructed with thickness of mortar joint about 5 mm. Generally, thickness of the mortar joint in the prototype wall lies in the range of 10 – 12 mm, thus the thickness of mortar joint in the half-scale model should be 5 – 6 mm to satisfy the scaling laws. The uniaxial compressive strength of masonry prism (f'_m) in the direction perpendicular to bed joints was determined after 28 days of curing in accordance with IS 1905 (BIS 1987). The average f'_m was found to be 5.2 MPa [COV 9.5%] and the modulus of elasticity of masonry (E_m) was calculated as the slope of the secant connecting 5% to 33% of the maximum compressive strength of the specimens (Kaushik et al. 2007, MSJC 2011) and it was found to be about 2000 MPa. Shear strength is required for the design of masonry panels when they are subjected to lateral loads. The initial shear strength of masonry (v_{m0}) from horizontal bed joint shear strength was determined by carrying out triplet test in accordance with BS EN 1052-3 (BSI 2002). The diagonal compressive strength of masonry (v_m) was determined in accordance with ASTM E 519 (ASTM 2010) using masonry wallettes of size 0.60 × 0.60 m. The average value of v_{m0} and v_m were found to be 0.43 MPa [COV 16%] and 0.44 MPa [COV 14%], respectively.

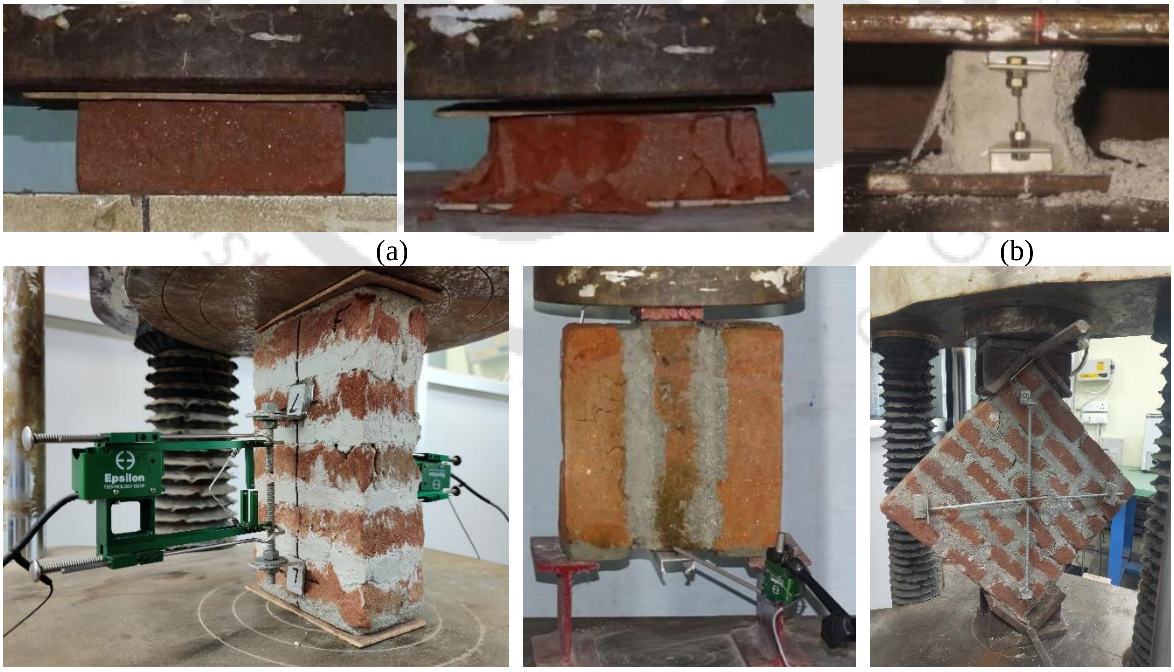

(a) (b)

(c) (d) (e)

Figure 3.2: Experimental tests on: (a) clay brick units; (b) mortar cubes; (c) masonry prisms, (d) masonry triplets, and (e) masonry wallettes.

The average compressive cube strength of M25 concrete (f_c) was 30.4 MPa, which was obtained by compressive test on concrete cubes as per IS 516 (BIS 2004). The modulus of elasticity of concrete (E_c) was obtained as 27570 MPa using IS456 (BIS 2000). The tensile properties of rebars were obtained by tension tests on bars in accordance with IS 1608 (BIS 2018). The average yield strength of 6 mm (longitudinal rebar) and 3 mm (transverse rebar) diameter bars was 549 MPa and 446 MPa, respectively, with the modulus of elasticity (E_s) as 1.91×10^5 MPa and 2.06×10^5 MPa, respectively.

Table 3.1: Material properties obtained in the experimental study.

Properties	Material	Mean Value (MPa)
Compressive strength, Elastic Modulus	Brick	$f_b = 15.41$ [COV 10%]
	Mortar	$f_j = 7.92$ [COV 8.83%]
	Masonry	$f'_m = 5.2$ [COV 9.46%], $E_m = 2000$
	Concrete (M25)	$f_c = 30.4$ [COV 16.8%], $E_c = 27570$
Yield strength, Elastic Modulus	Steel rebar (6ϕ)	$f_{yl} = 549$ [COV 0.98%], $E_s = 1.91 \times 10^5$
	Steel rebar (3ϕ)	$f_{yt} = 446$ [COV 1.15%], $E_s = 2.06 \times 10^5$
Initial shear strength	Masonry	$v_{m0} = 0.43$ [COV 16%]
Diagonal compressive strength	Masonry	$v_m = 0.44$ [COV 14%]

Note: COV = Coefficient of Variation; ϕ = diameter of bar; 6ϕ represents 6 mm diameter.

3.4 Test Procedure and Instrumentation

All specimens were constructed on an RC foundation beam of cross-section 250 mm × 250 mm. Reinforcement cages for the tie-columns were assembled and placed at the tie-column locations after constructing the bottom beam. Atop the foundation beam, masonry wall was constructed between the tie-columns up to the full height in three steps (not more than 0.5 m in a day) using solid half-scale burnt-clay bricks and mortar (about 5 mm thick) in English bond pattern. The average size of the half-scale clay brick units used was 120 mm × 60 mm × 40 mm, so two brick layers were provided in the out-of-plane direction in the alternate courses (stretcher courses) as shown in the sectional view of Fig. 3.3. All the horizontal and vertical joints in the masonry wall were filled with mortar. Concrete in the tie-columns was poured once the desired wall height was reached using formwork only on three faces of the tie-columns. Finally, the tie-beam was constructed along with an RC slab of 75 mm thickness.

(a) (b) (c)

Figure 3.3: Construction of the CM wall specimens: (a) Masonry wall construction, (b) Casting of tie-columns, (c) Tie-beam and slab construction.

The typical test setup for all the confined masonry wall specimens tested in the present study is shown in Fig. 3.4. The bottom foundation beam of the specimens was anchored rigidly at the base to the strong floor to prevent sliding and toppling of the specimens during the cyclic tests. The out-of-plane movement of the specimens was prevented by using steel buttress frames fitted with roller bearings at the slab level of the specimens. The lateral deformations of the specimens at different heights were recorded using four LVDTs, which were attached to the tie-columns. Moreover, two strain gauges were bonded to each longitudinal rebar at top and bottom at the critical locations where plastic hinges are expected to form. The imposed load (dead and live) due to the upper-story was applied by placing steel plates over the RC slab, and it was maintained such that the overburden pressure on the tie-beam (i.e., overburden load above tie-beam divided by surface area of tie-beam) is constant ($\sigma \approx 0.13$ MPa) throughout the test for all the specimens.

Quasi-static cyclic lateral loading was applied at the slab level using a servo-controlled hydraulic actuator of ±125 mm stroke length and 250 kN load capacity. The loading consisted of gradually increasing story drifts (ratio of lateral displacement to masonry wall height) from 0.10% till failure as per ACI 374 (2005) as shown in Fig. 3.5. Each displacement cycle was repeated three times at each drift ratio with a very low frequency of 0.02 Hz. All the responses during testing were recorded and processed with the help of a data acquisition system and LabVIEW.

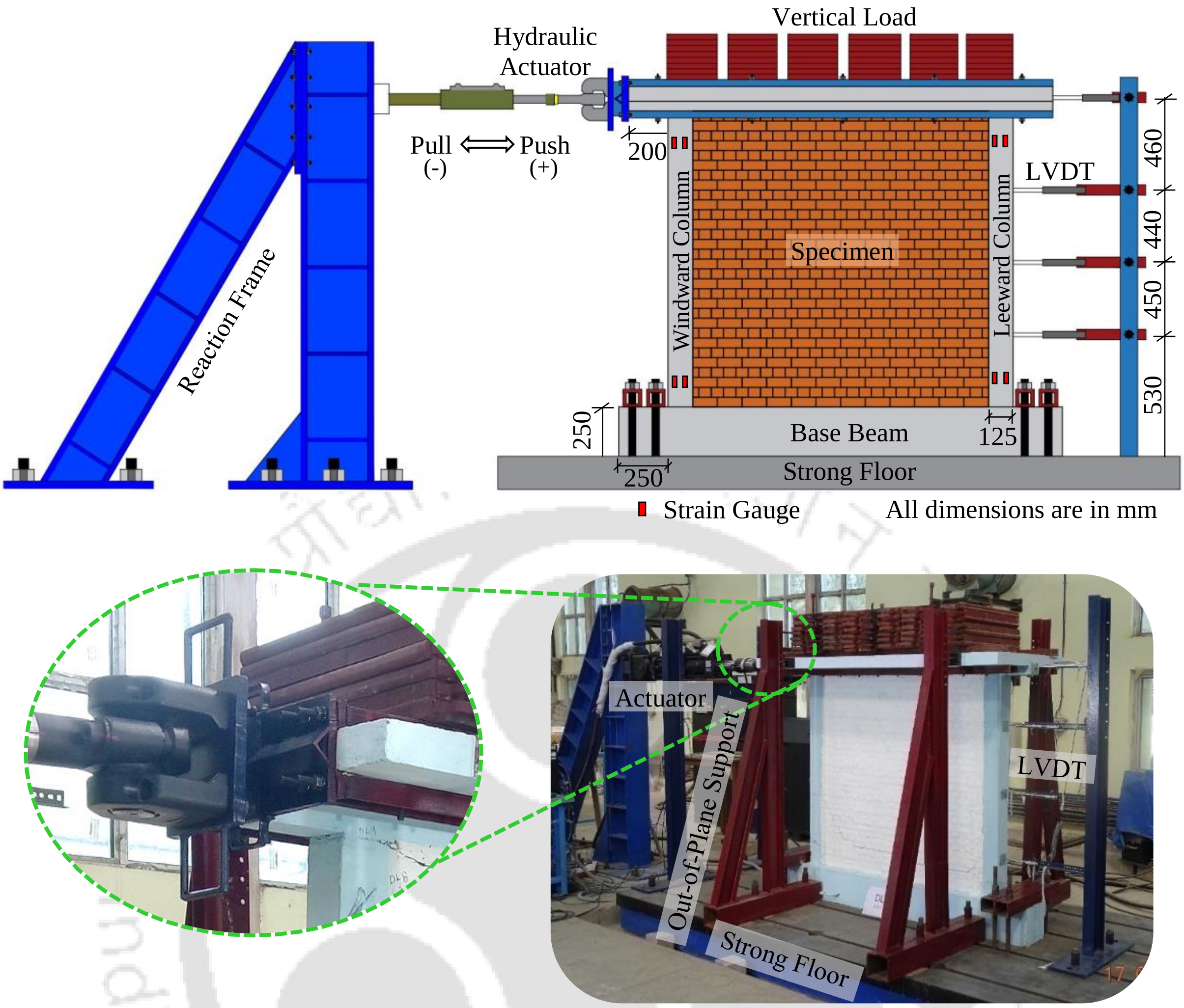

Figure 3.4: Experimental setup and instrumentation shown in schematic and during actual testing.

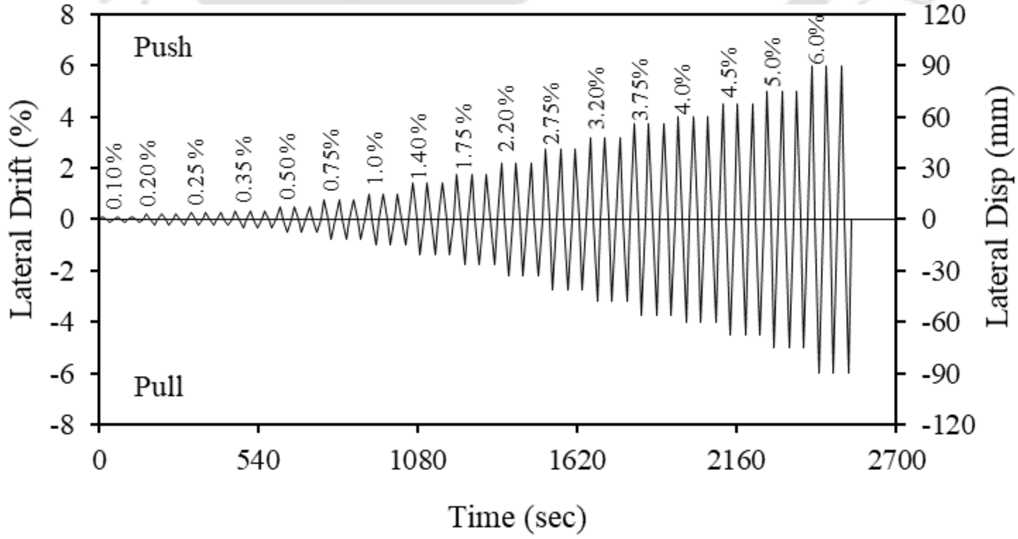

Figure 3.5: Cyclic loading history applied to the test specimens.

3.5 Response of Specimens

The lateral load behavior of the specimens during quasi-static cyclic testing in the form of hysteretic response (lateral load-lateral drift) for the applied three cycles of every lateral drift level is shown in Fig. 3.6. The hysteretic response showed symmetric loops in push and pull directions for all the specimens. As expected, pinching was observed in the response of all the specimens at higher drift levels because of significant damage. Sudden reduction in the lateral strength of the first specimen S1 is evident from the hysteresis curves at a drift level of about 4%. In the second specimen S2, the sudden reduction in the strength was not observed even when subjected to 6% drift. Though the lateral strength of the third specimen S3 was highest, it failed quite early due to severe damage in the tie-columns. Some test photographs and videos showing the lateral load response of the specimens are available at: https://www.iitg.ac.in/hemantbk/stud/bonisha.html.

3.5.1 Crack Pattern and Failure Mechanism

The crack pattern and resulting failure mechanisms observed during the tests provide an insight into the behavior of the specimens and effectiveness of the design methodologies adopted. Under the action of cyclic lateral loads, the three specimens behaved quite differently. The extent and type of damage were primarily governed by the characteristics of each wall. Figs. 3.6 and 3.7 show the observed cracking in the specimens during first notable cracking and lateral strength stages, respectively. Fig. 3.8 shows the load-deformation along with the final crack patterns. Damage observations are discussed in the following sections.

Specimen S1 (Aspect ratio 2)

As specimen S1 was slender, primarily flexural behavior was expected under lateral loads. True to this, the first crack that appeared in S1 was flexural in the left tie-column (windward column) near the bottom as observed in Fig. 3.6a at 0.35% drift and 38.4 kN load (average of push and pull loads). At 0.75% drift, interface cracks between tie-columns and walls, and additional flexural cracks in both the tie-columns were observed. Here the specimen achieved its strength of 46.7 kN in the pull direction, while the strength of 48.3 kN was achieved at the next drift level of 1% in the push direction. Fig. 3.7a shows the damage observed in S1 at this stage. The first shear crack formed at the top left beam-column joint at 1.75% drift. At about 4% drift, a reinforcing bar in the bottom of the left tie-column ruptured. The test was terminated at this stage when the lateral load dropped to about 13.9 kN, i.e., about 29% of the peak value. Fig. 3.8b shows the damage at the end of the test. The maximum recorded widths of the diagonal and vertical interface cracks were about 13 mm and 19 mm, respectively, at the end of the test. The maximum recorded bending deformation in the tie-columns was about 22 mm.

(c)

Figure 3.6: First notable cracks during testing of specimen: (a) S1, (b) S2, and (c) S3.

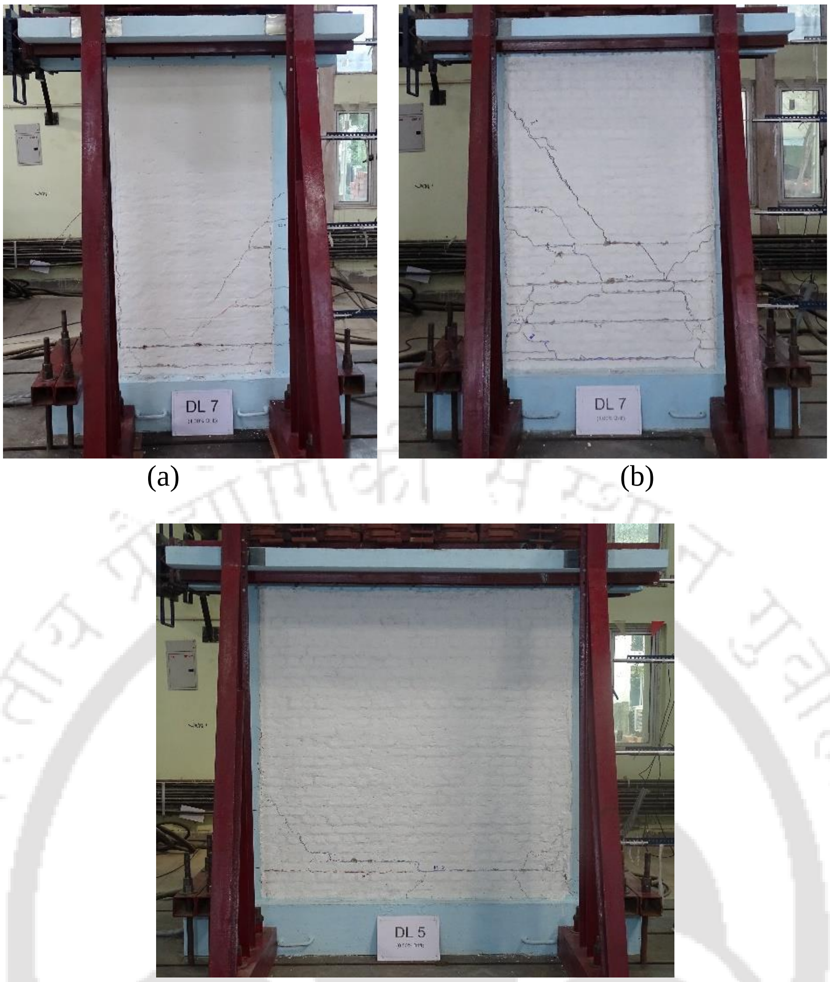

(a) (b)

(c)

Figure 3.7: Damage observed at peak lateral strength for: (a) S1, (b) S2, and (c) S3.

Specimen S2 (Aspect ratio 1.5)

Specimen S2 developed the first crack at the bed joint near the bottom part of the masonry wall at 0.2% drift level and a lateral load of 38.2 kN (Fig. 3.6b). During 0.75% drift level, several diagonal stair-stepped cracks in masonry wall and interface cracks between masonry and the windward tie-column were observed; the specimen achieved its peak strength of 52.6 kN in the pull direction at this drift. Similarly, the specimen achieved its strength of 59 kN in the push direction at the next drift level of 1%, where the cracks were also observed in the interface of masonry and leeward tie-column (Fig. 3.7b). The maximum bending deformation recorded in the tie-columns was in the range of 25 mm to 35 mm. The recorded width of different cracks was significantly higher (diagonal crack: 14 mm, interface crack: 40 mm) compared to the first specimen indicating severe damage in the wall. The test was terminated at 6% drift when the lateral strength reduced to about 19 kN, i.e., 35% of the peak value. Fig. 3.8d shows the damage at the end of the test.

Specimen S3 (Aspect ratio 1)

As expected from a relatively squat specimen, the first crack that appeared in S3 was a bed joint shear crack in the masonry wall near the bottom at a drift level of 0.25% and a lateral load of 65.7 kN was recorded (Fig. 3.6c). At about 0.5% drift level, diagonal stair-stepped crack and interface crack appeared at the left tie-column-to-wall interface, and the specimen achieved its peak strength of 82.3 kN in the push and 80 kN in pull direction (Fig. 3.7c). Further increase in the lateral drift resulted in the development of flexural and shear cracks in tie-columns. As expected, the width of the diagonal cracks was highest in this specimen (25 mm), while the maximum width of the interface crack (24 mm) was found to be lesser than that observed in S2. In this specimen too, significant bending of tie-columns was observed (maximum bending deformation of 25 mm). Severe damage to tie-columns and the rupture of the longitudinal reinforcement at the bottom of both the tie-columns resulted in termination of the test at 1.75% drift where the strength reduced to about 39 kN, i.e., 48% of the peak load (Fig. 3.8f).

Comparing the performance, the influence of aspect ratio on lateral load behavior of three specimens was apparent. When the configuration changed from slender to squat, initiation of damage pattern changed from flexural cracking of tie-columns to shear (sliding or diagonal) cracking of masonry. S3 achieved the lateral strength early (at only 0.50% drift) than S2 (at 0.82% drift) and S1 (at 0.87% drift). In past experimental studies, recorded drift at peak load varies from 0.17% to 0.74% for solid CM walls without horizontal reinforcements (detail discussion is provided in Chapter 5). Here, the obtained lateral drift at peak load was on the higher side possibly due to the use of soft masonry (E_m = 2000 MPa) in English bond pattern. In order to study the behaviour of tie-columns, it was important to apply further lateral drifts to the specimens. Thus, attempt was made (S1 and S2 were studied up to 4% and 6%, S3 was studied only up to 1.75% drift) to capture the response of tie-columns of CM walls with different AR under lateral loading. The tie-columns of the squat specimen S3 suffered the most severe damage and exhibited a sudden drop in strength after reaching the peak (Fig. 3.8e). The damage was uniformly distributed in the masonry wall in S1 and S2, whereas the damage was mostly concentrated in the bottom one-third part of S3 wall (Fig. 3.8f). Though the initiation of cracks and damage was different in the three specimens, finally, all the specimens failed due to shear failure of tie-columns after masonry suffered severe damage.

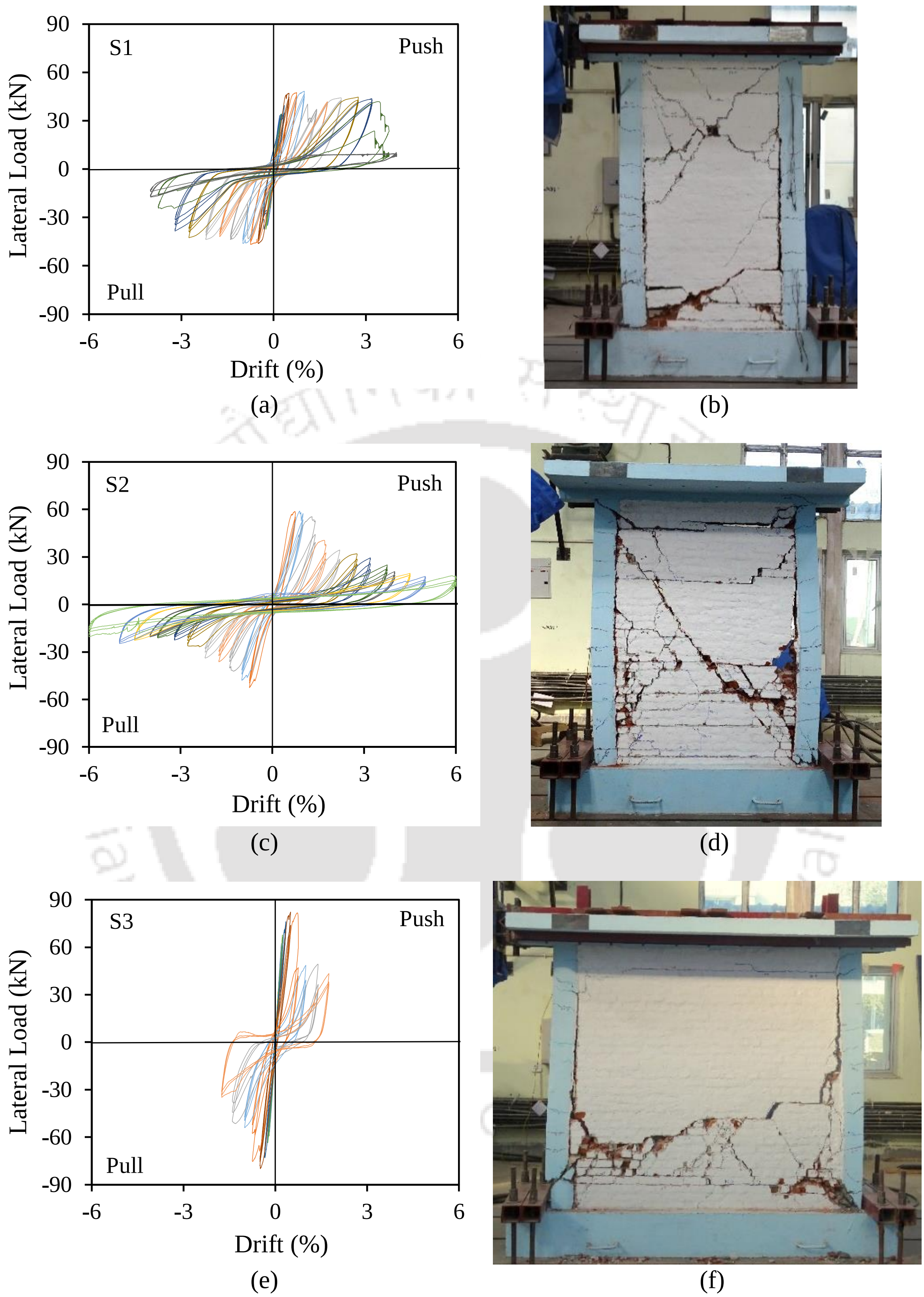

Figure 3.8: (a), (c), (e) Hysteretic response, (b), (d), (f) Damage observed in specimens S1, S2, and S3, respectively.

3.5.2 Deformation Response

Fig. 3.9 shows the maximum lateral displacement recorded at different drift levels by the LVDTs placed along the height of the right tie-column. The displacement profile can be generalized as the deflected shape of the single-story CM wall subjected to lateral load at the top. It can be observed that for the same load the deflection profile of the walls is not similar to each other. The recorded profile shows unsymmetrical bending of the tie-columns in S2 and S3, while it was symmetric in S1, which underwent well distributed lateral deformation along the height at all drift levels because of the lesser damage, especially in the tie-columns. As already discussed, the initiation of damage in S1 was due to the formation of flexural cracks in tie-columns. With increasing drift, the flexural cracks started forming along the whole length of the tie-columns in addition to the well-distributed damage in the masonry wall (Fig. 3.8b). However, plastic hinges were formed at the bottom of the tie-columns much after the lateral strength. On the other hand, failure pattern in S2 and S3 (Fig. 3.8 d and f) was governed by shear mode, and extensive damage was observed early in the tie-columns and masonry wall resulting in formation of plastic hinges at the bottom of tie-columns. With increasing lateral drift, the columns stopped deforming laterally near the locations of plastic hinges, while continuing to rotate at the hinges. Thus, the lateral deformation along the height of tie-columns was not uniform at all drift levels in S2 and S3 (Fig.3.9 b and c). Clearly, AR plays a significant role in the lateral deformability and deformation profile of CM walls.

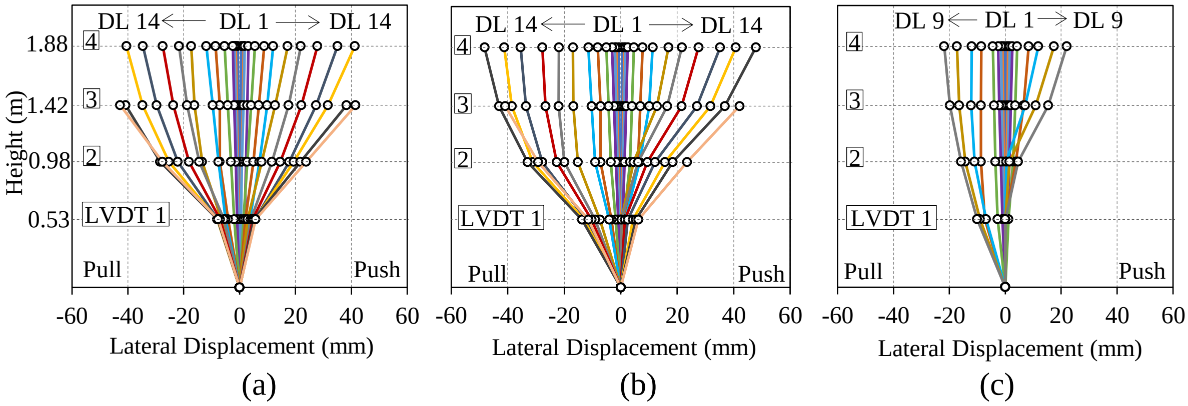

Figure 3.9: Deformation profile of specimens: (a) S1, (b) S2, and (c) S3. (DL=Drift Level)

3.5.3 Strain in Longitudinal Reinforcements of Tie-Columns

To assess the nonlinearity in tie-columns, the state-of-strain across the cross-section of tie-columns was determined with the help of strain gauge data. Pre-wired uniaxial strain gauges (HBM made) were used to record the strains at the most critical regions of tie-columns where plastic hinges are expected to develop. Four such critical cross-sections in tie-columns were considered for each specimen. Two strain gauges were bonded to each longitudinal rebar (one at the top and the other at the bottom) using cyanoacrylate adhesive. In total sixteen numbers of strain gauges (four strain gauges in each critical cross-section) were used on the longitudinal rebars of tie-columns as shown in Fig. 3.10. The maximum strain in rebars, recorded by the strain gauges at various locations, corresponding to the lateral drift values are shown in Fig. 3.10 and Tables 3.2, 3.3, and 3.4 for all three specimens. The strain gauges are designated by five symbol code, such as LCL1U. the first two letters LC or RC represents left or right tie-column in a CM specimen. The third letter L or R represents left or right longitudinal rebar in a tie-column cross-section. The fourth numeral 1 or 2 after the letter L or R represents the first or second longitudinal bar of a tie-column in left side or right side. The last letter U or D represents the top (up) or bottom (down) cross-section of a tie-column.

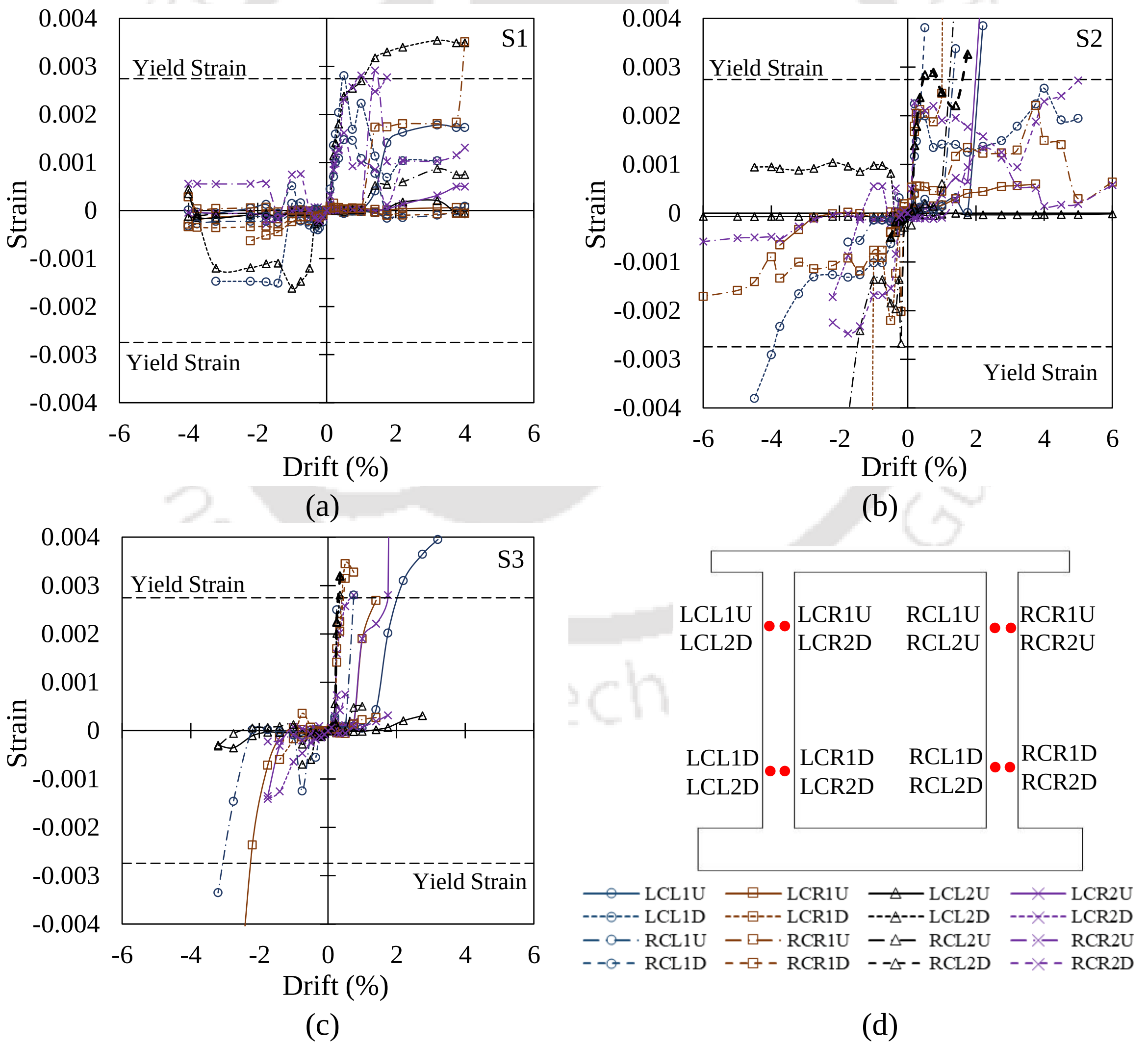

Figure 3.10: Envelope curves showing strain recorded at sixteen locations with respect to lateral drift for (a) S1, (b) S2, and (c) S3. Strain gauge location shown in (d).

Table 3.2: Typical strain values recorded at various column locations in S1.

Location	Strain Gauges	Peak Strain (μmm/mm)		Drift (%)		Status
		Tension (+)	Compression (-)	Push (+)	Pull (-)	
Left Column Up	LCL1U	1780.6	-57.8	2.75	-1.40	-
	LCR1U	62.1	-287.9	3.75	-3.75	-
	LCL2U	206.0	-164.1	2.75	-2.75	-
	LCR2U	498.0	-156.4	3.75	-1.40	-
Left Column Down	LCL1D	2805.0	-1515.0	0.50	-1.40	Yielded
	LCR1D	148.0	-632.0	0.20	-2.20	-
	LCL2D	2745.0	-1617.5	0.75	-1.00	Yielded
	LCR2D	2809.8	-286.2	0.75	-1.75	Yielded
Right Column Up	RCL1U	84.0	-329.0	3.75	-3.75	-
	RCR1U	3511.6	-29.8	3.75	-1.40	Yielded
	RCL2U	867.2	-121.9	2.75	-1.40	-
	RCR2U	-	-74.3	-	-1.40	-
Right Column Down	RCL1D	1474.0	-309.0	0.50	-0.50	-
	RCR1D	62.0	-359.0	0.25	-2.75	-
	RCL2D	-	-	-	-	-
	RCR2D	1617.5	-224.5	0.50	-0.20	-

Table 3.3: Typical strain values recorded at various column locations in S2.

Location	Strain Gauges	Peak Strain (μmm/mm)		Drift (%)		Status
		Tension (+)	Compression (-)	Push (+)	Pull (-)	
Left Column Top	LCL1U	3847	-	2.20		Yielded
	LCR1U	596	-656	3.75	-3.75	-
	LCL2U	-	-74.79	-	-0.75	-
	LCR2U	5059	-	2.20	-	Yielded
Left Column Bottom	LCL1D	2564	-2912	4.00	-4.00	Yielded
	LCR1D	2745	-2745	1.40	-1.40	Yielded
	LCL2D	1039	-396	-2.20	-0.35	-
	LCR2D	2074	-1725	0.20	-2.20	-
Right Column Top	RCL1U	3375	-598	1.40	-1.75	Yielded
	RCR1U	2206	-2020	3.75	-0.20	-
	RCL2U	4625	-4230	1.40	-1.75	Yielded
	RCR2U	1339	-585	2.20	-6.00	-
Right Column Bottom	RCL1D	3806	-404	0.50	-3.20	Yielded
	RCR1D	2046	-402	0.25	-0.50	-
	RCL2D	2841	-1376	0.50	-2.75	Yielded
	RCR2D	2745	-2470	0.50	-1.75	Yielded

Table 3.4: Typical strain values recorded at various column locations in S3.

Location	Strain Gauges	Peak Strain (μmm/mm)		Drift (%)		Status
		Tension (+)	Compression (-)	Push (+)	Pull (-)	
Left Column Top	LCL1U	3099.2	-95.0	2.20	-1.00	Yielded
	LCR1U	2745.0	-2366.6	1.75	-2.20	Yielded
	LCL2U	308.4	-355.6	2.75	-2.75	-
	LCR2U	2745.0	-1352.7	1.75	-1.75	Yielded
Left Column Bottom	LCL1D	2496.8	-102.8	0.25	-0.20	-
	LCR1D	3454.2	-598.8	0.50	-1.40	Yielded
	LCL2D	2745.0	-693.5	0.50	-0.75	Yielded
	LCR2D	2745.0	-1411.8	0.50	-1.75	Yielded
Right Column Top	RCL1U	2745.0	-3352.6	0.75	-3.20	Yielded
	RCR1U	268.7	-131.9	1.40	-0.75	-
	RCL2U	507.3	-321.7	1.00	-3.20	-
	RCR2U	318.9	-223.1	1.75	-1.75	-
Right Column Bottom	RCL1D	284.5	-553.5	0.20	-0.35	-
	RCR1D	3145.2	-30.0	0.50	-0.25	Yielded
	RCL2D	3201.3	-119.7	0.50	-0.20	Yielded
	RCR2D	751.9	-247.1	0.50	-0.50	-

The lateral load vs rebar strain (hysteretic) response at different sections of tie-columns is also shown in Figs. 3.11, 3.12, and 3.13 for all three specimens. For specimen S1, Strain gauge RCL2D was found to be not operational and was not considered for further analysis. Figs. 3.11, 3.12, 3.13, and Tables 3.2, 3.3, 3.4 show that during the testing of S1, only four strain gauges (three from bottom of left column and one from top of right column) recorded high strains corresponding to yielding of rebars. Similarly, nine strain gauges recorded yielding of bars in each of S2 and S3. In most of the cases, the strain recorded in tension was found to be higher when compared to compressive strain. Yielding of rebars and the maximum strain was recorded at a lower drift level near the left and right column at bottom locations when compared to the top locations. Most rebars at the bottom of tie-columns yielded at a low drift value of 0.5%, while those at the top yielded at a much higher lateral drift. The summary of yielding of reinforcement bars in the three specimens is shown in Fig. 3.14, which shows the minimum lateral drift values corresponding to yielding of these rebars at different locations in tie-columns.

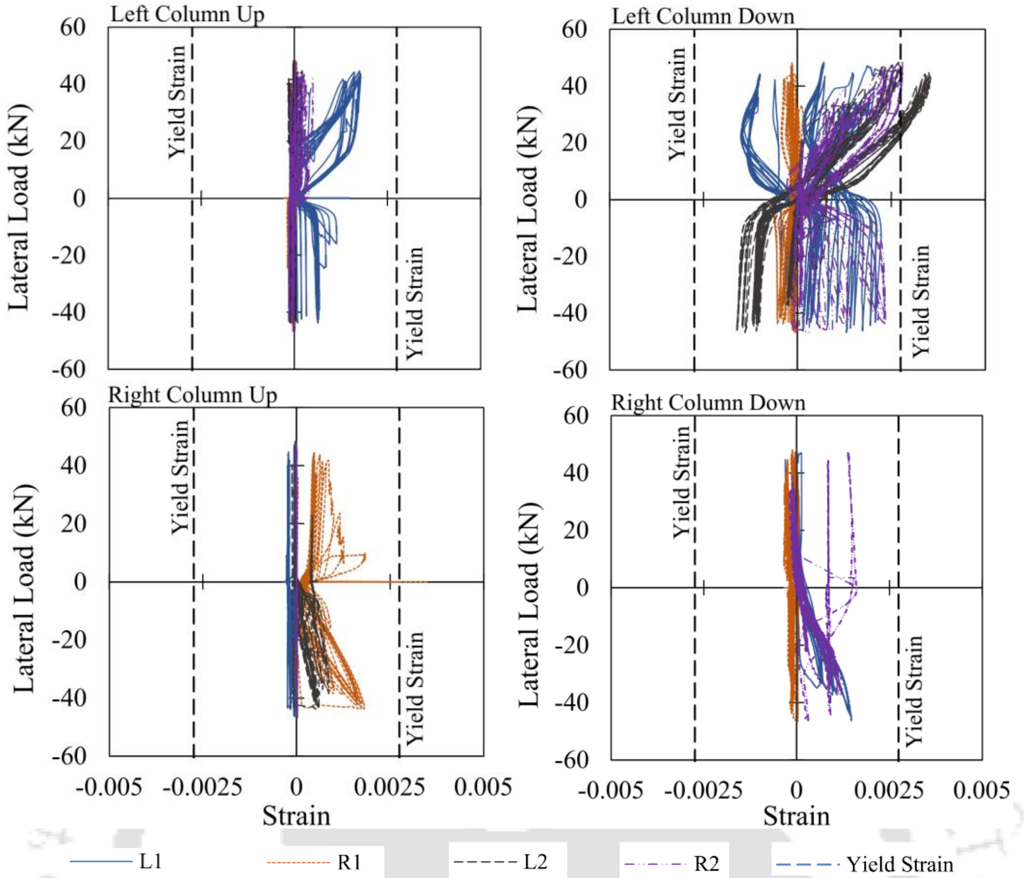

Figure 3.11: Lateral load-rebar strain response for different column locations in S1.

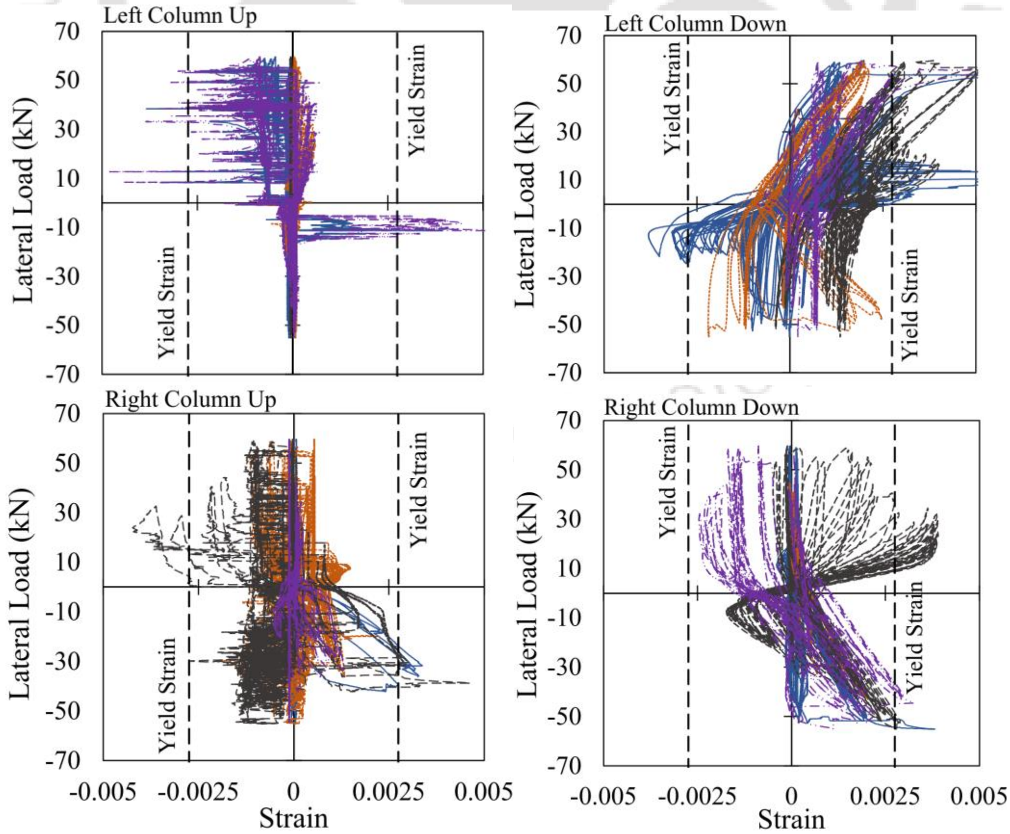

Figure 3.12: Lateral load-rebar strain response for different column locations in S2.

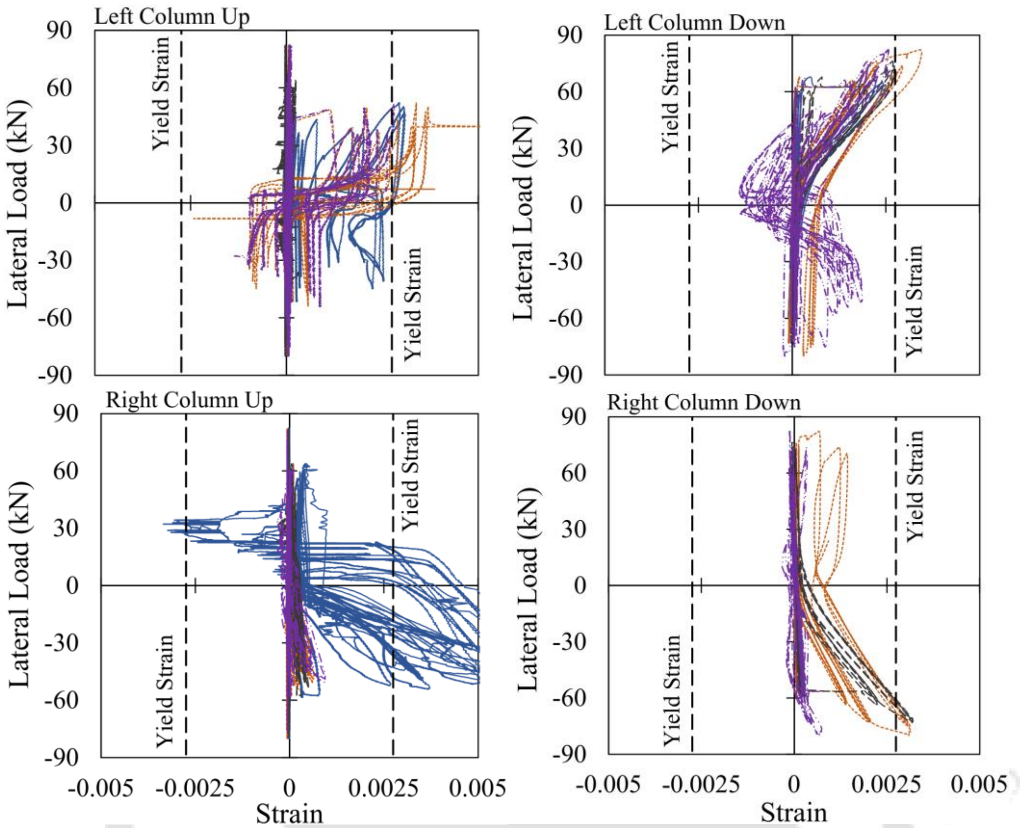

Figure 3.13: Lateral load-rebar strain response for different column locations in S3.

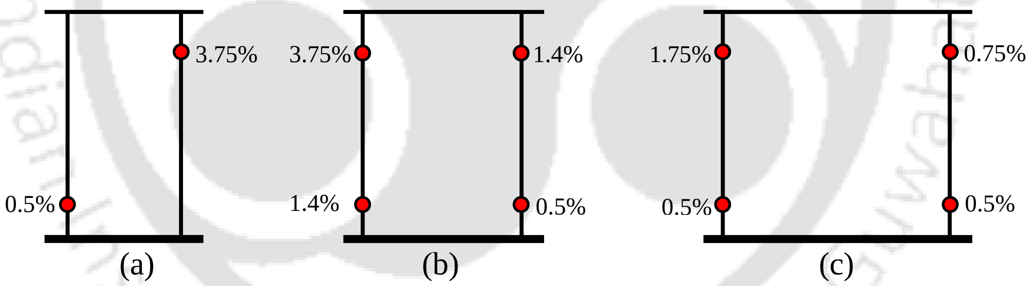

Figure 3.14: Comparison of the initial yielding of rebars and corresponding drift levels (in %) at the critical sections of tie-columns for specimen: (a) S1, (b) S2, (c) S3.

3.6 Evaluation of Influencing Parameters

The lateral load behavior of the test specimens is compared in terms of strength, stiffness, degradation of strength and stiffness, energy dissipation, damping, lateral deformation, and ductility.

3.6.1 Response Envelope Curves

The envelope backbone curves were plotted by joining the points of peak lateral load corresponding to the first hysteretic loop at each drift cycle. Fig. 3.15 shows the comparison of the envelope curves of all three specimens. It is evident that the lateral strength of CM wall increases as the aspect ratio of wall decreases. The experimentally obtained lateral strength ($V_{m,e}$) and residual strength at the end of the test (V_r) along with the corresponding drifts ($\delta_{m,e}$ and δ_r) for all the specimens are shown in Table 3.5. The obtained average $V_{m,e}$ was 48.3 kN, 59 kN, 82.3 kN for specimen S1, S2, and S3, respectively. Thus, $V_{m,e}$ of the walls S2 and S3 was about 1.2 and 1.7 times that of S1, respectively. Though the lateral strength increased with decreasing AR or increasing length (as H is constant), the shear stress in the masonry wall ($V_{m,e}$ /A_w), obtained by distributing the lateral load along masonry cross-section A_w, reduced from 0.51 MPa in S1 to 0.45 MPa in S2 and finally to 0.44 MPa in S3. Moreover, the lateral drift at peak load ($\delta_{m,e}$) decreases as AR of CM wall decreases. As given in Table 3.5, the relatively squat wall S3 achieved the strength early (at only 0.50% drift) than the comparatively slender walls S2 (at 0.82% drift) and S1 (at 0.87% drift). At the end of the tests, the average residual strengths were 13.9 kN, 19.2 kN, 39.1 kN corresponding to 4%, 5.9%, and 2.5% drift for S1, S2, and S3, respectively.

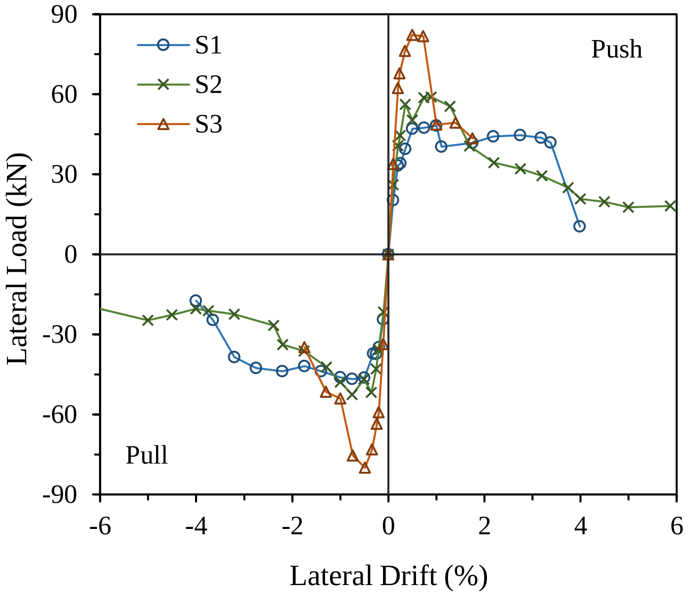

Figure 3.15: Comparison of envelope curves of specimens S1, S2, and S3.

Table 3.5: Summary of experimentally obtained hysteresis responses of the specimens.

ID	AR	$V_{m,e}$ (kN)			$\delta_{m,e}$ (%)			V_r (kN)			δ_r (%)			$V_{m,e}$ /A_w (MPa)
		Push	Pull	Avg	Push	Pull	Avg	Push	Pull	Avg	Push	Pull	Avg	
S1	2.0	48.3	46.7	47.5	1.00	0.75	0.87	10.4	17.4	13.9	4.0	4.0	4.0	0.51
S2	1.5	59.0	52.6	55.8	0.89	0.75	0.82	18.1	20.4	19.2	5.9	6.0	5.9	0.45
S3	1.0	82.3	80.0	81.1	0.50	0.49	0.50	43.4	34.9	39.1	1.8	3.2	2.5	0.44

3.6.2 Stiffness Degradation

The cyclic stiffness (K_c) was estimated for the first hysteresis cycle at each drift level as the slope of the line joining the positive and negative extreme points. The initial cyclic stiffness (K_{c0}) was found to be 14.7, 15.7, and 21.8 kN/mm for S1, S2, and S3, respectively. The cyclic stiffness at each drift level (K_c) was normalized with respect to the maximum or initial cyclic stiffness K_{c0} to obtain stiffness degradation (K_c/K_{c0}) at a particular drift level and plotted against the corresponding drift δ normalized with respect to the drift at the end of first loading cycle, δ_0 (Fig. 3.16a). It is observed that all the specimens followed almost a similar trend for cyclic stiffness degradation with in-plane drift. Among all the specimens, maximum common drift value was 1.75% (i.e., δ/δ_0 = 17.5) at which K_c/K_{c0} was about 0.1 for all the specimens indicating that the cyclic stiffness degraded to about 10% of K_{c0}.

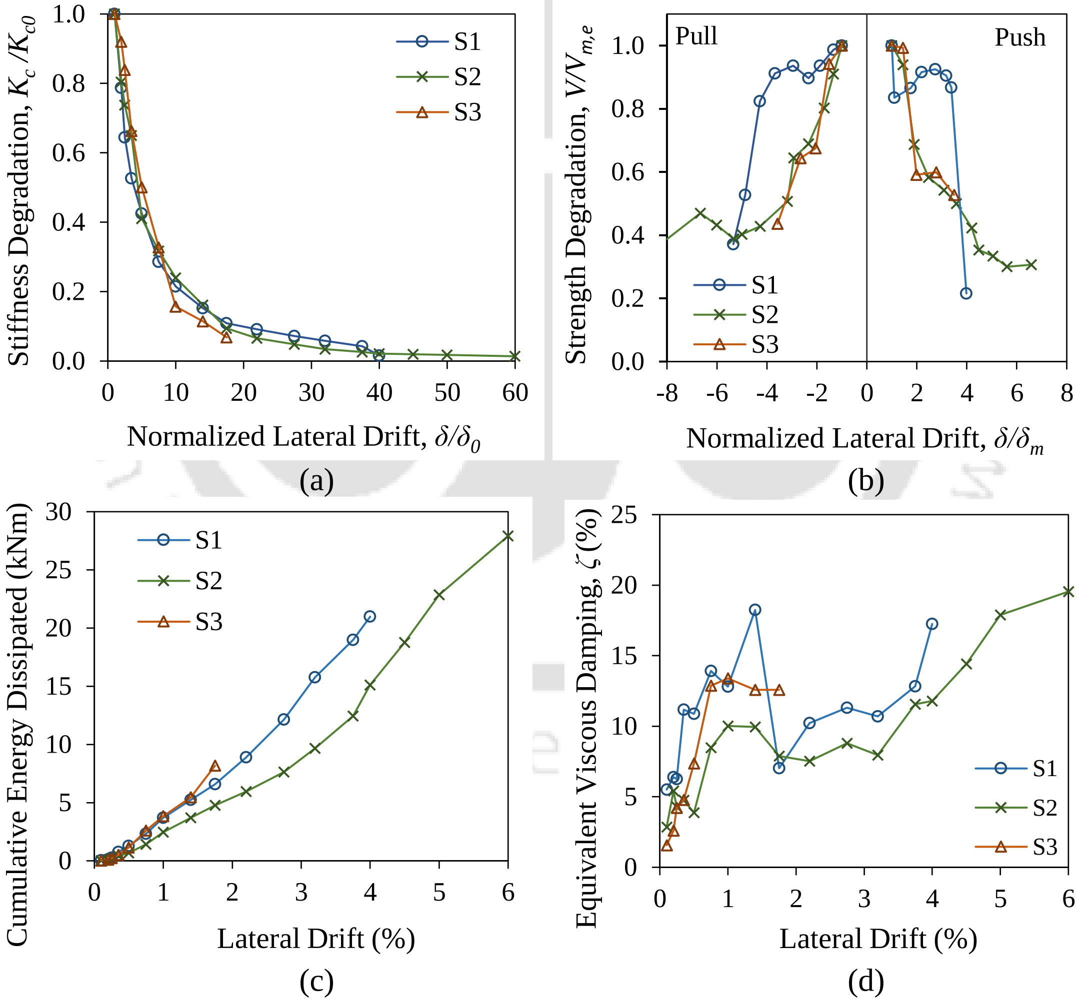

Figure 3.16: Comparison of hysteretic response in terms of: (a) stiffness degradation, (b) strength degradation, (c) cumulative energy dissipation, and (d) equivalent viscous damping.

3.6.3 Strength Degradation

The post-peak lateral loads obtained at different drift levels were normalized with $V_{m,e}$ and the obtained strength degradation ($V/V_{m,e}$) is plotted against $\delta/\delta_{m,e}$ as shown in Fig. 3.16b, which shows specimens S2 and S3 followed almost uniform strength degradation pattern. However, a slight increment in strength was observed in the slender wall S1 after initial degradation due to the confining effect of the closely spaced tie-columns as also mentioned in Gavilan et al. (2015). The ratio, $V/V_{m,e}$ was found to be 0.88, 0.69, and 0.48 at a maximum common drift of 1.75% for which $\delta/\delta_{m,e}$ = 2.0, 2.1, and 3.5 for S1, S2, and S3, respectively, signifying that with decreasing AR not only the peak strength reached earlier, but it also degraded more. Further, as the squat wall achieved the peak capacity at a smaller drift level, the drift factor was more for the squat wall at 1.75% drift.

3.6.4 Energy Dissipation

The energy dissipated in each displacement level was evaluated as the area enclosed under the hysteresis loops (3 loops or cycles per displacement level). The cumulative energy dissipation (E_{dc}) was calculated by summing up the energy dissipated in each displacement level. As shown in Fig. 3.16c, the cumulative energy dissipation (E_{dc}) was 21 kNm, 27.9 kNm, and 8.2 kNm for S1, S2, S3, respectively. Thus, maximum E_{dc} was observed in the case of S2 for which the hysteresis loops were most stable until a large lateral drift of about 6%. A comparison shows the minimum energy (about one-third of S2) was dissipated by S3 because of its early failure (Fig. 3.16c). Another parameter to analyze the energy dissipation capacity is damping. The equivalent viscous damping ratio (ζ), which is proportional to the energy dissipated in one hysteresis loop to the maximum strain energy of an equivalent elastic system (Chopra 2017), is plotted against the lateral drift in Fig. 3.16d. The value of ζ at failure is 17.3%, 19.5%, and 12.6%, respectively. Thus, similar to the energy dissipation, damping estimated at the failure was maximum in S2, while S3 exhibited the least damping.

3.7 Idealization of Lateral Load-Displacement Relationship

In order to simplify analysis and design, the experimentally obtained hysteretic response can be represented by an idealized bi- or trilinear resistance envelope. Adopting from Tomaževič (1999), three limit states in the observed behavior were first defined as follows:

a. Cracking Limit: It is represented by the lateral displacement and resistance at the formation of the first significant cracks in the masonry wall, which change the slope of the envelope.

b. Maximum Resistance: It is represented by the maximum lateral resistance achieved by the CM wall during the test, and the corresponding displacement.

c. Ultimate State: It is represented by the maximum attained displacement during the test, and the corresponding residual lateral resistance.

3.7.1 Idealization with Bilinear Relationship

The experimentally obtained hysteretic response can be idealized with an elastic-perfectly plastic bilinear envelope as shown in Fig. 3.17. The slope of the initial rising branch of the idealized envelope is called effective stiffness of the wall, K_i. It is calculated as the ratio of the cracking load ($V_{cr,e}$) to the corresponding displacement ($\Delta_{cr,e}$) of the wall obtained experimentally, i.e., $K_i = V_{cr,e} / \Delta_{cr,e}$. In the absence of a well-defined cracking point, $V_{cr,e}$ is recommended to be considered as 0.6 to 0.8 times $V_{m,e}$ (Tomaževič 1999, Tomaževič and Klemenc 1997a). Further, some empirical formulations are also discussed in Chapter 6 for the estimation of $V_{cr,e}$. For the three tested CM walls, the idealized bilinear envelopes in push and pull directions were developed as shown in Fig. 3.18a, b, c. The average values from push and pull directions for all three specimens are compared in Fig. 3.18d. The obtained average value of K_i was 11.6 kN/mm, 12.6 kN/mm, and 20.1 kN/mm for S1, S2, and S3, respectively (as given in Table 3.6). In case of the bilinear idealization, the maximum or ultimate resistance of the idealized envelope is defined as 90% of the experimentally obtained strength. The first point corresponds to the displacement at the idealized elastic limit Δ_e calculated as $\Delta_e = 0.9V_{m,e}/K_i$. The second point on the idealized envelope corresponds to the ultimate displacement $\Delta_{u,bl}$, where the idealized line intersects the descending branch of experimental response as shown in Fig. 3.17. The ductility factor is estimated as the ratio of $\Delta_{u,bl}$ to Δ_e and it was found to be 8.1, 4.7, and 3.3, for S1, S2, and S3, respectively.

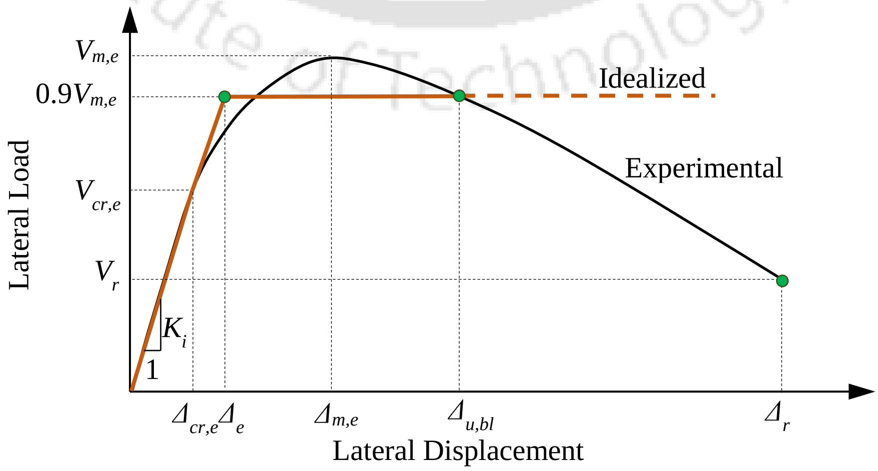

Figure 3.17: Idealization of experimental resistance envelope with bilinear relationship.

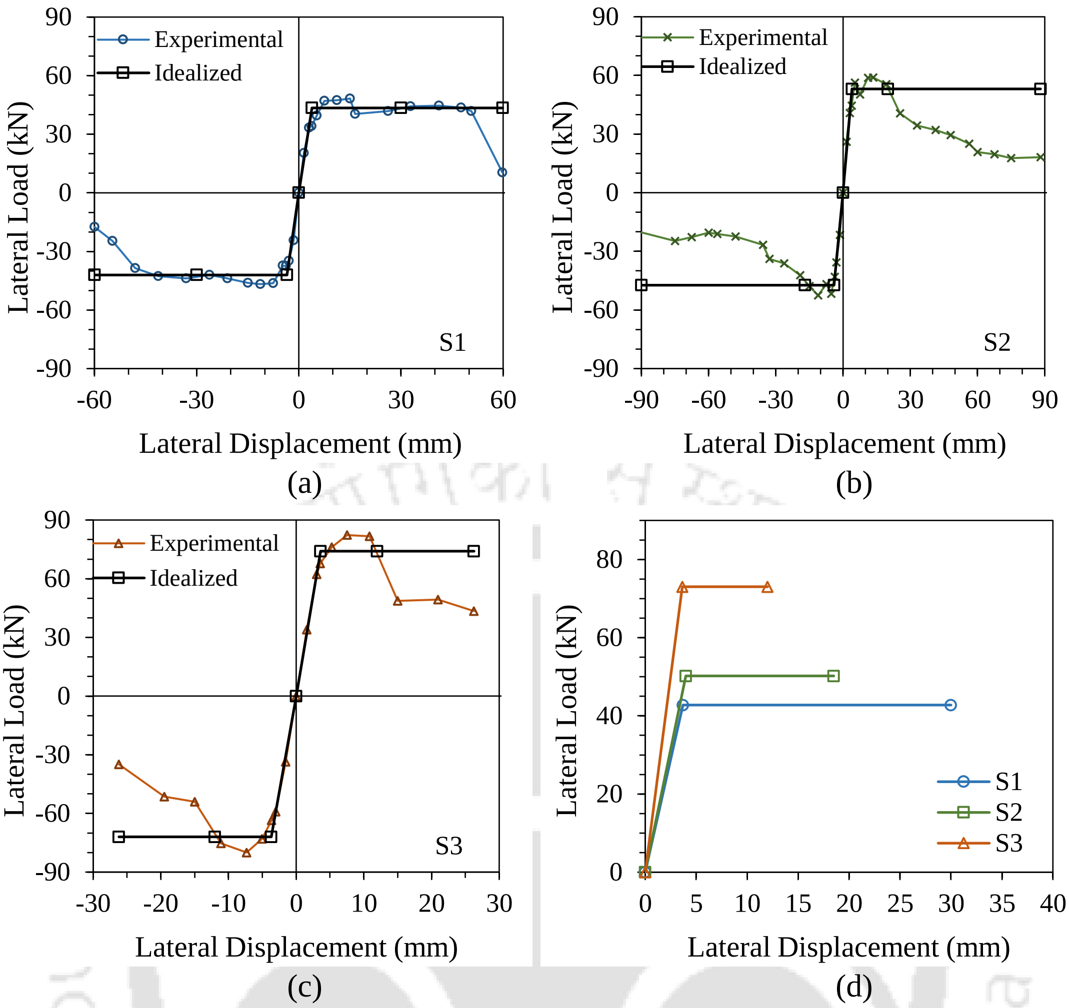

Figure 3.18: (a), (b), (c) Development of idealized envelopes with bilinear relationship for S1, S2, and S3, respectively; (d) Comparison of idealized bilinear curves of the three specimens.

Table 3.6: Parameters defining the idealized bilinear envelopes of the specimens.

Loading Direction	Specimen	K_e (kN/mm)	$0.9V_{m,e}$ (kN)	Δ_e (mm)	$\Delta_{u,bl}$ (mm)	μ
Push	S1	11.1	43.5	3.9	30.0	7.7
	S2	13.5	53.1	3.9	20.0	5.1
	S3	20.6	74.1	3.6	12.0	3.3
Pull	S1	12.0	-42.1	-3.5	-30.0	8.5
	S2	11.7	-47.3	-4.0	-17.0	4.7
	S3	19.5	-72.0	-3.7	-12.0	3.3
Average	S1	11.6	42.8	3.7	30.0	8.1
	S2	12.6	50.2	4.0	18.5	4.7
	S3	20.1	73.0	3.6	12.0	3.3

3.7.2 Idealization with Trilinear Relationship

The bilinear idealization is too simplistic for identifying different performance limit states; therefore, the experimentally obtained hysteretic response is also idealized with a trilinear envelope as shown in Fig. 3.19. The first point is the cracking point with lateral load $V_{cr,e}$ and lateral displacement $\Delta_{cr,e}$ obtained experimentally; the slope of this rising branch (K_i) is same as obtained from the bilinear relationship. The second point corresponds to the maximum resistance ($V_{m,e}$) without any reduction, and the corresponding displacement ($\Delta_{m,e}$). Generally, the ratio of lateral load at cracking to lateral strength ($V_{cr,e}/V_{m,e}$) varies from 0.6 to 0.8 in many past experimental studies (Tomaževič 1999, Tomaževič and Klemenc 1997a). In the present experimental study, it was found to be 0.72, 0.68, and 0.75 for S1, S2, and S3, respectively. The third point is corresponding to the ultimate state; it is recommended to consider the ultimate strength (V_u) at 20% strength degradation for practical considerations (i.e., $V_u = 0.8V_{m,e}$) rather than considering it at residual strength V_r corresponding to severe deterioration. Thus, the intersecting point of 80% strength line and the linear branch connecting $V_{m,e}$ and V_r gives the ultimate state. The corresponding displacement in post-peak regime is denoted as Δ_u and Δ_r (Fig. 3.19). For the tested CM walls, the idealized trilinear envelopes in push and pull directions were developed in Fig. 3.20a, b, c, and the average values from push and pull directions for all three specimens are compared in Fig. 3.20d.

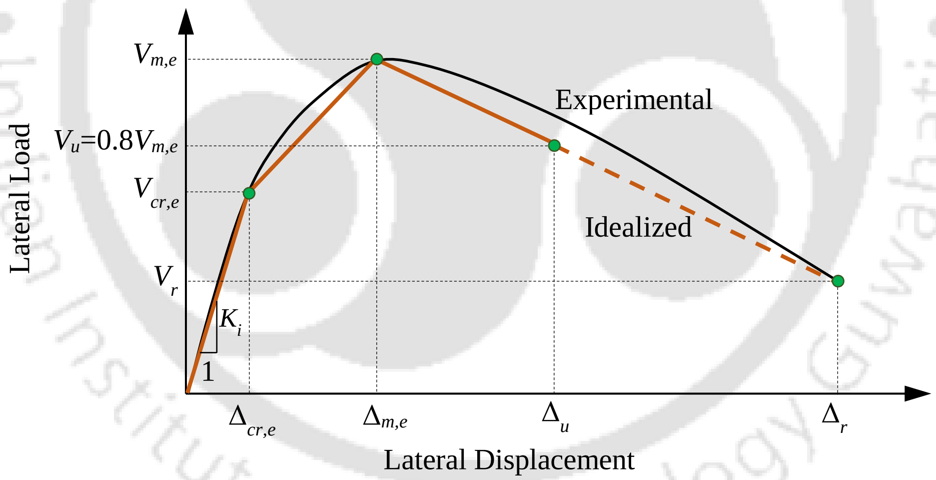

Figure 3.19: Idealization of experimental resistance envelope with trilinear relationship.

Comparison of the three specimens showed that as the aspect ratio of wall decreases by two times from slender (AR = 2) to squat (AR = 1), the lateral load corresponding to the initial cracking in the wall ($V_{cr,e}$) becomes higher for squat wall (60.7 kN) in comparison to slender wall (34.1 kN) at an almost same lateral displacement of 3 mm (0.2% drift level). On the other hand, the effective stiffness, K_i increases by around 1.74 times from slender to squat specimen. The estimated displacement ductility μ for S2 and S1 is around 1.4 and 2.5 times S3, respectively; which signifies that as aspect ratio decreases ductility of CM wall reduces drastically. From the trilinear idealized envelopes, it can be observed that the rate of stiffness degradation after initial cracking in wall is more for the squat wall S3 (almost two times) in comparison to the slender wall S1. The trilinear idealization of the load-deformation response of CM walls is extensively used in Chapter 6 to suggest relevant performance limit states for CM walls using data obtained in several past experimental as well as empirical studies. In Fig. 3.21, experimental, idealized bilinear, and idealized trilinear curves are plotted altogether for the three specimens. The maximum lateral resistance obtained from bilinear idealization for all three specimens was 90% of that obtained from experimental or trilinear idealized curve. Further, when CM wall changed from squat to slender, the ultimate displacement obtained from bilinear idealization varied from 0.8% to 2%, whereas it varied from 0.98% to 2.38% as per trilinear idealization.

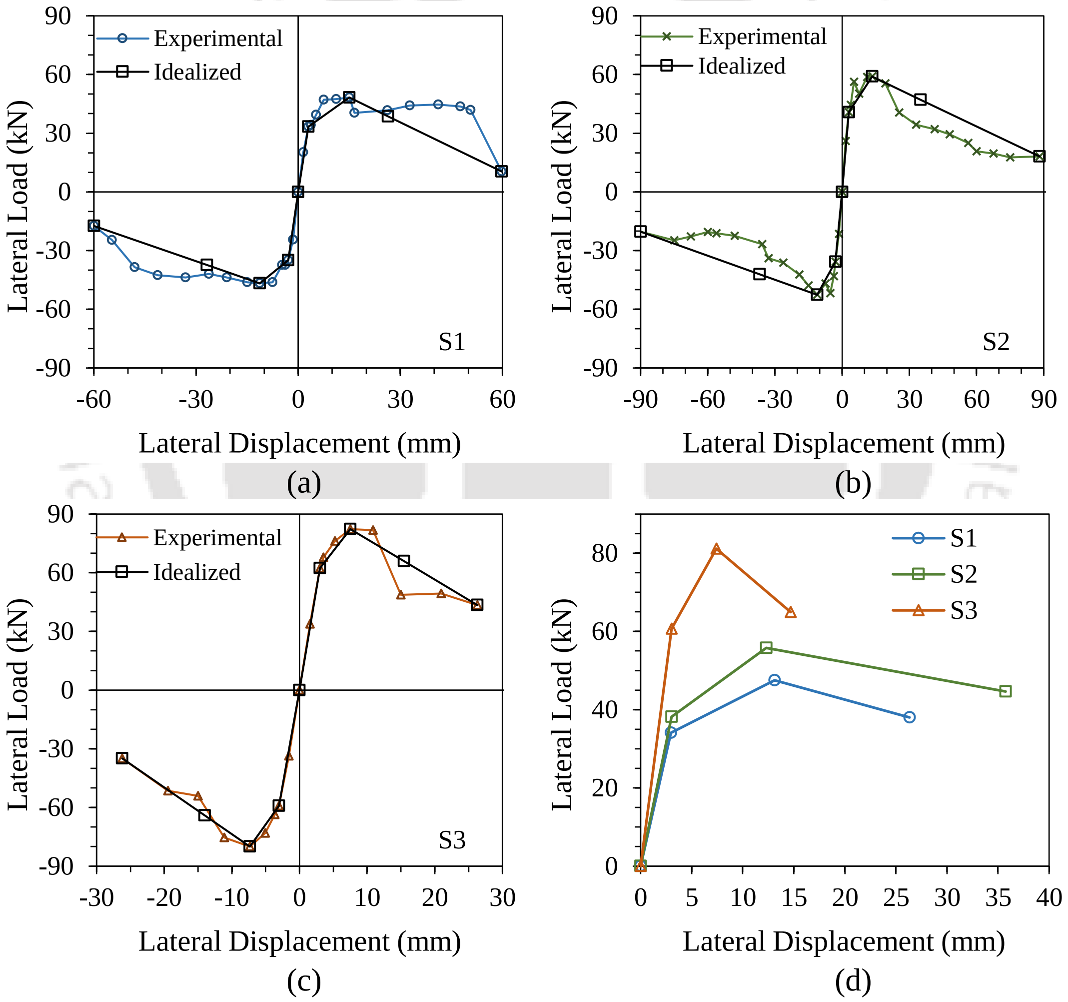

Figure 3.20: (a), (b), (c) Development of idealized envelopes with trilinear relationship for S1, S2, and S3, respectively; (d) Comparison of trilinear idealized envelopes of the three specimens.

Table 3.7: Parameters from the idealized load-displacement curves.

	ID	$V_{cr,e}$ (kN)	$V_{m,e}$ (kN)	V_r (kN)	V_u (kN)	K_i (kN/mm)	$\Delta_{cr,e}$ (mm)	$\Delta_{m,e}$ (mm)	Δ_r (mm)	Δ_u (mm)
Push	S1	33.3	48.3	10.4	38.6	11.1	2.99	15.0	59.8	26.4
	S2	40.7	59.0	18.1	47.2	13.5	3.01	13.4	88.1	34.9
	S3	62.3	82.3	43.4	65.8	20.6	3.02	7.5	26.3	15.5
Pull	S1	34.9	46.7	17.4	37.4	12.0	2.91	11.2	60.0	26.8
	S2	35.7	52.6	20.4	42.1	11.7	3.04	11.3	90.1	37.0
	S3	59.1	80.0	34.9	64.0	19.5	3.03	7.3	48.0	14.0
Average	S1	34.1	47.5	13.9	38.0	11.6	2.95	13.1	59.9	26.3
	S2	38.2	55.8	19.2	44.6	12.6	3.02	12.3	89.1	35.7
	S3	60.7	81.1	39.1	64.9	20.1	3.03	7.4	37.1	14.7

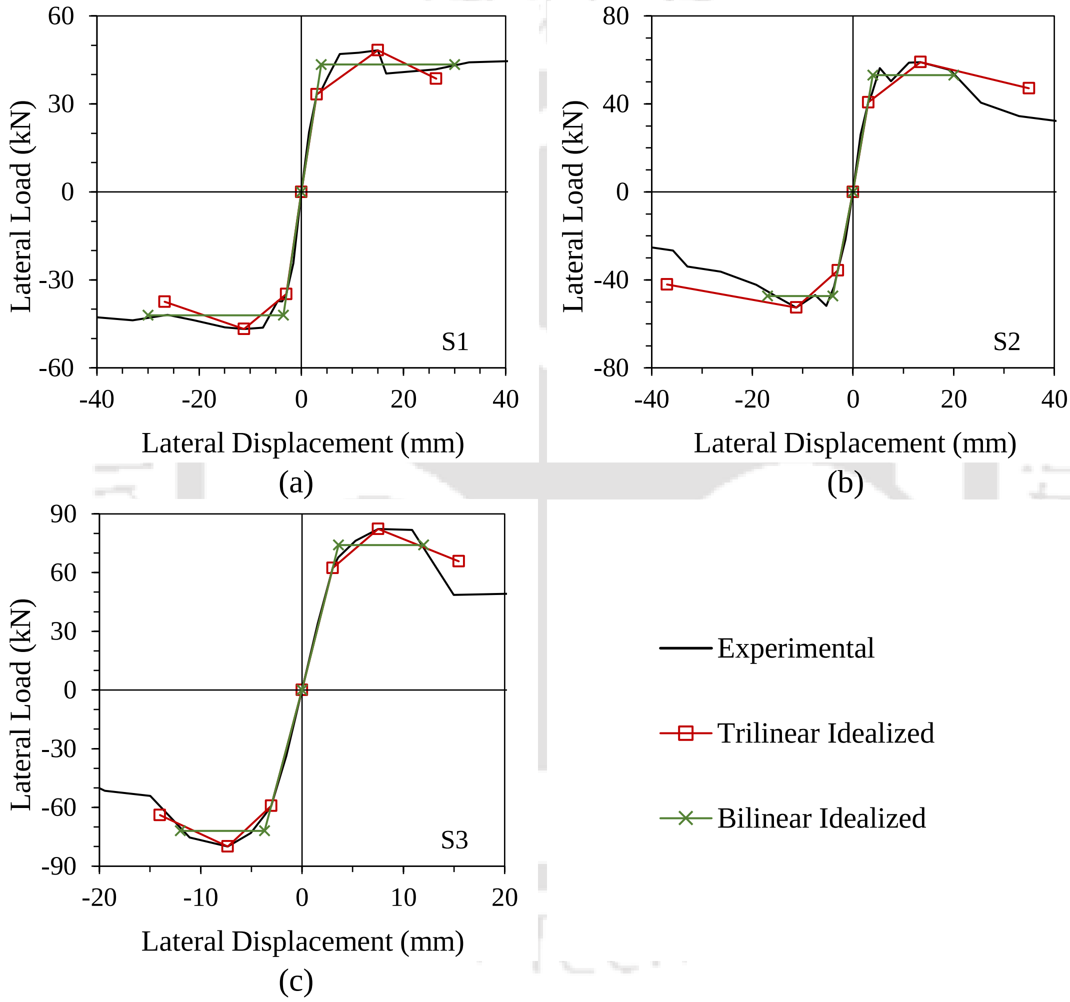

Figure 3.21: Comparison of experimental and idealized envelopes with bilinear and trilinear relationship for: (a) S1, (b) S2, and (c) S3.

3.8 Summary

Three half-scale CM walls with different aspect ratios were designed according to present international practice and the lateral load behavior was evaluated experimentally. In all the specimens, tie-elements were provided with similar sectional dimensions and nominal reinforcement as per the prevalent design guidelines. The intent of the study was to consider at least one slender CM wall (S1 with AR = 2.0), one wall with intermediate aspect ratio (S2 with AR = 1.5), and one relatively squat wall (S3 with AR = 1.0), so that representative behavior of all three cases can be studied. Appropriate design dead and live loads were applied by placing steel plates over the RC slab constructed over the CM specimens to replicate the realistic gravity loads before application of lateral loads. These specimens were subjected to quasi-static cyclic lateral loading. Some test photographs and videos are available at: https://www.iitg.ac.in/hemantbk/stud/bonisha.html

From the comparison of the experimental results, a strong influence of aspect ratio on lateral load responses was observed. When the aspect ratio of masonry panel of a CM wall reduced from 2.0 to 1.5, the lateral strength of CM wall increased by about 20% and it increases up to 70% when AR reduces to 1.0. However, the lateral drift capacity (corresponding to lateral strength) reduces by 43% and the developed shear stresses in the masonry panel decreased by about 13% when AR reduced from 2 to 1. In a relatively squat wall S3, significant degradation in post-peak strength was seen due to early damage in its tie-columns, and thus, the lowest dissipation of energy was observed for this wall when compared to the others. The idealized load-deformation relations also showed that as the aspect ratio decreases, the initial stiffness increases. However, due to the occurrence of severe damage, the ductility of CM wall reduces with decreasing aspect ratio. Further, the initiation of damage pattern changed from flexural cracking of tie-columns to shear cracking of masonry, and the uniform lateral deformability of the walls along the height drastically altered when the configuration of the CM wall changed from slender to squat. The strain gauge data also indicated that the drift values corresponding to yielding of rebars in tie-columns reduced with decreasing aspect ratio. It was inferred that the existing design methodologies for CM walls, especially for tie-columns, are required to be further improved by providing clear influence of aspect ratio.

Chapter 4
DEVELOPMENT OF V-D STRUT MODEL

CONTENTS

4.1 OVERVIEW

Over the years some modeling techniques have been developed for the analysis of CM buildings to capture failure modes and response under lateral loading with different degrees of refinement and precision. Masonry is an anisotropic and highly non-linear material and it exhibits complex behavior under different actions of forces due to the presence of mortar joints which act as planes of discontinuity. The complexity increases further for confined masonry (CM) where, in addition to masonry, RC confining members are constructed around the periphery of masonry walls such that the structure work in unison. Most design codes do not specify modeling schemes due to limited research, especially considering the highly variable masonry properties. Some analysis methods consider simple mathematical tools based on the equilibrium of forces at a joint, while some have been transferred into commercial software packages, making them available to engineers. The software-based numerical models have the superiority as software allows to define the geometric details, nonlinearity, and variety of choices to perform linear and nonlinear analyses.

Finite element (FE) modeling technique is quite commonly used for numerical simulation of any structure. For masonry structures, the FE analysis can be performed at a micro or macro level. Micro-modeling approaches are most suited for small structural elements in order to closely represent the heterogeneous states of masonry; whereas, macro-modeling approaches are used to represent the global structural behavior, where the distinction between the individual units and mortar joints is not made and material parameters are obtained from the masonry tests under homogeneous states of stress. Both FE micro- (Smoljanović et al. 2017, Amouzadeh Tabrizi and Soltani 2017), as well as macro-modeling (Okail et al. 2016, Medeiros et al. 2013, Janaraj and Dhanasekar 2014, Singhal 2014, Tripathy and Singhal 2019, and Yacila et al. 2019) approaches, have been used extensively in past for CM wall. However, the use of realistic and reliable FE models is limited as they are computationally intensive, complex, and require a large number of input parameters that are not available easily.

Therefore, researchers are coming up with modeling techniques that are based on simple modeling strategies, such as, Wide Column Model (WCM) or Strut-and-Tie Model (STM) as shown in Fig. 2.13 (NTC-M 2004, Brzev 2007, Brzev and Gavilán 2013 and 2016, Ghaisas et al. 2017, Rangwani and Brzev 2017). WCM has been recognized as a viable simplified model as this technique provides the opportunity for the structural analysis of CM structure with commercial computer programs. However, the hypothesis of monolithic behavior assumed in WCM does not provide the opportunity to study the behavior of tie-columns and complex force transmission in different elements under loading. The application of the basic strut-and-tie method is limited to determination of force resultants in members of the walls when the applied lateral load is provided and structure is determinate. The lateral capacity may be estimated from STM by reducing one unknown considering yielding of rebars or from limiting capacity of strut as suggested by Singhal (2014) and Tripathy and Singhal (2019). However, these STM strategies are not much helpful to predict other nonlinear responses of the structure, such as lateral load - lateral deformation profile. Both the models - WCM and STM - are mainly helpful for carrying out linear analysis for preliminary design purposes. Some researchers also attempted to extend the WCM and software based STM for nonlinear pushover analysis, where the nonlinearity (lumped hinge) was defined using the empirical backbone model of CM wall (Terán-Gilmore et al. 2009, Ranjbaran et al. 2012, Ahmad et al. 2012, Rankawat et al. 2021). However, the problem is to choose a reliable backbone model of CM wall as these mathematical models of the backbone parameters (stiffness, strength, and deformation parameters) are mainly based on a limited number of experimental studies with large variations in material and geometrical properties. Some past researchers have also attempted to use Equivalent Strut Model (ESM) for CM walls; in which the tie-elements can be separately modeled unlike WCM and instability issues can be removed with the rigid jointed confining frame, unlike STM, in addition to the capability of nonlinearity establishment in different elements. However, their applicability is limited because these studies considered failure modes in CM walls similar to that considered in masonry infilled frames (Kaushik and Sanganee 2010, Torrisi and Crisafulli 2017). None of these simplified models have the capability to realistically simulate the gravity load transfer from the tie-beams to the masonry walls. In this chapter, FE analysis will be carried out for the tested specimens and some other specimens tested in the past. After that, an attempt will be made to develop a simple analysis model that can reliably predict the linear and non-linear behavior of CM walls and their confining elements under gravity and lateral loading.

4.2 FE Model Development

The objective of the FE numerical evaluation was to develop a reliable three-dimensional (3D) FE model that can capture the influence of aspect ratio of CM walls on their lateral load behavior. The numerical models were developed in the FE software Abaqus.

4.2.1 Details of Specimens

The three tested half-scale CM wall specimens S1 (AR = 2.0), S2 (AR = 1.5), and S3 (AR = 1.0) were considered and the details of this first set of specimens are provided in Chapter 3. In addition, five more single-bay, single-story full-scale CM walls – ME 1, ME 2, ME 3, ME 4, and ME 5 - with different aspect ratios tested by Gavilán et al. (2015) were also considered to validate the FE model. The material and geometric properties of this second set of specimens are given in Table 4.1. The material models (for masonry, concrete, and steel) defined in the FE models are explained in the next section.

Table 4.1: Properties of the considered CM wall specimens.

Properties	ME 1	ME 2	ME 3	ME 4	ME 5
Compressive strength of masonry prism (f'_m), MPa	5.53	5.17	5.57	5.83	8.15
Modulus of elasticity of masonry (E_m), MPa	4252	4371	4288	4322	4556
Compressive strength of concrete (f_c), MPa	33.4	20.4	18	23.1	22.7
Yield strength of longitudinal rebars (f_{yl}), MPa	412 (9.5ϕ, 12.7ϕ)				
Yield strength of transverse rebars (f_{yt}), MPa	248 (6.35ϕ)				
Aspect ratio of wall (H_w/L_w)	2.75	1.73	1.32	1.04	0.68
CM wall length (L_w), mm	850	1350	1770	2250	3450
CM wall height (H_w), mm	2340				
Tie-column cross-section	150 mm × 120 mm				
Tie-beam cross-section	120 mm × 160 mm				
Tie-column longitudinal reinforcement	4 bars of 12.7ϕ				
Tie-beam longitudinal reinforcement	4 bars of 9.5ϕ at corners				
Tie-column transverse reinforcement	6.35ϕ at 180 mm c/c				
Tie-beam transverse reinforcement	9.5ϕ at 180 mm c/c				

Source: Data from Gavilán et al. (2015).
Note: ϕ = diameter of reinforcing bar in mm, c/c denotes the center-to-center distance between bars.

4.2.2 Material Modeling

The density and the elastic characteristics (elastic modulus and Poisson's ratio) of the materials were provided as inputs in the Abaqus FE program under general and mechanical behavior, respectively. In the plastic regime, the material behavior definition requires the yield stress as a function of plastic strain. The behavior of concrete and masonry is closer to brittle behavior and primarily lies between ideal brittle and ductile and they are considered as quasi-brittle materials. The constitutive material models, such as Concrete Smeared Cracking and Concrete Damaged Plasticity (CDP) models (Simulia 2016) have been used for masonry and concrete in past. Though the CDP model was originally developed for isotropic brittle materials (Lee and Fenves 1998, Lubliner et al. 1989), it has been extensively used for anisotropic materials, such as masonry through parameter adaptation (Grillanda et al. 2020, Yacila et al. 2019, Castellazzi et al. 2017, Valente and Milani 2016, Agnihotri et al. 2013). The CDP constitutive model captures the effect of damage associated with the failure mechanisms and works well under monotonic as well as cyclic loads. Therefore, the CDP model of Abaqus (Fig. 4.1) was used as a constitutive model to represent the behavior of concrete and masonry materials in all the specimens. All the parameters involved in CDP can be obtained from uniaxial, biaxial, and triaxial tests. However, in the absence of such data, the parameters can be determined by calibrating with the experimental results, and/or by using common values recommended in the literature. The parameters in the CDP models of masonry and concrete are discussed below in brief.

4.2.2.1 Yield surface and flow potential parameters

To describe the multi-dimensional behavior in the inelastic range, the CDP model assumes the Drucker-Prager strength criterion, modified by means of the parameter k_c (= 0.667), which approximates the yield surface to the Mohr-Coulomb criterion in the deviatoric plane. In addition, CDP assumes a non-associated flow law, which provides the necessary control to dilatancy by the parameter dilation angle. The value of the dilation angle is typically assumed from 5° to 51°; and in this study, it is taken as 10° and 12° in the first set and second set, respectively for masonry as also suggested in different studies for a moderate-to-low level of vertical compression (Grillanda et al. 2020, Castellazzi et al. 2017, Valente and Milani 2016). Dilation angle of 30° was considered for concrete for all the walls as also observed in different studies (Yacila et al. 2019, Michał and Andrzej 2015). Other required properties, to define the shape of the yield function or the potential flow, were taken as default values for all the walls from the Abaqus user manual as given in Table 4.2, e.g., flow potential eccentricity as 0.1, the ratio of initial equi-biaxial compressive yield stress to initial uniaxial compressive yield stress as 1.16. A high value of viscosity parameter can lead to an overestimation of the peak base shear in Abaqus/Standard. Though the viscosity parameter is optional for Abaqus/Explicit, a small value (1×10^{-5}) was still taken to take care of any convergence difficulties of the model in the softening branch, without compromising results (Simulia 2016, Grillanda et al. 2020).

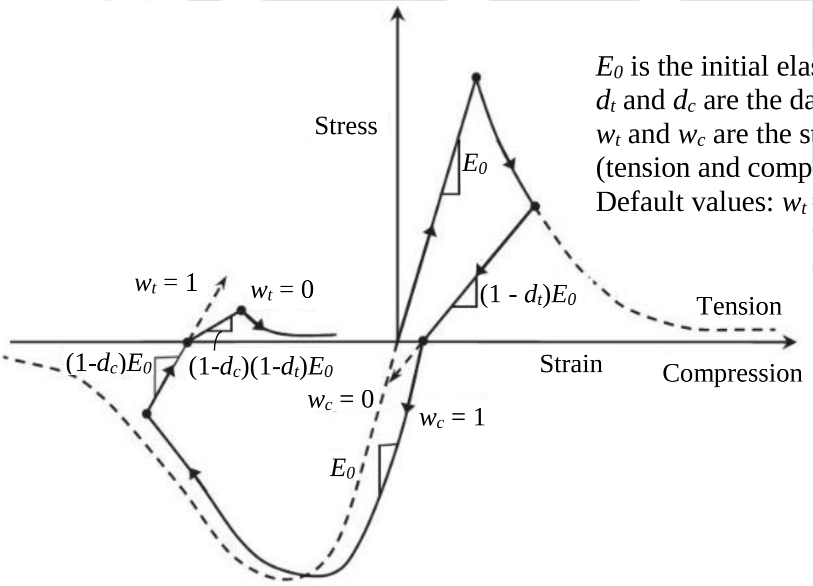

Figure 4.1: CDP Model of Abaqus under uniaxial load cycle (tension-compression-tension) (Simulia 2016).

Table 4.2: Values of basic material parameters adopted for the numerical simulations.

Parameter	Range	Value for		
		Masonry	Concrete	Steel
Density (in kN/m^3)	—	18	24	78.5
Poisson's ratio	—	0.18	0.20	0.30
Dilation angle (in degree)	$5^0 – 51^0$	10^0 or 12^0	30^0	—
Flow potential eccentricity	—	0.1	0.1	—
Ratio of initial equibiaxial compressive yield stress to initial uniaxial compressive yield stress	1.1 – 1.16	1.16	1.16	—
Ratio between second stress invariant on the tensile meridian and that on the compressive meridian (k_c)	0.5 – 1.0	0.667	0.667	—
Viscosity parameter	0 – 0.01	0.00001	0.00001	—

4.2.2.2 Material stress-strain parameters

The CDP model allows variation of the strength of the material in tension and compression with different damage parameters to model the degradation of strength and stiffness. Under tension, the stress increases linearly in the material till the failure stress (corresponds to the initiation of micro-cracks formation in the material), beyond which the stress-strain response drops down following a softening curve as shown in Fig. 4.1. Again, under compressive loading, the stress increases till the maximum stress is reached after which the strain-softening was observed. In addition, when the material is unloaded from a point beyond the peak load, some stiffness degradation takes place due to the occurrence and accumulation of damage. This behavior is simulated in the numerical analysis by the damage parameters d_t and d_c for tension and compression, respectively. For cyclic load analysis, Abaqus requires yield stress of material and values of damage parameters in the input as a function of inelastic strain. When damage is encountered, Abaqus converts inelastic strain to plastic strain using the input damage parameters. The damage parameters (d_c and d_t) for masonry and concrete were defined using the pivot rule formulation of Park et al. (1987). d_t and d_c can take the values between zero to one representing an undamaged and total loss of strength, respectively. Moreover, the CDP model considers the effect of opening and closing of cracks, i.e., the recovery of the compression stiffness upon crack closure when the load changes from tension to compression as shown in Fig. 4.1. w_t and w_c are the stiffness recovery factors for tension and compression, respectively, and default values ($w_t = 0$ and $w_c = 1$) were taken for the analyses.

The stress-strain curve for masonry in compression was developed in the present study using the masonry stress-strain model developed by Kaushik et al. (2007) as shown in Fig. 4.2. Residual strength of 20% of the peak stress was considered in the stress-strain definitions to avoid kinetic instabilities in the numerical model. For tension, a linear elastic pre-cracking stage followed by linear softening was considered for masonry. The tensile strength was estimated as a fraction of its compressive strength for properly fitting the experimental patterns (Fig. 4.3). The calibrated tensile strength of masonry was around 7% and 9% of compressive strength in the first set and second set of specimens, respectively as also observed in other studies (Medeiros et al. 2013). The post-peak behavior was modeled in such a way that masonry completely loses its tensile strength (residual strength is 10% of peak) at the ultimate strain that is equal to 10 times the strain corresponding to the peak tensile strength.

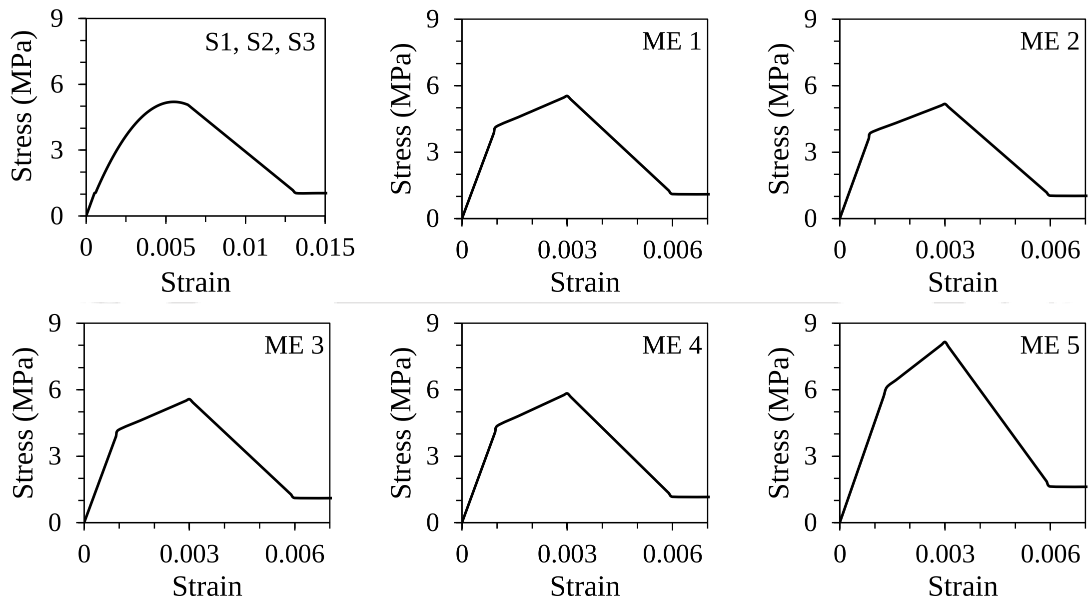

Figure 4.2: Stress-strain properties of masonry in compression for the selected specimens.

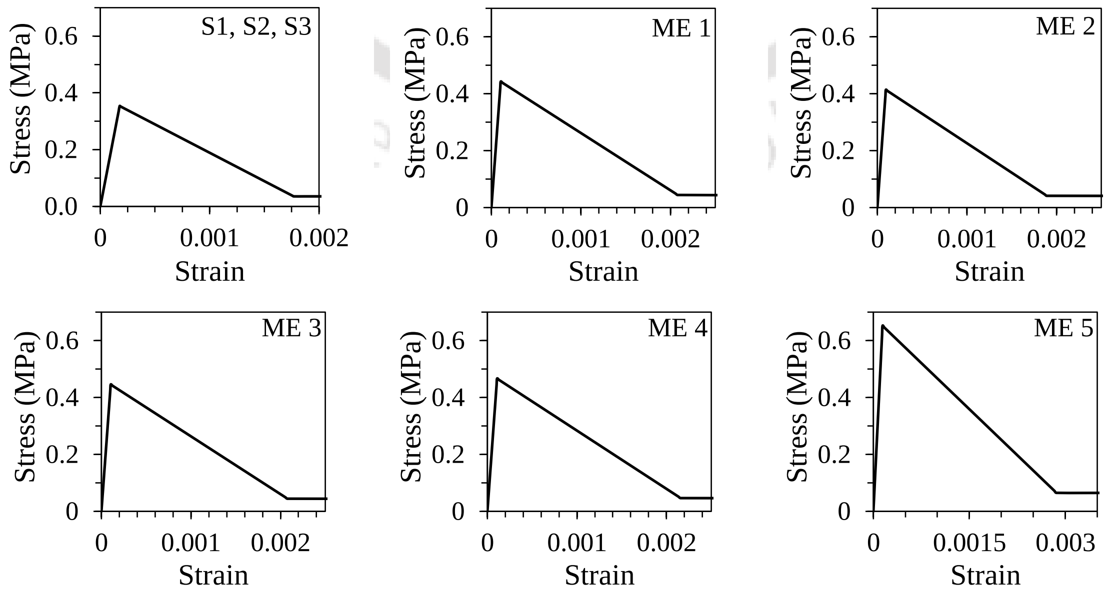

Figure 4.3: Stress-strain properties of masonry in tension for the selected specimens.

The stress-strain curve for concrete under compression was defined using the Kent and Park (1971) model without confinement as shown in Fig. 4.4. It has to be noted that the unconfined concrete model was used because the steel stirrups were modeled separately in the FE program. The tensile response of concrete was modeled based on the tension stiffening model (Wahalathantri et al. 2011) as shown in Fig. 4.5, in which the tensile strength was considered according to IS456 (BIS 2000). Residual strengths of 20% and 10% of the peak stress were considered in the stress-strain definitions in compression and tension, respectively.

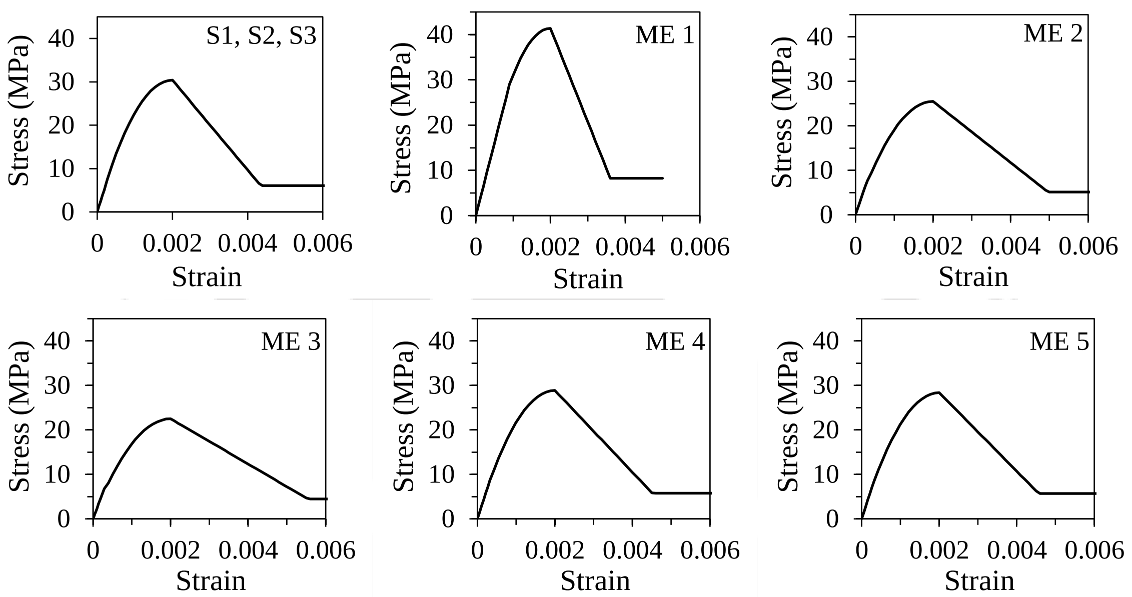

Figure 4.4: Stress-strain properties of concrete in compression for the selected specimens.

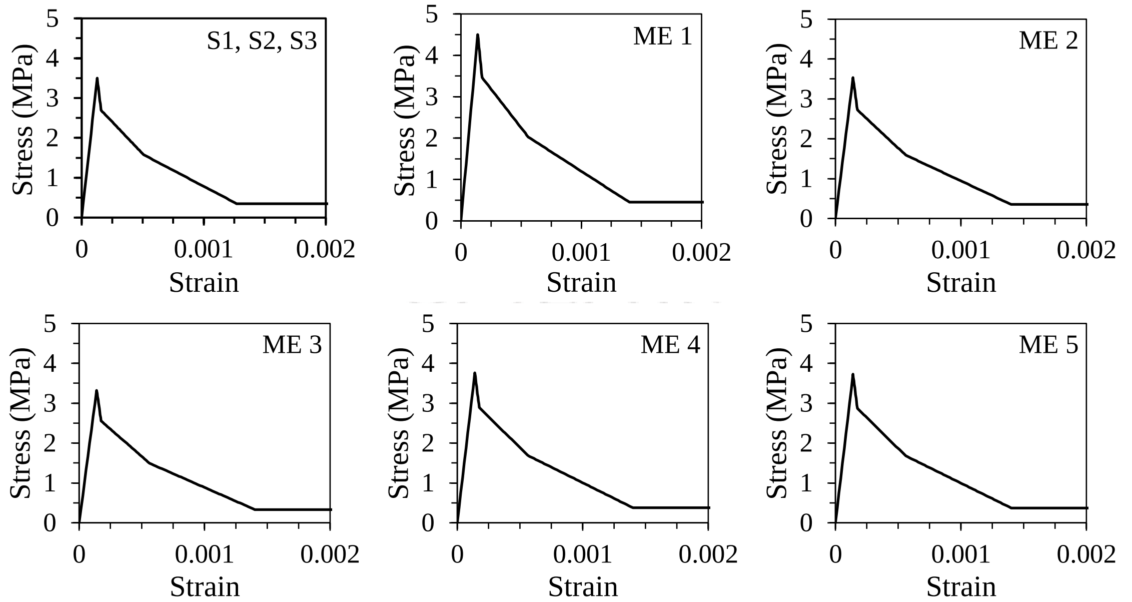

Figure 4.5: Stress-strain properties of concrete in tension for the selected specimens.

The material model used for steel reinforcement employs a uni-directional elastic-strain hardening response with three regions - an elastic region, a perfectly plastic, and a parabolic strain hardening region as shown in Fig. 4.6.

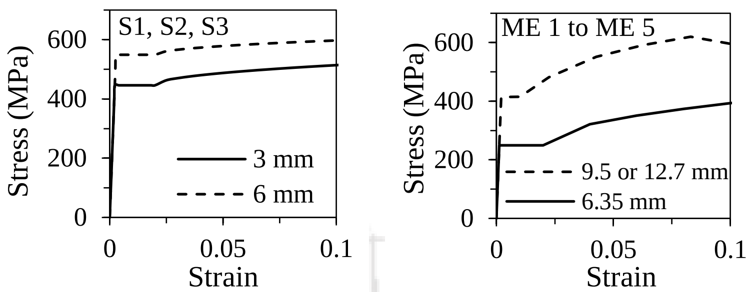

Figure 4.6: Stress-strain properties of steel rebars in tension for the selected specimens.

4.2.3 Model Characterization

The schematic of a typical finite element model for confined masonry walls is shown in Fig. 4.7. The components of confined masonry walls - concrete frame and masonry were modeled using three-dimensional solid (continuum) hexahedral (bricks) linear interpolation elements with 8 nodes and reduced integration (C3D8R) from the ABAQUS/Explicit element library. Due to the selected reduced integration, *Enhanced Hourglass* control was activated to avoid zero-energy deformation of the linear hexahedral element under bending. Steel reinforcing bars were modeled using *wire* feature associated with three-dimensional truss elements with two nodes (T3D2).

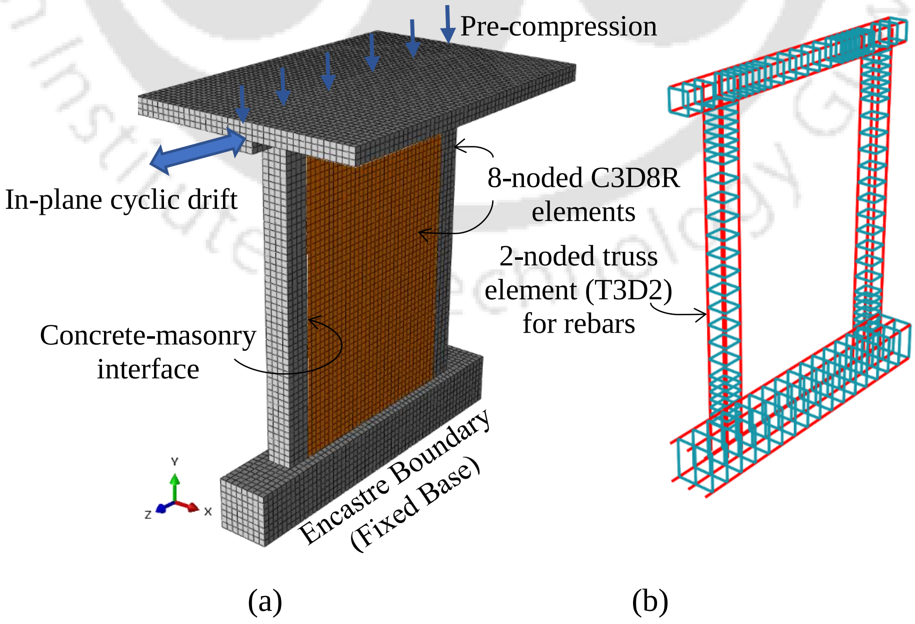

Figure 4.7: Schematic of a typical FE model representing various elements, loading, boundary conditions, interface, and constraints for the walls: (a) concrete and masonry elements, and (b) Embedded steel reinforcement.

The steel reinforcing bars were embedded in the surrounding concrete using relevant constraint conditions. The proper bonding between steel reinforcement (embedded truss elements) and concrete (host solid elements) was ensured in the numerical simulation by applying the *Embedded Element Constraints* between the truss and solid elements. This constraint allows the reinforcement nodes to displace exactly equal to the nodes of the surrounding concrete. Similar to the boundary condition used in the tests, the bottom surface of the bottom foundation beam was assumed to be fixed using the *Encastre* boundary condition. The contact between the masonry wall and concrete confining frame was simulated by assigning suitable interface properties by testing several possible interface scenarios. The mesh was continuously refined to achieve convergence in the numerical results. The analysis was carried out in Abaqus-Explicit solver in three steps, viz., Initial, Gravity and Pre-compression, and In-plane cyclic loading. The Initial step is mandatory and default for all the analysis, in which boundary conditions are initialized. In the next step, gravity load was applied along with the pre-compression load over the tie-beam as per the experimental program. This was followed by in-plane cyclic displacement-controlled loading, applied at the center of the top beam.

4.3 VALIDATION OF FE MODELS

4.3.1 Sensitivity Study

Different contact modeling was studied between masonry wall and concrete confining frame by testing several possible interface scenarios. For example, in interaction 1, all the four wall-tie interfaces were modeled using *Tie-Constraint*. In interaction 2, frictional properties, i.e., *Penalty Friction* with frictional coefficient in the tangential direction and *Hard* contact (pressure-overclosure relationship) in the normal direction with *Default* contact enforcement method and allowable contact separation, was assigned in all four interfaces. While in interaction 3, frictional properties were assigned only in the bottom interface, and the rest interfaces were modeled using *Tie-Constraint*. All three interaction properties were considered in the present comparative analysis, and results are discussed below.

The comparison showed that the FE model with interaction 2 captured the strength and stiffness very well (as shown in Fig. 4.8a); therefore, it was finally considered in further simulations. As the *Tie-Constraint* does not allow relative motion of the surfaces, it fails to represent the actual behavior. It is to be noted that in addition to frictional properties, cohesion is also generally defined at contact interfaces, but it is effective in the initial stage only and once it degrades only friction resists the deformation. Due to insufficient test data, cohesion was not considered here, and the interface was simulated with frictional properties as adopted in the past literature (Okail et al. 2016). The optimum value of the frictional coefficient was found to be 0.8 for the specimens S1 to S3 (first set) and 0.7 for ME 1 to ME 5 (second set). The mesh was refined to achieve convergence, and an optimum mesh size of 30 mm approximately was finally chosen for the elements of S1, S2, and S3 CM walls as shown in Fig. 4.8b. For specimens ME 1 to ME 5, 50 mm mesh also provides a good prediction (Fig. 4.8c).

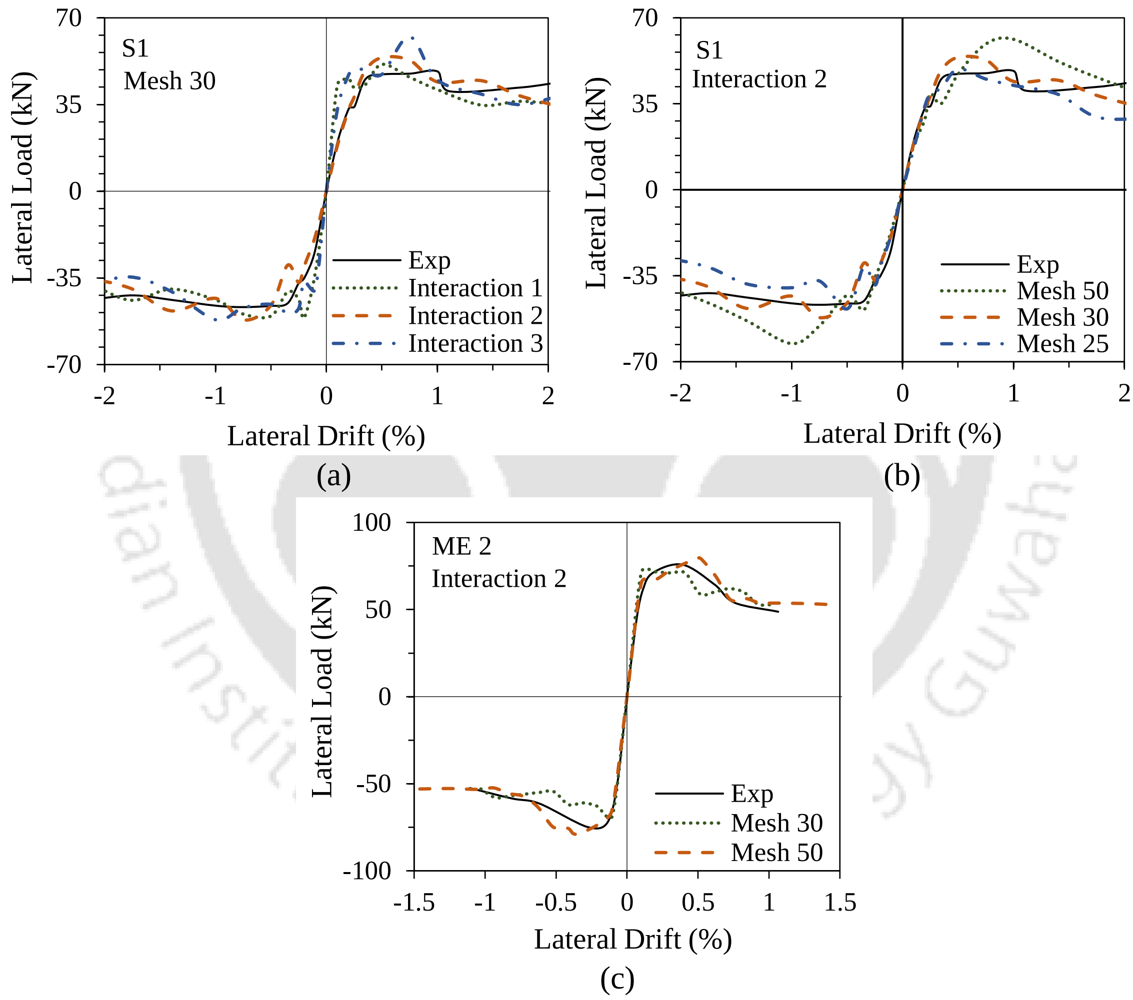

Figure 4.8: Sensitivity study for (a) masonry to concrete interface, and (b), (c) FE Mesh.

4.3.2 Results of FE Analyses

The numerically predicted lateral load responses of the CM wall specimens were compared with the experimentally obtained results in terms of envelope curve, damage, and yielding of rebars. Fig. 4.9 shows the comparison of the envelope curves obtained from the FE analysis with the experimental, and it was observed that the numerical pre- and post-peak responses matched the experimental results quite well. Further, the missing lateral load behavior was captured in the numerical simulation, particularly for the squat wall (S3) for which the test was terminated at a lateral drift of 1.75%. For the first set of walls (S1, S2, and S3), a maximum error of 14.5% was observed in the numerically obtained lateral strength ($V_{m,FE}$) as given in Table 4.3. For the second set of specimens (ME 1 to ME 5), the maximum error in the estimation of $V_{m,FE}$ was 10%. The maximum error in estimating the drift at lateral strength ($\delta_{m,FE}$) for the second set of walls was quite high, mainly because of the unavailability of the complete stress-strain behavior of materials.

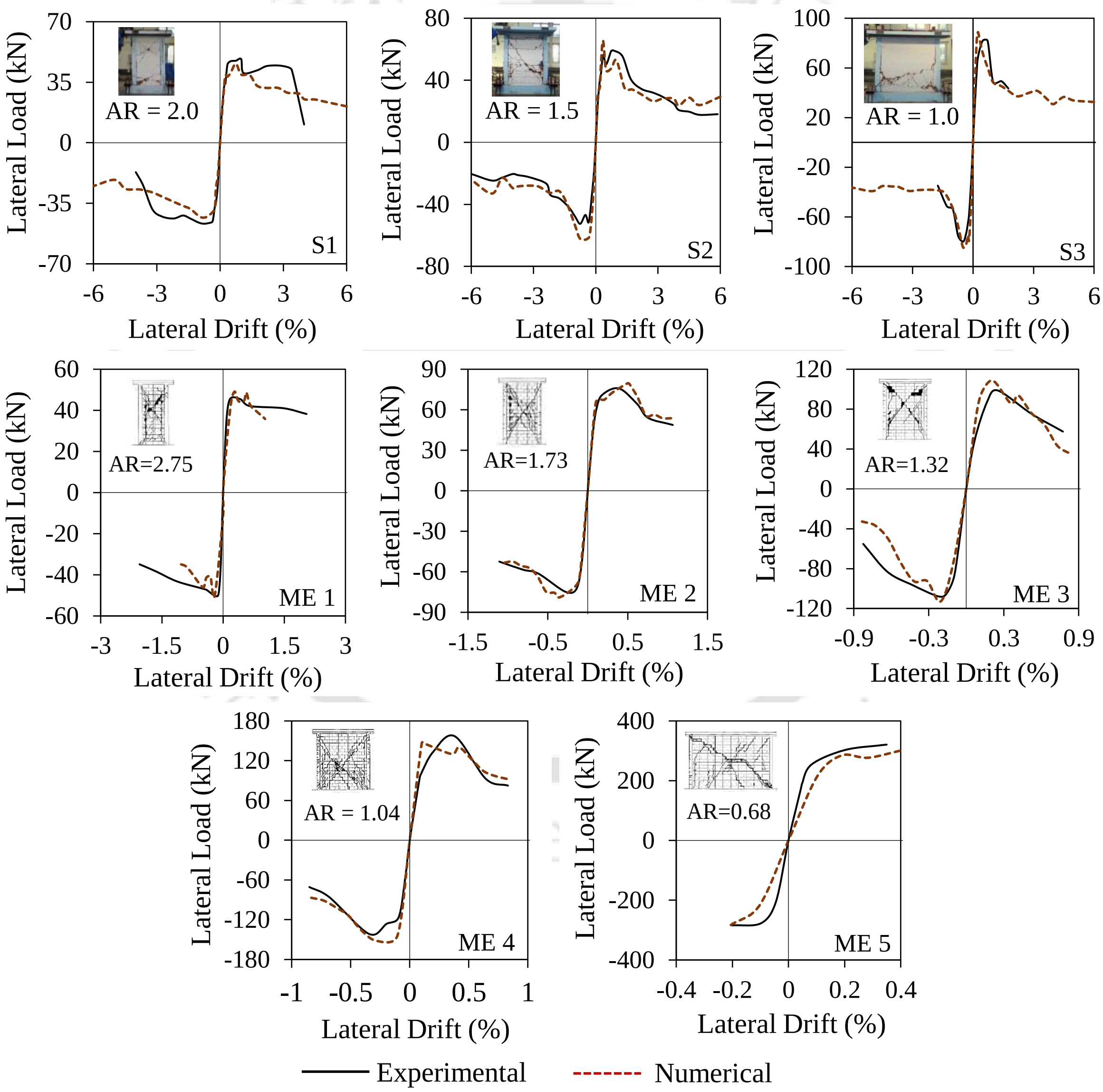

Figure 4.9: Comparison of envelope curves obtained from FE analyses with experimentally obtained curves for the selected specimens.

Table 4.3: Comparison of numerical and experimental lateral strengths and drifts.

Test Conducted	ID	AR	$V_{m,FE}$ (kN)			$\delta_{m,FE}$ (%)			Error (%)	
			Push	Pull	Avg	Push	Pull	Avg	$V_{m,FE}$	$\delta_{m,FE}$
Present study	S1	2.00	45.7	43.3	44.5	0.75	0.75	0.75	6.3	13.8
	S2	1.50	65.5	62.2	63.9	0.35	0.75	0.55	14.5	32.9
	S3	1.00	88.8	84.5	86.6	0.25	0.50	0.37	6.8	25.0
Past study	ME1	2.75	49.2	50.2	49.7	0.28	0.20	0.24	4.9	71.2
	ME2	1.73	79.4	79.0	79.2	0.49	0.36	0.43	5.2	26.9
	ME3	1.32	108.8	112.9	110.9	0.21	0.21	0.21	7.5	-12.5
	ME4	1.04	146.7	151.7	149.2	0.10	0.28	0.19	0.4	-47.9
	ME5	0.68	311.6	294.2	302.9	0.51	0.28	0.40	0.3	43.6

As Abaqus user graphic interface could not visualize cracks explicitly with the CDP model, *DAMAGET* (damage parameter in tension) plots were chosen as a representative of experimental damage (Fig. 3.5). As shown in Fig. 4.10, the higher values of the *DAMAGET* parameter were mainly noticed near both ends of tie-columns and along the diagonal in the masonry walls. However, such prominent damage in the diagonal region was not observed in the tests, especially in the S3 wall as the diagonal stair-stepped cracks formed near the bottom part of the wall and extended majorly through the wall to tie-column interfaces.

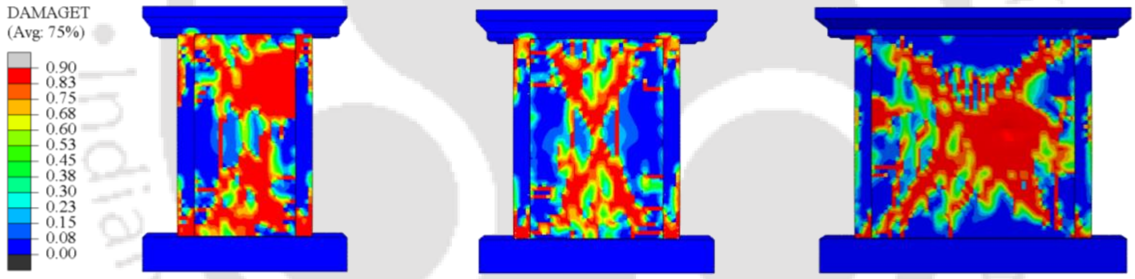

(a) (b) (c)

Figure 4.10: Variation in damage parameter in tension (*DAMAGET*) obtained from FE analyses: (a) S1, (b) S2, and (c) S3.

The nominal strain (*NE*) profiles and corresponding drifts at the first yielding of rebars for all the specimens are shown in Fig. 4.11. As also observed experimentally (Fig. 3.11), the lateral drift at the onset of bar yielding more or less decreases with decreasing AR of CM walls. In the FE study, masonry walls were modeled as a continuum without simulating individual bricks and mortar joints; therefore, the exact damage pattern with bed joint sliding failure could not be predicted in the numerical results and this is the limitation of the FE model. Even with this simplification, the developed FE models provided reasonable agreement with experimental lateral strength along with a satisfactory prediction of deformation capacity and damage. Thus, the FE results enable a better understanding of the development of stresses and strains in different members of the specimens, and also substantiated the influence of aspect ratio on yielding of tie-column reinforcement as observed during the experiments. The developed FE model will be further used in the latter part of this chapter and Chapter 7.

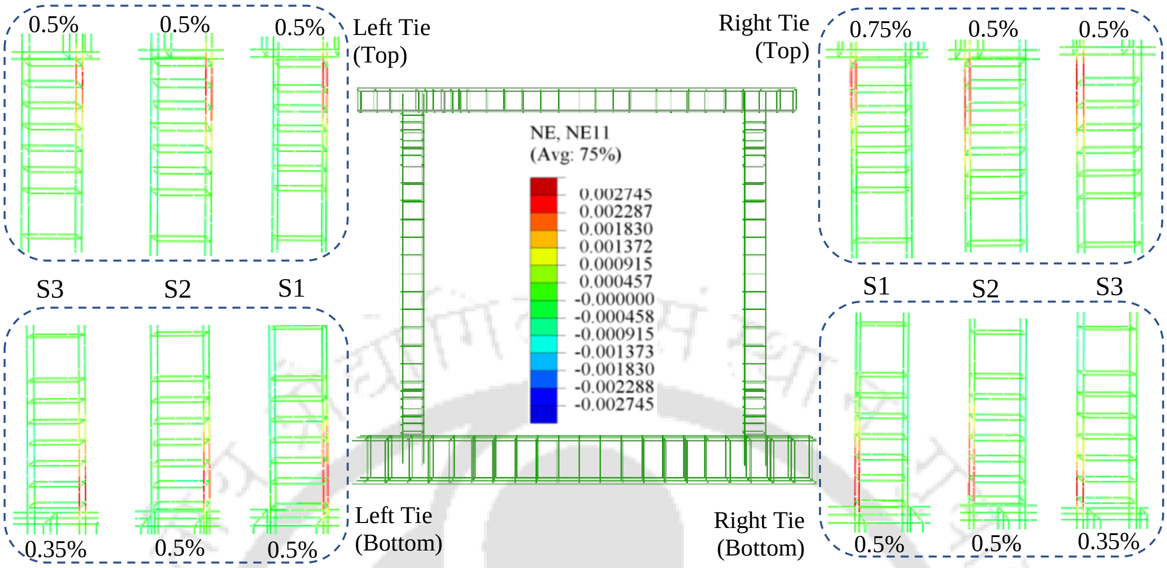

Figure 4.11: Nominal Strain (*NE*) profiles in tie-columns and corresponding lateral drifts (in %) at the first yielding of rebars for S1, S2, and S3 from the FE analyses.

4.4 Preliminary Comparative Study using Simplified Models

A comparative numerical study was first carried out using three simple modeling techniques including ESM as shown in Fig. 4.12 in SAP2000 to assess a suitable simplified model for CM walls. In model 1, masonry wall was discretized using four-noded shell elements (Fig. 4.12a), whereas, in model 2, masonry wall was modeled as an equivalent diagonal strut using two-noded beam elements (Fig. 4.12b). Additionally, a bare frame model (Fig. 4.12c) was also considered to study and compare the effectiveness of diagonal strut in the gravity load distribution of CM walls. The full-scale CM wall specimens ME 1, ME 2, ME 3, and ME 4 (Table 4.1) were considered in this section for which simple gravity load analyses were carried out to assess the suitability of the ESM in predicting the realistic load distribution and deformation behavior of CM walls.

In all three analytical models, tie-columns and tie-beams were modeled as centerline two-noded frame elements, and the joints of the tie-columns and tie-beams were treated as moment-resisting joints. The tie-columns were fixed at their base to simulate the experimental boundary conditions. The diagonal strut in model 2 was modeled using a frame element but with moment releases at both ends. For the preliminary study, the width of the diagonal strut was taken as one-fourth of the diagonal length of the strut as given for infilled

RC frame (Paulay and Priestley 1992), and thickness was taken as the actual thickness of the masonry wall. A vertical load of 0.5 MPa was applied above the tie-beam as distributed line load along its length to simulate the loading during experiments. Linear static analyses of the three models for each of the CM walls (ME 1, ME 2, ME 3, and ME 4) were first carried out under the action of gravity loads, and distribution of axial forces in different elements and deflection of tie-beam were compared for the three modeling strategies as shown in Figs. 4.13 and 4.14, respectively.

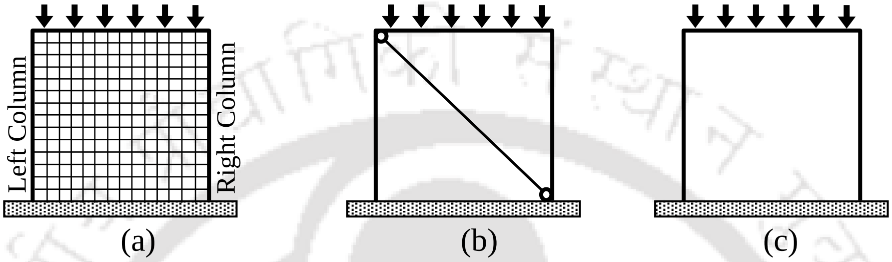

Figure 4.12: Analytical models studied: (a) Model 1 – masonry wall modeled using shell elements, (b) Model 2 – masonry wall modeled using a conventional single diagonal strut, (c) Model 3 – bare frame.

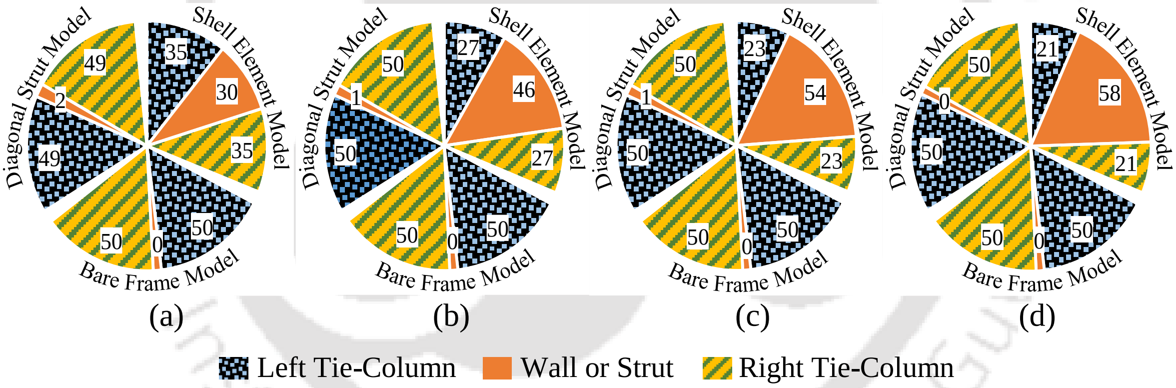

Figure 4.13: Comparison of axial force distribution (in percentage) in different members under gravity loads obtained using three modeling schemes for different CM wall specimens: (a) ME 1, (b) ME 2, (c) ME 3, and (d) ME 4.

The shell element model satisfies the basic mechanics of confined masonry wall under the action of gravity loads, and realistically simulates the gravity load distribution in different elements and flexural deflection of the tie-beam. Therefore, past researchers have simulated the masonry wall of CM buildings using shell element models in preliminary linear analysis to further develop models for nonlinear analysis and seismic design. Kaushik et al. (2008) studied the contribution of masonry infills in RC frames by conducting linear analysis using different diagonal strut models and validating the results with the shell element model. Kaushik and Sanganee (2010) used shell element models to develop a simplified equivalent diagonal strut model for CM walls and to further estimate the effective width of the diagonal strut for nonlinear analysis of CM walls. Ghaisas et al. (2017) also used shell element models to develop Strut-and-Tie models for seismic analysis and design of CM walls. Therefore, the shell model (Model 1) was considered as the realistic representative model for evaluating the gravity load resistance of different elements of a CM wall.

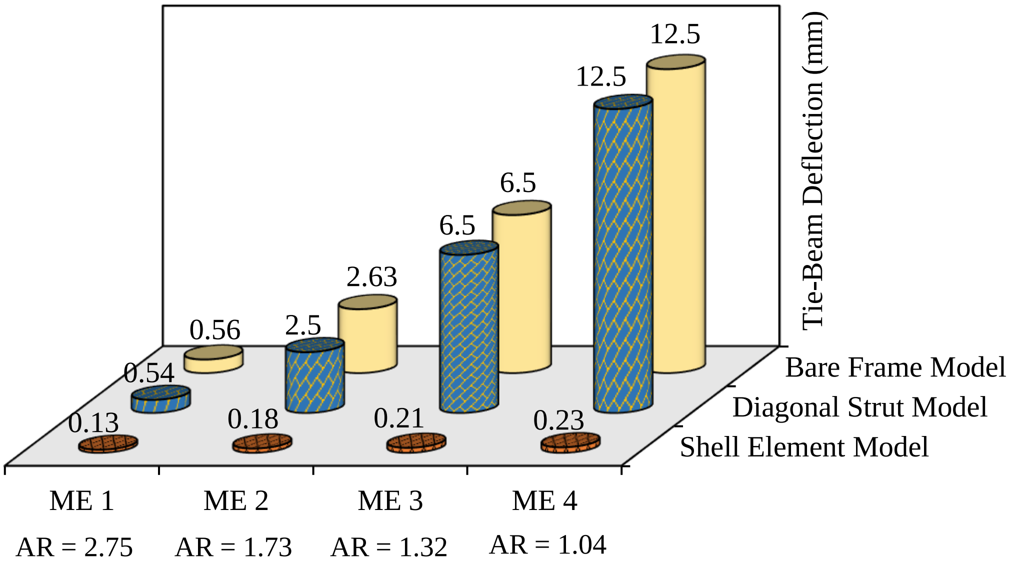

Figure 4.14: Comparison of maximum tie-beam deflection (in mm) under gravity loads in different CM wall specimens (ME 1, ME 2, ME 3, and ME 4) obtained using three modeling schemes.

It was observed that in all four walls as shown in Fig. 4.13, the axial forces in the tie-columns of the diagonal strut model (Models 2) were overestimated by about 50%. Almost all the gravity load was resisted by the tie-columns in Model 2 and negligible axial force was observed in the diagonal strut, which was almost similar to that observed in the case of the bare frame model (Model 3) in which the masonry was not even modeled. As already discussed, the masonry walls of CM buildings are expected to resist significant gravity loads; however, the diagonal strut was found to be incapable of sharing any gravity load coming from the top beam resulting in the entire gravity load being resisted by the tie-columns. Similarly, Fig. 4.14 shows the comparison of tie-beam deflection obtained using three modeling strategies. It was observed that the maximum deflection of the tie-beam is significantly large for the diagonal strut model (Model 2) just like the bare frame model (Model 3), which is not in agreement with the shell model (Model 1) exhibiting negligible tie-beam deflection. The diagonal strut does not also support the top beam due to which there is a significant vertical deformation of the top beam.

Both these observations contradict the realistic behavior of CM walls. Further, the actual distribution of axial forces (developed due to gravity loads) in masonry walls and tie-columns depends on the aspect ratio of CM wall (as shown in Fig. 4.13 with the shell model). As the tie-beam is cast after the construction of the masonry panel, a proper connection between tie-beam and masonry panel is naturally developed and a significant amount of vertical load is transferred to the masonry panel in CM structure. Though the flexural stiffness of the tie-beam is generally low, the CM wall and RC members act in a monolithic fashion, and deflection of the tie-beam is restricted because of the construction sequence. However, in the case of infilled RC frame, the flexural stiffness of the RC beam is significantly higher, and usually, there exists a small gap between the beam soffit and the masonry panel; thus, gravity load is not transferred to the infill. This peculiar behavior of CM walls must be simulated realistically in strut models in order to correctly design the tie-columns and masonry walls. The conventional diagonal strut model cannot simulate the gravity load transfer from the tie-beams resulting in a transfer of most of the axial loads onto the tie-columns.

4.5 Analysis for Gravity Loads

To simulate the realistic: (a) distribution of gravity loads in tie-columns and masonry walls, and (b) deformation profile of tie-beams, a novel modification to ESM has been attempted in this section. From the shell element model, contour plots of principal stresses for all the considered CM specimens were studied, and the formation of a vertical strut was clearly observed in addition to the diagonal struts under vertical and lateral loads, respectively, as shown in Fig. 4.15.

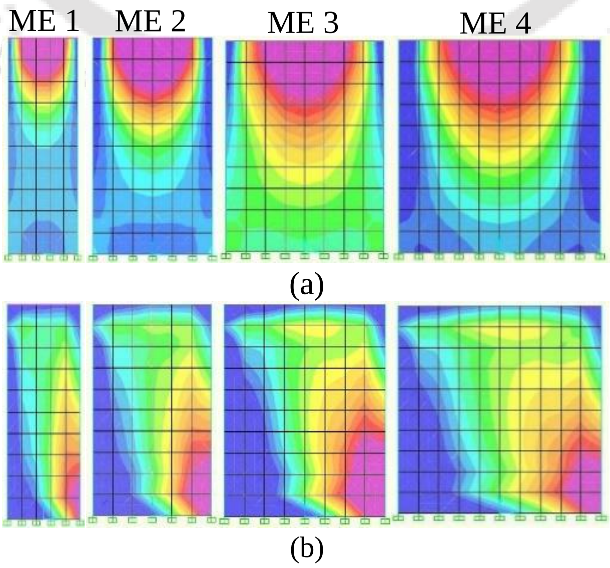

Figure 4.15: Contour plots of principal stress under (a) vertical, and (b) lateral load.

Therefore, in addition to the diagonal strut that resists the lateral earthquake load, a vertical strut connecting the center of the tie-beams in two adjacent floors was also considered in the ESM. It was observed that the axial forces cannot be realistically distributed simply by modeling an additional strut at the center of the tie-beam; the flexural stiffness (*EI*) of the tie-beams plays an important role. In reality, the entire length of the tie-beam is continuously supported over the masonry wall; therefore, the vertical deflection of the tie-beam under the action of gravity loads is very less (Fig. 4.14 with the shell model). Whereas, in this modified ESM the tie-beam is supported only at the central node resulting in comparatively higher vertical deflection of the tie-beam in the unsupported length. Therefore, a stiffness enhancement factor was suggested for the tie-beams, which ensures that the vertical deflection of the tie-beam along its entire length is negligible. More importantly, as discussed later, the stiffness enhancement factor helped in the realistic estimation of the axial forces in the tie-columns that matched quite well with that observed in the shell element model. In brief, a combination of both vertical and diagonal struts with enhanced tie-beam stiffness was considered as shown in Fig. 4.16. The newly developed ESM model is named as V-D (Vertical-Diagonal) strut model.

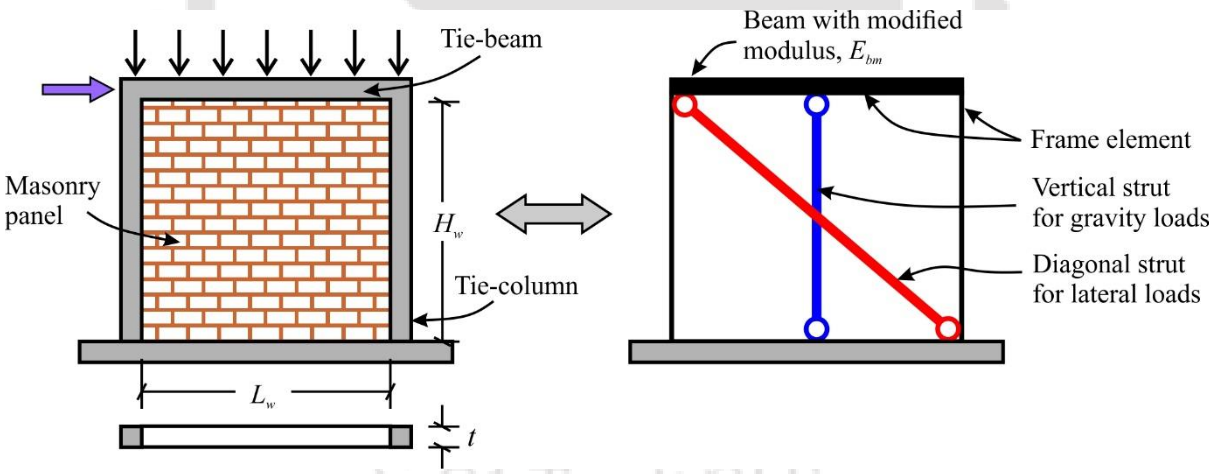

Figure 4.16: Typical CM wall and equivalent V-D strut model.

The thickness of the vertical strut can be considered as the actual thickness of the masonry wall. Estimation of another dimension of the vertical strut, i.e., vertical strut width (w_{vs}) was linked with the enhanced stiffness of the tie-beam ($E_{bm} = KE_b$) in order to reduce the tie-beam deflection (Δ) and get the realistic axial forces in tie-columns (AF); here K is the stiffness enhancement factor. For that, the influence of the input parameters w_{vs} and K on the output parameters Δ and AF was studied by carrying out a linear gravity load analysis of all the wall specimens modeled using the V-D strut model. Figs. 4.17a and 4.17b represent the influence of w_{vs} and K on AF and Δ, respectively, for ME 3 wall specimen. Similar procedure was applied for the other specimens also. Here the w_{vs} was normalized with the width of the masonry wall, and the obtained Δ and AF were normalized with the maximum tie-beam deflection and maximum axial force in tie-columns, respectively, obtained from the shell element model (Model 1). The stiffness enhancement factor K for the tie-beam is obtained by increasing the modulus of elasticity of concrete used in the tie-beam by 5, 10, 20, 30, and 40 times. It was obviously observed that in the case of ME 3, an increase in w_{vs} resulted in a reduction in Δ and AF for all values of K. Similar observation was also found in all other specimens.

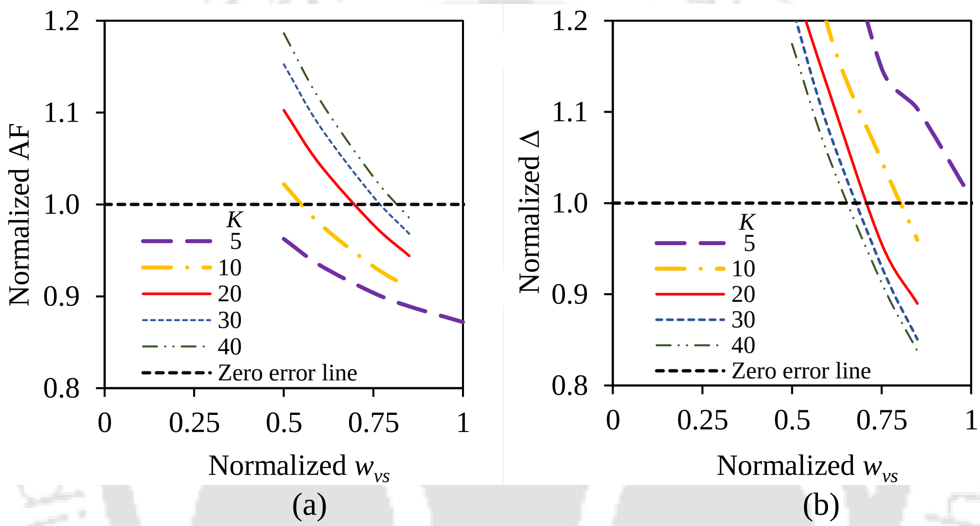

Figure 4.17: Variation of input parameters - vertical strut width (w_{vs}) and tie-beam stiffness enhancement factor (K) - in V-D strut model with the output parameters: (a) tie-column axial force (AF) and (b) tie-beam deflection (Δ) for ME 3 specimen.

After this, the aim was to get the absolute optimum input pair of $\{K, w_{vs}\}$ for which the output (Δ, AF) is similar to the one obtained from the shell element model (represented by the zero-error line). As explained in the preliminary study carried out in the present study, the shell element model for masonry gives a realistic representation of CM wall under linear gravity load analyses, thus, the errors were calculated with respect to the results obtained in the shell element model. The curves shown in Figs. 4.17(a) and 4.17(b) were then superimposed by taking the inverse of the normalized Δ values so that their intersection gives the minimum errors in prediction of AF and Δ for a particular value of K as shown in Fig. 4.18. The obtained pair of K and w_{vs} corresponding to the intersection point on the curve will be the optimum point.

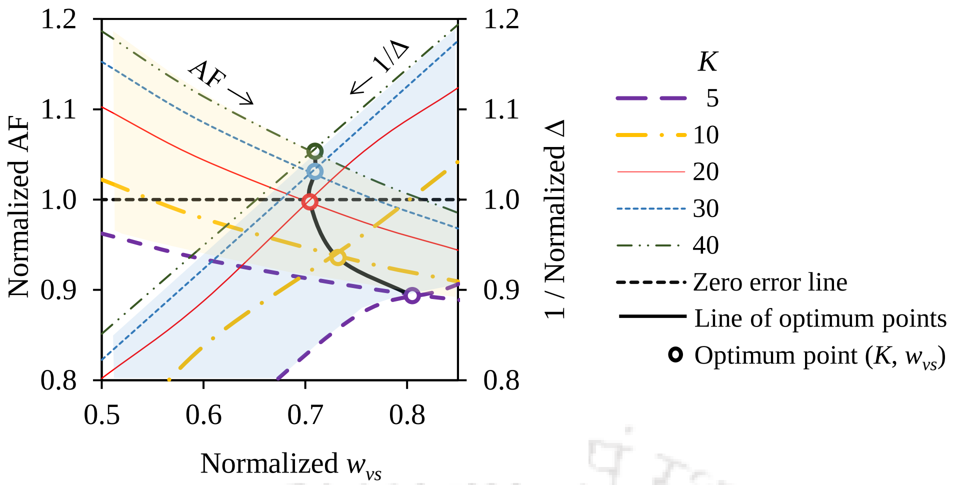

Figure 4.18: Evaluation of optimum K and w_{vs} values and line of optimum points for ME 3 specimen modeled using V-D strut model.

Using the same method, different optimum points for all the K values were then traced to locate the absolute optimum point, where the prediction error is the absolute minimum among all the optimum points (i.e., where the line of optimum points intersects the zero-error line). For the ME 3 specimen, as shown in Fig. 4.18, the absolute optimum point {K, w_{vs}} came out to be {20, 0.71L_w}.

Similarly, the lines of optimum points were obtained for all the specimens and are shown in Fig. 4.19. After observing all the absolute optimum {K, w_{vs}} pairs for CM walls with a wide range of aspect ratios (ME 1, ME 2, ME 3, and ME 4), it can be concluded that the K value lies in the range of 5 to 20 and the w_{vs} lies in the range of 0.63L_w to 0.9L_w as shown in Fig. 19. Further observations also showed that over a wide range of AR, the Δ and AF can also be found out effectively by selecting a single set of values for K and w_{vs}. This converges the K value to 20 (maximum required to simulate rigidity in tie-beams) and w_{vs} to 0.75L_w (average within the observed range). This observation is elucidated in Figure 4.20, which shows the comparison of the absolute optimum points and suggested values of {K, w_{vs}} for all the wall specimens. With the suggested combination of w_{vs} and K, the error in prediction of both Δ and AF was found to be less than 5% for most of the CM walls, except for the beam deflection in specimen ME 1, which had an unreasonably high aspect ratio of 2.75. Therefore, the suggested combination of the parameters {K = 20, w_{vs} = 0.75L_w} appears to be an excellent approximation.

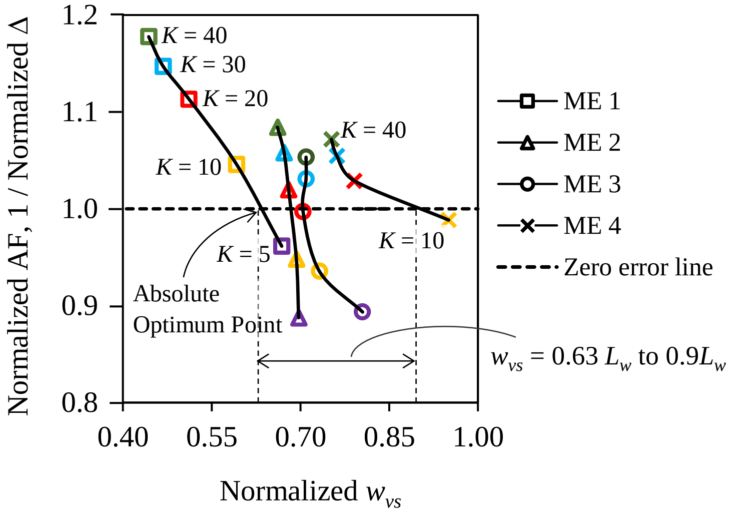

Figure 4.19: Lines of optimum points (K, w_{vs}) for specimens ME 1, ME 2, ME 3 and ME 4.

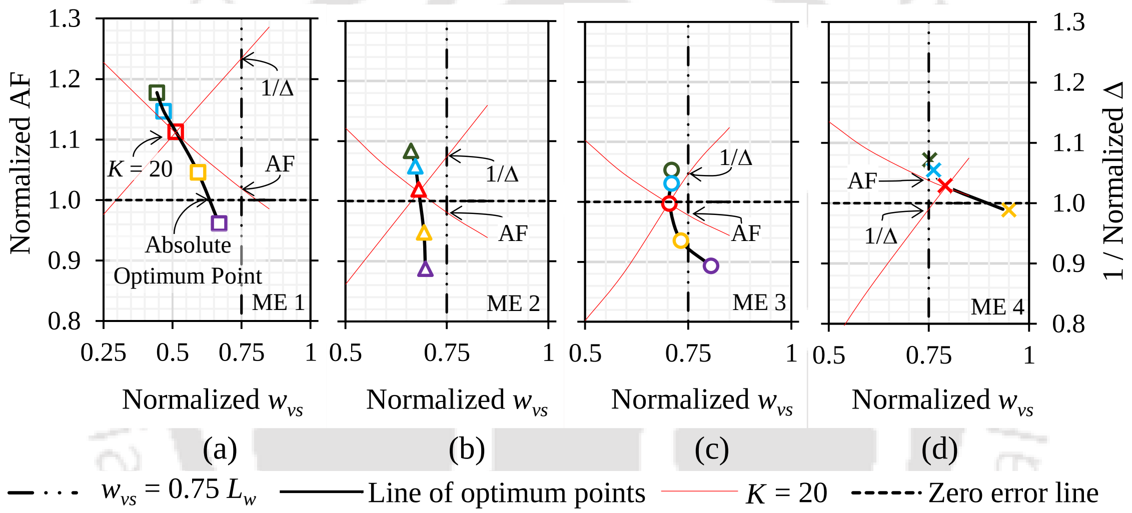

Figure 4.20: Comparison of the absolute optimum {K, w_{vs}} and suggested {K = 20, w_{vs} = 0.75L_w} values in V-D strut models for wall specimens: (a) ME 1, (b) ME 2, (c) ME 3, and (d) ME 4.

As far as the dimensions of the diagonal struts are concerned, thickness of the strut was considered as the actual wall thickness, and its width (w_{ds}) was decided such that the initial stiffness of the model under the action of lateral loads matches with that of the experimental values. Therefore, from the analysis, w_{ds} was found to be around one-third of the diagonal length of the member (L_d). The proposed modifications simulate the necessary conditions by which the tie-beam in the V-D strut model behaves as if it is supported over the wall along its whole length. These modifications in the numerical simulation accurate displacement of tie-beam in the V-D strut model and ensure realistic vertical load distribution in different elements of the CM wall. Therefore, the proposed V-D strut model is well established for linear analyses in this section. To evaluate the effectiveness of this model in simulating the nonlinear response of CM walls, nonlinear pushover analyses of the same specimens were carried out.

4.6 Analysis for Lateral Loads

All the four wall specimens ME 1, ME 2, ME 3, and ME 4 were again modeled using the proposed V-D strut model in SAP2000 for carrying out the nonlinear static analysis. As discussed in the previous section, K and w_{vs} were taken as 20 and $0.75L_w$, respectively, in order to simulate negligible beam deflection and realistic gravity load distribution on different members of the CM wall. w_{ds} was considered as one-third of the diagonal length of the wall L_d. The base of the tie-columns was assumed to be fixed to reflect the boundary conditions used in the experiments. Nonlinearity in all the members was modeled using lumped plasticity approach at specified hinge locations. Plastic hinges were assumed to form in the tie-columns at $l_p/2$ from the member ends; the plastic hinge length l_p was calculated using Paulay and Priestley (1992). Definition of flexural hinge properties for tie-columns involves axial load-moment interaction as the failure envelope and moment-rotation as the corresponding load-deformation relation. Flexural hinge properties were defined using FEMA 356 (2000), while force-controlled shear hinges were defined with user-defined properties. Flexural and shear strength for concrete sections were calculated using the material and section properties given in Table 4.1 using relevant Indian Standard (BIS 2000). Mander's confined concrete model (Mander et al. 1988) and default stress-strain data for reinforcing bars available in SAP2000 were used for generating the hinge properties. Nonlinearity was not defined in the tie-beams as damage was mostly observed in tie-columns in the experimental study. Plastic hinges were assumed to develop at the center of the diagonal struts, whose length was assumed to be about three-fourth of the strut length as suggested by Kaushik et al. (2009) and nonlinearity was defined with user-defined axial hinge properties provided by Kaushik et al. (2007).

Comparison of the experimental lateral load response of CM walls with their numerical predictions showed that the initial stiffness of both experimental and numerical models matched quite well; however, the strengths of the numerical models were significantly higher. This was expected because the predominant failure mode usually observed in CM structures is a brittle shear failure at the brick-mortar interface in the form of bed joint sliding or stepped cracks or a combination thereof. However, the approach used for modeling masonry walls in the V-D strut model considered only the compressive prism strength of masonry (f'_m)

resulting in consideration of only compressive mode of failure, which usually overpredicts the wall capacity. Therefore, it is necessary to model the nonlinearity in the diagonal strut in such a way that model simulates the lateral strength corresponding to the weakest failure mode in CM walls.

The weakest failure mode of a typical confined masonry wall depends primarily on the material properties, geometric characteristics (wall height, length, and thickness), reinforcement detailing, and gravity loads. Obviously, assuming that only f_m' will take into account of all these parameters is a gross postulation. Therefore, a term "effective shear strength of masonry (f_{ss})" was coined, which represents the minimum strength for the weakest failure mode in CM walls. The effective shear strength parameter of masonry was developed in the present study to limit the axial strength of the diagonal strut in the V-D strut model. For simplicity, f_{ss} was initially calibrated in a most simplistic way such that the predicted strength using the V-D strut model matches well with the experimental results of the relevant wall specimens of Gavilán et al. (2015). Regardless of the failure mode, the same stress-strain model using f_{ss} (instead of f_m') as the peak stress was utilized for the axial hinge definition in the diagonal strut as shown in Fig. 4.21. As f_{ss} represent the most critical failure mode in CM walls, its magnitude will be obviously less than f_m', which is also reflected in Fig. 4.21. The calibrated f_{ss} values obtained from the nonlinear SAP2000 analyses were 0.75 MPa, 1.1 MPa, 1.30 MPa, and 1.55 MPa for ME 1, ME 2, ME 3, and ME 4, respectively. Interestingly, f_m' represents only the material strength irrespective of the wall parameters; however, as the ratio of f_{ss} and f_m' increases with increasing AR. It can be observed from Fig. 4.22 that using these values both experimental and analytical results, in terms of initial stiffness and strength, matched very well. This shows that the effectiveness of the V-D strut model depends on the accurate prediction of f_{ss}.

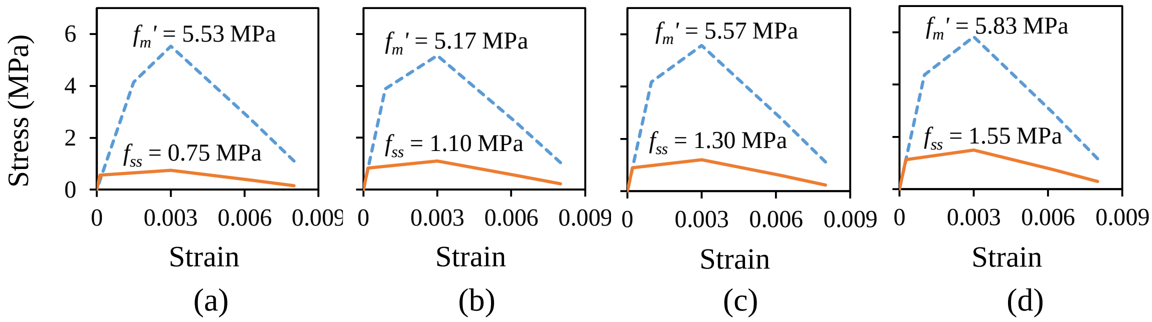

Figure 4.21: Modification in axial hinge property for the diagonal strut in V-D strut model of CM wall specimens: (a) ME 1, (b) ME 2, (c) ME 3, and (d) ME 4.

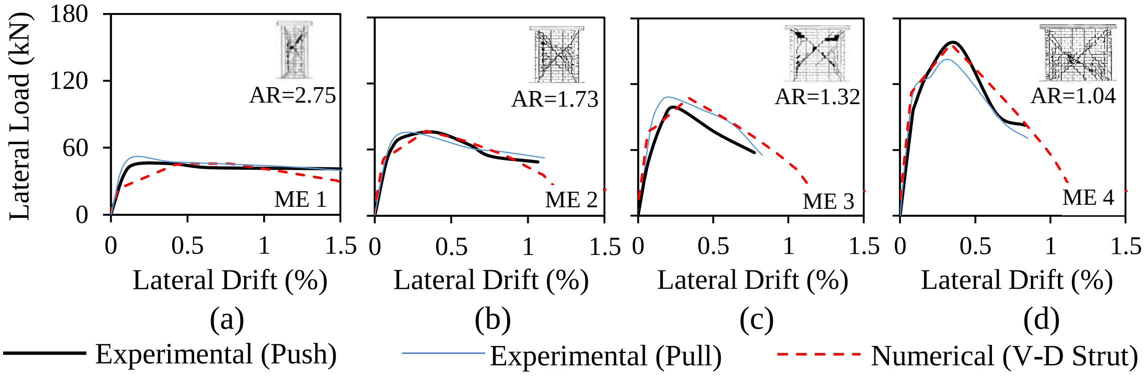

Figure 4.22: Lateral load-displacement behavior of CM walls modeled using V-D strut model considering effective shear strength of masonry (f_{ss}) for the nonlinearity definition in the diagonal strut: (a) ME 1, (b) ME 2, (c) ME 3, and (d) ME 4.

4.7 Characteristics of Diagonal Strut

In the previous section, the effective shear strength of masonry (f_{ss}) used for the axial hinge definition in the diagonal strut of the V-D strut model was simply calibrated in a most simplistic way such that the predicted lateral strength using the V-D strut model matches well with the experimental results. However, based on the available limited experimental data, it is difficult to develop a generalized method for the estimation of the effective shear strength of masonry. As the strength of strut, corresponding to various failure modes, depends on various parameters, a parametric FE study was carried out using the previously developed FE model incorporating the influence of all relevant parameters to develop a methodology for the estimation of f_{ss}.

4.7.1 Data obtained from Parametric FE Study

As explained earlier, a parametric FE study is essential to be carried out to build a database of the sensitivity of the in-plane strength of CM wall to different parameters related to material properties, geometric characteristics, reinforcement detailing, and gravity loads. As given in Table 4.4, six independent parameters were considered as variables, namely, compressive prism strength of masonry (f'_m), compressive strength of concrete (f_c), aspect ratio of wall (AR), gravity loads on tie-beams (σ), percentage of reinforcement in tie-columns (ρ_l), and wall thickness (t). The magnitude of variation in each parameter reflects the level of uncertainty associated with it. CM walls with five different aspect ratios were considered by varying the length of the wall, while the height of the masonry wall (H_w) was kept constant as 3 m.

Table 4.4: Details of parameters considered for the parametric FE analyses.

Sl no.	Parameter	Unit	Values	Comments and References
1	f'_m	MPa	3.0, 5.5, 8.5	Commonly practiced grade in India
2	f_c	MPa	20, 25, 30	Usual available grade of concrete
3	AR	—	0.75, 1.0, 1.25, 1.5, 1.75	AR_{min} = 0.75 (NTC-M 2017)
4	σ	MPa	0.1, 0.3, 0.65	σ_{min} = 0.1 MPa (Considering an exterior wall of a single-story building), σ_{max}= 0.627 MPa (Considering an interior wall of a 3-story high building)
5	ρ_l	%	0.6, 1.0, 1.5, 2	$(\rho_l)_{min}$= 0.6% (NTC-M 2017), $(\rho_l)_{max}$= 2% (NTC-M 2017)
6	t	mm	100, 200, 250	t_{min}= 100 mm (NTC-M 2017), t_{max}= 250 mm (Considering full brick thick wall)

Varying each parameter one at a time while keeping all other parameters constant resulted in 1620 numerical models, which were analyzed in Abaqus under gravity and cyclic lateral loads. A sensitivity study was carried out to understand the influence of each parameter on the lateral load behavior of CM wall. As shown in Fig. 4.23, the lateral strength of CM walls decreases with increasing AR, but increases with f'_m and t. The lateral strength was observed to be comparatively less sensitive to the percentage reinforcement in the members, concrete compressive strength, and gravity loads. The influence of σ on in-plane lateral strength was noticed at high σ only. Generally, the lateral resistance of CM buildings is found to be sensitive to the gravity loads because the bed joint friction is directly proportional to the gravity loads. Clearly, as expected the macro-modeling strategy adopted in the study could not simulate the joint friction appropriately. The influence of the three most sensitive parameters (AR, f'_m, and t) on the lateral strength of the CM walls was studied in more detail in the parametric study.

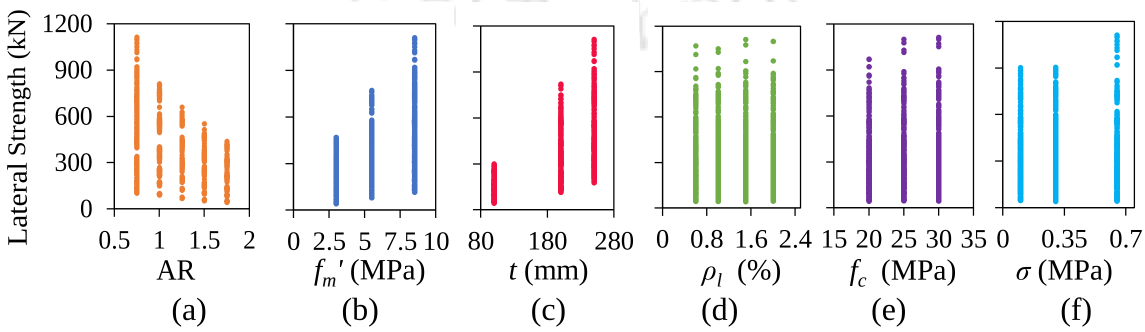

Figure 4.23: Sensitivity of lateral strength of CM walls obtained from the parametric 3D FE analyses to the six input parameters: (a) AR, (b) f'_m, (c) t, (d) ρ_l, (e) f_c, and (f) σ.

The peak lateral strength of CM walls obtained from the 1620 FE analyses was plotted against the AR of the corresponding walls for different wall thicknesses as shown in Fig. 4.24. In all three plots, three distinct bands can be seen, which correspond to three different masonry compressive strengths: 3 MPa, 5.5 MPa, and 8.5 MPa. The distinct bands are wider at lower AR, and subsequently get narrowed down with an increase in AR. Further, it was also observed that the bands are narrower for lower f_m'. Such distinct bands were formed because the lateral strength was found to be highly dependent on f_m', AR and *t*. Lateral strengths corresponding to the variation in all the other parameters (f_c, σ, and ρ_l) were embedded into these bands. The width of the bands increases for lower AR values for all the cases (three considered values of f_m' and *t*) because of the influence of other parameters on the lateral strength.

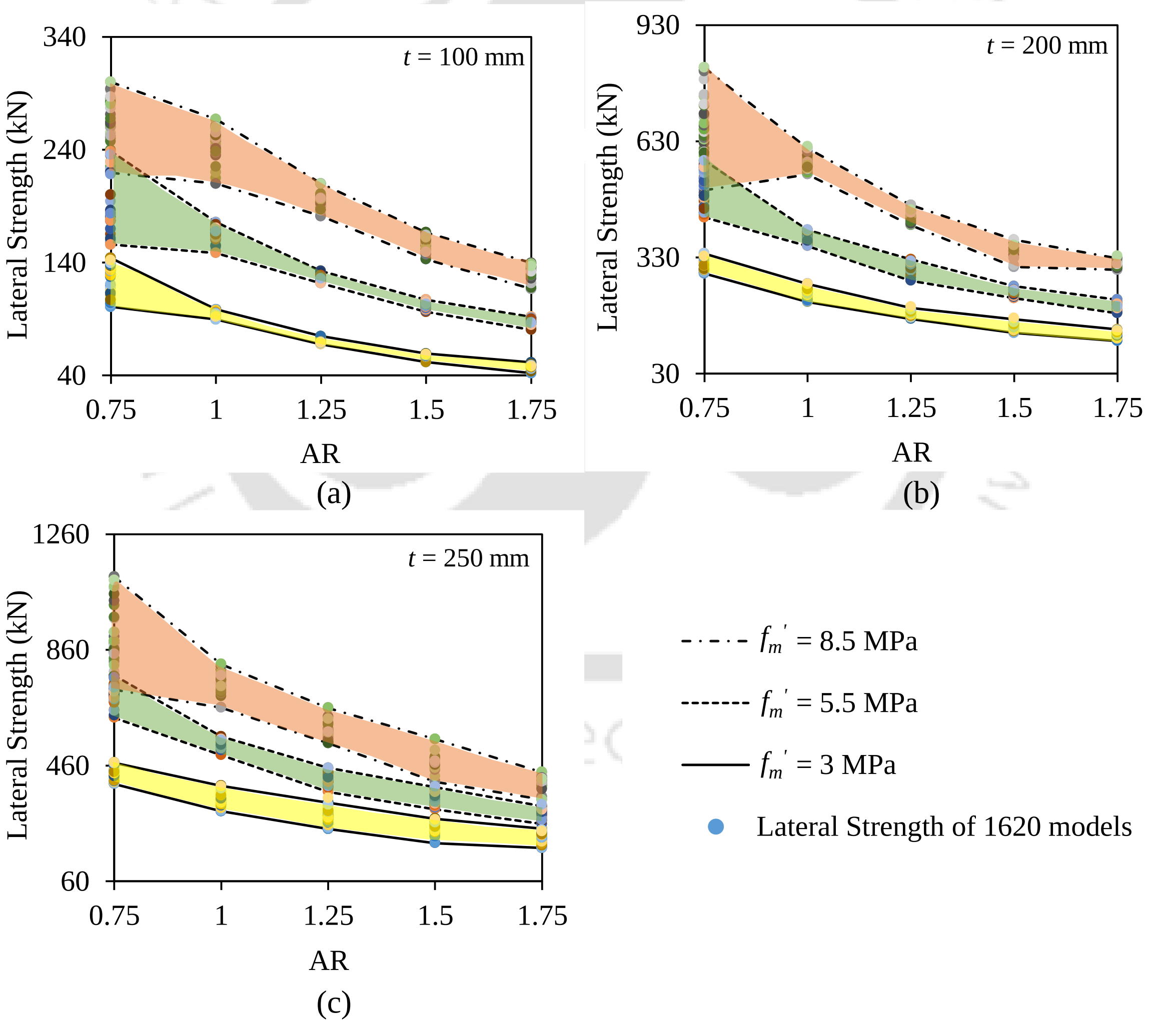

Figure 4.24: Variation in the in-plane shear capacity of CM walls obtained from the parametric 3D FE analyses with aspect ratio of wall for: (a) *t* = 100 mm, (b) *t* = 200 mm, (c) *t* = 250 mm.

For example, lower values of σ and ρ_l in CM wall specimens resulted in a significant reduction in the lateral strength; whereas, the strength increases dramatically for higher values of σ and ρ_l. Such a dramatic rise or fall in the lateral strength was more noticeable in the case of the lowest AR value. This is because lateral strength of squat specimens was already higher, and the variability in lateral strength was also found to be higher perhaps due to the following two reasons: (a) yielding of reinforcement in tie-columns before the failure of the masonry wall for low σ and ρ_l, (b) failure of masonry walls before yielding of reinforcement in tie-columns for high σ and ρ_l. Such different failure modes at lower AR resulted in higher variability in the lateral strengths observed in Fig. 4.24.

4.7.2 Data for Effective Shear Strength of Masonry (f_{ss}) and Empirical Formulation

In this section, all 1620 CM wall models, which were considered in the FE parametric study, were again simulated using the V-D strut model and analyzed in SAP2000. Lateral strength obtained from the pushover analysis of all these models was calibrated with the data (lateral strength) obtained from the parametric FE analyses, and the required minimum strength of the diagonal strut in the axial hinge definition, i.e., f_{ss} instead of f'_m was obtained. The obtained f_{ss} values were then collected in a database and associated with the respective geometrical and mechanical features for each CM wall specimen. As masonry walls in CM structures are well confined with surrounding tie-members; various other parameters in addition to the masonry compressive strength influence the lateral strength, as also observed in the previous section. The influence of various parameters on f_{ss} values is shown in Fig. 4.25. It was observed that f_{ss} was most sensitive to f'_m followed by AR and t, and least to σ, f_c, and ρ_l. However, for lower values of AR, f_{ss} was also found to be quite sensitive to σ.

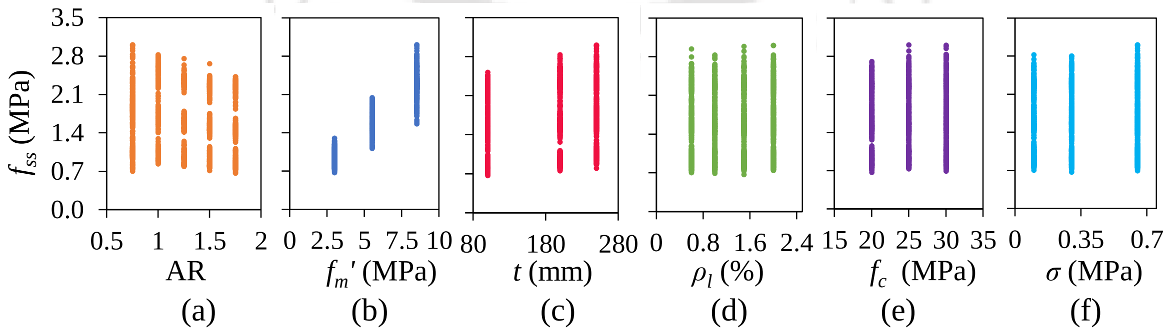

Figure 4.25: Sensitivity of effective shear strength of masonry (f_{ss}), obtained using V-D strut models considering the lateral strength obtained from the parametric 3D FE analyses, to the six input parameters: (a) AR, (b) f'_m, (c) t, (d) ρ_l, (e) f_c, and (f) σ.

Fig. 4.25 also shows large variability of f_{ss} with the input parameters; therefore, f_{ss} cannot be estimated considering just one or two parameters for the sake of simplicity. In view of this complex nature of dependence of f_{ss} on different parameters, a generalized method for the assessment of f_{ss} must be developed considering all the six parameters. Therefore, empirical equations were developed for estimation of f_{ss} by carrying out unconstrained multiple variable linear regression analysis of the data obtained from the pushover analyses of all the 1620 V-D strut models. As discussed earlier, that lower AR resulted in higher variability in lateral strength compare to AR values greater than 1.0 (Fig. 4.24). Further, it was also observed from Fig. 4.25a that for lower bound values, f_{ss} is directly proportional to aspect ratio for AR ≤ 1, and it was inversely proportional for AR > 1. Thus, considering this peculiar sensitivity of f_{ss} with AR, two empirical relations given in Equations (4.1) and (4.2) were developed for two different ranges of aspect ratios; AR ≤ 1 and AR > 1. Fig. 4.26 shows the comparison of the numerically obtained and empirically predicted values of f_{ss} for the considered CM specimens. Fig. 4.26 shows high coefficients of determination (around 0.98) confirming the effectiveness of the developed empirical equations in predicting the f_{ss} values.

$$f_{ss} = 0.096 t^{0.217} f_m'^{0.827} f_c^{0.081} \rho_l^{0.018} (1+\sigma)^{0.235} \mathrm{AR}^{0.101} \qquad \text{for AR} \le 1 \tag{4.1}$$

$$f_{ss} = \frac{0.134 t^{0.133} f_m'^{0.886} f_c^{0.107} \rho_l^{0.002} (1+\sigma)^{0.004}}{\mathrm{AR}^{0.248}} \qquad \text{for AR} > 1 \tag{4.2}$$

here, f_{ss}, f_m', f_c, σ are in MPa; ρ_l is in %; t is in mm; and AR is dimensionless.

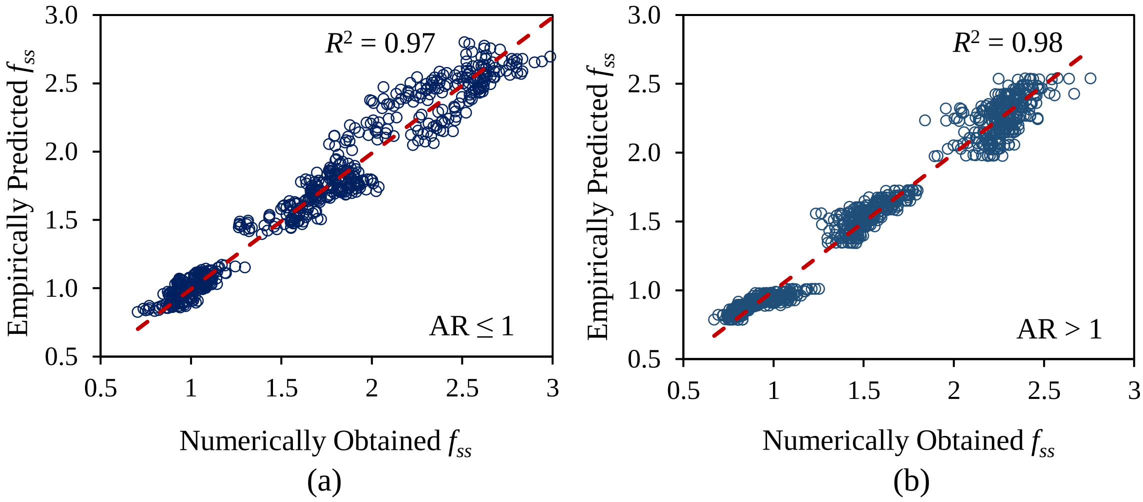

Figure 4.26: Comparison of the numerically obtained and empirically predicted f_{ss} (in MPa) for the considered CM specimens in the parametric study with aspect ratio: (a) less than or equal to 1, and (b) greater than 1.

4.8 VALIDATION OF PROPOSED V-D STRUT MODEL

To evaluate the effectiveness of the proposed V-D strut model in predicting the lateral load behavior of CM walls, the three test specimens of the present study and thirty-five CM wall specimens tested by fourteen past research teams (Table 4.5) were simulated using the V-D strut model and nonlinear pushover analyses were carried out in SAP2000. The f_{ss} value was obtained for each of the walls using the developed empirical Equations (4.1) and (4.2).

Table 4.5: Comparison of in-plane lateral strength of CM walls obtained from the V-D strut model with experimentally obtained values

Sl no.	Study	Model ID	AR	f'_m (MPa)	t (mm)	ρ_l (%)	f_c (MPa)	σ (MPa)	f_{ss} (MPa)	$\frac{V_{m,VD}}{V_{m,e}}$
1	Aguilar et al. (1996)	MO	1.02	3.5	125	1.5	20.0	0.49	1.087	0.84
2	Iiba et al. (1996)	IDM	1.39	5.35	115	2.4	28.0	1.05	1.470	0.64
3	Yoshimura et al. (1996)	4-H0V0	0.75	14.7	100	3.1	31.7	0.84	3.646	0.88
		1-H0V0	0.75	18.8	100	2.8	30.6	0.84	4.448	1.08
4	Yoshimura et al. (2000)	H1-H0V0-HC	0.75	13.4	100	2.8	33.8	1.80	3.740	0.84
		H1-H0V0-LC	0.75	18.7	100	2.8	32.2	0.84	4.447	1.39
		H1-H0V0-T*	0.75	12.3	100	2.8	28.1	-0.11	2.622	1.50
		L1-H0V0-HC	0.75	18.4	100	2.8	23.3	1.80	4.718	0.80
		L1-H0V0-LC	0.75	18.8	100	2.8	30.6	0.84	4.448	1.09
		L1-H0V0-T	0.75	18.4	100	2.8	24.5	-0.11	3.618	1.28
5	Kumazawa and Ohkubo (2000)	ISM	1.24	5.58	115	2.4	29.8	1.33	1.621	0.87
6	Yáñez et al. (2004)	Pattern 1-CMU*	0.63	6.04	140	1.1	23.9	0	1.536	1.82
		Pattern 1-Clay	0.63	6.89	140	1.1	23.9	0	1.711	1.38
7	Marinilli and Castilla (2004)	M1	0.77	6.8	150	2.3	23.8	0.39	1.890	1.40
		M2+	1.63	6.8	150	2.3	23.8	0.39	1.780	0.96
		M3+	2.59 1.19	6.8	150	2.3	23.8	0.39	1.588 1.924	1.14
		M4+	2.59	6.8	150	2.3	23.8	0.39	1.588	1.00
8	Zabala et al. (2004)	3	1.00	2.9	200	2	20.0	0.36	1.032	1.10
		4	1.00	2.9	200	2	20.0	0.36	1.032	0.97
9	Bourzam et al. (2008a)	JCM	1.53	9	100	2	20.0	0.40	2.206	0.89
10	Kuroki et al. (2010)	CMWO-01*	0.79	28.3	100	2.8	26.3	0.48	5.888	1.52
		CMWO-07*	0.79	10.4	100	2.8	21.1	0.48	2.528	1.76
11	Matošević et al. (2014)	A	1.31	2.6	190	0.8	43.8	0.54	0.882	0.69
12	Singhal and Rai (2014)	SC_{NT}+	1.25	8.8	65	2.7	33.1	0.1	2.212	1.26
13	Gavilán et al. (2015)	ME 1	2.75	5.53	120	2.8	33.4	0.5	1.342	1.47
		ME 2	1.73	5.17	120	2.8	20.4	0.5	1.345	1.22
		ME 3	1.32	5.57	120	2.8	18.0	0.5	1.516	1.26
		ME 4	1.04	5.83	120	2.8	23.1	0.5	1.721	1.10
		ME 5	0.68	8.15	120	2.8	22.7	0.5	2.174	1.02
		ME 6+	0.78	8.99	120	2.8	25.5	0.5	2.413	0.88
		ME 7+	0.78	6.54	120	2.8	29.8	0.5	1.879	0.85
14	Quiroz et al. (2017)	A1-1	1.07	3.74	205	0.8	20.6	0.16	1.189	0.99
		A1-2	1.07	3.74	205	0.8	20.6	0.16	1.189	0.92
		A2-1	1.07	3.74	205	0.5	20.6	0.16	1.188	1.18
		A2-2	1.07	3.74	205	0.8	20.6	0.16	1.189	0.82
15	Present study	S1	2.00	5.20	125	0.7	30.4	0.13	1.304	1.12
		S2	1.50	5.20	125	0.7	30.4	0.13	1.400	1.21
		S3	1.00	5.20	125	0.7	30.4	0.13	1.421	1.25

* Not included in the initial error estimation; + Walls with multiple bays.

As shown in Fig. 4.27 and Table 4.5, the numerically predicted lateral strengths (using V-D strut model) of all the specimens ($V_{m,VD}$) were then compared with the experimentally obtained lateral strength ($V_{m,e}$). The comparison study showed that the uses of f_{ss} obtained from the proposed empirical equations in the V-D strut model very well predict the lateral strength of CM walls. Further, it was observed that the developed model can also predict the lateral load behavior of multi-span CM wall specimens marked with plus signs (+), i.e., M2, M3, M4, SC_{NT}, ME 6, and ME 7. The average error in prediction of the lateral strength came out to be only 5% (mean of $V_{m,VD}$ / $V_{m,e}$ = 1.05) with a standard deviation of 21%, if the results corresponding to those studies marked with an asterisk (*) were not considered. For the marked four specimens — H1-H0V0-T, Pattern 1-CMU, CMWO-01, and CMWO-07, the model overpredicted the experimental results. Interestingly, all these specimens had very low AR (less than 0.8); moreover, these specimens had some contrasting points discussed below in comparison to the rest of the specimens. As shown in Table 4.5, Yoshimura et al. (2000) tested two sets of CM wall specimens (H series and L series) considering the height of the applied lateral forces at 1.11 and 0.67 times the height of wall, respectively.

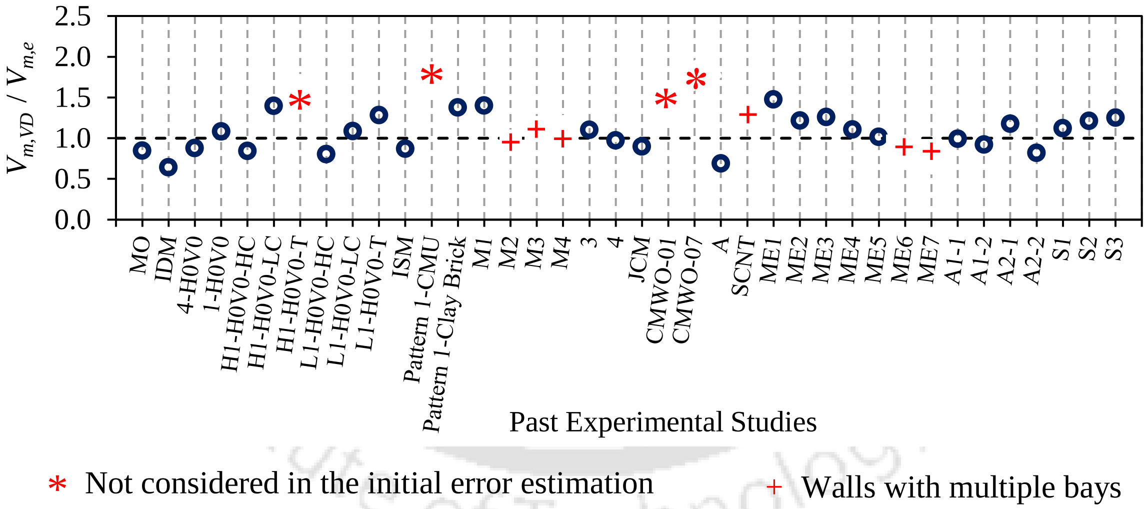

Figure 4.27: Comparison of in-plane lateral strength of CM walls obtained from the V-D strut model and past experimental studies.

From the tests it was noticed that most of the L series specimens failed in shear. On the other hand, the H series specimens failed in flexure. In addition to this, H1-H0V0-T specimen (marked with asterisk) of Yoshimura et al. (2000) was tested with negative gravity stress. Pattern 1-CMU specimen of Yáñez et al. (2004) was tested with hollow concrete masonry unit. The remaining two marked specimens (CMWO-01 and CMWO-07) were tested by Kuroki et al. (2010) who used high strength masonry in the construction. As these conditions were not considered in the present study in the development of the V-D strut model as well as in the empirical equations developed for estimation of effective shear strength of masonry, these studies were excluded in the initial error estimation. If all the studies were considered, including the four studies (marked by *), the error in estimation of lateral strength of confined masonry wall went up to 12% (mean of $V_{m,VD}/V_{m,e}$ = 1.12) with a standard deviation of 28%. To gain more insight in the obtained results, the number of studies for which the model overestimate or underestimate the lateral strength is shown in Table 4.6 along with the average error in underestimation or overestimation. For single-bay CM specimens, the average error in prediction of lateral strength is 18% and 31% for underestimation and overestimation cases, respectively. Whereas, for multi-bay CM specimens, the average error in prediction of lateral strength is 11% and 14% for underestimation and overestimation cases, respectively.

In addition, the numerically obtained pushover curves were compared with the experimental lateral load envelope for all the considered CM walls as shown in Fig. 4.28. Overall, it is quite clear from the above discussion and comparison that the V-D strut model is very effective in prediction of not only the lateral strength of confined masonry walls, but it can also predict the complete nonlinear lateral load response of single as well as multi-span CM walls with sufficient accuracy. The simplicity and versatility of the V-D strut model make it a better choice for seismic analysis of confined masonry walls if compared with the other available analytical models that use equivalent diagonal strut approach for nonlinear simulation of CM walls.

Table 4.6: Lateral Strength prediction of CM walls using V-D strut model: underestimated and overestimated cases.

CM wall specimen	Quantity	Underprediction	Overprediction	Total
Single bay (Total = 32)	No. of cases	12	20	-
	Average of ($V_{m,VD}/V_{m,e}$)	0.85	1.31	1.13
	Average error (%)	18	31	13
Multi bay (Total = 6)	No. of cases	3	3	-
	Average of ($V_{m,VD}/V_{m,e}$)	0.9	1.14	1.02
	Average error (%)	11	14	2
All 38 Specimens	Average of ($V_{m,VD}/V_{m,e}$)	-	-	1.12
	Standard deviation	-	-	0.28

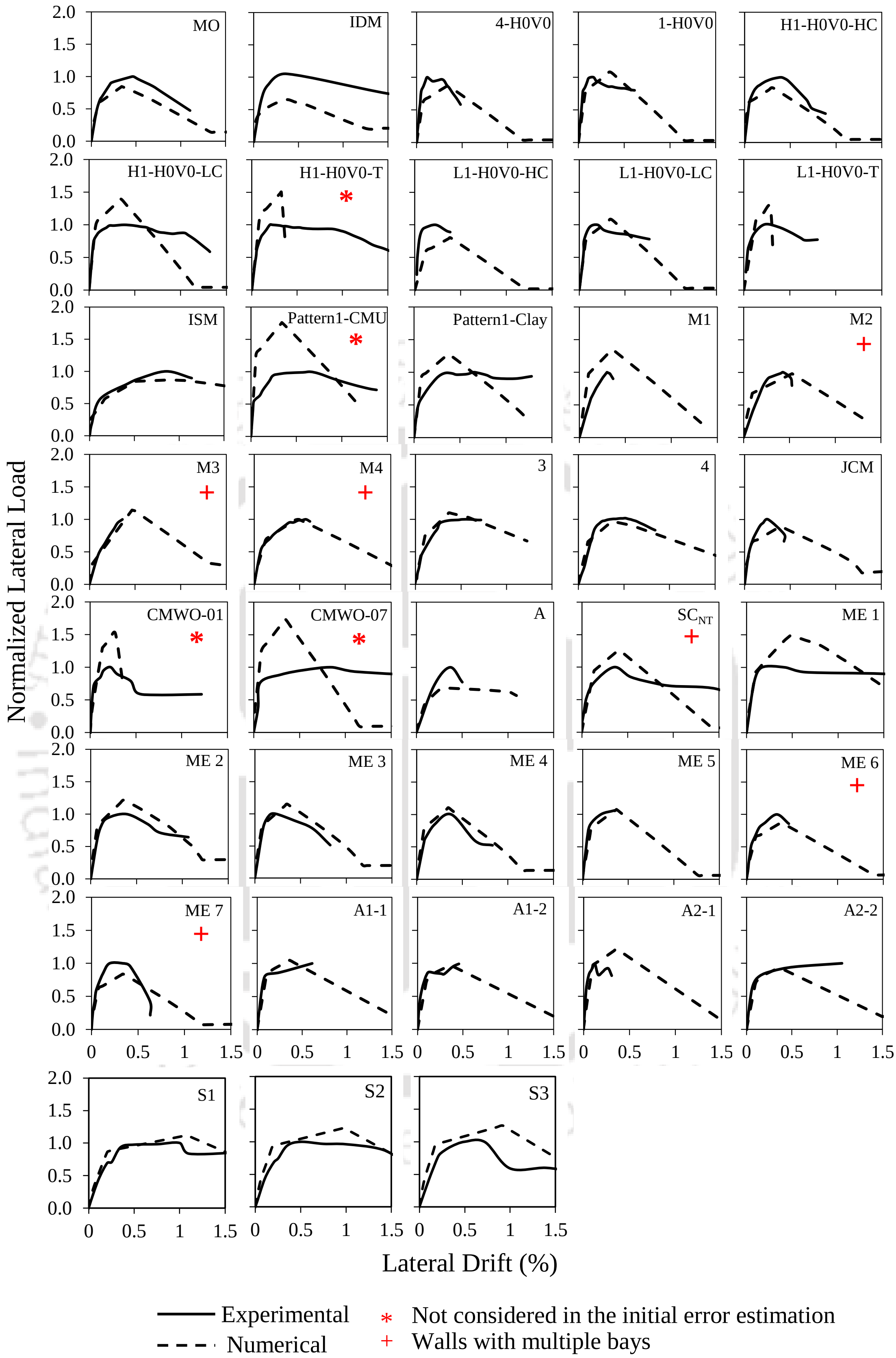

Figure 4.28: Comparison of the lateral load response of CM walls obtained in several past experimental studies with that predicted by the V-D strut model. The lateral load is normalized with respect to the lateral strength obtained experimentally.

4.9 SUMMARY

Confined masonry is a riveting choice for building construction technology due to its economic viability for low-tech construction in seismic regions. Though numerous studies on seismic analysis approaches for CM buildings have been carried out, the approaches bear certain limitations. Application of the available analysis techniques in a nonlinear range with the motive of displacement-based design is limited and not enough literature is available on it. The use of realistic and reliable FE models is rather limited due to lack of relevant input data and excessive computational effort and time.

From a preliminary study, it was observed that the equivalent diagonal strut model (ESM), which is a reliable modeling technique for infilled RC structures, needs some important modifications for the application in CM structures. Based on gravity load analyses, ESM was modified and a new vertical-diagonal (V-D) strut model was developed in which a vertical strut was also modeled, in addition to the diagonal strut, to simulate realistic tie-beam deflection and tie-column axial forces. Further, the stiffness of the tie-beam was enhanced 20 times in order to obtain representative load and deformation profile. Nonlinear static analyses showed that the use of masonry prism strength (f_m') in the definition of nonlinearity in the diagonal strut overestimates the lateral strength because of the unique failure modes of the CM walls. In order to simulate the realistic failure of CM walls, a new term “Effective Shear Strength of Masonry (f_{ss})” was defined that corresponds to the lowest strength of masonry considering all the possible failure modes; f_{ss} was used for defining the nonlinearity in the diagonal strut.

To establish a method for assessment of f_{ss}, FE parametric study was first carried out in Abaqus considering six relevant and most important parameters. The FE model was developed using the present tested specimens and some specimens with different aspect ratios tested in the past. The lateral strength values obtained from 1620 models developed in the parametric study were then used to calibrate the results of V-D strut model in SAP2000 to estimate f_{ss}. Further, two empirical equations were also developed for the estimation of f_{ss} by carrying out multiple variable linear regression analysis of the analytical data. The effectiveness of the empirical equations and V-D strut model was validated using several past experimental studies. It was observed that the developed V-D strut model was able to suitably capture the linear and nonlinear behavior of CM walls with acceptable accuracy. The developed analysis method using V-D strut model and f_{ss} is extremely simple and effective to use, as it needs only a few easily available input parameters and well-established principles of ESM. In the present form, the developed V-D strut model does not take into account the out-of-plane response of CM walls. Applicability of the model in the case of multi-story CM walls is required to be ascertained by validating it with experimental results. The accuracy of the developed model can be further improved by calibrating it with additional experimental studies.

Chapter 5
ASSESSMENT OF DESIGN PROVISIONS

CONTENTS

5.1 OVERVIEW

Seismic design codes are unique to a particular region or country, and reflect the state-of-the art in that country in that field. They take into account the local seismology, accepted level of seismic risk, building typologies, materials, and methods used in construction; though some of the codes have become international in nature because of the exhaustive coverage of different clauses. Confined masonry has been embraced in many countries as an affordable and resilient seismic solution for low-rise buildings. Especially, in Latin American countries, such as Mexico, Chile, and Peru, it is a popular and widely adopted construction practice for buildings even up to six-story high (Brzev 2007). Several guidelines have been developed over the years to provide basic details on Confined masonry and promote its construction practice as mentioned in Chapter 2. Some countries have developed standard design provisions for CM walls: Mexico (NTC-M 2017), Peru (NT E.070 2019), Chile (NCh2123 2003), Argentina (INPRES-CIRSOC 103 2018), Colombia (NSR-98 2010), Costa Rica (CSCR 2002), Europe (CEN 2005), and China (GB 50003 2011). Also, the Indian code for

Confined masonry is under development and it is expected to be published soon (BIS 2021). The essence of structural design is to identify the possible failure mechanisms, predict the resistance or capacity at failure, and determine if this capacity is larger than the expected demands on the structure. The structural behavior of CM walls can be divided into the responses to vertical loading and in-plane lateral loading. Compressive failure in CM wall may occur due to very large vertical load on the wall or low compressive strength of masonry used for the construction of CM wall and it is characterized by crushing of masonry as shown in Fig. 5.1(a). Under lateral seismic loading, damages in CM buildings usually take place at the first story level mainly under two major failure modes: shear (bed-joint sliding and/or diagonal-tension) and flexure (Figs. 5.1b, c, and d). The failure due to only vertical loading is not considered a critical issue for CM walls, as masonry wall is always designed in such a way that it experiences relatively small axial compressive stress. Although individual failure mechanism is theoretically possible, the observed damages in CM walls are generally in a combination of different modes under the action of gravity and lateral seismic loading. Due to seismic loading, shear-induced damages in the form of diagonal cracking were more common in CM structures compared to flexure-induced damages. The confining effect by the tie-elements will limit the damage to the masonry wall and prevent wall instability. The occurrence of a given failure mechanism depends on a particular combination of different factors related to material properties, wall geometry, boundary condition, type, and magnitude of loading.

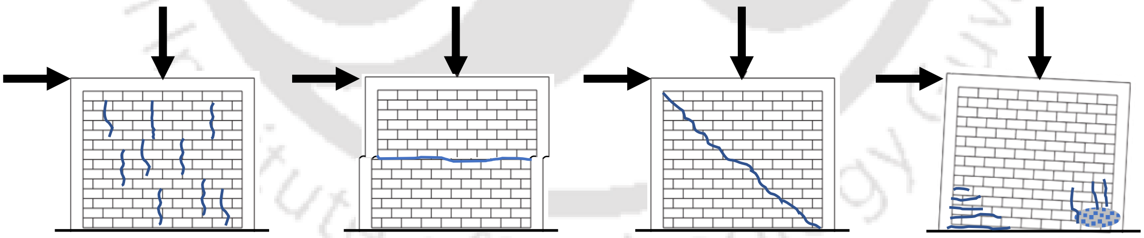

(a) (b) (c) (d)

Figure 5.1: Schematic of possible failure modes in CM walls under vertical and lateral loading: (a) compression, (b) bed-joint sliding shear, (c) diagonal-tension shear, and (d) flexure.

In all the available design codes, the basic concepts for CM construction are almost common; however, they convey a large dispersion of rules and many gaps, especially related to material properties, in-plane and out-of-plane capacity, design and detailing provisions for tie-members, etc. The guidelines are still under development and are non-conclusive on methods to be adopted in design and detailing of different elements in a typical CM building instead of prescriptive approaches. Thus, there is a need to assess the efficacy of the existing codes in safely predicting the design lateral forces of CM walls of different configurations.

5.2 Shear Strength Provisions

Masonry has high compressive strength, but comparatively lower shear and flexural strength. Failure of a CM wall is mostly characterized by the composite action of masonry and tie-columns. In case of low vertical load, weak horizontal mortar joint, and low concrete shear strength, seismic loads can cause bed-joint sliding shear failure of the wall (Fig. 5.1b). Further, the initial damage characteristic of diagonal-tension shear behavior is diagonal cracking in the mortar or masonry units from the center of the masonry wall to the tie-columns along the compression strut (Fig. 5.1c).

5.2.1 Contribution of Different Elements

In a CM wall, the effects of lateral earthquake loads are mainly resisted by the masonry panel initially, while the confining elements do not play a significant role. Once the cracking takes place in masonry walls of confined masonry (either in masonry units or in mortar joints), the maonsry panels becomes less effective in resisting the lateral forces. If the lateral force continues to increase, the masonry panel typically begins to lose strength, and at this stage the vertical reinforcement in tie-columns becomes engaged in resisting the tensile and compressive stresses, thereby providing additional deformability. The ultimate failure occurs when the tie-columns completely fail in shear by the extension of diagonal shear failure of the masonry panel into the tie-columns (Meli et al. 2011). In general, the design shear strength (V_{des}) of confined masonry walls is the combined resistance coming from: (i) masonry panels, considering the influence of vertical axial compression (V_{mas}), (ii) tie-columns (V_{tc}), and (iii) wall horizontal reinforcements (V_{wr}) if any. Eq. (5.1) shows the combined resistances from the masonry walls, tie-columns, and wall horizontal reinforcement. All the available equations will be first converted to this simplistic form before comparing their effectiveness in estimating the lateral strength of CM walls.

$$V_{des} = V_{mas} + V_{tc} + V_{wr} \tag{5.1}$$

The recommended equations for the design shear strength in different codes are provided in Table 5.1. The contribution of different parts and the associated safety factors in the design shear strength provisions provided in different design codes will be studied in detail here.

Table 5.1: Estimation of shear strength of CM wall using different codes.

Country Code	Equations for V_{des}	Eq.
Mexico (NTC-M 2017)	$V_{des} = V_{mas} + V_{wr}$ where, $V_{mas} = \{F_S f_{AR}(0.5v_{md} + 0.3\sigma)A\} \le 1.5F_S f_{AR} v_{md} A$; $V_{wr} = F_S \eta \rho_h f_{yh} A$ $f_{AR} = \begin{cases} 1.5 & \text{for } H/L \le 0.2 \\ 1.0 & \text{for } H/L \ge 1.0 \end{cases}$; $\rho_h = A_{sh}/s_h t$; $\eta = \frac{V_{mas}}{F_S \rho_h f_{yh} A}(k_0 k_1 - 1) + \eta_s$ (wall in axial compression); $\eta = k_1 \eta_s$ (wall in axial tension); $\eta_s = \begin{cases} 0.75 & \text{for } f'_m \ge 9\text{ MPa} \\ 0.55 & \text{for } f'_m \le 6\text{ MPa} \end{cases}$; $k_0 = \begin{cases} 1.3 & H/L \le 1.0 \\ 1.0 & H/L \ge 1.5 \end{cases}$; $k_1 = (1 - \alpha_s \rho_h f_{yh}) \ge (1 - 0.1\alpha_s A_{gn} f'_m)$; $\alpha_s = 0.45\text{ MPa}^{-1}$; if $(\rho_h f_{yh}) > (0.1\alpha_s A_{gn} f'_m)$, then η_s should be multiplied by $\{0.1A_{gn} f'_m / (\rho_h f_{yh})\}$.	(5.2)
Peru (NT E.070 2019)	$V_{des} = V_{mas} = F_S\{0.5 f_{AR} v_{md} + 0.23\sigma\}A$ (For clay and concrete units) $V_{des} = V_{mas} = F_S\{0.35 f_{AR} v_{md} + 0.23\sigma\}A$ (For silica lime units) where, $1/3 \le f_{AR} = V_b L/M \text{ or } L/H \le 1$	(5.3)
Chile (NCh2123 2003)	$V_{des} = V_{mas} = \{F_S(0.45v_{md} + 0.24\sigma)A\} \le 0.35 v_{md} A$	(5.4)
Argentina (INPRES-CIRSOC 103 2018)	$V_{des} = V_{mas} = \{F_S(v_{md} + 0.4\sigma)A\} \le 2F_S v_{md} A$	(5.5)
Colombia (NSR-98 2010)	$V_{des} = V_{mas} = \left\{F_S\left(0.08\sqrt{0.75 f'_m} + 0.33\sigma\right)A_w\right\} \le 0.17F_S\sqrt{0.75 f'_m}A_w$	(5.6)
Costa Rica (CSCR 2002)	$V_{des} = V_{mas} + V_{wr}$ where, $V_{mas} = F_S\left(0.5\sqrt{f'_m} + 0.3\sigma\right)0.8A$; $V_{wr} = \left(A_{sh} f_{yh} d_{sc}\right)/s_h$	(5.7)
Eurocode EN 1996-1-1 (CEN 2005)	$V_{des} = V_{mas} = \left(1/\gamma_{m,masonry}\right)(v_{mk0} + 0.4\sigma)A = 0.5(v_{mk0} + 0.4\sigma)A$	(5.8)
China (GB50003 2011)	$V_{des} = V_{mas} + V_{tc}$ where, $V_{mas} = F_s \eta_c v_{md}(A - A_{cc})$; $V_{tc} = F_s\left(\xi_c f_{tcc} A_{cc} + 0.08 f_{ylc} A_{slc}\right)$; η_c = 1.1 if column spacing < 3 m, else 1; ξ_c = 0.5 for one central column, 0.4 for more than one	(5.9)
India (BIS CED-39 2021*)	$V_{des} = V_{mas} = \{F_S f_{AR}(0.5v_m + 0.4\sigma)A\} \le 1.5 v_m A$ where, $f_{AR} = \begin{cases} 1.55 & H/L \le 0.2 \\ (1.7 - 0.7H/L) & 0.2 < H/L \le 1.0 \\ 1.0 & H/L > 1.0 \end{cases}$	(5.10)

* Code under development

5.2.1.1 Contribution of masonry wall

The contribution of V_{mas} in shear strength depends on the physical model describing the failure mechanism. In diagonal shear failure (Fig. 5.1c), shear cracks are caused by principal tensile stresses developed in the masonry wall under the action of lateral loads (tensile strength hypothesis). On the other hand, the resistance offered against shear sliding in masonry under the action of the lateral loads (Fig. 5.1b) is developed by friction and adhesion between bricks and mortar (friction hypothesis). Design shear strength of CM wall at the onset of cracking is based on either of these two hypotheses. Once cracking initiates, the vertical axial compression improves its shear resistance by developing frictional forces across the cracks (Yoshimura et al. 2000). According to most of the codes, the generalized equation (Eq. 5.11) for estimation of V_{mas} can be expressed as a combination of important parameters:

$$V_{mas} = F_S (av_{md} + b\sigma) f_{AR} A_d \tag{5.11}$$

where, a (varies from 0.16 to 1.1) and b (varies from 0.23 to 0.4) are the constants to take care of different proportions of v_{md} and σ considered in design codes indicating that most of the codes try to remain quite conservative by limiting the shear strength. The effect of overburden pressure is not included in the Chinese code (i.e., b = 0). f_{AR} is the wall aspect ratio factor (varies from 0.33 to 1.55) and is considered only in codes of Mexico, India, and Peru; F_s is the strength modification factor and mainly ranges from 0.4 to 0.8 for most of the codes; however, the value is more than 1 for the Chinese code; the cross-sectional area A_d includes the area of tie-columns with the masonry wall section in most codes, but not all and is considered differently (around 80% to 100% of total gross-section) in different design codes; σ is overburden pressure on the CM wall; and v_{md} is the design shear strength of masonry due to tension, which is obtained from the diagonal compression test (giving v_m) with appropriate design factor. However, in Eurocode 6, it is the characteristic initial shear strength of masonry under zero compressive stress (v_{mk0}) due to shear sliding obtained from the triplet test. Further, Colombian and Costa Rican codes consider shear strength of masonry in terms of $\sqrt{f'_m}$ as an estimate of the v_{md}. Codes use different safety factors for the evaluation of the design value of masonry shear strength as given in Table 5.2 when the experimentally obtained value is utilized in design equations. Again, codes recommended indicative values of shear strength of masonry (Table 5.3), if the experimental data are not available.

Table 5.2: Design shear strength of masonry (v_{md}) from the experimental value.

Country Code	Mathematical relationships	Eq.
Mexico (NTC-M 2017)	$v_{md} = \dfrac{v_m}{1+2.5c_v}$	(5.12)
Peru (NT E.070 2019)	$v_{md} = v_m - \text{SD}$	(5.13)
Chile (NCh2123 2003)	$v_{md} = v_m - 0.431\times(v_{m5} - v_{m1})$	(5.14)
Argentina (INPRES-CIRSOC 103 2018)	$v_{md} = 0.75v_m(1-1.45c_v)$	(5.15)
Eurocode EN 1996-1-1 (CEN 2005)	$v_{mk0} = 0.8v_{m0}$	(5.16)
China (GB50003 2011)	$v_{md} = \dfrac{1}{1.8}(v_m - 1.645\text{SD})$	(5.17)
India (BIS 2021)	$v_{md} = v_m$	(5.18)

Table 5.3: Design shear strength of masonry (v_{md}) from indicative values recommended in codes.

Country Code	Indicative value of shear strength of masonry (v_{md})	Remarks
Mexico (NTC-M 2017)	0.2 MPa	Unit: crafted solid clay brick, extruded clay brick, concrete block, solid or concrete brick Mortar: must comply the standard Masonry: Type I
Peru (NT E.070 2019)	$v_{md} \le 0.319\sqrt{f'_m}$ or, 0.5 MPa to 1.1 MPa (when test data for f'_m is not available)	Unit: different class, different type - clay, concrete, silica lime; 4.9 MPa to 17.6 MPa Mortar: 1:4 for clay otherwise 1:0.5:4 Masonry: 3.4 MPa to 10.1 MPa.
Chile (NCh2123 2003)	0.2 MPa to 0.6 MPa	Unit: different class, 4.5 MPa to 16 MPa Mortar: 5 MPa to 15 MPa
Argentina (INPRES-CIRSOC 103 2018)	0.15 MPa to 0.26 MPa	Unit: solid ceramic brick, hollow ceramic and hollow concrete block Mortar: normal, intermediate and high strength with 5 MPa to 15 MPa.
Eurocode EN 1996-1-1 (CEN 2005)	0.1 MPa to 0.4 MPa	Unit: different type – clay, calcium silicate, aggregate concrete, autoclaved aerated concrete, manufactured stone, dimensioned natural stone Mortar: general-purpose (1 MPa to 20 MPa), thin layer, light mortar
China (GB50003 2011)	$v_{md} = \zeta_N\, v_{m0}$ where, ζ_N =0.8 to 3.92; v_{m0} = 0.06 MPa to 0.17 MPa	ζ_N =0.8 to 2.05 for solid and perforated brick, and 1.23 to 3.92 for concrete block depending on masonry type v_{m0} = 0.06 MPa to 0.17 MPa are based on: Unit: solid or perforated clay brick, solid or perforated concrete brick, autoclaved sand-lime or flyash-lime brick, concrete and light aggregate concrete block, rubble Mortar: 2.5 to more than 10 MPa
India (BIS 2021)	$v_{md} = 0.16\sqrt{f'_m}$ when test data is not available: $f'_m = 4 \times$ permissible compressive stress ≈ 1 MPa – 12.2 MPa	Permissible compressive stress is obtained from IS 1905 for: Unit: 3.5 MPa to 40 MPa Mortar: 0.5 MPa to 10 MPa.

5.2.1.2 Contribution of tie-columns

The contribution of the tie-columns (V_{tc}) in the shear resistance comes mainly after severe cracking in masonry wall (Meli et al. 2011). Some experimental investigations also observed that the lateral strength of CM wall is affected by the reinforcement in tie-elements (Kato et al. 1992, Quiroz et al. 2017). The longitudinal reinforcement in tie-columns contributes to shear capacity by the dowel action (Tomaževič and Klemenc 2007a, Riahi et al. 2007, Bourzam et al. 2008a). On the contrary, a few studies have also reported that the longitudinal reinforcements in tie-columns mainly improve the ductility of CM walls and their effect on lateral strength is insignificant (Marques and Lourenço 2013). Most of the design codes estimate the design shear at the onset of cracking while neglecting the contribution from longitudinal reinforcement of tie-columns; however, the cross-sectional area of tie-columns is considered in the overall sectional area of the wall. The Chinese code (GB50003 2011) considers the contribution to the shear strength of CM wall by the concrete and reinforcement used in the central tie-column or constructional column if any (Eq. 5.19 as well as Eq. 5.9):

$$V_{tc} = F_s \left(\xi_c f_{tcc} A_{cc} + 0.08 f_{ylc} A_{slc} \right) \tag{5.19}$$

where, ξ_c is the participation service factor of the central constructional column and the value is 0.5 if one column is arranged in the center, 0.4 if more than one column is arranged; f_{tcc} is the tensile strength of concrete in the constructional column; f_{ylc} is the yield strength of longitudinal rebar in the constructional column; A_{cc} is the total cross-sectional area of middle constructional columns; and A_{slc} is the total area of longitudinal reinforcement in them.

5.2.1.3 Contribution of horizontal reinforcement in wall

The seismic response of CM walls can be improved by placing horizontal reinforcement within the mortar joints anchored into the tie-columns. The bed-joint reinforcement helps to delay the formation of diagonal cracks in masonry walls (Aguilar et al. 1996, Kumazawa, and Ohkubo 2000, Cruz et al. 2019). However, this approach is not commonly adopted in practice in some countries because of the unavailability of small diameter bars with a high yield stress, the use of low strength masonry that inhibit improvement in the shear strength due to joint reinforcement, and the associated costs in providing additional steel. Moreover, limited experimental research on the influence of horizontal reinforcement on shear strength deter some code developers from adopting such reinforcement. Design codes of Mexico and Costa Rica consider the contribution of the horizontal rebars (V_{wr}) in V_{des} as shown in Eqs. (5.2) and (5.7).

5.2.2 Estimation of Design Shear Strength

Table 5.4 shows the design value of shear strength of confined masonry wall along with the variation in the values of different input parameters for the tested CM walls - S1, S2, and S3 (details are given in Chapter 3) obtained using nine different codes. As the specimens had no central tie-column (single bay wall), so tie-columns' contribution part is zero (V_{tc} = 0), but the area of tie-columns was included while calculating the cross-sectional area of the walls in most of the codes as also discussed earlier. Further, the contribution of horizontal reinforcement is not considered (V_{wr} = 0), as these bars were not provided in the tested specimens. Thus, V_{des} will be governed by only V_{mas}. In Mexican and Indian code, the shear strength for the squat walls having H/L (ratio of total height to total length) less than 1 (i.e. S3 of H/L = 0.93) is enhanced using the factor f_{AR}. On the other hand, the shear strength of slender walls having H/L greater than 1 (i.e. S1 and S2 of H/L = 1.63 and 1.3, respectively) is reduced by a similar factor in the Peruvian code; this factor is applied on the first part of the equation only, i.e., on v_{md} (Eq. 5.3). v_{md} obtained using the experimental data with different factors for different codes is found to vary from 0.17 MPa (in Colombia) to 0.44 MPa (in India), i.e., a difference of about 2.6 times. Similarly, considering all factors, the estimated V_{des} finally underlines a difference of about 3 times between the maximum (for Argentina) and the minimum (for Peru and Chile) values predicted for the three considered specimens.

Table 5.4: Different parameters in Eq. (5.11) and estimation of design shear strength for specimen S1, S2, and S3 using Eqs. (5.1) to (5.11).

Country Code	F_s	a	b	f_{AR} for S1	f_{AR} for S2	f_{AR} for S3	v_{md} (MPa)	σ (MPa)	A_d	$V_{des} = V_{mas}$ (kN) S1	S2	S3
Mexico	0.70	0.50	0.30	1.00	1.00	1.04	0.37	0.13	A	19.8	24.7	36.2
Peru	0.55	0.50*b	0.23	0.62	0.77	1.00	0.41	0.13	Lt_e	10.8	16.1	28.2
Chile	0.50	0.45	0.24		-		0.43	0.13	A	11.7	14.6	20.4
Argentina	0.80	1.00	0.40		-		0.30	0.13	A	34.9	43.6	61.0
Colombia	0.60	1.00	0.33		-		0.17*d	0.13	A_w	11.7	15.6	23.4
Costa Rica	0.40*a	0.16	0.24		-		0.36*e	0.13	0.8A	11.7	15.5	23.3
Europe	0.50	1.00	0.40		-		0.35*f	0.13	A	25.3	31.6	44.2
China	1.11	1.00*c	0		-		0.22	0.13	A-A_{cc}	30.0	37.6	52.6
India	0.80	0.50	0.40	1.00	1.00	1.05	0.44	0.13	A	27.2	34.0	49.9

*a F_s = 0.6, 0.55, and 0.4 for Class A, B, and C masonry, respectively;
*b a = 0.5 for clay and concrete masonry units, and 0.35 for silica lime units;
*c a = 1.1 if constructional column spacing < 3 m, else 1;
*d $0.08\sqrt{0.75 f'_m}$ instead of v_{md}; *e $\sqrt{f'_m}$ instead of v_{md}; *f v_{mk0} instead of v_{md}

5.3 Flexural Strength Provisions

Masonry members are subjected to flexural stresses due to lateral loads or eccentricity of gravity loads. Though flexural failure is not a common failure mode in CM walls, the walls with higher aspect ratio or higher moment-to-shear ratio are susceptible to it (Gavilán 2020, Varela-Rivera et al. 2019). Walls are subjected to compression stresses at one end and tensile stresses at the other. Flexural damage is characterized by horizontal cracking in wall and yielding of longitudinal reinforcement in tie-columns on the tension side of the wall, along with crushing of bricks or concrete on the compression side. A mixed shear-flexure failure mechanism has been more frequently observed in case of CM walls (Marques and Lourenço

2019). Several other factors, like vertical axial load and the amount of longitudinal steel in the tie-columns affect the flexural capacity of CM walls.

5.3.1 Contribution of Different Elements

Under the combined action of axial load and in-plane bending moment, the flexural capacity of a CM wall can be evaluated based on the moment developed for an equilibrium of forces in the cross-section of the wall (Fig. 5.2). The strain diagram shows that a portion of the panel is in tension, while the remaining portion is in compression. It is usually assumed that the masonry and concrete are not able to resist tension, thus longitudinal reinforcement in the tension tie-column resists all the tensile stresses and the compression stresses are resisted by concrete, masonry, and longitudinal reinforcement in the compression zone as shown in Fig. 5.2. Estimation of design flexural strength (M_{des}) for CM walls is recommended in six design codes as given in Table 5.5. Most of the codes use the assumption of triangular stress distribution of compression stresses. However, Eurocode 6 does not consider the contribution of compression steel for flexural strength estimation and considers rectangular stress distribution (CEN 2005, Marques and Lourenço 2019). In general, the design flexural strength of CM walls (M_{des}) is obtained as a combined strength from: (i) tension and compression stresses in longitudinal steel of tie-columns (M_{sl}), and (ii) flexural compressive stress on the masonry wall (M_p) as given in Eqs. (5.20) and (5.21) as:

$$M_{des} = M_{sl} + M_p \tag{5.20}$$

$$M_{des} = F_M\, p\left(f_{yl} A_{sl} d_s\right) + q\left(P d_{sc}\right) \tag{5.21}$$

here, p and q are the factors governing the contribution of the two terms mentioned above.

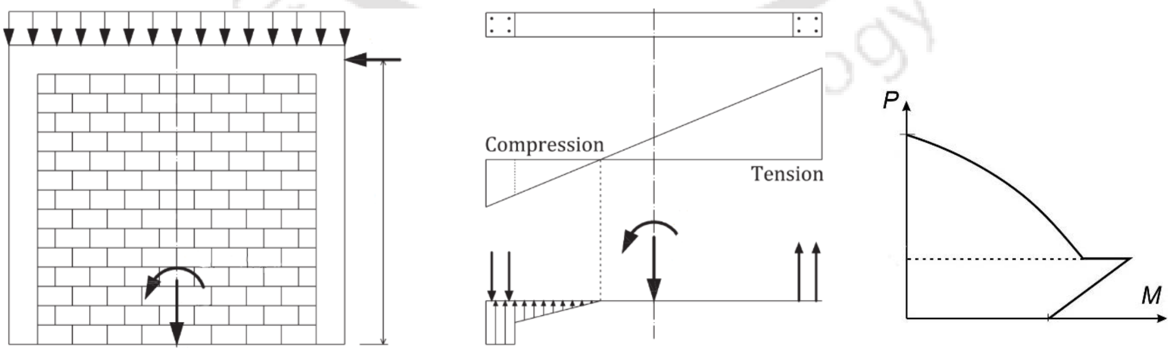

(a) (b) (c)

Figure 5.2: CM wall subjected to combined axial and bending loads: (a) forces acting on the wall, (b) strain and internal force distributions, (c) interaction diagram (Meli et al. 2011, BIS 2021).

Table 5.5: Estimation of the in-plane moment of resistance of CM wall.

Country Code	Equation for M_{des}	Eq.
Mexico (NTC-M 2017)	$M_{des} = F_M f_{yl} A_{sl} d_s + 0.3Pd_{sc}$ if $0 \le P \le P_D/3$ $M_{des} = \left(1.5F_M f_{yl} A_{sl} d_s + 0.15P_D d_{sc}\right)\left(1 - P/P_D\right)$ if $P > P_D/3$	(5.22)
Peru (NT E.070 2019)	$M_{des} = F_M \left\{ f_{yl} A_{sl} \left(0.8L\right) + 0.9P\left(0.5L\right) \right\}$	(5.23)
Chile (NCh2123 2003)	$M_{des} = 0.5F_M f_{yl} A_{sl} d_s + 0.2Pd_{sc}$ if $0 \le P \le P_D/3$ $M_{des} = \left(1.5 \times 0.5F_M f_{yl} A_{sl} d_s + 0.1P_D d_{sc}\right)\left(1 - P/P_D\right)$ if $P > P_D/3$	(5.24)
Costa Rica (CSCR 2002)	$M_{des} = F_M A_{sl} f_{yl} \left(0.5L\right)\left(1 + \frac{P}{A_{sl} f_{yl}}\right)\left(1 - \frac{c_1}{L}\right)$ where, $\frac{c_1}{L} = \frac{(\alpha + \beta)}{(2\alpha + 0.72)}$, $\alpha = \frac{A_{sl} f_{yl}}{tLf'_m}$, and $\beta = \frac{P}{tLf'_m}$	(5.25)
Eurocode EN 1996-1-1 (CEN 2005)	$M_{des} = \left(1/\gamma_{m,masonry}\right) f_{yl} A_{sl} (d_{sc} - 0.4x) + P(0.5L - 0.4x)$ where, $x = \frac{P + A_{sl}\left(f_{yl}/\gamma_{m,steel}\right)}{0.8 \times 0.85\left(f'_m/\gamma_{m,masonry}\right)t}$	(5.26)
India (BIS 2021)	$M_{des} = F_M f_{yl} A_{sl} d_s + 0.3Pd_{sc}$ if $0 \le P \le P_D/3$ $M_{des} = \left(1.5F_M f_{yl} A_{sl} d_s + 0.15P_D d_{sc}\right)\left(1 - P/P_D\right)$ if $P > P_D/3$	(5.27)

In design codes of Mexico, Chile, and India, two separate equations are recommended for design flexural strength estimation for two different ranges of axial load (low and high): $0 < P \le P_D/3$ and $P > P_D/3$, where, P is the axial compressive load on the CM wall, and P_D is the design axial compressive strength of CM wall. Under low axial load condition, p is one for most of the codes (except 0.5 in Chile), and q ranges from 0.2 to 1. Whereas under high axial load condition, p varies from 0 to 1, and q varies from 0 to 0.1. F_M is the strength modification factor for the first term and it ranges from 0.65 to 0.9; d_s and d_{sc} are the lever arm factors for the moment generated in the two terms.

5.3.2 Estimation of Design Axial Compressive Strength

The cross-section of a CM wall is composed of the cross-sectional area of a masonry wall and adjacent RC confining columns. When a CM wall is subjected to a uniformly distributed vertical load at the top tie-beam, the wall is assumed to behave monolithically with an equal vertical deformation for the three sections. The vertical reactive force at the wall base in each three material sections is proportional to the stiffness and cross-sectional area of the material, which provides the individual contribution to the resistance to compressive loading. The equations for P_D recommended in different codes are provided in Table 5.6.

Table 5.6: Design compressive strength of CM wall.

Country Code	Equations for P_D	Eq.
Mexico (NTC-M 2017)	$P_D = F_P F_E (f'_{md} A + \sum A_{sl} f_{yl})$ where, $F_E = (1-(2e_c/t))\{1-(H_e/30t)^2\}$	(5.28)
Chile (NCh2123 2003)	$P_D = 0.4 F_E f'_m A$, where, $F_E = 1-(H/40t)^3$	(5.29)
India (BIS 2021)	$P_D = F_E (0.4 f'_m A_w + 0.45 n f_{ck} A_c + 0.75 n f_{yl} A_{sl})$ where, F_E is taken from Table 9 of IS 1905 (1987)	(5.30)

The design compressive strength (P_D) of confined masonry walls recommended in a few design codes can be suitably represented by Eqs. (5.31) and (5.32) as:

$$P_D = P_m + P_{tc} \tag{5.31}$$

$$P_D = F_P F_E \left\{ c\left(f'_m A_w\right) + d\left(n f_c A_c\right) + e\left(n f_{yl} A_{sl}\right) \right\} \tag{5.32}$$

As given in these equations, P_D is a function of the vertical compressive resistances of the masonry wall (P_m), and resistance of tie-columns including the contribution from concrete and longitudinal steel (P_{tc}) in the tie-columns. Here c, d, and e are the constants governing the contribution of three terms given in the equation, n is the number of tie-columns in the CM wall, A_c is the cross-sectional area of concrete in tie-column excluding the cross-sectional area of the longitudinal reinforcing steel in the tie-column, A_{sl} is the total area of longitudinal steel in each end tie-column, F_P is the strength modification factor, and F_E is a reduction factor allowing for the effects of slenderness and eccentricity of loading. The values of different factors used in different codes are compared by evaluating P_D for the specimens tested in the current study (as given in Chapter 3). As shown in Table 5.7, the Chilean code (Eq. 5.29) considers only the contribution of masonry in P_D estimation (d = 0, e = 0 in Eq. 5.32). In addition to masonry, Mexican code (Eq. 5.28) also considers the contribution of longitudinal steel in tie-columns without considering the concrete contribution. However, all three terms are considered in the draft Indian code (Eq. 5.30). It is to be noted that for Mexico and Chile code: $A_w = A$ in Eq. (5.32).

Table 5.7: Estimation of design axial strength for specimen S1, S2, and S3 using Eq. (5.32).

Sl. No.	Country Code	F_P	F_E	c	d	e	n	P_D (kN)		
								S1	S2	S3
1	Mexico	0.6	0.90	0.73	0	1.00	2	322.3	386.1	513.8
2	Chile	1.0	0.97	0.40	0	0	2	251.2	314.0	439.5
3	India	1.0	0.81	0.40	0.45	0.75	2	579.6	632.2	737.5

5.3.3 Estimation of Design Flexural Strength

Table 5.8 gives values of all the input parameters used in Eq. (5.21) and the estimated design flexural strengths (M_{des}) for the tested specimens S1, S2, and S3. For all the tested specimens, P is less than $P_D/3$, thus the final M_{des} were considered for that axial load condition. In Table 5.8, considerable variation of the input parameters can be observed for different codes; variation of d_s and d_{sc} showed that both the terms are about 0.5L for the Costa Rican code (also in Eq. 5.25), i.e., the values are minimum for the Costa Rican code. From the comparison of M_{des} for different codes, it was observed that the Costa Rican code predicts the lowest value of M_{des}, while the European and Indian codes predict the highest, which is almost twice as large.

Table 5.8: Estimation of design flexural strength for S1, S2, and S3 using Eq. (5.21).

Sl.	Country Code	Axial load condition	F_M	p	d_s	q	P	d_{sc}	M_{des} (kNm) S1	S2	S3
1	Mexico	$0 \le P \le P_D/3$	0.80	1.00	L-b_t	0.30	P	L-0.5b_t	48.0	63.1	95.1
		$P > P_D/3$	0.60	1.43*	L- b_t	0.14*	P_D	L-0.5b_t	-	-	-
2	Peru	-	0.65	1.00	0.8L	0.90	P	0.5L	37.0	47.8	71.1
3	Chile	$0 \le P \le P_D/3$	0.90	0.50	L- b_t	0.20	P	L-0.5b_t	27.5	36.3	55.0
		$P > P_D/3$	0.90	1.40*	L- b_t	0.09*	P_D	L-0.5b_t	-	-	-
4	Costa Rica	-	0.76	1.00	0.5L(1-c_1/L)	0.76	P	0.5L(1-c_1/L)	25.9	34.7	54.6
5	Europe	-	0.87	1.00	L-0.5b_t -0.4x_u	1.00	P	0.5L-0.4x_u	51.9	69.5	107.9
6	India	$0 \le P \le P_D/3$	0.87	1.00	L- b_t	0.30	P	L-0.5b_t	51.8	68.0	102.2
		$P > P_D/3$	0.87	1.45*	L- b_t	0.14*	P_D	L-0.5b_t	-	-	-

* when $P > P_D/3$: p= 1.5(1-P/P_D), q = 0.15(1-P/P_D) for Mexico and India and p = 0.75(1-P/P_D), q = 0.10(1-P/P_D) for Chile. b_t = width of a tie-column = 125 mm; x_u = depth to the neutral axis of the wall section from compression side = 244.4 mm; c_1/L = 0.13, 0.12, 0.10 for S1, S2, and S3, respectively.

5.4 Comparative Assessment of Codes

5.4.1 Assessment using Present Experimental Results

In order to assess the safety margins in different codes, the design shear strength (V_{des}) and design flexural strength (M_{des}) of the three tested specimens were compared with the experimental results. From the codal formulation, it can be noticed that the design values of shear for CM wall (Table 5.1) are mainly based on the cracking of masonry wall (i.e., the contribution of tie-columns is not directly considered), so V_{des} was first compared with the experimental lateral load at cracking ($V_{cr,e}$) as shown in Fig. 5.3(a). The ratio ($V_{des}/V_{cr,e}$) obtained using different codes varies from 0.32 to 1.02 for S1, 0.38 to 1.14 for S2, and 0.34

to 1 for S3. Comparatively, Argentinian, Chinese, and Indian codes recommend a higher shear value for design with the ratio ranging from 0.8 to 1.14, indicating lesser safety margins. On the other hand, codes such as - Peru, Chile, Colombia, and Costa Rica provide higher safety margins by recommending the strength ratios varying from 0.32 to 0.46.

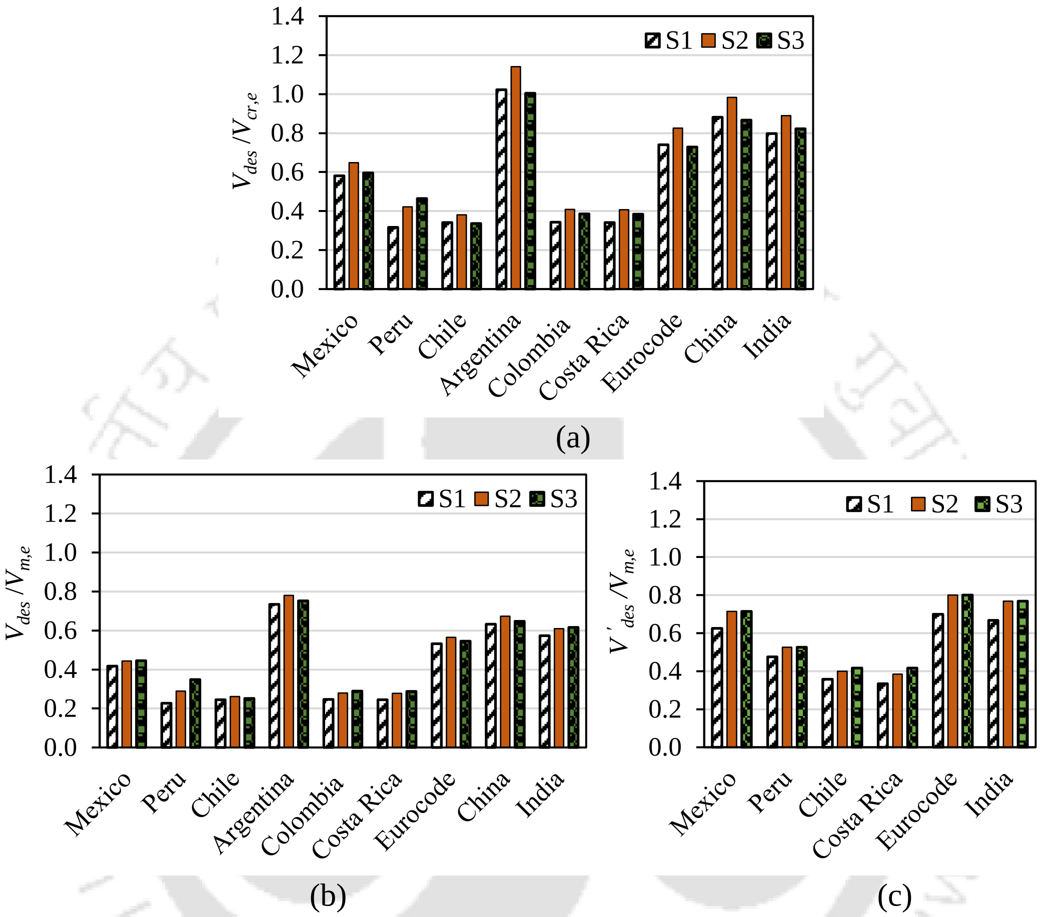

Figure 5.3: Comparison of (a) design shear and shear strength at cracking, (b) design shear and lateral strength, and (c) shear from design flexural strength and lateral strength.

Similarly, as shown in Fig. 5.3(b), if the design shear strength values are compared with the experimentally obtained lateral strengths, the ratio ($V_{des}/V_{m,e}$) obtained using different codes varies from 0.23 to 0.73 for S1, 0.26 to 0.78 for S2, and 0.25 to 0.75 for S3; i.e., a reduction of around 1.4 times, as the peak lateral strength was around 1.4 times the cracking lateral load. Subsequently, for the comparative assessment in flexure, M_{des} was first approximately converted to equivalent lateral load (V'_{des}) by dividing it with the height of the wall (H). Fig. 5.3(c) illustrates the comparison of $V'_{des}/V_{m,e}$ ratio obtained for different codes (0.3 to 0.7 for S1, and 0.4 to 0.8 for S2 and S3). It has to be noted that the lateral strength ratio (design-to-experimental) obtained from flexure theory may not actually represent the safety margin, as the failure may not correspond to flexure. To gain more clarity on this, section analysis was carried out using the mean values of the material strengths to evaluate the moment capacity of the CM walls. The obtained yield moment capacities were 55 kNm, 77 kNm, and 118 kNm, and the ultimate moment capacities were 76 kNm, 103 kNm, and 151 kNm for S1, S2, and S3, respectively. The obtained equivalent lateral loads at yield moment (37 kN, 51 kN, and 79 kN for S1, S2, and S3, respectively) were lesser than $V_{m,e}$, but higher than the cracking load ($V_{cr,e}$). This comparison highlights that the moment at yielding in all the specimens was attained after reaching $V_{cr,e}$. Similarly, the equivalent lateral loads obtained from the ultimate moment were 51 kN, 69 kN, and 101 kN for S1, S2, and S3, respectively. In case of the wall S1, the equivalent load was almost equal to $V_{m,e}$, whereas, for the other two specimens it was significantly higher than $V_{m,e}$. It can be inferred from here that the slender specimen S1 reached its flexural capacity, but the other two specimens did not. In addition, considering that the flexure capacity of walls S2 and S3 is higher than their shear capacity, the estimated $V'_{des}/V_{m,e}$ values should be significantly higher and dissimilar from the values that were obtained for wall S1.

5.4.2 Assessment using Past Experimental Results

In addition to the three specimens tested in the present study, nine CM walls tested in past studies were also investigated by estimating the design values of shear and flexural strengths using different seismic codes (as given in Tables 5.9 and 5.10). In these nine solid, single-story, single-bay CM specimens, H/L varies from 0.62 to 1.62. Out of these, two specimens can be categorized as slender with H/L = 1.62 (ID 6) and 1.52 (ID 7); these are comparable with S1 and S2. Similarly, four specimens can be categorized as relatively squat with H/L = 0.97 to 1 (ID: 1, 4, 5, 8); these are comparable with S3. Longitudinal reinforcement percentage in tie-columns of these specimens (ρ_l) varies from 0.79 to 2.82, and σ varies from 0 to 0.5 MPa. Material properties such as: f'_m varies from 3.5 to 9 MPa; v_m varies from 0.25 to 1.1 (minimum strength for specimen 1 of Aguilar et al. 1996; and maximum strength for specimen 6 of Bourzam et al. 2008a); f_c and f_{yl} are almost similar with the present specimens.

Values of the input parameters for the design lateral strength estimation of CM wall, such as, v_{md}, f_{AR}, and P_D obtained for all the twelve specimens are shown in Fig. 5.4. The coefficient of variation (c_v) for the estimation of v_{md} was assumed as 0.2. The maximum values of v_{md} obtained by all the codes correspond to the test specimens of Bourzam et al. (2008a) as the experimentally obtained v_m (=1.1) was very high (Fig. 5.4a); however, Colombian and Costa Rican codes consider $\sqrt{f'_m}$ as an estimate of v_{md}, which resulted in lesser values compared to others as f'_m was comparatively lesser. Further, v_m was used as v_{m0} for Eurocode as the triplet test data was not provided in these past studies. Overall, the draft Indian code directly considers experimentally obtained shear strength as v_{md}; naturally v_{md} values given by the other codes are lesser. In some cases, the Costa Rican code also gives higher v_{md} in terms of $\sqrt{f'_m}$. On the other hand, the Chinese and Colombian codes always give lower v_{md} values. The additional influence of aspect ratio of CM walls has been considered in the codes of Mexico, Peru, and India by using f_{AR} primarily for either squat or slender specimens as shown in Fig. 5.4(b).

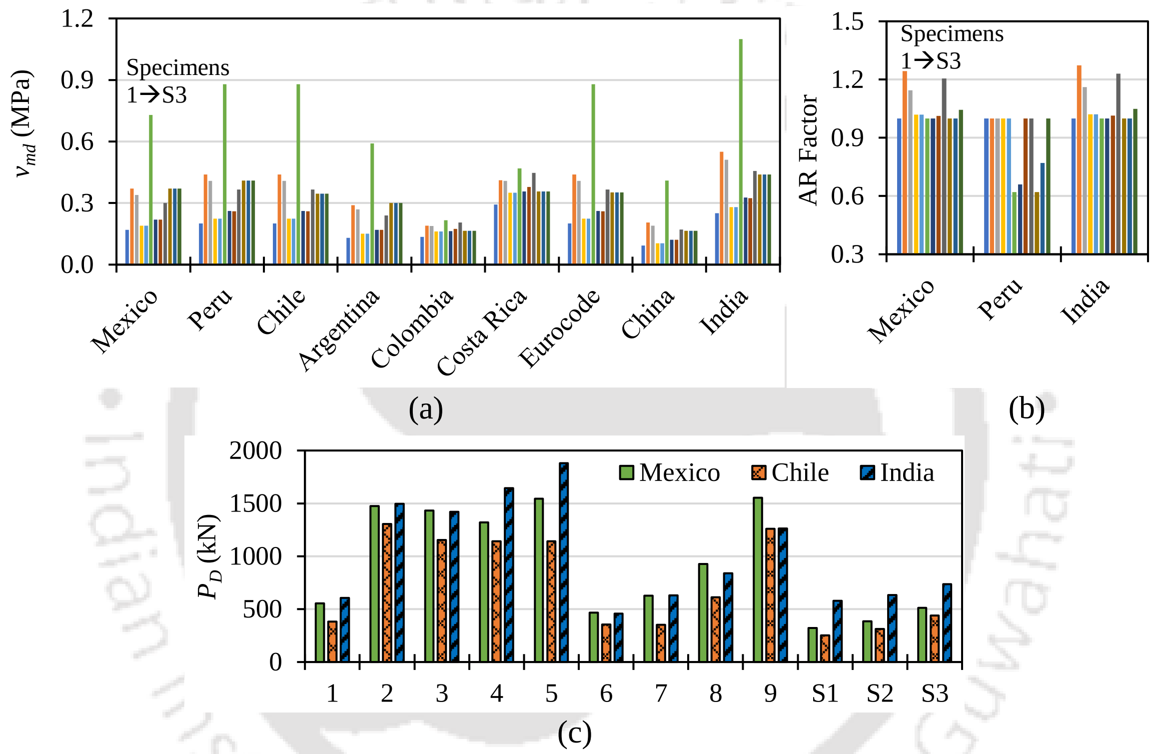

Figure 5.4: Variation in different parameters for the twelve specimens: (a) design shear strength of masonry (v_{md}), (b) wall aspect ratio factor, and (c) design axial resistance (P_D).

For example, shear strength of the squat specimen (H/L = 0.62) tested by Yáñez et. al (2004) is enhanced by 1.24 or 1.27 when the codes of Mexico or India are used, respectively. Similarly, shear strength of the slender specimen (H/L = 1.62) tested by Bourzam et. al (2008a) was reduced by 0.62 when Peru code was used. Further, Fig. 5.4(c) shows a significant variation in P_D due to the difference in material and geometric properties of the specimens. The rest of the input parameters for the estimation of V_{des} and M_{des} can be obtained from Tables 5.4 and 5.8, respectively. It is to be noted that for all the specimens, the reported ultimate failure mode was shear failure.

The design-to-experimental strength ratios (global safety factors) under shear and flexure for all twelve specimens were evaluated as given in Tables 5.9 and 5.10. In Table 5.9(a), the design shear strength is compared against the experimental shear at cracking, and significant variation was observed in the safety margins in different codes against shear failure ($V_{des}/V_{cr,e}$ ranges from 0.21 to 1.31). Some of the codes, such as Peruvian and Chilean codes provide a higher safety margin (i.e. lower value of $V_{des}/V_{cr,e}$) compared to some other codes, such as, draft Indian, Argentinian, Chinese codes, and Eurocode. Even after considering all the partial safety factors associated with the design shear strength of CM wall, the ratio $V_{des}/V_{cr,e}$ was greater than one for some cases. Again, to gain more knowledge on the results, the design shear strengths were also compared against the experimental lateral strength ($V_{des}/V_{m,e}$) as shown in Table 5.9(b), which shows that the predicted design values are higher (say $V_{des}/V_{m,e}$ > 0.75) with draft Indian, Argentinian codes, and Eurocode.

Further, the variation of equivalent $V'_{des}/V_{m,e}$ ratio under flexure is shown in Table 5.10, where it can be noticed that the ratio varies from 0.3 to 1.7. The values indicate that codes, such as Mexican, Peruvian, Indian, and Eurocode estimate relatively high design flexural strength for most specimens. A combined shear and flexure behavior in terms of design-to-experimental lateral strength is shown in Fig. 5.5 to provide a simplistic visual comparison between different codes. The blank spaces in Table 5.10, as well as the bar diagram (Fig. 5.5), indicate that some codes (Argentina, Colombia, and China) do not have design flexural strength provisions. The high variability in the design-to-experimental strength ratios, i.e., the safety margins, obtained from all the codes against shear and flexural failure mode for the twelve specimens indicates the inconsistencies in the design force estimation.

Table 5.9(a): Comparison of safety margins against shear (at cracking).

Study	ID	H/L	$\frac{V_{cr,e}}{V_{m,e}}$	$V_{m,e}$ (kN)	For Shear Resistance: $V_{des}/V_{cr,e}$								
					Mexico (2017)	Peru (2019)	Chile (2003)	Arg (2018)	Col (2006)	CR (2002)	EC (2005)	China (2011)	India (2021)
Aguilar et. al (1996)	1	1.00	0.73	140.6	0.49	0.35	0.21	0.65	0.48	0.35	0.60	0.31	0.78
Yáñez et. al (2004)	2	0.62	0.67	191	0.74	0.56	0.46	1.09	0.47	0.75	1.03	1.06	1.31
M and C (2004)	3	0.77	0.66	215.4	0.71	0.51	0.44	1.07	0.53	0.47	0.90	0.71	1.19
Zabala et. al (2004)	4	0.97	0.70	118	0.76	0.61	0.52	1.28	0.83	0.79	1.07	0.84	1.26
Zabala et. al (2004)	5	0.97	0.68	207	0.61	0.45	0.33	0.99	0.62	0.51	0.78	0.49	0.98
Bourzam et. al (2008a)	6	1.62	0.86	81.4	0.52	0.31	0.37	0.91	0.26	0.31	0.79	0.69	0.87
Gavilán et. al (2015)	7	1.52	0.94	75.8	0.50	0.31	0.25	0.78	0.45	0.35	0.64	0.38	0.81
Gavilán et. al (2015)	8	0.98	0.64	157	0.56	0.41	0.28	0.84	0.55	0.43	0.70	0.41	0.89
Gavilán et. al (2015)	9	0.67	0.78	320.8	0.46	0.29	0.23	0.63	0.37	0.41	0.51	0.34	0.75
Present Study	S1	1.63	0.72	47.5	0.58	0.32	0.34	1.02	0.34	0.34	0.74	0.88	0.80
Present Study	S2	1.30	0.68	55.8	0.65	0.42	0.38	1.14	0.41	0.41	0.83	0.98	0.89
Present Study	S3	0.93	0.75	81.15	0.60	0.46	0.34	1.00	0.39	0.38	0.73	0.87	0.82

Arg = Argentina; Col = Colombia; CR = Costa Rica; EC = Eurocode; M and C = Marinilli and Castilla

Table 5.9(b): Comparison of safety margins against shear (at maximum strength).

Study	ID	H/L	$\frac{V_{cr,e}}{V_{m,e}}$	$V_{m,e}$ (kN)	For Shear Resistance: $V_{des}/V_{m,e}$ Mexico (2017)	Peru (2019)	Chile (2003)	Arg (2018)	Col (2006)	CR (2002)	EC (2005)	China (2011)	India (2021)
Aguilar et. al (1996)	1	1.00	0.73	140.6	0.36	0.26	0.16	0.47	0.35	0.26	0.44	0.23	0.57
Yáñez et. al (2004)	2	0.62	0.67	191	0.50	0.38	0.31	0.73	0.31	0.50	0.68	0.71	0.87
M and C (2004)	3	0.77	0.66	215.4	0.47	0.34	0.29	0.71	0.35	0.31	0.59	0.47	0.79
Zabala et. al (2004)	4	0.97	0.70	118	0.53	0.43	0.37	0.90	0.58	0.55	0.75	0.59	0.88
Zabala et. al (2004)	5	0.97	0.68	207	0.41	0.31	0.23	0.68	0.42	0.35	0.53	0.34	0.67
Bourzam et. al (2008a)	6	1.62	0.86	81.4	0.45	0.26	0.32	0.78	0.22	0.27	0.68	0.60	0.75
Gavilán et. al (2015)	7	1.52	0.94	75.8	0.47	0.29	0.24	0.73	0.42	0.33	0.60	0.35	0.76
Gavilán et. al (2015)	8	0.98	0.64	157	0.36	0.26	0.18	0.54	0.35	0.27	0.45	0.26	0.57
Gavilán et. al (2015)	9	0.67	0.78	320.8	0.36	0.23	0.18	0.50	0.29	0.32	0.40	0.27	0.59
Present Study	S1	1.63	0.72	47.5	0.42	0.23	0.25	0.73	0.25	0.25	0.53	0.63	0.57
Present Study	S2	1.30	0.68	55.8	0.44	0.29	0.26	0.78	0.28	0.28	0.57	0.67	0.61
Present Study	S3	0.93	0.75	81.15	0.45	0.35	0.25	0.75	0.29	0.29	0.54	0.65	0.62

Arg = Argentina; Col = Colombia; CR= Costa Rica; EC = Eurocode; M and C = Marinilli and Castilla

Table 5.10: Comparison of safety margins against flexure.

Study	ID	H/L	ρ_l (%)	$V_{m,e}$ (kN)	For Flexural Resistance: $V'_{des}/V_{m,e}$ Mexico (2017)	Peru (2006)	Chile (2003)	Arg (1991)	Col (2006)	CR (2002)	EC (2005)	China (2001)	India (2017)
Aguilar et. al (1996)	1	1.00	1.51	140.6	0.9	0.8	0.5			0.4	1.0		1.0
Yáñez et. al (2004)	2	0.62	1.12	191.0	1.0	0.7	0.6			0.5	1.1		1.1
M and C (2004)	3	0.77	2.25	215.4	1.2	0.9	0.7			0.7	1.4		1.3
Zabala et. al (2004)	4	0.97	0.79	118.0	1.1	0.9	0.7			0.7	1.4		1.2
Zabala et. al (2004)	5	0.97	2.01	207.0	1.6	1.2	0.9			0.8	1.7		1.7
Bourzam et. al (2008)	6	1.62	2.01	81.4	0.6	0.4	0.3	-	-	0.3	0.6	-	0.6
Gavilán et. al (2015)	7	1.52	2.82	75.8	1.6	1.2	0.9			0.6	1.4		1.7
Gavilán et. al (2015)	8	0.98	2.82	157.0	1.3	1.0	0.8			0.6	1.4		1.4
Gavilán et. al (2015)	9	0.67	2.82	320.8	1.1	0.8	0.6			0.6	1.2		1.1
Present Study	S1	1.63	0.72	47.5	0.6	0.5	0.4			0.3	0.7		0.7
Present Study	S2	1.30	0.72	55.8	0.7	0.5	0.4			0.4	0.8		0.8
Present Study	S3	0.93	0.72	81.2	0.7	0.5	0.4			0.4	0.8		0.8

Arg=Argentina; Col=Colombia; CR=Costa Rica; EC=Eurocode; M and C = Marinilli and Castilla

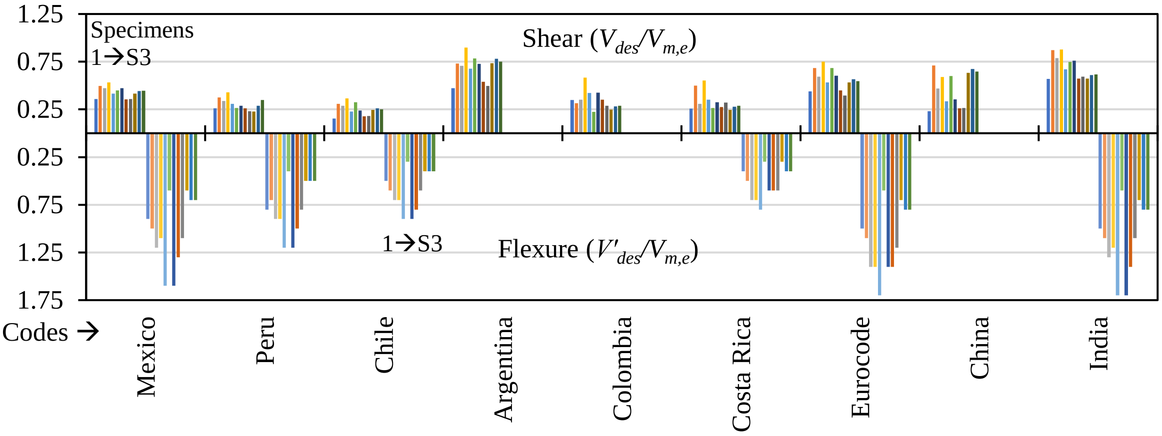

Figure 5.5: Variation in design-to-experimental strength ratios obtained from all the codes against shear and flexural failure mode for the twelve specimens.

5.5 SUMMARY

Seismic performance of confined masonry buildings has been reported as adequate even under high levels of seismic excitations, mainly because of the unique construction practice followed in such buildings and confining action of the RC tie-elements around the masonry panels of the building. The cost of construction of this building type is generally less than a similar-sized infilled RC frame building. Therefore, CM is a natural alternate construction choice for seismically active regions, especially in economically weaker sectors of society. However, due to the lack or deviation of available design codes, the application of this construction system is limited. The failure modes of CM walls under lateral seismic loading mainly depend on their geometric parameters and boundary conditions. As shear-induced damages are more common in CM walls, most of the design formulations are based on shear behaviour. The behavior under flexure has not received much attention in research and thus only a few codes provide the design formulations. All the available formulations for the design shear and design flexural strengths of CM walls provided in the seismic design codes of several countries are assembled in this chapter. The variations associated with different input parameters of different formulations are studied by estimating the design forces for the three tested specimens in the present study, as well as those tested in several past studies.

A comparative study was carried out for the design-to-experimental strength ratios to study the safety margins adopted in different codes against shear and flexural failure. A large variation was observed in the estimated safety margins in different codes against shear failure (0.21 to 1.31) as well as flexural failure (0.3 to 1.7). This highlights the inconsistent estimation of design strength by design codes and limitations of some of the design codes in safely designing the CM walls against shear and flexure failure. Such inconsistencies may arise due to limited experimental data and uncertain material properties of masonry. Systematic experimental and FE studies are required to be carried out considering all important parameters to improve the existing design codes of CM buildings, and hence their construction practice, in different parts of the world.

Chapter 6
DEVELOPMENT OF LATERAL LOAD - DISPLACEMENT BACKBONE MODEL

CONTENTS

6.1 OVERVIEW

Seismic behavior of confined masonry has been a subject of experimental studies from several years. On the basis of observed behavior and analyses of test results, backbone curve models for the prediction of lateral in-plane resistance-displacement envelope curve of CM wall, idealized by a trilinear relationship, have been suggested by different researchers. However, the variation associated with material properties, detailing of tie-elements, construction practices, etc., are huge in different experimental studies across the world. This makes the formulation of a generalized analytical backbone model for CM walls a difficult task for an approximate prediction of their lateral load response. Some models and guidelines are available in the literature to estimate the lateral strength, stiffness, and deformability of a typical CM wall; however, most of the models are specific to considered wall specimens.

Therefore, a large dispersion is generally observed in the estimated parameters due to the huge variation in material properties of masonry, detailing of tie-elements, and construction practices in different parts of the world. Clearly, unless validated, these models may not work well with CM practiced in different places. Further, most of these models have been developed using simplified linear or polynomial equations that are highly influenced by the relations originally developed for reinforced masonry, URM, or infilled RC frames; and they neglect the nonlinear interaction of confining elements with masonry walls. Thus, there is a need for carrying out a comparative evaluation of existing prediction models for understanding their effectiveness in estimating the strength, stiffness, and deformability of different CM walls tested in different regions of the world, and further to develop a generalized nonlinear backbone profile for CM walls that may be used for performance-based seismic analysis and design.

6.2 Lateral Load - Displacement Models

Seismic design of structures highly depends on their characteristic force-deformation relationship, which is defined as a function of three most important parameters - strength, stiffness, and deformability or ductility. The lateral strength of a structure assures the ability to safely resist the applied lateral loads, sufficient lateral stiffness is required to maintain required resistance to lateral deformation, and ductility makes sure that the structure is able to deform beyond the elastic range and dissipate seismic energy through plastic deformations without failure. The in-plane lateral load response of CM walls in the past studies can be summarized with an idealized lateral load-deformation envelope curve as shown in Fig. 6.1 (Flores and Alcocer 1996, Meli et al. 2011).

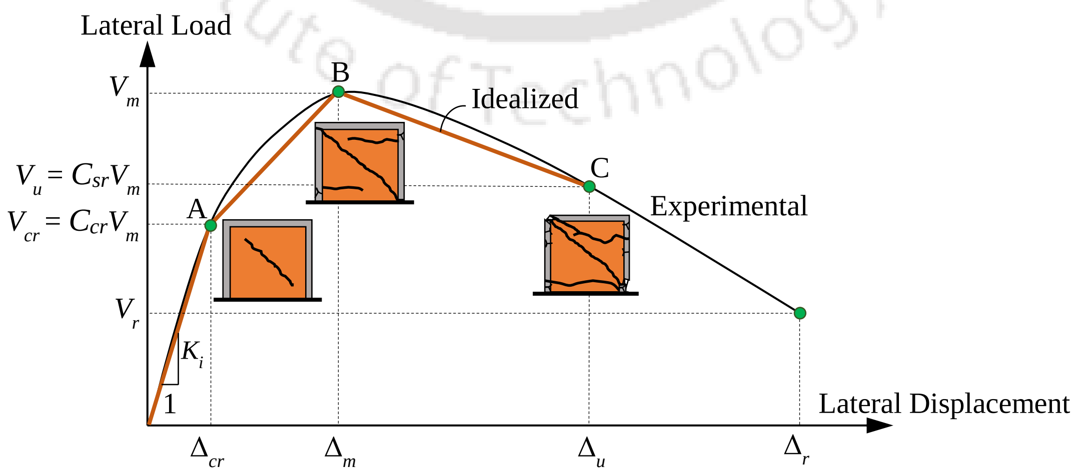

Figure 6.1: Idealized trilinear load-deformation curve for CM walls subjected to lateral loads.

Trilinear variation in the backbone curve has been most popularly recommended in past studies. The lateral load response of CM walls can be assumed to be linearly elastic until the formation of the first visible crack in masonry wall (point A) corresponding to the cracking strength V_{cr} and deformation Δ_{cr}. At a higher drift excursion level, the cracks concentrate along the diagonals and extend towards the tie-columns, resulting in a significant decrease in the wall stiffness until the lateral strength V_m is achieved at a corresponding displacement of Δ_m (point B). This post-cracking behavior (branch A-B) is directly influenced by the friction and brick interlock in the masonry panel, and by the shear resistance of tie-columns. With further drift, the CM wall experiences strength deterioration due to failure of masonry and tie-elements in different modes until point C is reached corresponding to ultimate load V_u and displacement Δ_u. The post-peak behavior (descending branch B-C) and stiffness of the panel at large deformations are mainly governed by the cross-sectional area and reinforcement detailing of the tie-columns. The trilinear approximation is generally not considered beyond point C, which is followed by a rapid reduction in lateral loads with increasing displacements (V_r and Δ_r represent residual strength and corresponding displacement). C_{cr} and C_{sr} are the reduction factors used to reduce V_m to V_{cr} and V_u, respectively.

6.2.1 Models Developed in Past Studies

Some simplified models have been developed in past studies for the approximate prediction of lateral load response of CM walls. Some of these models were developed based on limited experimental studies followed by finite element simulations (Tomaževič and Klemenc 1997a, Marinilli and Castilla in 2006, Bourzam et al. 2008a, 2008b, Gavilán et al. 2015, Singhal and Rai 2016); while some were based on regression analysis of data obtained in past experimental studies (Flores and Alcocer 1996, Riahi et al. 2009, Marques and Lourenço 2013, Marques and Lourenço 2019). The models for all the three points of the force-displacement idealized envelope curve were suggested only by Flores and Alcocer (1996), and Riahi et al. (2009); the rest of the models were mainly developed for predicting lateral force characteristics. The equations recommended in past studies for the prediction of lateral strength ($V_{m,p}$), lateral load at cracking ($V_{cr,p}$), and lateral load at ultimate limit ($V_{u,p}$) of CM walls are given in Table 6.1. In all the studies, the primary contribution to the lateral strength was considered to be provided by masonry walls only (cracking strength as well as maximum strength), and influence of axial loads, aspect ratio, longitudinal reinforcement in tie columns (including the dowel action), number of tie columns, and confinement effect of ties was additionally considered in some studies.

Table 6.1: Estimation of lateral shear at the three critical damage stages of CM walls.

Study	Equations	Eq.
Flores and Alcocer (1996)	$V_{m,p} = \text{Min}\left\{\left(0.5v_m + 0.3\sigma\right)A;\ 1.5v_m A\right\} + 0.3\left(1.26 d_{bl}^2 \sqrt{f_c f_{yl}}\right)$	(6.1a)
	$V_{cr,p} = \text{Min}\left\{\left(0.5v_m + 0.3\sigma\right)A;\ 1.5v_m A\right\}$, or $V_{cr,p} = 0.8V_{m,p}$	(6.1b)
	$V_{u,p} = C_{sr}V_{m,p}\ ;\ C_{sr} = 0.9$	(6.1c)
Tomaževič and Klemenc (1997a)	$V_{m,p} = \left[\left\{1 + \sqrt{c_i^{\,2}\left(1 + \sigma/v_m\right) + 1}\right\} \Big/ \left(c_i f_{AR}\right)\right] v_m A_w + \left(0.8059 n_r d_{bl}^2 \sqrt{f_c f_{yl}}\right)$ where, $c_i = 2\alpha_i \dfrac{f_{AR}}{\text{AR}},\ \alpha_i = \dfrac{5}{4},\quad f_{AR} = \begin{cases} 1.0 & \text{AR} \le 1 \\ \text{AR} & 1 < \text{AR} < 1.5 \\ 1.5 & \text{AR} \ge 1.5 \end{cases}$	(6.2a)
	$V_{cr,p} = 0.7V_{m,p}$ to $0.8V_{m,p}$	(6.2b)
	$V_{u,p} = C_{sr}V_{m,p}\ ;\ C_{sr} \ge 0.7$	(6.2c)
Marinilli and Castilla (2006)	$V_{m,p} = \left(0.47v_m + 0.29\sigma\right)\left(A - nA_c\right) + 4200n$ (in kg cm)	(6.3a)
	$V_{cr,p} = \left(0.47v_m + 0.29\sigma\right)A$ (in kg cm)	(6.3b)
Bourzam et al. (2008a, b)	$V_{m,p} = \left\{\sqrt{1 + \left(\sigma/v_m\right)} \Big/ f_{AR}\right\} v_m A_w + \left(0.537 n n_r d_{bl}^2 \sqrt{f_c f_{yl}}\right)$	(6.4a)
	$V_{m,p} = \left[\left\{1 + \sqrt{c_i^{\,2}\left(1 + \sigma/v_m\right) + 1}\right\} \Big/ \left(c_i f_{AR}\right)\right] v_m A_w + \left(0.537 n n_r d_{bl}^2 \sqrt{f_c f_{yl}}\right)$	(6.4b)
	$V_{m,p} = \left[A_w \big/ \left\{f_{AR}\left(1 + v_m/f'_m\right)\right\}\right]\left(\sqrt{v_m^{\,2} + \sigma v_m\left(1 - v_m/f'_m\right) - \sigma^2 v_m/f'_m}\right) + \left(0.537 n n_r d_{bl}^2 \sqrt{f_c f_{yl}}\right)$	(6.4c)
	$V_{cr,p} = 0.6V_{m,p}$ to $0.8V_{m,p}$	(6.4d)
	$V_{u,p} = C_{sr}V_{m,p}\ ;\ C_{sr} = 0.4$ to 0.8	(6.4e)
Riahi et al. (2009)	$V_{m,p} = \left(0.21v_m + 0.363\sigma + 0.0141\sqrt{\rho_l f_c f_{yl}}\right)A$	(6.5a)
	$V_{cr,p} = \text{Min}\left\{\left(0.424v_m + 0.374\sigma\right)A;\ v_m A\right\}$ or	(6.5b)
	$V_{cr,p} = 0.7V_{m,p}$	(6.5c)
	$V_{u,p} = C_{sr}V_{m,p}\ ;\ C_{sr} = 0.8$	(6.5d)
Marques and Lourenço (2013)	$V_{m,p} = \left\{\left(0.49v_m + 0.53\sigma\right) - 0.14\left(H/L\right) - \left(A_w/A\right) + 1\right\}A$	(6.6a)
	$V_{cr,p} = 0.8V_{m,p}$	(6.6b)
	$V_{u,p} = C_{sr}V_{m,p}\ ;\ C_{sr} = 0.8$	(6.6c)
Singhal and Rai (2016)	$V_{m,p} = \left(0.7L_i/L_p + 2.15\right)\left\{\text{Min}\left(0.2 + 0.4\sigma;\ 0.25\sqrt{f'_m}\right)\right\}A_w$	(6.7)
Gavilán et al. (2015)	$V_{cr,p} = \text{Min}\left\{\left(0.5v_m + 0.3\sigma\right) f_{AR} A;\ 1.5v_m f_{AR} A\right\}$ where, $f_{AR} = \begin{cases} 1.55 & H/L \le 0.2 \\ \left(1.69 - 0.69H/L\right) & 0.2 < H/L < 1.0 \\ 1.0 & H/L \ge 1.0 \end{cases}$	(6.8)
Marques and Lourenço (2019)	$V_{m,p} = \left(0.5f_{AR}v_m + 0.4\sigma\right)A$; where, $f_{AR} = 1.15 - 0.15H/L$	(6.9a)
	$V_{m,p} = \left\{\left(0.45v_m + 0.3\sigma\right) + 0.4\sqrt{f_c}\left(1 + n_i\right)nA_c/A\right\}A$	(6.9b)

The three equations (Eqs. 6.4a, 6.4b, and 6.4c) of Bourzam et al. (2008a) represents the consideration of three different methods for the prediction of masonry wall contribution in the lateral strength depending on three different failure hypotheses: failure at a critical in-plane tensile strength as per Turnšek and Čačovič (1971), failure at a critical tensile strength by considering the interaction effect of confining elements developed by Tomaževič and Klemenc (1997a), and failure by a critical biaxial combination of normal principal stresses following the study of Sucuoğlu and McNiven (1991). The ultimate lateral load before failure has been simply formulated as a function of the lateral strength as: $V_{u,p} = C_{sr}V_{m,p}$, where C_{sr} is the strength reduction factor.

The analytical models for the initial lateral stiffness of CM walls, defining the slope of the first branch of the idealized backbone curve, are mainly developed considering the flexural and shear deformations of wall as observed in Flores and Alcocer (1996), Tomaževič and Klemenc (1997a), and Bourzam et al. (2008b). The contribution of RC confining elements to lateral stiffness is not considered explicitly; however, in the calculation of the moment of inertia of wall section, gross sectional area including the dimensions of the tie-columns with attributed masonry mechanical characteristics is considered. Singhal and Rai (2016) combined the method developed by Rai et al. (2014) and Drysdale et al. (1999) to estimate the initial stiffness of CM wall. To model the degradation of stiffness after cracking, Tomaževič and Klemenc (1997a) proposed a model for degraded or secant stiffness as a function of initial stiffness and extent of damage in walls at characteristic damage stages. The damage index I_d is suggested as 0.25, 0.5, and 1, respectively, at first cracking, maximum load, and ultimate limit for which the stiffness is 2% of initial stiffness. Further, it was suggested that the degraded strength beyond the post-peak region should not be more than 70% of the maximum lateral strength. The degraded stiffness proposed by Bourzam et al. (2008b) is similar to that given in Tomaževič and Klemenc (1997a) except for the values of the coefficients, and also that the ultimate limit is considered for 5% of initial stiffness.

Many of the past research studies have mainly focused on the force characteristics of CM walls; with the increasing popularity of performance-based design, deformation capacity has also been addressed in a limited number of studies. Deformation capacity is a very complex parameter that depends on many variables related to material and geometrical properties, overburden loading, etc. Especially after cracking it becomes more difficult to formulate analytical models for drift at different performance levels because of the complex interaction between tie-columns and masonry walls in addition to the heterogeneity and highly nonlinear behavior of masonry. The lateral drift values corresponding to different damage stages or at critical points on the backbone curves have been recommended in past studies as given in Table 6.2. On the basis of wall characteristics, drift at different damage stages was proposed by Riahi et al. (2009) using linear regression analysis of several past experimental test results. In that proposal, the ultimate drift limit was considered against 80% residual strength ($V_{u,p}$ = $0.8V_{m,p}$). The drift at cracking can be evaluated from the initial stiffness if the lateral load at cracking is also known. As per Flores and Alcocer (1996), the lateral drift limits are 0.3% and 0.5% at peak lateral load and at ultimate limit corresponding to 10% strength degradation ($V_{u,p}$ = 0.9$V_{m,p}$), respectively.

Table 6.2: Estimation of lateral stiffness and drift limits of CM walls.

Parameter	Researchers	Analytical model for lateral strength of CM wall	Eq.
Initial Stiffness	Flores and Alcocer (1996), Tomaževič and Klemenc (1997a)	$K_{i,p} = \left(\dfrac{H_w^{3}}{\beta E_m I} + \dfrac{\kappa H_w}{G_m A}\right)^{-1}$ where, κ = 1.2, β = 3 for cantilever, 12 for fixed ended wall	(6.10)
	Bourzam et al. (2008b)	$K_{i,p} = \left(\dfrac{H_w^{3}}{\beta E_{eqv} I} + \dfrac{\kappa H_w}{G_{eqv} A}\right)^{-1}$ where, $E_{eqv} = \dfrac{E_m A_w + 2E_c A_c}{A_w + 2A_c}$; $G_{eqv} = \dfrac{G_m A_w + 2G_c A_c}{A_w + 2A_c}$	(6.11)
	Riahi et al. (2009)	$K_{i,p} = 100V_{cr,p} / \left(H\delta_{cr,p}\right)$ where, $V_{cr,p}$ is taken from Eq. (6.5b) or (6.5c), and $\delta_{cr,p}$ from Eq. (6.17)	(6.12)
	Singhal and Rai (2016)	$K_{i,p} = \left(0.29 + 0.26 L_i / L_p\right)\left(\dfrac{H_w^{3}}{3E_m I} + \dfrac{H_w}{G_m A_w}\right)^{-1}$	(6.13)
Degraded or Secant Stiffness	Tomaževič and Klemenc (1997a)	$K_{d,p} = K_{i,p}\left(1 - \sqrt{1.28 I_d - 0.32}\right)$	(6.14)
	Bourzam et al. (2008b)	$K_{d,p} = K_{i,p}\left(1 - \sqrt{1.805 I_d - 0.451}\right)$	(6.15)
Lateral Drift at Cracking	Flores and Alcocer (1996), Tomaževič and Klemenc (1997a)	$\delta_{cr,p} = \left(V_{cr,p} / K_{i,p}\right)\left(100 / H_w\right)$	(6.16)
	Riahi et al. (2009)	$\delta_{cr,p} = f_\delta V_{cr,p} / A\sqrt{f_m'}$ where, f_δ = 1.13 for clay brick wall and 0.72 for concrete block wall	(6.17)
Lateral Drift at Peak Strength	Flores and Alcocer (1996)	$\delta_{m,p} = 0.3\%$	(6.18)
	Riahi et al. (2009)	$\delta_{m,p} = 0.65\delta_{u,p}$	(6.19)
Lateral Drift at Ultimate Limit	Flores and Alcocer (1996)	$\delta_{u,p} = 0.5\%$	(6.20)
	Riahi et al. (2009)	$\delta_{u,p} = f_\delta \mu V_{m,p} / A\sqrt{f_m'}$ where, $\mu = \mathrm{Min}\left\{1.3 + 0.5 / \left(V_{m,p}/A\right)^{2} ;\ 6\right\}$	(6.21)

6.2.2 Status of Existing Codes of Practice

Some seismic codes provide relations to estimate the design shear strength of CM walls, as mentioned in Chapter 5. Removing all the design safety factors, the different codal formulations were used in this section to evaluate their effectiveness in predicting the lateral strength of CM wall. Thus, the generalized equation of codes for the prediction of lateral shear strength of CM wall can be expressed as:

$$V_{cr,p} = av_m(A - n_i A_c) + b\sigma(A - n_i A_c) + cf_{tc}A_c + df_{yl}n_r A_{sl} \tag{6.22}$$

where, *a, b, c, d* are the coefficients representing the contribution of different parameters. As the codal formulations are mainly based on a conservative approach by considering the design lateral load at the initial cracking stage, only the first two terms are considered in the codes except for the Chinese code, in which the last two terms are also included to consider the contribution of concrete and steel in the intermediate columns of multi-bay specimens. As mentioned previously, Mexico and Indian codes consider wall aspect ratio factor in the coefficient of the first two terms in Eq. 6.22, and the Peruvian code considers an aspect ratio factor in the coefficient of the first part. Table 6.3 summarizes the values of different coefficients involved in Eq. 6.22, where some of the coefficients (*a*, *b*, *c*, *d*) are specified directly in some design codes, while some are derived in the present study by combining the influence of one or more parameters.

Table 6.3: Coefficients in the generalized equation for strength estimation (Eq. 6.22).

Design Code	Coefficients used in Eq. (6.22)			
	a	*b*	*c*	*d*
Mexico (NTC-M 2017): [Mex]	0.5 to 0.75	0.3 to 0.45	-	-
Peru (NT E.070 2019): [Per]	0.167 to 0.5	0.23	-	-
Chile (NCh2123 2003): [Chl]	0.45	0.24	-	-
Argentina (INPRES-CIRSOC 103 2018): [Arg]	1	0.4	-	-
Colombia (NSR-98 2010): [Col]	0.08	0.3	-	-
Costa Rica (CSCR 2002): [CR]	0.13	0.24	-	-
Eurocode (CEN 2005): [EC]	1	0.4	-	-
China (GB 50003 2011): [Chn]	1 or 1.1	0	0.5 or 0.4	0.08
India (BIS 2021): [Ind]	0.5 to 0.775	0.4 to 0.62	-	-

The deformation capacity of CM walls has been defined in a few design codes and it is defined only in terms of recommended drift values for different damage stages. The Peruvian code allows up to 0.125% drift limit to prevent initial cracking in wall and this limit may go up to 0.5% for economically repairable damage. Similarly, Mexican code suggests an inter-story drift limit at peak strength of 0.5% and 0.4% for walls made using solid and hollow units, respectively.

6.3 EXPERIMENTAL DATA

Several experimental studies have been carried out on CM walls under quasi-static monotonic or cyclic loads as well as dynamic loads on shake table to understand and characterize the lateral load behavior of CM construction system. Table 6.4 gives details of relevant experimental studies carried out by 24 research teams with a total of 166 CM wall specimens. However, specimens having more than one-story, openings, horizontal wall reinforcement, joint reinforcement at wall-to-tie interfaces, and additional moment on top were removed from the database, and finally, seventy-eight specimens were selected as given in Table 6.4. This database contains seventy single-bay CM specimens in addition to eight multi-bay specimens from the studies of Marinilli and Castilla (2004), Singhal and Rai (2014), and Gavilán et al. (2015). The scaling ratio of the considered specimens ranges from full-scale to one-fifth scale, in which 35 specimens were constructed in full-scale, 34 in half-scale, 6 had one-third scaling, and one-fifth scaling was used in the remaining 3 specimens.

Table 6.4: Database of CM wall specimens tested in previous studies.

Sl.	Experimental Study	Scale	Parameters studied	Considered Specimen ID
1	Kato et al. (1992)	0.5	tie-detailing	A, B, C, D
2	Aguilar et al. (1996)	1	wall reinforcement, % opening	MO
3	Iiba et al. (1996)	0.5	unit type, tie-column reinforcement	IDM, IDJ, HDJ
4	Yoshimura et al. (1996)	0.5	tie-detailing, wall reinforcement	4-H0V0, 1-H0V0
5	Tomaževič and Klemenc (1997a)	0.2	common practice for comparison with URM	AH-1/2/3
6	Yoshimura et al. (2000)	0.5	axial load, load application point, wall reinforcement	H/L1-H0V0-HC/LC/T
7	Kumazawa and Ohkubo (2000)	0.5	horizontal wall reinforcement	ISM
8	Yoshimura et al. (2004a)	0.5	masonry type, axial load, load application point, anchorage, wall reinforcement, 3D effect	2D-H/L1-H0V0-48/84-1/2
9	Yáñez et al. (2004)	1	unit type, % opening	Pattern 1-CMU/Clay Brick
10	Marinilli and Castilla (2004)	1	no. of tie-columns	M1/2/3/4
11	Zabala et al. (2004)	1	tie-column reinforcement, axial load, wall reinforcement	1, 2, 3, 4
12	Gouveia and Lourenço (2007)	0.5	wall reinforcement	W2.4
13	Bourzam et al. (2008 a, b)	0.5*	common practice, axial load	JCM, CM30J-1/2
14	Kuroki et al. (2010)	0.5	confining scheme for opening	CMWO-01/07
15	Wijaya et al. (2011)	1	wall to tie-column connection	A, C
16	Bourzam et al. (2013)	0.5*	unit type	CM60J
17	Matošević et al. (2014)	0.67	wall to tie-column connection	A/B-1/2/3
18	Singhal and Rai (2014)	0.5	wall to tie-column connection	SC_{NT}, SC_{CT}, SC_{FT}
19	Gavilán et al. (2015)	1	aspect ratio	ME1/2/3/4/5/6/7
20	Quiroz et al. (2017)	1	tie-detailing	A1/2-1/2
21	Varela-Rivera et al. (2019)	1	aspect ratio, axial load	M1/2/3/4/5/6
22	Cruz et al. (2019)	1	wall to tie-column connection	MB0
23	Gavilán (2020)	1	moment on top	M1/2-1
24	Present study	0.5	aspect ratio	S1/2/3

*full-scale masonry pier was tested

6.3.1 Variation of Different Parameters

In an attempt to understand the influence of different parameters on the lateral load response of tested CM walls, the following information was extracted from the reported experimental results: material properties, which vary significantly with geographical location; geometric properties and reinforcement detailing; loading data; and force-displacement envelope curves in terms of maximum strength ordinates, initial stiffnesses and drift limits. In some studies, some of the data were missing, and in that case, the required values were considered based on usual practice. The ranges of some important input parameters along with their occurrence frequency in the database can be observed in Fig. 6.2.

6.3.2 Material and Loading Parameters

Among all the parameters, the variation associated with masonry property is found to be the highest. In the considered test database, the compressive strength of masonry prism (f'_m) ranges from 1.7 MPa to 61 MPa (Fig. 6.2). This huge variation is due to the adoption of combinations of different types of masonry unit and mortar at different places. Different types of masonry units, such as hand-made clay bricks, machine-made clay bricks, solid concrete blocks, concrete units, hollow clay units, multi-perforated clay bricks, hollow concrete blocks, etc., were used in different studies, resulting in significant variation of compressive strength of masonry unit f_b (4 to 60 MPa). Substantial variation was also found in the compressive strength of mortar f_j from 6 to 63 MPa, due to the use of different compositions of cement, sand, and lime, etc. The sand to cement ratio in mortar was found to vary from 2.5 to 6, whereas, half or equal ratio of lime to cement ratio was also observed in some mortar mixture. In these specimens, the shear strength of masonry (v_m) varies from 0.24 to 2.74 MPa. Not all studies have reported v_m; the missing v_m values were evaluated as $0.184\sqrt{f'_m}$ as suggested by Riahi et al. (2007). The higher v_m values (> 1.0) were reported in Kato et al. (1992), Iiba et al. (1996), Yoshimura et al. (2004), Bourzam et al. (2008a, 2008b, 2013), Kuroki et al. (2010), and Cruz et al. (2019). The concrete used in these specimens had compressive strength (f_c) of 10 MPa to 44 MPa. The material strengths used in the one-fifth scale specimens tested by Tomaževič and Klemenc (1997a) were very low compared to the other studies: f_b = 1.09 MPa, f_j = 0.45 MPa (with C:S: L = 0.4: 11: 1), f'_m = 1.27 MPa, and f_c = 10.8 MPa; therefore, these are not compared here. Further, all studies have not reported the modulus of elasticity of materials (E_m, E_c, G_m, and G_c); the missing values were evaluated using $E_m = 550\, f'_m$ for masonry and $E_c = 5000\sqrt{f_{ck}}$ for concrete. The missing shear modulus of masonry was estimated using its general relationship with the modulus of elasticity recommended in past studies: $G_m = 0.4E_m$. The lateral loading was simulated mostly by applying quasi-static cyclic loads in most of the specimens, and shake table dynamic loads in a few cases. Axial loads in different test specimens range from -0.1 MPa to 1.8 MPa. The negative axial load was considered in two specimens of Yoshimura et al. (2000), while in some studies, there was no overburden pressure (Kato et al. 1992 and Yáñez et al. 2004).

6.3.3 Geometry and Detailing Parameters

In the database, the aspect ratio of specimens (AR = H_w/L_w) ranges from 0.6 to 2.75, if individual single panels are considered; however, the lower limit reduces to 0.3, if multi-bay CM specimens with more than two tie-columns are considered as a single unit. The effectiveness of confinement provided to CM walls by RC tie-elements depends on various factors, such as number, location, and size of tie-elements, grade of concrete, grade of steel, reinforcement percentage, etc. In the considered experimental studies, minimum two and maximum four numbers of tie-columns have been used in CM specimens. The full-scale thickness of masonry wall used in the specimens ranges from 115 mm to 286 mm; whereas, the full-scale in-plane width of tie-column ranges from 100 mm to 400 mm. To show the variation associated with the cross-section of different specimens, a dimensionless parameter nA_c/A, which varies from 0.07 to 0.32, is presented in Fig. 6.2. Moreover, as explained earlier, the post-peak behavior of CM walls is also governed by the reinforcement detailing of tie-columns. Huge variation is observed in the amount of longitudinal steel provided in tie-columns of different specimens; one to six numbers of longitudinal rebars, with full-scale diameter ranging from 8 mm to 38 mm amounting to 0.5% to 6.6% of the cross-sectional area of tie-columns, have been used in these studies. While, shear reinforcement was not provided at all in some specimens (Zabala et al. 2004, Varela-Rivera et al. 2019), spiral hoops were provided in some of the specimens with single longitudinal rebar (Yoshimura et al. 1996, 2000, 2004a, Varela-Rivera et al. 2019), and commonly used stirrups were provided in rest of the specimens. The full-scale diameter of these stirrups ranges from 6 mm to 12 mm with full-scale spacing ranging from 50 mm to 440 mm (at the end of tie-columns) indicating a wide range of shear capacities of tie-columns. Further, in some experimental studies, it was observed that the bonding between the masonry wall and RC tie-elements can be improved with the help of joint reinforcement (anchorage) or toothed edges to delay the undesirable cracking and separation at the wall-to-tie-column interface. The considered test database contains 8 single-bay and 2 multi-bay specimens with toothed connections (Wijaya et al. 2011, Matošević et al. 2015, Quiroz et al. 2017, Singhal and Rai 2014). As already discussed, the specimens with joint reinforcement are not considered in the present study.

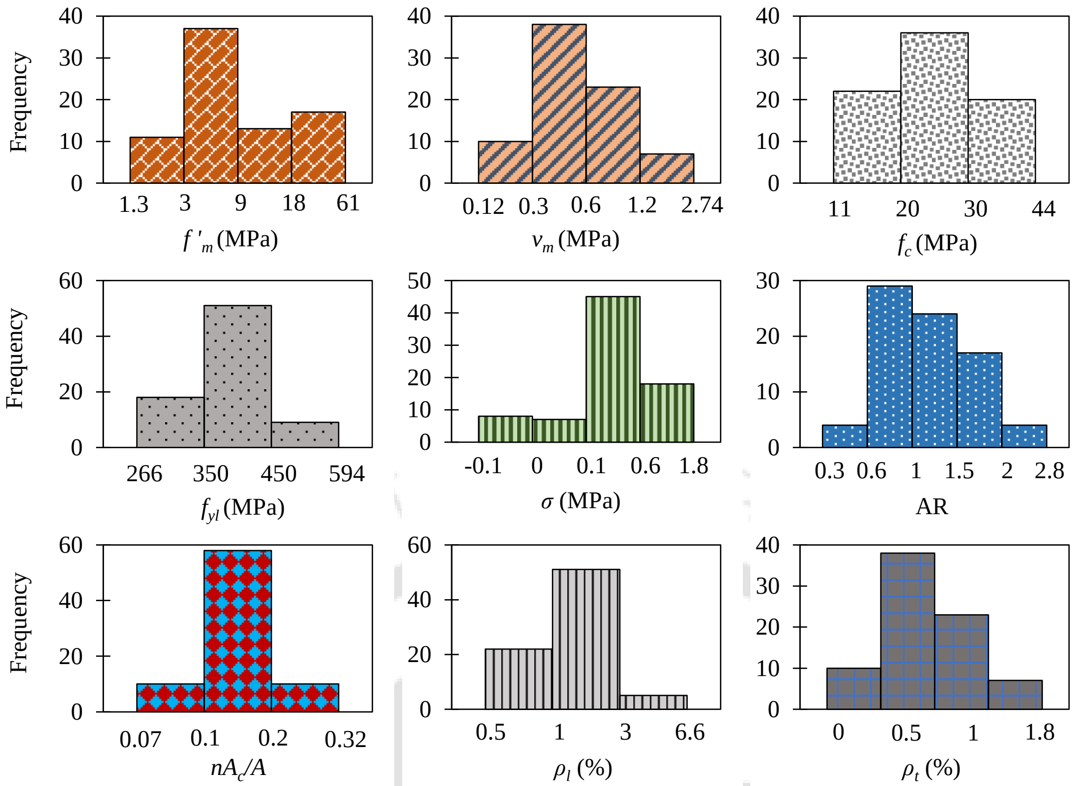

Figure 6.2: Histogram showing range and frequency of occurrence of some important parameters in the considered database of CM wall specimens tested in the past.

Clearly good variation can be observed in different parameters considered in the experiments; this will provide prospect to realistically assess the effectiveness of all equations in predicting the lateral loads and deformations of CM walls considering the variations in different parameters.

6.4 Summarized Influence of Important Parameters

Depending upon the availability of materials, cost, climatic condition, living habits, and tradition, different types of brick unit and mortar combinations have been adopted for confined masonry construction in different parts of the world. A few past studies have shown that the type of masonry used in the construction changes the lateral load response of confined masonry walls (Iiba et al. 1996, Yáñez et al. 2004, Yoshimura et al. 2004a). For example, the study of Yáñez et al. (2004) showed that when hollow clay brick masonry units having compressive strength f_b of 25.9 MPa were used, CM specimens demonstrated larger strength and stiffness degradation than when concrete masonry units (f_b = 9.68 MPa) were used, although the former specimens reached larger lateral strength. From different studies, it was found that the axial load improves the lateral strength (around 30%) of CM walls (Yoshimura et al. 2000, Zabala et al. 2004, Varela-Rivera et al. 2019). Aspect ratio (AR) of masonry panel is one of the governing factors from the consideration of damage pattern and failure modes. Seismic behavior of squat CM walls with AR less than or around one is mostly governed by shear deformations. When AR is higher or more than one, the flexural deformations become predominant in CM walls. With a decrease in aspect ratio, lateral strength of CM wall increases; whereas, the drift corresponding to it reduces (Gavilán et al. 2015, Varela-Rivera et al. 2019). An increase in the number of tie-columns improves the lateral load response of CM wall as observed by Marinilli and Castilla (2004). Further, an increase in the percentage reinforcement (longitudinal or transverse) in tie-columns or tie-beams results in a substantial increase of lateral capacity and deformation response of CM walls (Kato et al. 1992, Iiba et al. 1996, Zabala et al. 2004, Quiroz et al. 2017). However, excessive longitudinal reinforcement may trigger brittle shear failure if not designed properly for shear failure mode. Lateral ties also play a vital role in the behavior of CM walls. After formation of the initial diagonal crack when lateral load increases, the crack gets propagated to tie-columns leading to shear concentration at the ends of the tie-columns. Thus, adequate transverse reinforcement is needed to achieve desired deformation and energy dissipation characteristics; Kato et al. (1992) observed that 3.8 times increase in ρ_l resulted in 1.5 times increase in the lateral capacity. Similarly, though the cracking drift remains the same and only a slight increment was observed in ultimate drift with 4 times increase in ρ_t, the drift at lateral strength increases by 1.4 times and goes up to 2.7 times. Iiba et al. (1996) observed that 4 times increase in ρ_l with 2 times increase in ρ_t did not result in any significant increase in the lateral capacity; however, $\delta_{m,e}$ increases by 2 times and a slight increment was observed in $\delta_{u,e}$. Zabala et al. (2004) showed that 1.5 times increase in ρ_l, along with 2 times increase in σ, increases the lateral capacity of confined masonry walls by around 2 times; whereas, $\delta_{m,e}$ increases around 3 times and a slight increase was observed in $\delta_{u,e}$. Quiroz et al. (2017) observed 1.3 times increase in ρ_l results in the increase in the lateral capacity by 1.4 times, whereas $\delta_{m,e}$ and $\delta_{u,e}$ increase by around 4 times.

As observed in different models, the output parameters – stiffness, strength and lateral drift capacity of a CM wall are functions of different input variables related to material properties, geometric characteristics, overburden pressure, reinforcement detailing, etc. The developed models were based on the consideration of different combinations of input parameters by mainly observing and analyzing the experimentally obtained responses. All the parameters involved in the development of stiffness, strength, and drift capacity of CM walls are shown in Table 6.5.

Table 6.5: Input parameters considered in different formulations.

Output Parameters of CM wall	Input properties considered						
	Material Parameters			Load	Geometrical	Detailing	Others
	Masonry	Concrete	Steel	Parameters	Parameters	Parameters	
Lateral load at cracking, $V_{cr,p}$	v_m, f'_m	f_{tc}^*	f_{yl}^*	σ	A, AR, A_c^*, n_i^*	A_{sl}^*, n_r^*	–
Lateral capacity, $V_{m,p}$	v_m, f'_m	f_c	f_{yl}	σ	A, A_c, n, n_i, L_i/L_p, AR	A_{sl}, n_r, d_{bl}, ρ_l	–
Ultimate lateral load, $V_{u,p}$	–	–	–	–	–	–	$V_{m,p}$
Initial stiffness, $K_{i,p}$	E_m, G_m	E_c, G_c	–	–	H_w, A, I, L_i/L_p	–	β, $V_{cr,p}$, $\delta_{cr,p}$
Degraded stiffness, $K_{d,p}$	–	–	–	–	–	–	I_d, $K_{i,p}$, $V_{m,p}$, $V_{u,p}$
Drift at cracking, $\delta_{cr,p}$	unit type, f'_m	–	–	–	H_w, A	–	$K_{i,p}$, $V_{cr,p}$
Drift at capacity, $\delta_{m,p}$	–	–	–	–	–	–	$\delta_{u,p}$
Drift at ultimate load, $\delta_{u,p}$	unit type, f'_m	–	–	–	A	–	$V_{m,p}$

* wall with intermediate tie-columns

The analytical models for the estimation of lateral load at cracking are mainly based on Coulomb's friction model along with v_m, f'_m, σ, and A. Effect of aspect ratio was also considered in some equations (Gavilán et al. 2015, and codes of Mexico, Peru, and India). In addition, contribution of intermediate tie-columns on the lateral strength of confined masonry walls is considered in Chinese code using parameters f_{tc}, f_{yl}, n_r, n_i, A_c, A_{sl} (marked with asterisk in Table 6.5). Similarly, main parameters considered for lateral capacity prediction are v_m, f'_m, σ, and A; AR is considered in Eqns. (6.2a), (6.4a), (6.4b), (6.4c), (6.6a), and (6.9a) (Tomaževič and Klemenc 1997, Bourzam et al. 2008a, Marques and Lourenço 2013, Marques and Lourenço 2019). Most of the equations, such as Eqs. (6.1a), (6.2a), (6.3a), (6.4a), (6.4b), (6.4c), (6.5a), considered the contribution by the tie-columns using the parameters f_c, f_{yl}, n_r, n, n_i, A, A_c, A_{sl}, d_{bl}, ρ_l (Flores and Alcocer 1996, Tomaževič and Klemenc 1997a, Marinilli and Castilla 2006, Bourzam et al. 2008a, and Riahi et al. 2009). Along with the main parameters, one additional geometrical parameter L_i/L_p (ratio of total centerline length of internal confining elements to centerline length of confining elements at perimeter of the wall), is considered in Singhal and Rai (2016), which gives a constant minimum multiplying factor of 2.15 in lateral strength, irrespective of variation in materials and detailing of tie-elements.

The analytical models for the initial lateral stiffness of CM walls are mainly proposed considering the flexural and shear deformations using parameters E_m, G_m, H_w, A, I, and β (with values 3 or 12). Additional parameters E_c and G_c are considered in Bourzam et al. (2008b) by formulating equivalent stiffness values from masonry and concrete. Singhal and

Rai (2016) on the other hand considered one additional geometrical parameter L_i/L_p along with the main parameters, which gives a constant minimum multiplying factor of 0.29. The analytical models for the degraded lateral stiffness of CM walls after cracking (Eqs. 6.14, 6.15) were developed based on the initial stiffness and the extent of damage using the parameter I_d. For the drift estimation at different damage stages, unit type, f_m', H_w and A are mainly considered.

6.5 Estimation of Responses using Available Models

The experimental data collected from seventy-eight confined masonry walls tested in the past studies (including the three specimens tested in the present study) were used to understand the efficacy of several existing models in estimating the lateral loads at various damage stages, initial lateral stiffness, and lateral drift at various damage stages.

6.5.1 Lateral Load – at Initial Cracking, Maximum Capacity, and Failure

The effectiveness of all the equations suggested in the past studies and design codes of some countries in predicting the lateral strength as well as the lateral load at cracking of confined masonry walls was evaluated by utilizing them for all the seventy-eight CM walls tested in the past experimental studies. Tables 6.6 and 6.7 show the experimentally obtained lateral loads, and the ratio of predicted to experimental lateral loads for all the specimens at strength ($V_{m,p}/V_{m,e}$) and cracking ($V_{cr,p}/V_{cr,e}$) levels. In these two tables, the first seventy specimens are single-bay specimens and the last eight specimens have multiple bays. Figs. 6.3 and 6.4 show the graphical comparison of the experimentally obtained lateral load carrying capacity and lateral load at cracking, respectively, for all the seventy-eight CM walls with their predictions. The dotted line represents the mean value (± standard deviation) of the predicted to experimental load ratio for the specimens. Tables 6.6 and 6.7, or Figs. 6.3 and 6.4 show huge variations in the overestimation or underestimation of the lateral strength as well as the lateral load at cracking obtained using all the equations. The predicted mean values of the lateral strength appear to be quite accurate if the equations of Marques and Lourenço (2013), Marques and Lourenço (2019) (Eq. 9a), Riahi et al. (2009), and Flores and Alcocer (1996) are used; the standard deviations are also quite low for these equations (Fig. 6.3). Similarly, the mean values of lateral load at cracking were predicted with acceptable accuracy using the design codes of Peru, Chile, and Colombia (Fig. 6.4).

Table 6.6: Comparison of predicted and experimentally obtained lateral strengths for all the specimens.

Sr	Experimental Study and Model Id	$V_{m,e}$ (kN)	$V_{m,p}/V_{m,e}$										
			M&L 3	M&L 2	S&R	M&L 1	Ria	Bzm 1	Bzm 2	Bzm 3	M&C	T&K	F&A
1	Kato et al. (1992) - A	230	1.0	0.7	0.2	0.8	0.5	1.3	1.6	1.3	0.8	1.3	0.8
2	Kato et al. (1992) - B	235	1.0	0.7	0.2	0.8	0.4	1.0	1.3	0.9	0.8	1.3	0.8
3	Kato et al. (1992) - C	167	1.4	1.0	0.2	1.1	0.5	1.5	2.0	1.4	1.2	1.5	1.1
4	Kato et al. (1992) - D	147	1.6	1.1	0.3	1.3	0.6	1.2	1.7	1.1	1.3	1.7	1.2
5	Aguilar et al. (1996) - MO	141	1.1	0.7	1.7	0.8	0.9	1.3	1.5	1.2	1.1	1.2	0.6
6	Iiba et al. (1996) - IDM	114	1.1	0.7	1.2	0.9	0.8	0.9	1.0	0.8	1.2	1.0	0.7
7	Iiba et al. (1996) - IDJ	140	1.0	0.8	1.0	0.9	0.7	0.9	1.1	0.9	1.2	1.0	0.7
8	Iiba et al. (1996) - HDJ	135	1.0	0.8	1.0	1.0	0.7	0.7	1.0	0.7	1.2	1.0	0.8
9	Yoshimura et al. (1996) - 4-H0V0	240	0.6	0.5	0.8	0.6	0.5	0.8	1.0	0.8	0.7	1.0	0.5
10	Yoshimura et al. (1996) - 1-H0V0	236	0.7	0.6	0.8	0.6	0.5	0.9	1.1	0.9	0.8	1.1	0.6
11	Tomaževič and Klemenc (1997a) - AH-1	2.3	1.5	0.8	2.4	0.6	1.1	1.0	1.1	0.9	36.5	1.1	0.8
12	Tomaževič and Klemenc (1997a) - AH-3	1.8	1.9	1.0	3.0	0.8	1.4	1.2	1.4	1.1	45.5	1.4	0.9
13	Tomaževič and Klemenc (1997a) - AH-2	1.6	2.2	1.1	3.5	0.9	1.6	1.4	1.6	1.2	52.3	1.6	1.1
14	Yoshimura et al. (2000) - H1-H0V0-HC	264	0.8	0.7	1.2	0.9	0.7	0.9	1.0	0.8	0.8	1.0	0.7
15	Yoshimura et al. (2000) - H1-H0V0-LC	186	0.8	0.7	1.0	0.8	0.7	1.2	1.4	1.1	1.0	1.4	0.7
16	Yoshimura et al. (2000) - H1-H0V0-T	103	0.9	0.5	0.5	0.4	0.6	1.3	1.7	1.3	1.2	1.6	0.6
17	Yoshimura et al. (2000) - L1-H0V0-HC	343	0.6	0.6	0.9	0.7	0.5	0.8	0.9	0.7	0.7	0.9	0.5
18	Yoshimura et al. (2000) - L1-H0V0-LC	239	0.6	0.6	0.8	0.6	0.5	0.9	1.1	0.9	0.8	1.1	0.5
19	Yoshimura et al. (2000) - L1-H0V0-T	150	0.7	0.4	0.4	0.4	0.5	1.1	1.4	1.0	0.9	1.3	0.5
20	Kumazawa and Ohkubo (2000) - ISM	115	1.3	1.0	1.4	1.2	1.0	1.1	1.3	1.0	1.3	1.2	0.8
21	Yoshimura et al. (2004a) - 2D-H1-H0V0-48-2	149	1.2	1.0	0.9	1.1	0.8	1.9	2.3	1.8	1.4	2.3	1.1
22	Yoshimura et al. (2004a) - 2D-H1-H0V0-84-2	158	1.3	1.2	1.1	1.3	1.0	2.0	2.5	1.9	1.4	2.5	1.2
23	Yoshimura et al. (2004a) - 2D-L1-H0V0-48-1	149	0.9	0.7	0.9	0.8	0.7	1.3	1.6	1.2	1.1	1.6	0.7
24	Yoshimura et al. (2004a) - 2D-L1-H0V0-84-1	140	1.1	0.9	1.3	1.0	0.9	1.5	1.8	1.4	1.3	1.8	0.9
25	Yáñez et al. (2004) - Pattern 1-CMU-1	117	1.9	1.1	1.7	1.2	1.1	2.2	2.7	2.1	1.6	2.7	1.1
26	Yáñez et al. (2004) - Pattern 1-CMU-2	130	1.7	1.0	1.5	1.0	1.0	2.0	2.5	1.8	1.4	2.4	1.0
27	Yáñez et al. (2004) - Pattern 1-Clay Brick-1	162	1.4	0.9	1.2	0.9	0.8	1.7	2.2	1.6	1.2	2.1	0.9
28	Yáñez et al. (2004) - Pattern 1-Clay Brick-2	191	1.2	0.8	1.0	0.8	0.7	1.5	1.8	1.4	1.0	1.8	0.7
29	Marinilli and Castilla (2004) - M1	215	1.1	0.8	1.3	0.9	0.9	2.4	2.7	2.3	1.0	1.8	0.8
30	Zabala et al. (2004) - 1	118	2.1	1.1	2.6	1.2	1.2	1.8	2.4	1.7	1.5	2.4	1.0
31	Zabala et al. (2004) - 2	93	2.7	1.4	3.3	1.5	1.5	2.3	3.1	2.2	1.9	3.0	1.3
32	Zabala et al. (2004) - 3	207	1.4	0.8	1.9	0.9	1.1	1.4	1.8	1.3	1.0	1.7	0.8
33	Zabala et al. (2004) - 4	235	1.2	0.7	1.6	0.8	0.9	1.3	1.5	1.2	0.9	1.5	0.7
34	Gouveia and Lourenço (2007) - W2.4	95	1.1	0.8	1.3	1.0	0.8	0.8	1.0	0.7	1.4	1.0	0.7
35	Gouveia and Lourenço (2007) - W2.4	95	1.1	0.8	1.3	1.0	0.8	0.8	1.0	0.7	1.4	1.0	0.7
36	Bourzam et al. (2008a) - JCM	81	1.2	0.9	0.8	0.9	0.7	1.2	1.5	1.0	1.7	1.5	0.9
37	Bourzam et al. (2008b) - CM30J-1	78	1.3	0.9	0.9	1.0	0.8	1.2	1.6	1.1	1.8	1.6	0.9
38	Bourzam et al. (2008b) - CM30J-2	161	0.8	0.7	0.9	0.8	0.6	0.9	1.1	0.8	1.0	0.9	0.7
39	Kuroki et al. (2010) - CMWO-01	194	0.7	0.6	0.7	0.6	0.5	1.1	1.3	1.0	0.9	1.3	0.6
40	Kuroki et al. (2010) - CMWO-07	83	1.3	1.0	1.5	1.1	1.1	1.8	2.2	1.7	1.7	2.1	1.1
41	Wijaya et al. (2011) - A	51	2.5	1.1	3.4	0.7	1.6	2.3	3.2	2.1	2.5	3.2	1.1
42	Bourzam et al. (2013) - CM60J	92	1.3	1.0	0.7	1.1	0.8	1.3	1.7	1.2	1.7	1.7	1.0
43	Matošević et al. (2014) - A1	156	1.5	0.8	1.2	0.9	0.9	0.9	1.1	0.8	1.0	1.1	0.7
44	Matošević et al. (2014) - A2	125	1.8	0.9	1.5	1.2	1.0	1.1	1.4	0.9	1.3	1.4	0.9
45	Matošević et al. (2014) - A3	180	1.2	0.7	1.1	0.8	0.7	0.8	1.0	0.6	0.9	1.0	0.6
46	Gavilán et al. (2015) - ME1	46	2.7	1.0	1.9	1.1	1.6	2.1	2.5	2.0	2.4	2.5	1.1
47	Gavilán et al. (2015) - ME2	76	1.6	0.9	1.8	1.0	1.2	1.4	1.6	1.3	1.7	1.6	0.9
48	Gavilán et al. (2015) - ME3	99	1.4	0.9	1.8	1.0	1.2	1.3	1.6	1.3	1.5	1.6	0.9
49	Gavilán et al. (2015) - ME4	157	1.0	0.7	1.5	0.8	0.9	1.2	1.4	1.1	1.0	1.4	0.6
50	Gavilán et al. (2015) - ME5	321	0.7	0.6	1.1	0.7	0.7	1.0	1.2	0.9	0.7	1.2	0.5
51	Varela-Rivera et al. (2019) - M1	80	2.2	1.9	2.1	1.7	1.3	2.9	4.1	2.7	2.6	4.1	1.8
52	Varela-Rivera et al. (2019) - M2	53	2.7	2.0	2.3	1.9	1.5	2.4	3.4	2.2	3.2	3.3	2.1
53	Varela-Rivera et al. (2019) - M3	65	2.5	1.9	2.4	1.9	1.5	2.1	2.9	1.9	2.8	2.9	1.9
54	Varela-Rivera et al. (2019) - M4	26	4.2	2.4	2.8	2.3	1.9	3.0	5.1	2.8	5.2	5.1	2.8
55	Varela-Rivera et al. (2019) - M5	35	3.5	2.1	2.7	2.2	1.8	2.5	4.0	2.2	4.1	4.0	2.3
56	Varela-Rivera et al. (2019) - M6	45	2.9	2.0	2.6	2.1	1.7	2.1	3.3	1.8	3.4	3.3	2.0

	$V_{m,e}$	M&L3	M&L2	S&R	M&L1	Ria	Bzm1	Bzm2	Bzm3	M&C	T&K	F&A
57 Cruz et al. (2019) - MB0	301	1.0	0.8	0.8	0.8	0.9	1.6	2.0	1.4	0.9	2.1	0.8
58 Gavilán (2020) - M1-1	189	1.2	1.1	1.6	1.3	1.1	1.1	1.3	0.9	1.2	1.3	0.8
59 Gavilán (2020) - M2-1	219	1.1	1.2	2.0	1.4	1.2	1.4	1.6	1.3	1.2	1.6	0.8
60 Present study - S1	48	2.1	0.7	1.1	0.8	0.8	1.3	1.7	1.2	2.2	1.4	0.7
61 Present study - S2	56	1.9	0.7	1.2	0.8	0.8	1.3	1.6	1.2	2.0	1.3	0.8
62 Present study - S3	81	1.5	0.7	1.3	0.8	0.8	1.5	2.0	1.4	1.6	1.8	0.7
63 Wijaya et al. (2011) - C	43	3.0	1.3	4.1	0.8	1.9	2.8	3.8	2.5	3.0	3.8	1.3
64 Matošević et al. (2014) - B1	167	1.4	0.7	1.1	0.9	0.8	0.9	1.1	0.7	1.0	1.1	0.6
65 Matošević et al. (2014) - B2	131	1.8	0.9	1.5	1.1	1.0	1.1	1.3	0.9	1.2	1.3	0.8
66 Matošević et al. (2014) - B3	129	1.6	0.9	1.5	1.1	0.9	1.1	1.3	0.9	1.3	1.3	0.8
67 Quiroz et al. (2017) - A1-1	230	1.6	0.8	1.0	1.0	0.7	1.3	1.7	1.2	0.9	1.6	0.7
68 Quiroz et al. (2017) - A1-2	248	1.5	0.7	1.0	0.9	0.6	1.2	1.6	1.1	0.8	1.5	0.7
69 Quiroz et al. (2017) - A2-1	179	2.1	1.0	1.3	1.3	0.8	1.7	2.2	1.5	1.1	1.9	0.9
70 Quiroz et al. (2017) - A2-2	248	1.5	0.7	1.0	0.9	0.6	1.2	1.6	1.1	0.8	1.5	0.7
71 Marinilli and Castilla (2004) - M2	269	1.5	0.7	1.1	0.7	0.7	2.4	2.6	2.3	0.9	1.4	0.6
72 Marinilli and Castilla (2004) - M3	245	1.7	0.7	1.2	0.8	0.8	2.6	2.9	2.5	1.0	1.6	0.7
73 Marinilli and Castilla (2004) - M4	310	2.2	0.6	1.0	0.6	0.6	2.5	2.7	2.4	0.9	1.3	0.5
74 Gavilán et al. (2015) - ME6	95	1.0	0.4	0.7	0.3	0.6	1.3	1.5	1.3	1.6	1.0	0.4
75 Gavilán et al. (2015) - ME7	90	1.1	0.5	0.9	0.4	0.8	1.1	1.3	1.1	1.8	1.2	0.5
76 Singhal and Rai (2014) - SC_{NT}	98	1.0	0.4	0.8	0.3	0.7	1.0	1.2	1.0	1.6	1.1	0.4
77 Singhal and Rai (2014) - SC_{CT}	690	0.7	0.5	0.9	0.5	0.6	0.9	0.9	0.8	0.6	0.9	0.4
78 Singhal and Rai (2014) - SC_{FT}	835	1.0	0.5	1.2	0.6	0.7	0.9	0.9	0.8	0.6	0.9	0.5

M&L3 = Marques and Lourenço (2019) (Eq. 9b); M&L2 = Marques and Lourenço (2019) (Eq. 9a); S&R = Singhal and Rai (2014); M&L1 = Marques and Lourenço (2013) (Eq. 6a); Ria = Riahi et al. (2009); Bzm1 = Bourzam et al. (2008a) (Eq. 4a); Bzm2 = Bourzam et al. (2008a) (Eq. 4b); Bzm3 = Bourzam et al. (2008a) (Eq. 4c); M&C = Marinilli and Castilla (2006); T&K = Tomaževič and Klemenc (1997a); F&A = Flores and Alcocer (1996).

Table 6.7: Comparison of predicted and experimentally obtained lateral loads at cracking for all the specimens.

Sr	Experimental Study and Model Id	$V_{cr,e}$ (kN)	$V_{cr,p}/V_{cr,e}$ Gav	Ria	M&C	F&A	Mex	Per	Chl	Arg	Col	CR	EC	Chn	Ind
1	Kato et al. (1992) - A	150	1.2	1.0	1.1	0.8	1.2	0.8	1.0	2.3	0.5	0.7	2.3	2.3	1.2
2	Kato et al. (1992) - B	150	1.2	1.0	1.1	0.8	1.2	0.8	1.0	2.3	0.5	0.7	2.3	2.3	1.2
3	Kato et al. (1992) - C	120	1.5	1.2	1.4	1.0	1.5	1.0	1.3	2.9	0.6	0.8	2.9	2.9	1.5
4	Kato et al. (1992) - D	100	1.7	1.5	1.6	1.2	1.7	1.2	1.6	3.5	0.7	1.0	3.5	3.5	1.7
5	Aguilar et al. (1996) - MO	103	0.8	0.8	0.8	0.7	0.8	0.7	0.7	1.4	0.9	1.1	1.4	0.8	1.0
6	Iiba et al. (1996) - IDM	79	0.9	0.7	0.9	0.7	0.9	0.7	0.8	1.4	0.9	0.9	1.4	0.7	1.1
7	Iiba et al. (1996) - IDJ	100	1.0	1.0	1.0	0.8	1.0	0.7	0.9	1.8	1.0	1.2	1.8	1.2	1.2
8	Iiba et al. (1996) - HDJ	90	1.1	1.2	1.1	0.9	1.1	0.8	1.0	2.0	1.1	1.3	2.0	1.3	1.3
9	Yoshimura et al. (1996) - 4-H0V0	173	0.7	0.6	0.6	0.5	0.7	0.6	0.5	1.1	0.6	0.7	1.1	0.7	0.8
10	Yoshimura et al. (1996) - 1-H0V0	186	0.7	0.6	0.6	0.5	0.7	0.6	0.5	1.1	0.6	0.7	1.1	0.8	0.8
11	Tomaževič and Klemenc (1997a) - AH-1	1.1	1.3	1.1	1.3	1.1	1.3	1.0	1.1	2.2	1.7	1.9	2.2	1.1	1.6
12	Tomaževič and Klemenc (1997a) - AH-3	0.6	2.4	2.0	2.3	2.0	2.4	1.7	2.0	3.9	3.0	3.5	3.9	2.0	2.9
13	Tomaževič and Klemenc (1997a) - AH-2	0.6	2.4	2.0	2.3	2.0	2.4	1.7	2.0	3.9	3.0	3.5	3.9	2.0	2.9
14	Yoshimura et al. (2000) - H1-H0V0-HC	175	1.0	0.7	0.9	0.7	1.0	0.8	0.8	1.4	0.9	0.9	1.4	0.7	1.2
15	Yoshimura et al. (2000) - H1-H0V0-LC	130	1.0	0.9	0.9	0.7	1.0	0.8	0.8	1.6	0.8	1.0	1.6	1.1	1.1
16	Yoshimura et al. (2000) - H1-H0V0-T	72	0.8	0.7	0.7	0.5	0.8	0.7	0.7	1.5	0.6	1.0	1.5	1.6	0.8
17	Yoshimura et al. (2000) - L1-H0V0-HC	240	0.8	0.6	0.7	0.6	0.8	0.6	0.6	1.1	0.7	0.7	1.1	0.6	0.9
18	Yoshimura et al. (2000) - L1-H0V0-LC	190	0.7	0.6	0.6	0.5	0.7	0.6	0.5	1.1	0.6	0.7	1.1	0.8	0.8
19	Yoshimura et al. (2000) - L1-H0V0-T	105	0.7	0.6	0.6	0.4	0.7	0.6	0.6	1.3	0.6	0.9	1.3	1.4	0.7
20	Kumazawa and Ohkubo (2000) - ISM	80	1.1	0.8	1.1	0.8	1.1	0.9	1.0	1.8	1.1	1.1	1.8	0.8	1.2
21	Yoshimura et al. (2004a) - 2D-H1-H0V0-48-2	88	1.8	1.5	1.5	1.2	1.8	1.6	1.4	3.1	1.5	2.1	3.1	2.7	1.9
22	Yoshimura et al. (2004a) - 2D-H1-H0V0-84-2	96	1.9	1.7	1.7	1.3	1.9	1.7	1.5	3.2	1.6	2.1	3.2	2.6	2.1
23	Yoshimura et al. (2004a) - 2D-L1-H0V0-48-1	88	1.2	1.1	1.1	0.8	1.2	1.1	1.0	2.1	1.0	1.4	2.1	1.7	1.3
24	Yoshimura et al. (2004a) - 2D-L1-H0V0-84-1	140	0.9	0.8	0.8	0.6	0.9	0.7	0.7	1.4	0.8	0.9	1.4	1.0	1.0
25	Yáñez et al. (2004) - Pattern 1-CMU-1	60	2.6	1.8	2.0	1.4	2.6	2.1	1.9	4.2	1.7	2.6	4.2	4.2	2.6
26	Yáñez et al. (2004) - Pattern 1-CMU-2	68	2.3	1.6	1.7	1.2	2.3	1.9	1.7	3.7	1.6	2.3	3.7	3.7	2.4
27	Yáñez et al. (2004) - Pattern 1-Clay Brick-1	147	1.2	0.8	0.9	0.6	1.2	0.9	0.9	1.9	0.8	1.1	1.9	1.9	1.2

28 Yáñez et al. (2004) - Pattern 1-Clay Brick-2	128	1.4	0.9	1.0	0.7	1.4	1.1	1.0	2.2	0.9	1.3	2.2	2.2	1.4
29 Marinilli and Castilla (2004) - M1	134	1.4	1.1	1.1	0.9	1.4	1.1	1.0	2.1	1.0	1.4	2.1	1.7	1.5
30 Zabala et al. (2004) - 1	65	1.8	1.7	1.7	1.4	1.8	1.7	1.6	3.2	2.2	3.0	3.2	2.6	2.0
31 Zabala et al. (2004) - 2	65	1.8	1.7	1.7	1.4	1.8	1.7	1.6	3.2	2.2	3.0	3.2	2.6	2.0
32 Zabala et al. (2004) - 3	155	1.0	1.0	0.9	0.8	1.0	0.9	0.8	1.6	1.1	1.4	1.6	1.1	1.1
33 Zabala et al. (2004) - 4	160	0.9	0.9	0.9	0.8	0.9	0.8	0.8	1.6	1.1	1.4	1.6	1.1	1.1
34 Gouveia and Lourenço (2007) - W2.4	58	1.1	0.9	1.1	0.9	1.1	0.9	0.9	1.8	1.1	1.1	1.8	0.9	1.3
35 Gouveia and Lourenço (2007) - W2.4	58	1.1	0.9	1.1	0.9	1.1	0.9	0.9	1.8	1.1	1.1	1.8	0.9	1.3
36 Bourzam et al. (2008a) - JCM	70	1.0	0.9	1.0	0.7	1.0	0.7	0.9	1.9	0.6	0.7	1.9	1.7	1.1
37 Bourzam et al. (2008b) - CM30J-1	70	1.0	0.9	1.0	0.7	1.0	0.7	0.9	1.9	0.6	0.7	1.9	1.7	1.1
38 Bourzam et al. (2008b) - CM30J-2	101	1.0	1.0	1.0	0.8	1.0	0.7	0.9	1.8	0.7	0.8	1.8	1.2	1.2
39 Kuroki et al. (2010) - CMWO-01	136	0.9	0.7	0.8	0.6	0.9	0.8	0.7	1.5	0.7	1.0	1.5	1.2	0.9
40 Kuroki et al. (2010) - CMWO-07	33	2.4	2.2	2.1	1.8	2.4	2.1	2.0	4.0	2.1	2.7	4.0	3.0	2.7
41 Wijaya et al. (2011) - A	38	1.4	1.2	1.4	1.0	1.4	1.4	1.3	2.9	1.3	2.0	2.9	2.9	1.4
42 Bourzam et al. (2013) - CM60J	72	1.3	1.2	1.2	0.9	1.3	0.8	1.2	2.5	0.7	1.0	2.5	2.2	1.4
43 Matošević et al. (2014) - A1	113	0.9	0.9	0.9	0.7	0.9	0.8	0.8	1.6	0.7	0.8	1.6	1.1	1.1
44 Matošević et al. (2014) - A2	89	1.2	1.2	1.1	0.9	1.2	1.0	1.0	2.0	0.9	1.0	2.0	1.3	1.3
45 Matošević et al. (2014) - A3	125	0.8	0.8	0.8	0.7	0.8	0.7	0.7	1.4	0.6	0.7	1.4	1.0	1.0
46 Gavilán et al. (2015) - ME1	45	0.9	0.9	0.9	0.8	0.9	0.6	0.8	1.5	1.1	1.3	1.5	0.9	1.1
47 Gavilán et al. (2015) - ME2	71	0.9	0.9	0.8	0.7	0.9	0.6	0.7	1.5	0.9	1.1	1.5	0.9	1.0
48 Gavilán et al. (2015) - ME3	88	0.9	0.9	0.9	0.7	0.9	0.7	0.8	1.5	1.0	1.2	1.5	1.0	1.0
49 Gavilán et al. (2015) - ME4	101	1.0	1.0	0.9	0.8	1.0	0.8	0.8	1.6	1.1	1.3	1.6	1.0	1.1
50 Gavilán et al. (2015) - ME5	252	0.8	0.7	0.6	0.5	0.8	0.6	0.6	1.2	0.7	0.9	1.2	0.8	0.9
51 Varela-Rivera et al. (2019) - M1	60	2.4	2.2	2.2	1.7	2.4	2.2	2.1	4.5	1.6	2.1	4.5	4.0	2.5
52 Varela-Rivera et al. (2019) - M2	35	3.0	2.7	2.8	2.2	3.0	2.2	2.7	5.7	2.0	2.7	5.7	5.1	3.2
53 Varela-Rivera et al. (2019) - M3	50	2.4	2.3	2.3	1.8	2.4	1.7	2.1	4.4	1.7	2.1	4.4	3.6	2.6
54 Varela-Rivera et al. (2019) - M4	20	3.4	3.1	3.2	2.4	3.4	1.7	3.0	6.5	2.3	3.1	6.5	5.8	3.6
55 Varela-Rivera et al. (2019) - M5	28	2.8	2.6	2.6	2.1	2.8	1.5	2.4	5.1	2.0	2.5	5.1	4.2	3.0
56 Varela-Rivera et al. (2019) - M6	20	4.4	4.3	4.2	3.4	4.4	2.5	3.8	7.8	3.3	3.8	7.8	5.8	4.9
57 Cruz et al. (2019) - MB0	163	1.3	1.2	1.2	1.0	1.3	1.2	1.2	2.4	0.8	1.0	2.4	2.1	1.4
58 Gavilán (2020) - M1-1	143	1.0	0.6	1.1	0.6	1.0	1.0	0.9	1.7	1.2	1.2	1.7	0.6	1.0
59 Gavilán (2020) - M2-1	174	1.0	0.7	1.1	0.7	1.0	1.0	1.0	1.8	1.3	1.3	1.8	0.7	1.0
60 Present study - S1	34	0.9	0.9	0.9	0.7	0.9	0.6	0.8	1.8	0.8	1.2	1.8	1.6	1.0
61 Present study - S2	38	1.1	1.0	1.0	0.8	1.1	0.8	0.9	2.0	0.9	1.3	2.0	1.8	1.1
62 Present study - S3	61	1.0	0.8	0.9	0.7	1.0	0.9	0.8	1.8	0.8	1.1	1.8	1.6	1.0
63 Wijaya et al. (2011) - C	25	2.2	1.9	2.1	1.5	2.2	2.2	2.0	4.4	2.0	3.0	4.4	4.4	2.2
64 Matošević et al. (2014) - B1	117	0.9	0.9	0.8	0.7	0.9	0.7	0.8	1.5	0.7	0.8	1.5	1.0	1.0
65 Matošević et al. (2014) - B2	92	1.1	1.2	1.1	0.9	1.1	0.9	1.0	2.0	0.9	1.0	2.0	1.3	1.3
66 Matošević et al. (2014) - B3	90	1.2	1.2	1.1	0.9	1.2	1.0	1.0	2.0	0.9	1.0	2.0	1.3	1.3
67 Quiroz et al. (2017) - A1-1	130	1.3	1.1	1.2	0.9	1.3	1.2	1.1	2.4	0.9	1.2	2.4	2.1	1.4
68 Quiroz et al. (2017) - A1-2	167	1.0	0.9	0.9	0.7	1.0	0.9	0.9	1.8	0.7	0.9	1.8	1.6	1.1
69 Quiroz et al. (2017) - A2-1	172	1.0	0.9	0.9	0.7	1.0	0.9	0.8	1.8	0.7	0.9	1.8	1.6	1.1
70 Quiroz et al. (2017) - A2-2	167	1.0	0.9	0.9	0.7	1.0	0.9	0.9	1.8	0.7	0.9	1.8	1.6	1.1
71 Marinilli and Castilla (2004) - M2	210	0.9	0.7	0.7	0.6	0.9	0.7	0.7	1.4	0.7	0.9	1.4	1.7	1.0
72 Marinilli and Castilla (2004) - M3	140	1.3	1.1	1.1	0.9	1.3	1.1	1.0	2.0	1.0	1.3	2.0	2.5	1.4
73 Marinilli and Castilla (2004) - M4	160	1.1	0.9	0.9	0.7	1.1	0.9	0.9	1.8	0.9	1.1	1.8	2.7	1.3
74 Gavilán et al. (2015) - ME6	65	0.7	0.5	0.5	0.4	0.7	0.5	0.5	1.1	0.6	0.9	1.1	1.5	0.7
75 Gavilán et al. (2015) - ME7	61	0.8	0.5	0.6	0.4	0.8	0.6	0.6	1.3	0.7	1.0	1.3	1.8	0.8
76 Singhal and Rai (2014) - SC_{NT}	66	0.8	0.5	0.6	0.4	0.8	0.6	0.5	1.2	0.7	1.0	1.2	1.6	0.8
77 Singhal and Rai (2014) - SC_{CT}	473	0.9	0.6	0.6	0.5	0.9	0.6	0.5	1.1	0.6	0.8	1.1	1.0	1.0
78 Singhal and Rai (2014) - SC_{FT}	628	0.9	0.6	0.6	0.5	0.9	0.5	0.5	1.0	0.6	0.8	1.0	1.0	1.0
	$V_{cr,e}$	Gav	Ria	M&C	F&A	Mex	Per	Chl	Arg	Col	CR	EC	Chn	Ind

Gav = Gavilán et al. (2015); Mex = Mexico Code (NTC-M 2017); Per = Peruvian Code (NT E.070 2019); Chl = Chilean Code (NCh2123 2003); Arg = Argentinian Code (INPRES 2018); Col = Colombian Code (NSR-98 2010); CR = Costa Rican Code (CSCR 2002); EC = Eurocode (CEN 2005); Chn = Chinese Code (GB 50003 2011); and Ind = Indian Code (BIS 2021).

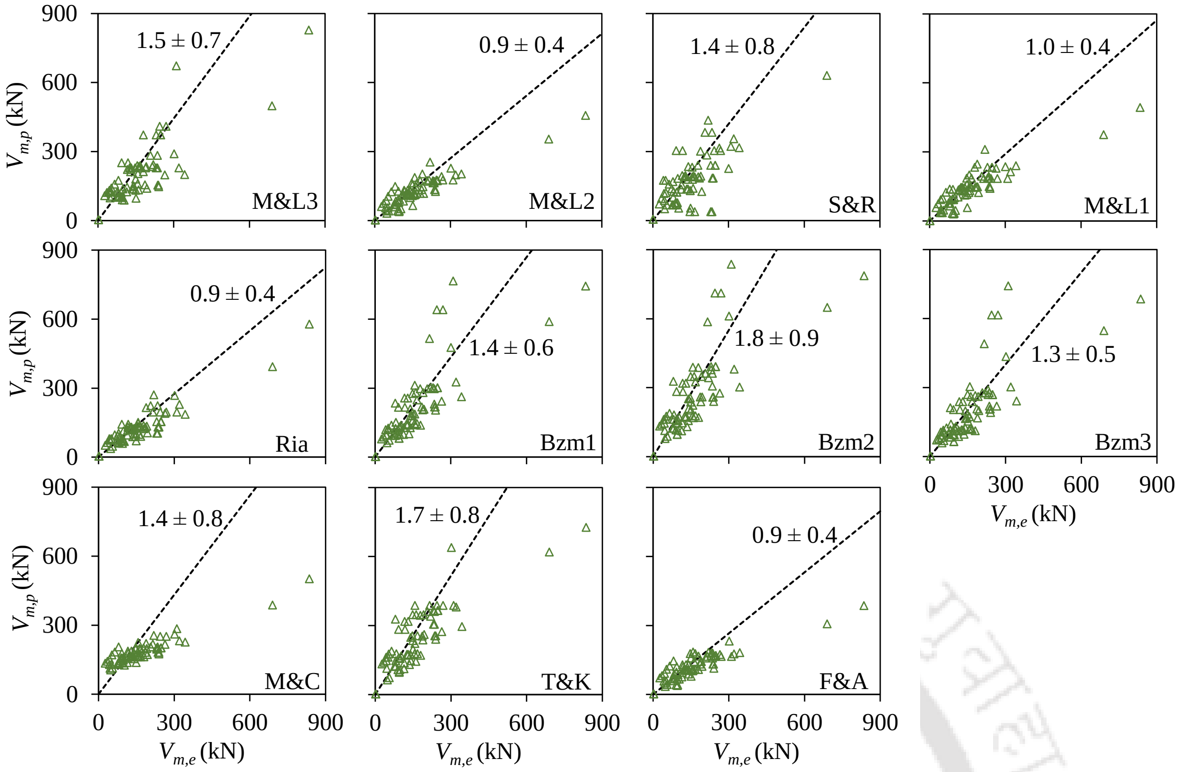

Figure 6.3: Effectiveness of different equations in predicting the lateral strength (numbers inside the chart represent mean $V_{m,p}/V_{m,e}$, i.e., slope of the dotted line, with standard deviation).

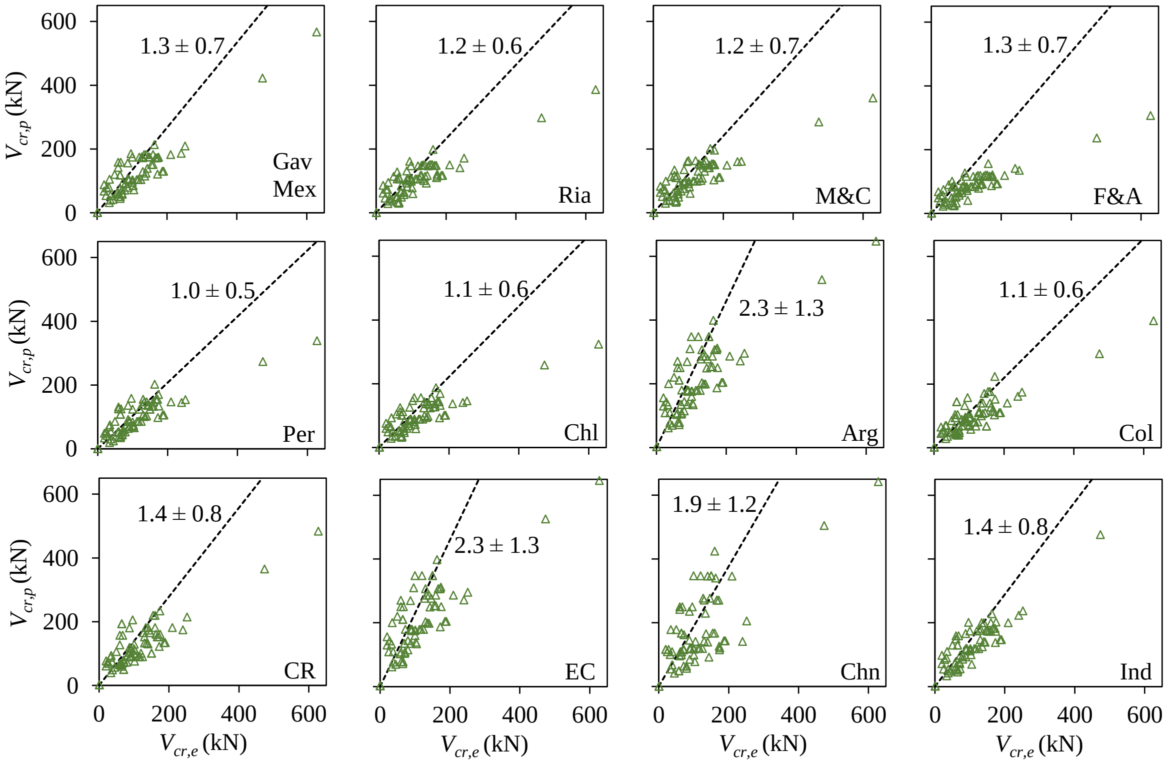

Figure 6.4: Effectiveness of different equations in predicting the lateral load at cracking (numbers inside the chart represent mean $V_{cr,p}/V_{cr,e}$, i.e., slope of the dotted line, with standard deviation).

To gain more insight into the obtained results, the number of studies for which the equations overestimate or underestimate the lateral strength of confined masonry walls are shown in Table 6.8 along with the average error obtained in the underestimation or overestimation of the strength. For single-bay CM specimens, the average error in prediction of lateral strength is lower for underestimated cases (varying from 5% to 44%) than that for overestimation cases (varying from 35% to 90%). Clearly, when the equations overestimate the lateral strength, the overestimation is done with a big margin of error. The second part of the lateral strength equation (Eq. 6.3a) proposed by Marinilli and Castilla (2006) gives a constant minimum additive lateral strength of 82 kN as a contribution by the tie-elements, thus the predicted lateral capacities were very high (maximum error goes up to 326%) in comparison to the experimental values for the one fifth-scale specimens of Tomaževič and Klemenc (1997a) as given in Table 6.6, whose total lateral strengths were observed to be just 1.6 kN to 2.3 kN from the experimental study. These three specimens were therefore removed from the database of Marinilli and Castilla (2006) while evaluating the accuracy of the model in lateral capacity estimation. Again, in case of multi-bay confined masonry specimens, the average error in prediction of lateral strength is almost similar for the underestimated (varying from 6% to 101%) and overestimated (varying from 14% to 105%) cases. The mean values and standard deviation of predicted to experimental strength ratios obtained for all seventy-eight specimens (also shown in Fig. 6.3) shows the variation in predicted to experimental lateral strength ratios across all the specimens using all the equations considered in the study. Similarly, the four available equations suggested in past studies for predicting the lateral load of CM walls at initial cracking (Table 6.1), along with the nine equations provided in the design codes (Table 6.3), were also evaluated using the experimental database to compare their effectiveness as shown in Table 6.9. For single-bay CM specimens, the average error in prediction is lower for underestimated cases (varying from 13% to 35%) than that observed in overestimated cases (varying from 63% to 141%). Clearly, the equations predict with much larger errors whenever they overestimate the lateral loads. On the other hand, for multi-bay specimens most of the equations underestimate the cracking load with mean prediction error varying from 3% to 58%; and the mean overprediction error varying from 0% to 96%, where the equations proposed by the design codes of Argentina, Eurocode, and China mostly overestimate the load.

Table 6.8: Lateral strength prediction: underestimated and overestimated cases.

Equation →	M&L3	M&L2	S&R	M&L1	Ria	Bzm1	Bzm2	Bzm3	M&C	T&K	F&A
Single-bay CM wall specimens (Total 70)											
No. of underestimated cases	16	51	22	42	47	16	4	22	19	6	51
Average of ($V_{m,p}/V_{m,e} < 1$)	0.79	0.77	0.70	0.80	0.73	0.87	0.95	0.81	0.84	0.94	0.73
Average error (%)	26	30	44	24	36	15	5	23	19	6	36
No. of overestimated cases	54	19	48	28	23	54	66	48	48	64	19
Average of ($V_{m,p}/V_{m,e} > 1$)	1.71	1.42	1.79	1.35	1.37	1.60	1.90	1.54	1.73	1.86	1.45
Average error (%)	71	42	79	35	37	60	90	54	73	86	45
Multi-bay CM wall specimens (Total 8)											
No. of underestimated cases	3	8	4	8	8	2	2	3	4	2	8
Average of ($V_{m,p}/V_{m,e} < 1$)	0.89	0.54	0.82	0.53	0.69	0.87	0.94	0.86	0.75	0.88	0.50
Average error (%)	13	86	21	90	44	15	6	16	33	13	101
No. of overestimated cases	5	0	4	0	0	6	6	5	4	6	0
Average of ($V_{m,p}/V_{m,e} > 1$)	1.51	-	1.14	-	-	1.82	2.05	1.91	1.50	1.27	-
Average error (%)	51	-	14	-	-	82	105	91	50	27	-
All 78 Specimens											
Average of $V_{m,p}/V_{m,e}$	1.48	0.90	1.40	0.97	0.92	1.45	1.84	1.33	1.44	1.72	0.88
Standard deviation	0.69	0.39	0.79	0.39	0.35	0.57	0.85	0.55	0.81	0.84	0.43

Table 6.9: Prediction of lateral loads at cracking: underestimated and overestimated cases.

Equation →	Gav	Ria	M&C	F&A	Mex	Per	Chl	Arg	Col	CR	EC	Chn	Ind
Single-bay CM wall specimens (Total 70)													
No. of underestimated cases	25	39	32	30	25	46	43	0	40	25	0	19	13
Average of ($V_{cr,p}/V_{cr,e} < 1$)	0.87	0.82	0.82	0.85	0.87	0.78	0.81	-	0.74	0.83	-	0.81	0.88
Average error (%)	15	21	22	17	15	28	24	-	35	21	-	23	13
No. of overestimated cases	45	31	38	40	45	24	27	70	30	45	70	51	57
Average of ($V_{cr,p}/V_{cr,e} > 1$)	1.66	1.70	1.63	1.68	1.66	1.64	1.72	2.41	1.66	1.78	2.41	2.30	1.64
Average error (%)	66	70	63	68	66	64	72	141	66	78	141	130	64
Multi-bay CM wall specimens (Total 8)													
No. of underestimated cases	6	7	7	7	6	7	8	0	7	4	0	2	4
Average of ($V_{cr,p}/V_{cr,e} < 1$)	0.83	0.63	0.64	0.68	0.83	0.65	0.65	-	0.69	0.83	-	0.97	0.82
Average error (%)	20	58	56	47	20	54	55	-	46	20	-	3	22
No. of overestimated cases	2	1	1	1	2	1	0	8	1	4	8	6	4
Average of ($V_{cr,p}/V_{cr,e} > 1$)	1.23	1.08	1.07	1.13	1.23	1.06	-	1.37	1.00	1.13	1.37	1.96	1.18
Average error (%)	23	8	7	13	23	6	-	37	0	13	37	96	18
All 78 Specimens													
Average of $V_{cr,p}/V_{cr,e}$	1.33	1.16	1.20	1.27	1.33	1.04	1.11	2.30	1.09	1.39	2.30	1.88	1.45
Standard deviation	0.70	0.65	0.66	0.70	0.70	0.48	0.61	1.30	0.60	0.77	1.30	1.19	0.75

As discussed earlier, the equations proposed by Marques and Lourenço (2013), Marques and Lourenço (2019) (Eq. 9a), Riahi et al. (2009), and Flores and Alcocer (1996) provide a comparatively accurate estimation of experimental strength values; whereas, the design codes of Peru, Chile, and Colombia provide better prediction of lateral load at cracking on an average when data for all the seventy-eight CM walls are considered. Some studies have proposed equations for estimation of both cracking load and lateral strength (Riahi et al. 2009, Marinilli and Castilla 2006, and Flores and Alcocer 1996); average value (± standard deviation) of predicted cracking strength to predicted lateral strength ratios were found to be 0.86 ± 0.26, 0.57 ± 0.18, and 0.95 ± 0.04, respectively. In fact, the cracking load predicted by Riahi et al. (2009) using Eq. (6.5b) comes out to be higher (maximum 1.6 times) than the lateral strength using Eq. (6.5a) in nineteen single-bay specimens. It is to be noted here that the lateral strength or lateral load at cracking predicted using any of the equations were quite high for some of the single-bay CM specimens, such as walls with 0.5% longitudinal reinforcement in tie-columns of CM walls tested by Varela-Rivera et al. (2019), CMWO-07 wall of Kuroki et. al (2010), wall with low reinforcement and axial load of Zabala et al., concrete masonry unit walls of Yáñez et. al (2004), and one-fifth scaled specimens of Tomaževič and Klemenc (1997a) as given in Tables 6.6 and 6.7. This is understandable as all the models are unable to consider the influence of the variation in input parameters considered in these specimens. Thus, if these specimens are removed, the maximum overestimation error reduces to 64% (from 90%) and 90% (from 141%), respectively, for the prediction of lateral strength and lateral load at cracking of single-bay CM specimens. With these studies removed from the database, the lateral strength predicted using Marques and Lourenço (2013) and Singhal and Rai (2016) provide better prediction on an average for single and multi-bay specimens, respectively; and the cracking load estimated using Gavilán et al. (2015) and codes of Mexico and India provide good prediction on an average both for single as well as multi-bay specimens. Further, for the comparative analyses of all the models, the ultimate lateral strength before failure is considered at 20% degradation of peak lateral strength, i.e., $V_{u,p} = 0.8V_{m,p}$.

6.5.2 Initial Lateral Stiffness

The effectiveness of the four equations in predicting the initial lateral stiffness (Table 6.2) was evaluated by utilizing them on all the seventy-eight CM walls tested in the past experimental studies as given in Table 6.10. Eqs. (10) and (11) (Flores and Alcocer 1996 or Tomaževič and Klemenc 1997a and Bourzam et al. 2008b) highly overestimate the initial stiffness in most of the cases, as these equations were derived on the basis of experimental behavior of URM walls (also shown in Fig. 6.5). However, the equations work well when used in their own studies, for example, Bourzam et al. (2008b) provides accurate estimation for their own experimental study using β = 12. High variation in the predicted stiffnesses is evident in Fig. 6.5 that shows the scattering of data points representing the predicted stiffness in relation to the experimentally obtained stiffnesses for all the studies. Fig. 6.5 also shows the mean values of the ratios of predicted to experimental stiffnesses for all the experimental studies along with their standard deviations. Table 6.11 gives the total number of experimental studies for which the equations provide overestimation or underestimation of lateral stiffness. For single-bay specimens, Singhal and Rai (2016) and Riahi et al. (2009) underestimate the stiffness most with higher errors. The other equations mostly overestimate the stiffness with very high errors. For eight multi-bay specimens, all equations except for that proposed by Singhal and Rai (2016) and Riahi et al. (2009) overestimate the stiffness by large margins. None of the equations estimate the lateral stiffness with acceptable accuracy; though, considering all the seventy-eight specimens, Riahi et al. (2009) provide a reliable estimation with slightly higher than acceptable values of standard deviation (also observed in Fig. 6.5).

Table 6.10: Estimation of initial lateral stiffness using existing equations.

Sr.	Experimental Study and Model Id	AR	$K_{i,e}$ (kN/mm)	$K_{i,p}/K_{i,e}$					
				S&R	Ria	Bzm		T&K, F&A	
						β=12	β=3	β=12	β=3
1	Kato et al. (1992) - A	1.53	150	0.3	0.4	2.4	1.3	2.0	0.9
2	Kato et al. (1992) - B	1.53	150	0.3	0.4	2.4	1.3	2.0	0.9
3	Kato et al. (1992) - C	1.53	120	0.4	0.4	3.0	1.6	2.5	1.1
4	Kato et al. (1992) - D	1.53	100	0.5	0.5	3.5	1.9	3.0	1.3
5	Aguilar et al. (1996) - MO	1.02	38	0.4	0.6	4.7	2.8	2.0	0.9
6	Iiba et al. (1996) - IDM	1.39	60	0.2	0.3	3.1	1.6	1.3	0.5
7	Iiba et al. (1996) - IDJ	1.53	1250	0.0	0.0	0.3	0.2	0.3	0.1
8	Iiba et al. (1996) - HDJ	1.53	1286	0.0	0.0	0.3	0.1	0.3	0.1
9	Yoshimura et al. (1996) - 4-H0V0	0.75	288	0.3	0.3	1.7	1.2	1.3	0.6
10	Yoshimura et al. (1996) - 1-H0V0	0.75	311	0.4	0.3	1.8	1.3	1.6	0.7
11	Tomaževič and Klemenc (1997a) - AH-1	1.58	1.8	0.3	1.5	9.4	4.6	1.8	0.8
12	Tomaževič and Klemenc (1997a) - AH-3	1.58	2.4	0.3	1.2	7.2	3.5	1.4	0.6
13	Tomaževič and Klemenc (1997a) - AH-2	1.58	1.0	0.6	2.7	16.8	8.1	3.3	1.4
14	Yoshimura et al. (2000) - H1-H0V0-HC	0.75	224	0.4	0.3	2.0	1.4	1.5	0.7
15	Yoshimura et al. (2000) - H1-H0V0-LC	0.75	181	0.6	0.5	3.2	2.2	2.7	1.2
16	Yoshimura et al. (2000) - H1-H0V0-T	0.75	86	0.8	0.9	4.8	3.4	3.7	1.6
17	Yoshimura et al. (2000) - L1-H0V0-HC	0.75	400	0.3	0.2	1.4	1.0	1.2	0.5
18	Yoshimura et al. (2000) - L1-H0V0-LC	0.75	288	0.4	0.3	2.0	1.4	1.7	0.7
19	Yoshimura et al. (2000) - L1-H0V0-T	0.75	175	0.6	0.5	3.1	2.2	2.7	1.2
20	Kumazawa and Ohkubo (2000) - ISM	1.24	23	0.2	1.0	5.2	2.9	1.2	0.5
21	Yoshimura et al. (2004a) - 2D-H1-H0V0-48-2	0.77	368	0.8	0.4	3.7	2.6	3.7	1.6
22	Yoshimura et al. (2004a) - 2D-H1-H0V0-84-2	0.77	324	1.1	0.5	4.6	3.2	4.7	2.0
23	Yoshimura et al. (2004a) - 2D-L1-H0V0-48-1	0.77	368	0.3	0.3	1.6	1.1	1.4	0.6
24	Yoshimura et al. (2004a) - 2D-L1-H0V0-84-1	0.77	392	0.3	0.2	1.4	1.0	1.2	0.5
25	Yáñez et al. (2004) - Pattern 1-CMU-1	0.63	146	0.4	0.6	2.7	2.3	1.4	0.6
26	Yáñez et al. (2004) - Pattern 1-CMU-2	0.63	165	0.4	0.5	2.4	2.1	1.2	0.5
27	Yáñez et al. (2004) - Pattern 1-Clay Brick-1	0.63	73	0.5	0.8	4.3	3.7	1.5	0.6
28	Yáñez et al. (2004) - Pattern 1-Clay Brick-2	0.62	106	0.3	0.6	3.0	2.6	1.0	0.4
29	Marinilli and Castilla (2004) - M1	0.78	48	1.1	1.6	7.8	5.4	5.1	2.2
30	Zabala et al. (2004) - 1	1.00	47	0.4	1.5	6.5	4.0	2.3	1.0

31	Zabala et al. (2004) - 2	1.00	28	0.7	2.6	10.8	6.7	3.8	1.6
32	Zabala et al. (2004) - 3	1.00	33	0.6	2.1	9.1	5.6	3.1	1.4
33	Zabala et al. (2004) - 4	1.00	43	0.5	1.7	7.0	4.3	2.4	1.1
34	Gouveia and Lourenço (2007) - W2.4	1.17	73	0.2	0.5	3.4	1.9	1.3	0.6
35	Gouveia and Lourenço (2007) - W2.4	1.17	73	0.2	0.5	3.4	1.9	1.3	0.6
36	Bourzam et al. (2008a) - JCM	1.53	135	0.1	0.2	1.0	0.6	0.7	0.3
37	Bourzam et al. (2008b) - CM30J-1	1.53	135	0.1	0.2	1.0	0.6	0.7	0.3
38	Bourzam et al. (2008b) - CM30J-2	1.53	191	0.1	0.1	0.7	0.4	0.5	0.2
39	Kuroki et al. (2010) - CMWO-01	0.79	285	0.5	0.2	2.6	1.8	2.4	1.0
40	Kuroki et al. (2010) - CMWO-07	0.79	56	1.0	0.7	6.3	4.3	4.5	2.0
41	Wijaya et al. (2011) - A	1.06	5	1.4	3.6	24.5	14.3	8.0	3.5
42	Bourzam et al. (2013) - CM60J	1.53	163	0.2	0.2	1.2	0.6	1.0	0.4
43	Matošević et al. (2014) - A1	1.31	44	0.7	0.6	10.0	5.4	4.2	1.8
44	Matošević et al. (2014) - A2	1.31	35	0.9	0.7	12.1	6.6	5.3	2.3
45	Matošević et al. (2014) - A3	1.31	44	0.7	0.6	8.8	4.8	4.2	1.8
46	Gavilán et al. (2015) - ME1	2.75	13	0.3	1.0	5.0	1.8	2.8	1.2
47	Gavilán et al. (2015) - ME2	1.73	20	0.5	0.8	4.7	2.1	3.8	1.7
48	Gavilán et al. (2015) - ME3	1.32	21	0.8	1.1	6.3	3.3	5.4	2.3
49	Gavilán et al. (2015) - ME4	1.04	54	0.5	0.5	3.4	2.0	2.9	1.3
50	Gavilán et al. (2015) - ME5	0.68	134	0.5	0.4	2.3	1.7	2.1	0.9
51	Varela-Rivera et al. (2019) - M1	1.10	22	1.2	1.4	9.0	5.0	7.0	3.1
52	Varela-Rivera et al. (2019) - M2	1.54	11	1.2	2.1	12.1	5.5	8.8	3.8
53	Varela-Rivera et al. (2019) - M3	1.54	23	0.6	1.0	5.8	2.6	4.1	1.8
54	Varela-Rivera et al. (2019) - M4	2.57	3	1.5	5.3	22.6	8.0	14.2	6.1
55	Varela-Rivera et al. (2019) - M5	2.57	6	0.7	2.5	11.1	3.9	6.7	2.9
56	Varela-Rivera et al. (2019) - M6	2.57	4	0.9	3.3	14.8	5.3	9.0	3.9
57	Cruz et al. (2019) - MB0	1.03	153	0.3	0.4	2.1	1.3	1.4	0.6
58	Gavilán (2020) - M1-1	1.06	32	0.1	0.7	0.4	0.3	0.5	0.2
59	Gavilán (2020) - M2-1	1.05	39	0.4	0.9	2.2	1.6	1.4	0.6
60	Present study - S1	2.00	12	0.4	1.5	11.8	5.1	2.9	1.2
61	Present study - S2	1.50	13	0.6	1.7	13.6	6.8	3.9	1.7
62	Present study - S3	1.00	20	0.8	1.5	11.5	7.1	4.2	1.8
63	Wijaya et al. (2011) - C	1.06	2	4.6	11.3	77.5	45.0	25.4	11.0
64	Matošević et al. (2014) - B1	1.31	39	0.8	0.7	11.3	6.2	4.7	2.0
65	Matošević et al. (2014) - B2	1.31	29	1.1	0.9	14.5	7.9	6.3	2.7
66	Matošević et al. (2014) - B3	1.31	37	0.8	0.7	10.3	5.6	4.9	2.1
67	Quiroz et al. (2017) - A1-1	1.07	118	0.2	0.4	3.9	2.5	1.1	0.5
68	Quiroz et al. (2017) - A1-2	1.07	108	0.2	0.4	4.2	2.7	1.2	0.5
69	Quiroz et al. (2017) - A2-1	1.07	98	0.3	0.4	4.7	3.0	1.4	0.6
70	Quiroz et al. (2017) - A2-2	1.07	108	0.2	0.4	4.2	2.7	1.2	0.5
71	Marinilli and Castilla (2004) - M2	0.78	44	1.5	1.8	9.8	6.8	5.6	2.4
72	Marinilli and Castilla (2004) - M3	0.78	49	1.3	1.6	8.9	6.1	5.0	2.2
73	Marinilli and Castilla (2004) - M4	0.78	84	0.9	0.9	5.8	4.0	2.9	1.3
74	Gavilán et al. (2015) - ME6	0.61	45	0.9	0.7	4.6	3.5	3.1	1.3
75	Gavilán et al. (2015) - ME7	0.55	35	1.1	0.9	5.9	4.7	3.6	1.6
76	Singhal and Rai (2014) - SC$_{NT}$	0.55	31	1.3	1.1	7.0	5.5	4.5	1.9
77	Singhal and Rai (2014) - SC$_{CT}$	0.40	202	0.8	0.4	2.7	2.3	2.4	1.0
78	Singhal and Rai (2014) - SC$_{FT}$	0.26	298	0.9	0.4	2.6	2.4	2.3	1.0
		AR	$K_{i,e}$	S&R	Ria	Bzm	Bzm	T&K,	F&A

Bzm = Bourzam et al. (2008b) (Eq. 11)

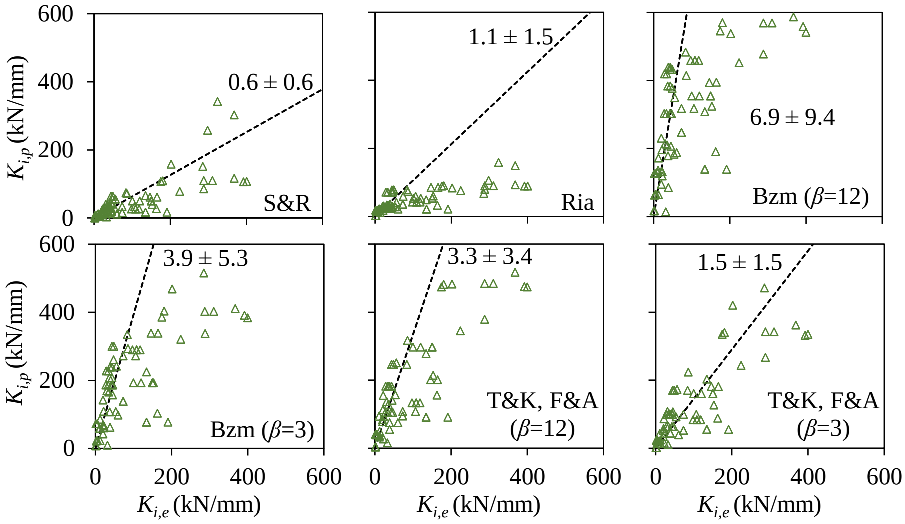

Figure 6.5: Effectiveness of different equations in predicting the lateral stiffness (numbers inside the chart represent mean $K_{i,p}/K_{i,e}$, i.e., slope of the dotted line, with standard deviation).

Table 6.11: Prediction of initial lateral stiffness: underestimated and overestimated cases.

Equation →	S&R	Ria	Bzm β=12	Bzm β=3	T&K, F&A β=12	T&K, F&A β=3
Single-bay CM wall specimens (Total 70)						
No. of underpredicted cases	62	50	4	9	7	35
Average of ($K_{i,p}/K_{i,e}$ < 1)	0.44	0.48	0.45	0.53	0.55	0.56
Average error (%)	126	114	123	90	80	78
No. of overpredicted cases	8	20	66	61	63	35
Average of ($K_{i,p}/K_{i,e}$ > 1)	1.65	2.56	7.37	4.36	3.61	2.31
Average error (%)	65	156	637	336	261	131
Multi-bay CM wall specimens (Total 8)						
No. of underpredicted cases	4	5	0	0	0	1
Average of ($K_{i,p}/K_{i,e}$ < 1)	0.9	0.6	-	-	-	1.0
Average error (%)	16	54	-	-	-	1
No. of overpredicted cases	4	3	8	8	8	7
Average of ($K_{i,p}/K_{i,e}$ > 1)	1.30	1.48	5.90	4.42	3.69	1.69
Average error (%)	30	48	490	342	269	69
All 78 Specimens						
Average of $K_{i,p}/K_{i,e}$	0.63	1.06	6.86	3.92	3.34	1.45
Standard deviation	0.58	1.48	9.45	5.29	3.44	1.49

6.5.3 Lateral Drift at Initial Cracking, Lateral Strength, and Ultimate Load at Failure

Lateral drift of a structure is expressed as a ratio of top lateral displacement to the height of the structure. Equations for estimation of lateral drift at different limit states have been suggested by Riahi et al. (2009) as given in Eqs. (6.17), (6.19), and (6.21). On the other hand, Flores and Alcocer (1996) suggested constant values for drift at lateral strength and ultimate load at failure (Eqs. 6.18 and 6.20). Though the drift values at different damage stages can also be obtained indirectly using the stiffness (initial and degraded) equations suggested by Tomaževič and Klemenc (1997a), and Bourzam et al. (2008b) using lateral load values, the estimated lateral load or stiffness were not closer to the experimentally obtained values as observed previously, and thus, those methods were not considered for drift estimation. Table 6.12 shows the experimental and predicted lateral drift values obtained at different damage stages for sixty-three confined masonry walls, for which the experimentally reported drift values were obtained satisfactorily. The effectiveness of individual equations in predicting the lateral drifts is also evaluated in Fig. 6.6, in which the mean value of predicted to experimental drift ratios and its standard deviation is also shown for each equation. Table 6.13 gives the total number of experimental studies for which the equations provide underestimation or overestimation of lateral drifts at different damage stages.

As observed, the mean value of lateral drift at cracking load predicted using the two available methods considering all sixty-three confined masonry wall specimens varies from 0.05% to 0.14%. It was further observed that Flores and Alcocer (1996) mostly underpredict the lateral drift at cracking load with an average error of 125%. Whereas, the overpredicted cases are more when Riahi et al. (2009) was used for prediction. The obtained average error was 56% in underprediction and 113% in overprediction. The mean values and standard deviation of predicted to experimental lateral drift at cracking show that both the methods are not suitable for drift estimation at cracking load (also shown in Fig. 6.6). Further, the mean value of the lateral drift at lateral strength predicted using the two methods is around 0.3%, and both the equations mostly underpredict the drift at lateral strength. Interestingly, the average error in underprediction of the mean values is lower than the error obtained in the overprediction cases. Though the mean ratio of predicted to experimental drift at lateral strength values are approximately 1.0, the standard deviation is quite high with both methods. Again, the mean value of lateral drift at ultimate limit predicted using both the methods is around 0.5%, and both of the methods underpredict the observed ultimate drift in experimental studies. The average error in underprediction is quite high compared to overpredicted cases.

Table 6.12: Estimation of lateral drift (%) of CM walls at the three damage stages using existing equations.

Sr.	Studies	$\delta_{cr,e}$	$\delta_{cr,p}$			$\delta_{m,e}$	$\delta_{m,p}$		$\delta_{u,e}$	$\delta_{u,p}$	
		Exp	Ria	F&A β=12	F&A β=3	Exp	Ria	F&A	Exp	Ria	F&A
1	Kato et al. (1992) - A	0.08	0.21	0.04	0.08	0.62	0.28	0.30	1.17	0.43	0.5
2	Kato et al. (1992) - B	0.08	0.21	0.04	0.08	0.24	0.28	0.30	0.85	0.43	0.5
3	Kato et al. (1992) - C	0.08	0.21	0.04	0.08	0.23	0.31	0.30	0.94	0.48	0.5
4	Kato et al. (1992) - D	0.08	0.21	0.04	0.08	0.17	0.31	0.30	0.75	0.48	0.5
5	Aguilar et al. (1996) - MO	0.12	0.15	0.05	0.08	0.44	0.45	0.30	0.67	0.70	0.5
6	Yoshimura et al. (1996) - 4-H0V0	0.05	0.12	0.02	0.03	0.11	0.17	0.30	0.36	0.26	0.5
7	Yoshimura et al. (1996) - 1-H0V0	0.05	0.11	0.02	0.03	0.16	0.16	0.30	0.61	0.25	0.5
8	Yoshimura et al. (2000) - H1-H0V0-HC	0.07	0.13	0.04	0.05	0.38	0.15	0.30	0.55	0.23	0.5
9	Yoshimura et al. (2000) - H1-H0V0-LC	0.06	0.11	0.02	0.03	0.30	0.16	0.30	1.00	0.25	0.5
10	Yoshimura et al. (2000) - H1-H0V0-T	0.07	0.06	0.01	0.02	0.20	0.18	0.30	1.00	0.28	0.5
11	Yoshimura et al. (2000) - L1-H0V0-HC	0.05	0.13	0.03	0.04	0.32	0.15	0.30	0.36	0.23	0.5
12	Yoshimura et al. (2000) - L1-H0V0-LC	0.06	0.11	0.02	0.03	0.17	0.16	0.30	0.51	0.25	0.5
13	Yoshimura et al. (2000) - L1-H0V0-T	0.05	0.06	0.01	0.02	0.21	0.17	0.30	0.75	0.26	0.5
14	Kumazawa and Ohkubo (2000) - ISM	0.27	0.21	0.26	0.47	0.61	0.28	0.30	1.48	0.44	0.5
15	Yoshimura et al. (2004a) - 2D-H1-H0V0-48-2	0.02	0.07	0.01	0.01	0.20	0.11	0.30	0.26	0.17	0.5
16	Yoshimura et al. (2004a) - 2D-H1-H0V0-84-2	0.03	0.09	0.01	0.01	0.20	0.11	0.30	0.47	0.17	0.5
17	Yoshimura et al. (2004a) - 2D-L1-H0V0-48-1	0.02	0.08	0.02	0.02	0.10	0.16	0.30	0.22	0.24	0.5
18	Yoshimura et al. (2004a) - 2D-L1-H0V0-84-1	0.03	0.11	0.02	0.03	0.03	0.16	0.30	0.40	0.25	0.5
19	Yáñez et al. (2004) - Pattern 1-Clay Brick-1	0.10	0.10	0.06	0.07	0.54	0.39	0.30	1.12	0.60	0.5
20	Yáñez et al. (2004) - Pattern 1-Clay Brick-2	0.06	0.10	0.06	0.07	0.64	0.39	0.30	1.08	0.60	0.5
21	Marinilli and Castilla (2004) - M1	0.13	0.09	0.03	0.04	0.36	0.24	0.30	0.42	0.37	0.5
22	Zabala et al. (2004) - 1	0.05	0.06	0.04	0.07	0.16	0.23	0.30	0.63	0.36	0.5
23	Zabala et al. (2004) - 2	0.09	0.06	0.04	0.07	0.18	0.23	0.30	0.76	0.36	0.5
24	Zabala et al. (2004) - 3	0.18	0.08	0.05	0.09	0.54	0.26	0.30	0.71	0.40	0.5
25	Zabala et al. (2004) - 4	0.14	0.08	0.05	0.09	0.50	0.26	0.30	0.91	0.40	0.5
26	Gouveia and Lourenço (2007) - W2.4	0.08	0.13	0.07	0.12	0.29	0.27	0.30	0.56	0.41	0.5
27	Gouveia and Lourenço (2007) - W2.4	0.08	0.13	0.07	0.12	0.29	0.27	0.30	0.56	0.41	0.5
28	Kuroki et al. (2010) - CMWO-01	0.04	0.13	0.01	0.02	0.19	0.21	0.30	0.44	0.33	0.5
29	Kuroki et al. (2010) - CMWO-07	0.05	0.15	0.03	0.04	0.85	0.31	0.30	3.01	0.48	0.5
30	Wijaya et al. (2011) - A	0.26	0.09	0.05	0.08	0.75	0.34	0.30	1.08	0.53	0.5
31	Bourzam et al. (2013) - CM60J	0.03	0.20	0.05	0.08	0.03	0.32	0.30	0.47	0.49	0.5
32	Matošević et al. (2014) - A1	0.17	0.27	0.04	0.07	0.30	0.60	0.30	0.37	0.93	0.5
33	Matošević et al. (2014) - A2	0.17	0.27	0.04	0.07	0.41	0.63	0.30	0.54	0.96	0.5
34	Matošević et al. (2014) - A3	0.19	0.27	0.04	0.07	0.35	0.67	0.30	0.46	1.03	0.5
35	Gavilán et al. (2015) - ME1	0.15	0.15	0.05	0.14	0.40	0.30	0.30	1.55	0.46	0.5
36	Gavilán et al. (2015) - ME2	0.15	0.16	0.03	0.08	0.39	0.38	0.30	0.70	0.58	0.5
37	Gavilán et al. (2015) - ME3	0.18	0.16	0.03	0.06	0.25	0.38	0.30	0.47	0.59	0.5
38	Gavilán et al. (2015) - ME4	0.08	0.15	0.03	0.04	0.38	0.34	0.30	0.46	0.53	0.5
39	Gavilán et al. (2015) - ME5	0.08	0.15	0.03	0.04	0.35	0.32	0.30	0.35	0.49	0.5
40	Varela-Rivera et al. (2019) - M1	0.11	0.17	0.04	0.06	0.75	0.57	0.30	1.03	0.88	0.5
41	Varela-Rivera et al. (2019) - M2	0.13	0.17	0.04	0.10	1.50	0.57	0.30	1.84	0.88	0.5
42	Varela-Rivera et al. (2019) - M3	0.09	0.20	0.05	0.11	0.75	0.50	0.30	2.43	0.76	0.5
43	Varela-Rivera et al. (2019) - M4	0.28	0.17	0.07	0.19	2.00	0.57	0.30	2.66	0.87	0.5
44	Varela-Rivera et al. (2019) - M5	0.19	0.20	0.08	0.22	1.00	0.49	0.30	2.28	0.75	0.5
45	Varela-Rivera et al. (2019) - M6	0.18	0.23	0.09	0.25	0.75	0.46	0.30	1.88	0.71	0.5
46	Cruz et al. (2019) - MB0	0.05	0.14	0.04	0.07	0.38	0.18	0.30	0.72	0.28	0.5
47	Gavilán (2020) - M1-1	0.19	0.17	0.36	0.56	0.62	0.24	0.30	0.64	0.38	0.5
48	Gavilán (2020) - M2-1	0.20	0.14	0.14	0.18	0.59	0.17	0.30	0.60	0.26	0.5
49	Present study - S1	0.20	0.12	0.06	0.15	0.87	0.45	0.30	3.34	0.70	0.5
50	Present study - S2	0.20	0.12	0.05	0.11	0.82	0.45	0.30	1.40	0.70	0.5
51	Present study - S3	0.20	0.12	0.05	0.07	0.50	0.45	0.30	0.87	0.70	0.5
52	Wijaya et al. (2011) - C	0.54	0.09	0.05	0.08	1.40	0.34	0.30	2.46	0.53	0.5
53	Matošević et al. (2014) - B1	0.20	0.27	0.04	0.07	0.38	0.60	0.30	0.47	0.93	0.5
54	Matošević et al. (2014) - B2	0.21	0.27	0.04	0.07	0.65	0.63	0.30	0.76	0.96	0.5
55	Matošević et al. (2014) - B3	0.16	0.27	0.04	0.07	0.39	0.67	0.30	0.60	1.03	0.5
56	Marinilli and Castilla (2004) - M2	0.23	0.09	0.03	0.04	0.55	0.24	0.30	0.56	0.37	0.5

57	Marinilli and Castilla (2004) - M3	0.14	0.09	0.03	0.04	0.38	0.24	0.30	0.38	0.37	0.5
58	Marinilli and Castilla (2004) - M4	0.09	0.09	0.03	0.04	0.48	0.24	0.30	0.67	0.37	0.5
59	Gavilán et al. (2015) - ME6	0.10	0.15	0.03	0.03	0.32	0.30	0.30	0.32	0.47	0.5
60	Gavilán et al. (2015) - ME7	0.09	0.16	0.02	0.03	0.19	0.31	0.30	0.41	0.48	0.5
61	Singhal and Rai (2014) - SC_{NT}	0.10	0.09	0.02	0.03	0.40	0.25	0.30	0.85	0.38	0.5
62	Singhal and Rai (2014) - SC_{CT}	0.12	0.09	0.02	0.03	0.48	0.22	0.30	1.07	0.34	0.5
63	Singhal and Rai (2014) - SC_{FT}	0.15	0.08	0.02	0.03	0.49	0.22	0.30	1.79	0.33	0.5
		Exp	Ria	F&A	F&A	Exp	Ria	F&A	Exp	Ria	F&A

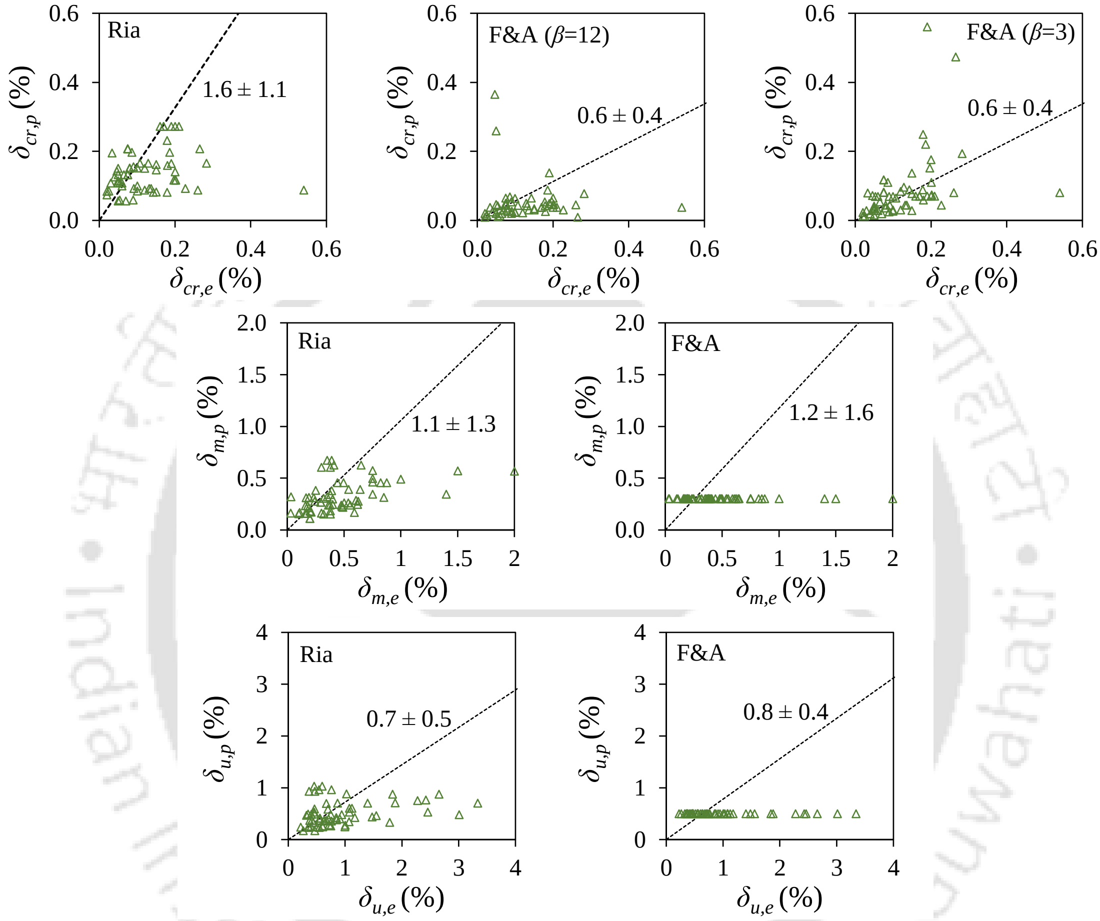

Figure 6.6: Effectiveness of different equations in predicting the lateral drift at different damage stages (numbers inside the chart represent mean $\delta_{cr,p}/\delta_{cr,e}$ or $\delta_{m,p}/\delta_{m,e}$ or $\delta_{u,p}/\delta_{u,e}$, i.e., slope of the dotted line, with standard deviation).

6.6 RECOMMENDATIONS ON BACKBONE ENVELOPES

Based on assessment of the past experimental results and formulations, a backbone envelope for lateral load-deformation of CM walls can be defined using three distinct stages corresponding to: cracking point, maximum strength point, and ultimate deformation point on the backbone envelope. Fig. 6.7(a) shows the developed trilinear envelopes for all seventy-eight CM walls obtained using their experimental data. For a better comparison, the envelopes are also plotted in Fig. 6.7(b) by normalizing the lateral loads with respect to their corresponding lateral strength.

Table 6.13: Lateral drift prediction: underestimated and overestimated cases.

Equation →	Ria	F&A (β=12)	F&A (β=3)
Drift at Initial Cracking			
Average ± Stdev of $\delta_{cr,p}$ (%)	0.14 ± 0.06	0.05 ± 0.05	0.09± 0.09
No. of underpredicted cases	21	57	57
Average of ($\delta_{cr,p} / \delta_{cr,e} < 1$)	0.64	0.44	0.44
Average error (%)	56	125	125
No. of overpredicted cases	42	6	6
Average of ($\delta_{cr,p} / \delta_{cr,e} > 1$)	2.13	1.68	1.68
Average error (%)	113	68	68
Average of $\delta_{cr,p} / \delta_{cr,e}$	1.63	0.56	0.56
Standard deviation	1.09	0.45	0.45
Drift at Maximum Capacity			
Average ± Stdev of $\delta_{m,p}$ (%)	0.33 ± 0.15	0.30± 0	
No. of underpredicted cases	45	41	
Average of ($\delta_{m,p} / \delta_{m,e} < 1$)	0.62	0.58	
Average error (%)	62	71	
No. of overpredicted cases	18	20	
Average of ($\delta_{m,p} / \delta_{m,e} > 1$)	2.16	2.40	
Average error (%)	116	140	
Average of $\delta_{m,p}/ \delta_{m,e}$	1.06	1.18	
Standard deviation	1.28	1.58	
Drift at Ultimate Load			
Average ± Stdev of $\delta_{u,p}$ (%)	0.50 ± 0.23	0.50± 0	
No. of underpredicted cases	49	45	
Average of ($\delta_{u,p} / \delta_{u,e} < 1$)	0.50	0.56	
Average error (%)	101	78	
No. of overpredicted cases	14	18	
Average of ($\delta_{u,p} / \delta_{u,e} > 1$)	1.51	1.32	
Average error (%)	51	32	
Average of $\delta_{u,p} / \delta_{u,e}$	0.72	0.78	
Standard deviation	0.50	0.43	

The trilinear backbone curves of seventy-eight CM walls show the high variability associated with all three damage stages. Though researchers have suggested various equations for the prediction of lateral load at cracking, it can also be simply estimated from the lateral strength of CM walls as: $V_{cr,p} = C_{cr}V_{m,p}$, where C_{cr} is a reduction factor that varies from 0.6 to 0.8 in different studies as already discussed in Table 6.1. For the considered experimental database, C_{cr}, taken as $V_{cr,e} /V_{m,e}$, is found to vary from 0.35 to 1.0 with mean value of 0.7 and standard deviation of 0.13. Clearly, from both the experimental database and the available equations, the mean lateral load at cracking can be suitably taken as 70% of the mean lateral strength. Similarly, the ultimate lateral load before failure can be taken from available equations as: $V_{u,p} = C_{sr}V_{m,p}$, where C_{sr} is the strength reduction factor. Taking clue from the data obtained experimentally and that prescribed by different relations, the present study recommends C_{sr} as 0.8. Thus, the recommended value of lateral load at ultimate limit (in the post-peak region) is 80% of the lateral strength.

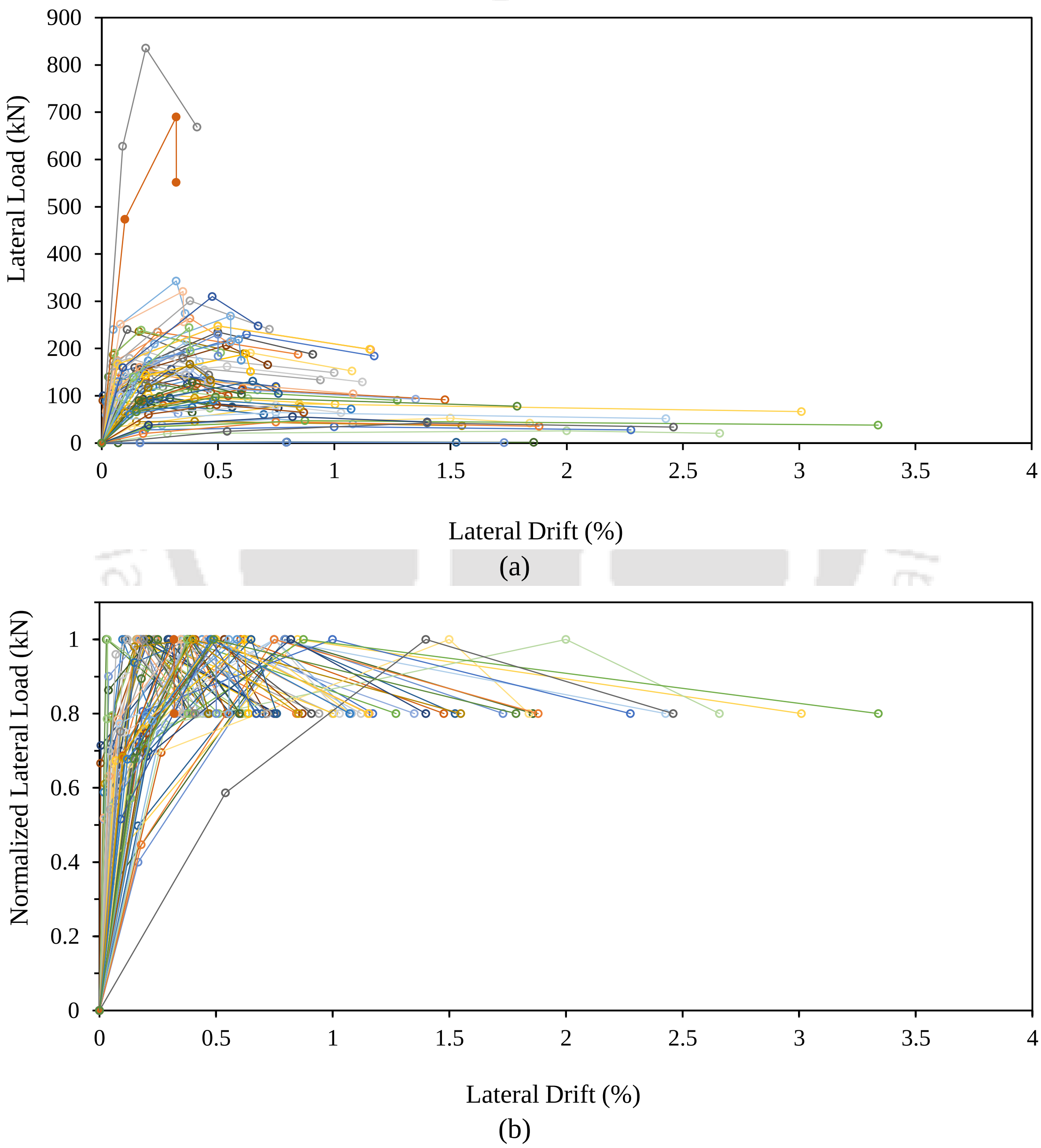

Figure 6.7: Trilinear lateral load – deformation envelopes for seventy-eight experimental studies: (a) actual envelopes, and (b) by normalizing the lateral loads with lateral strength.

Even though various equations have been suggested in the past studies for the prediction of different deformation levels for confined masonry walls, it was observed that the predicted results are significantly different from the experimentally obtained results and observations. The lateral loads at various stages can be predicted with a better confidence level; however, the same is not true for deformations because of the high level of uncertainty in deformation prediction, especially in the nonlinear range. The lateral displacement corresponding to the cracking load can be estimated from the in-plane initial stiffness and lateral cracking load of the wall. However, the displacement corresponding to the maximum load and ultimate load before collapse are difficult to predict due to the complex failure mechanism of masonry. For the considered experimental database, the lateral drift at cracking ($\delta_{cr,e}$) varies from 0.01% to 0.54% (mean 0.11, and standard deviation 0.08). In the seventy-eight experimental studies, the lateral drift at lateral strength ($\delta_{m,e}$) is observed to vary from 0.03% to 2.0% (mean 0.46, standard deviation 0.33). The ultimate drift for 20% strength degradation of the wall ($\delta_{u,e}$) is observed to vary from 0.22% to 3.34% (mean 0.94, standard deviation 0.67).

The scattered experimental data points representing three damage stages corresponding to the cracking stage, maximum resistance stage, and ultimate deformation stage in the post-peak regime are shown in Fig. 6.8 by removing the outliers from the dataset. The normalized trilinear envelope curve shown in Fig. 6.8 is developed from the mean values of the suggested load and deformation values as discussed above. To facilitate the designers in estimating the lateral load response of CM walls, an idealized trilinear lateral load-deformation curve is also developed as shown in Fig. 6.9. The recommendations include simple relations to estimate not only the lateral loads at three critical points, but also the corresponding lateral drift values. The mathematical formulations are derived by unconstrained multiple variable linear regression analysis of the experimentally obtained data by removing the outliers. As clear from Fig. 6.9 and already discussed in Fig. 6.8, the recommended lateral loads corresponding to the cracking stage and the ultimate deformation stage are actually derived from the lateral strength values observed from past experimental and analytical studies. The recommended equations for estimation of lateral drifts, shown in Fig. 6.9, are comparatively much simpler as they require lesser input parameters than that required by other existing equations given in Tables 6.1 and 6.2. Moreover, the recommended equations for lateral drifts estimate the values at different damage stages with better accuracy as evident from the comparison of Figs. 6.6 and 6.10.

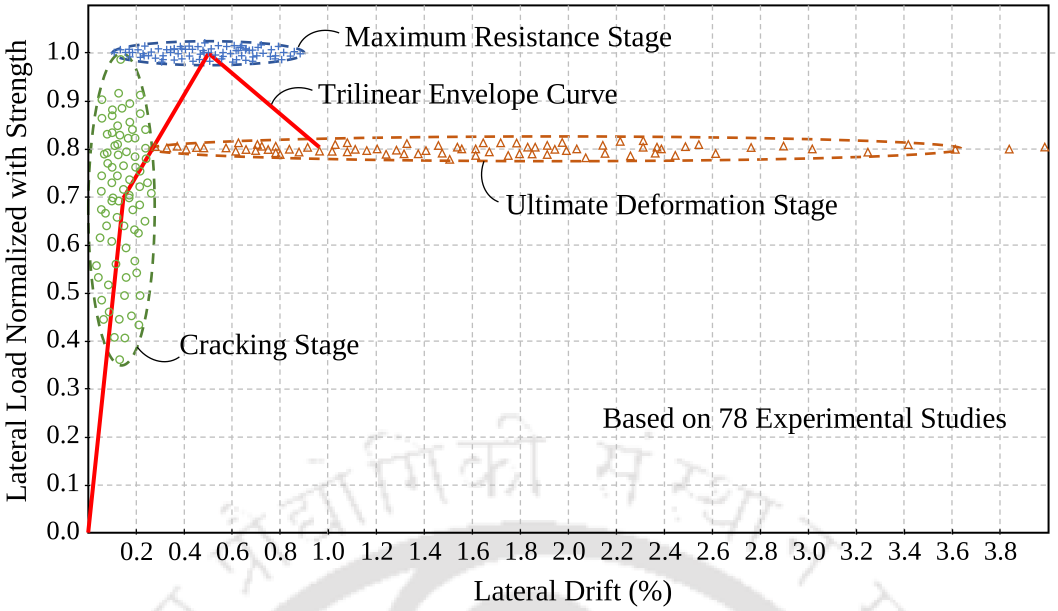

Figure 6.8: Development of the normalized trilinear envelope curve from the experimental responses.

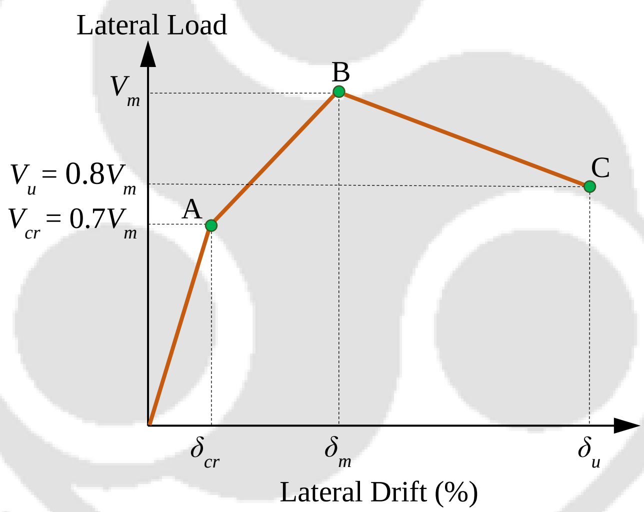

$V_{cr} = 0.7V_m$	
$V_m = \left[\dfrac{(f'_m)^{0.4}(nA_c/A)^{0.9}}{(\mathrm{AR})^{0.7}}\right](1+\sigma)A$	
$V_u = 0.8V_m$	
Clay Brick Masonry	Concrete Block Masonry
$\delta_{cr} = (\mathrm{AR})^{0.125}(f'_m)^{-0.983}$	$\delta_{cr} = (\mathrm{AR})^{-4.1}(f'_m)^{-1.5}$
$\delta_m = 1.5\ (\mathrm{AR})\ (\delta_{cr})$	$\delta_m = 3.7\ (\mathrm{AR})\ (\delta_{cr})$
$\delta_u = 2.0\ (\delta_m)$	$\delta_u = 1.8\ (\delta_m)$

Figure 6.9: Recommended Idealized trilinear lateral load – deformation curve for CM walls.

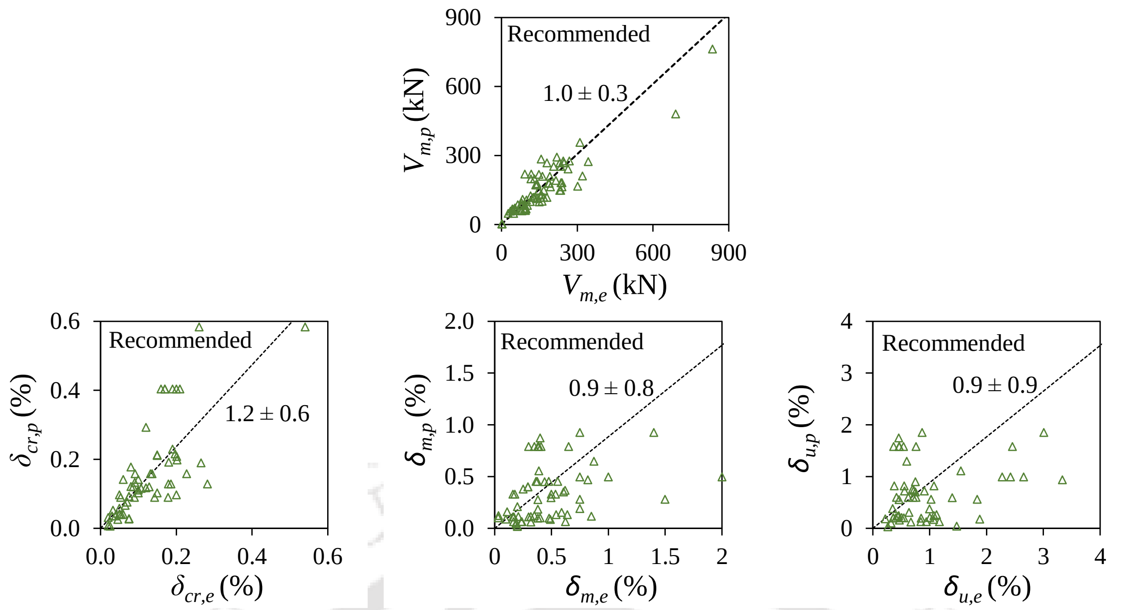

Figure 6.10: Effectiveness of the recommended empirical equations in predicting the lateral strength and lateral drift at the three damage stages.

6.7 SUMMARY

Seismic analysis and performance-based design of confined masonry walls require accurate representation of lateral stiffness, strength, and deformation capacity. Several past experimental testing of CM walls demonstrated that there are a number of parameters that significantly influence the lateral load response of CM walls. The in-plane hysteretic responses of CM walls have been commonly idealized in the past as trilinear lateral load-deformation envelope curves using different formulations available in the literature. However, these models, which assume different sets of parameters that may differ regionally, are difficult to be generalized because of their specific calibration for particular CM wall schemes. Large variations in important parameters, such as compressive (f'_m = 1.7 MPa to 61 MPa) and shear (v_m = 0.24 to 2.74 MPa) strength of masonry, compressive strength of concrete (f_c = 10 to 44 MPa), wall aspect ratio (H_w/L_w = 0.3 to 2.75), longitudinal reinforcement in tie-columns (0.5% to 6.6% of the cross-sectional area), cross-sectional area of tie-columns with respect to the total area (nA_c/A = 0.07 to 0.32), and vertical axial load on walls (σ = -0.1 to 1.8 MPa), introduce many challenges in developing idealized load-deformation envelop curves for analysis and design of CM walls.

Most of the past studies have concentrated on prediction of lateral loads, while only a few have recommended some methods for lateral drift estimation at different damage stages. From the comparison of the existing models, it was observed that the lateral strength equation recommended by Marques and Lourenço (2013) provides comparatively better prediction. Similarly, Gavilán et al. (2015) provides better prediction of cracking load. As far as the prediction of lateral drifts at different damage stages are concerned, the available two methods (Riahi et al. 2009 and Flores and Alcocer 1996) show very large variations. This is primarily because of huge variation in the lateral drifts observed in the past experimental studies due to sensitivity of lateral load response of masonry walls to different parameters.

Keeping these uncertainties into consideration, it becomes imperative to try and obtain even simpler empirical equations for prediction of complete lateral load response of CM walls. Therefore, in the present study, an easy-to-use trilinear backbone curve model is developed for CM walls on the basis of past experimental results. The developed model uses simple geometric, loading, and material parameters as input variables, and characterize the lateral load response of CM walls into three different damage stages – those corresponding to – cracking load, strength, and ultimate load. The predicted strength and drift values not only demonstrate better mean and standard deviations compared to the existing equations, but also show much better fit with the experimentally obtained responses. The proposed simplified load-deformation envelop model will provide an additional tool to the users in nonlinear seismic analysis for performance-based design. The results of the study can also be used to further improve the analysis and design guidelines for CM buildings. The uncertainties, especially in the prediction of ultimate deformation, highlights the large variability in available test results, and thus, more experimental investigations are required to develop a more refined backbone curve model.

Chapter 7
DESIGN FORCE ESTIMATION IN DIFFERENT MEMBERS

CONTENTS

7.1 OVERVIEW

In confined masonry buildings, masonry structural walls are confined on all four sides with reinforced concrete (RC) vertical and horizontal confining elements. Though masonry walls are the primary load-resisting members in CM walls, the RC confining members, particularly the tie-columns, play a key role in improving the structural integrity or stability and preventing extensive damage to masonry walls during an earthquake. Unlike the beams and columns in RC frame structures, the confining members of CM are generally not designed for seismic loads as there is not enough literature available to estimate the design forces. Some simplistic guidelines, mostly based on thumb rules, are available for controlling the minimum dimensions and minimum reinforcement detailing in confining elements. Only a few design codes recommend additional criteria, albeit in a limited manner, for seismic design of tie-members. For example, the Argentina code (INPRES-CIRSOC 103 2018) has some guidelines to estimate the design axial strength of tie-columns as a fraction of the wall shear. Peru code (NT E.070 2019) provides guidelines to evaluate the ultimate internal design forces (shear, tensile, and compression forces) for the confining elements. The confining columns are to be designed for shear force equal to a fraction of the design shear strength of the masonry wall depending upon the length of the wall and number of the tie-columns in the CM wall. Using this method, the shear force in tie-column of one bay CM walls comes out to be 50% of the design shear strength of the masonry wall; it is not clear if such values of design forces are adequate for tie-columns design. Mexico code (NTC-M 2017) suggests a simple methodology for estimation of minimum reinforcement area in tie-columns. Most of the existing design codes provide prescriptive provisions for the confining elements, such as guidelines on minimum cross-sectional size, number, diameter, spacing of longitudinal and transverse rebars. For instance, some codes simply suggest providing four bars as longitudinal reinforcement (diameter ranging from 5 mm to 12 mm) and 6 mm diameter ties in confining elements for acceptable seismic performance (Meli et al. 2011).

Because of the fact that confining elements are not typically designed through detailed structural calculations, the design and detailing of these elements are solely dependent on engineers' judgement and experience in construction practices. This can sometimes result into unnecessary large-sized tie-members without fully utilizing the material strength that the tie-members can additionally provide to the structure. On the other extreme, masonry walls of CM buildings may not resist the design forces as per the expectations and may fail prematurely if inadequate tie-columns are provided. This results in a potential seismic risk to these buildings, especially under bigger earthquake shakings where nonlinear response is expected from masonry walls as well as tie-elements of CM walls. These deficiencies related to inadequate design of tie-columns in CM buildings were observed during some of the past earthquakes, such as 2003 Tecomán, Mexico earthquake, 1985 Llolleo, and 2010 Maule, Chile earthquakes (Brzev 2007, Brzev and Mitra 2018). In 2010 Chile earthquake, the failure of tie-columns due to insufficient longitudinal and transverse reinforcement resulted in damage to masonry walls of some CM buildings (Fig. 7.1).

For seismic design of masonry infilled RC frame buildings, which resemble the CM buildings in appearance and materials used, several design codes recommend minimum design forces for RC columns though the columns are not subjected to any significant force resultants until infill walls are damaged (Kaushik et al. 2006). This is to ensure the safety of such buildings in case of failure of brittle masonry infill walls after which the entire loads are transferred to

RC frame. In case of CM walls too, it is important to distribute the seismic base shear to both masonry walls and tie-columns appropriately, and then design these members for improving their seismic performance during intense shakings. Clearly, a systematic design approach for the elements of CM buildings is of utmost importance for satisfactory performance.

Figure 7.1: Damage in CM walls due to premature failure of tie-columns in 2010 Chile earthquake of magnitude 8.8 (Brzev and Mitra 2018).

7.2 Influence of Tie-Members on Seismic Behavior of CM Walls

A few past experimental studies have shown the importance and significance of tie-elements in CM wall constructions by considering variations in their numbers, location, size, and their reinforcement content. The presence of more than two tie-columns in a CM wall is a common practice due to the limitation imposed in various codes on the length of the masonry panels to improve their lateral stability. The influence of additional number of tie-columns in a CM wall was studied by Marinilli and Castilla (2004) by testing four full-scaled CM walls with three different configurations of intermediate tie-columns. The first specimen was a regular single bay squat CM wall having aspect ratio (AR = H_w/L_w) of 0.78 (M1), second was with one intermediate tie-column making two panels of 1.65 aspect ratio (M2), third wall was with one intermediate tie-column having panels of 2.5 and 1.24 aspect ratio (M3), and the fourth wall was with two intermediate tie-columns having 2.63 aspect ratio for each of the three panels (M4). The quasi-static cyclic lateral load test showed that the inclusion of tie-columns increases the initial stiffness, strength, and ductility of CM walls, and allows a better damage distribution in the masonry panels in conjunction with a lesser and uniform spacing.

Another big influential parameter is the size of tie-columns as observed in the experimental study of San Bartolomé et al. (2010). In this study, lateral load performance of two identical CM walls (2.4m × 2.4m × 0.13m) with two different tie-column widths - M1 with 200 mm (AR = 1) and M2 with 400 mm (AR = 1.25) - were compared. Both the walls had horizontal wall reinforcement made with same materials; however, M2 had 5% additional vertical reinforcement in the tie-columns. From the test results, it was observed that wall M2 had significantly higher lateral strength mainly because of the greater concrete occupied area (33% of total area) than in M1 (17% of total area). The results of the tests also concluded that the tie-columns of M2 were oversized. The failure mechanism of M1 may be characterized by composite action of wall and tie-columns as the diagonal cracking in masonry wall propagated into the tie-columns. On the other hand, a vertical separation crack was observed between the wall and tie-columns in M2 with significant cracks in tie-columns. Thus, according to Meli et al. (2011), when tie-elements of a CM wall have larger sections (inplane dimension) or significant relative stiffness in comparison to masonry panel, the behavior of a CM wall is similar to infilled RC frames.

There is no consensus in the past literature on the influence of longitudinal and transverse reinforcement in tie-columns on the lateral strength of CM walls, though the lateral deformability and ductility have been found to consistently improve with increasing reinforcement content. It was observed in the shake table testing of CM walls with different variations in the tie-columns' axial reinforcement that four times increase in tie-columns' longitudinal reinforcement percentage (ρ_l) along with two times increase in transverse reinforcement percentage (ρ_t) did not result in any significant increase in the lateral strength of CM walls. However, the drift at peak lateral strength (δ_m) increased by two times and a slight increment was observed in the drift at ultimate load (δ_u) (Iiba et al. 1996). Contrary to this, from the quasi-static cyclic lateral load testing of four half-scaled CM walls with different tie-column reinforcement, Kato et al. (1992) observed that 3.8 times increase in ρ_l

resulted in 1.5 times increase in the lateral strength and 1.4 times increase in δ_m. Further, the drift capacity increased by 2.7 times with four times increase in ρ_t, though the cracking drift remained the same and only a slight increment was observed in δ_u. From the quasi-static cyclic lateral load testing of CM walls with different variations of overburden load and tie-column reinforcement, Zabala et al. (2004) found that 1.5 times increase in ρ_l, along with two times increase in overburden pressure (σ), increased the lateral load capacity of CM walls by around 2 times; whereas, δ_m increases by around 3 times and a slight increase was observed in δ_u. Quasi-static cyclic lateral load testing carried out on four full-scaled CM walls with different tie-element reinforcement also demonstrated that 1.3 times increase in ρ_l results in 1.4 times increase in the lateral capacity of CM; whereas, δ_m and δ_u increases by around 4 times (Quiroz et al. 2017).

Again, from different experimental and analytical investigations of CM walls under lateral loading, it was observed that the maximum lateral load resistance of a CM wall is generally around 1.4 times the lateral load resistance at the initial cracking, i.e., initial cracking occurs at 70% of lateral strength. For that, the tie-columns should have adequate strength and deformability to deliver sufficient confinement to the masonry wall by not allowing the brittle shear failure to occur under lateral loading. Therefore, it is essential to first understand how the load distribution takes place between masonry wall and tie-columns of a CM wall under the influence of relevant parameters so that a systemic, safe, and economical design methodology for the tie-columns can be proposed.

7.3 Distribution of Forces in CM Members

In CM buildings, it is assumed that initially the masonry wall resists the effect of lateral earthquake loads while the confining elements do not play a significant role. Once the cracking takes place in masonry units or mortar joints, the masonry panel becomes less effective in transferring the loads and the tie-columns become engaged in confining the masonry walls, thereby indirectly resisting the loads. Thus, it is very important to have the information on the required strength of the tie-columns for safe and affordable design of CM buildings. The forces developed in the members of a CM wall under lateral loading were investigated in the present study by adopting two methodologies: (a) using available equations for lateral strength estimation, and (b) by finite element (FE) simulation. In the first methodology, the existing equations for lateral strength estimation of CM wall were utilized for extracting the forces developed in the members of seventy-eight CM wall specimens tested in the past. Whereas, in the second methodology, FE simulation was first carried out on three CM walls tested previously by the authors. This was followed by a parametric FE study considering variations in several important input parameters for development of a generalized force distribution model.

7.3.1 Distribution of Forces based on Existing Formulations

As already explained in Chapter 6, some formulations have been recommended in past studies for the prediction of lateral strength of CM walls. In the existing methods, the lateral load at the initial cracking is mostly formulated with parameters related to only masonry wall; on the other hand, the lateral strength is formulated as additive resistance from masonry wall and tie-columns using different influencing parameters (Table 6.1). However, these formulations do not directly provide an estimation of individual member's (masonry wall and tie-columns) contribution to the strength. In the present study, an indirect method was followed to estimate the distribution of forces. In this approach, as given in Table 7.1, the contribution of masonry wall and tie-columns was arranged or separated (wherever possible) from the original equations in such a way that the additive resistance of these two terms provides the same lateral strengths that were obtained from the original equations. This methodology helped attaining some knowledge on the considered influence of tie-columns in existing formulations of lateral strength of CM wall. Here, the contribution of tie-columns represents combined resistance from all the tie-columns in a CM wall.

Table 7.1: Estimation of lateral strength of CM walls using existing formulations.

Formulations	Contribution of Masonry Wall	Contribution of Tie-columns
1. F&A	$\text{Min}\{(0.5v_m + 0.3\sigma)A;\ 1.5v_m A\}$	$0.3\left(1.26 d_{bl}^2 \sqrt{f_c f_{yl}}\right)$
2. T&K	$\left[\left\{1+\sqrt{c_i^2(1+\sigma/v_m)+1}\right\}/(c_i f_{AR})\right] v_m A_w$	$0.8059 n_r d_{bl}^2 \sqrt{f_c f_{yl}}$
3. M&C	$(0.47v_m + 0.29\sigma)(A - nA_c)$ (in kg cm)	$4200n$ (in kg cm)
4a. Bzm1	$\left\{\sqrt{1+(\sigma/v_m)}/f_{AR}\right\} v_m A_w$	$\begin{cases} 0.4 n n_r d_{bl}^2 \sqrt{f_c f_{yl}}, \text{ if } s \geq 2l_d \\ n n_r \times \max\left(\frac{2}{3}R_c, \frac{1}{3}R_c + R_{st}\right)^*, \text{ if } s \geq 2l_d \end{cases}$
4b. Bzm2	$\left[\left\{1+\sqrt{c_i^2(1+\sigma/v_m)+1}\right\}/(c_i f_{AR})\right] v_m A_w$	
4c. Bzm3	$\left[A_w/\{f_{AR}(1+v_m/f'_m)\}\right]\left(\sqrt{v_m^2 + \sigma v_m(1 - v_m/f'_m) - \sigma^2 v_m/f'_m}\right)$	
5. Ria	$(0.21v_m + 0.363\sigma)A$	$0.0141\sqrt{\rho_l f_c f_{yl}}\,A$
6. S&R	$\left\{\text{Min}\left(0.2 + 0.4\sigma;\ 0.25\sqrt{f'_m}\right)\right\} A_w$	$(0.7L_i/L_p+1.15)$ times masonry wall part
7. M&L3	$(0.45v_m + 0.3\sigma)A$	$0.4\sqrt{f_c}(1+n_i)nA_c$

*$R_{st} = f_{yt}A_{sv}$; R_c is obtained from $\frac{0.256}{f_c d_{bl}} R_c^2 + \frac{2 f_{yt} A_{sv}}{f_c d_{bl}} R_c - \frac{f_{yt} A_{sv} s - \pi d_{bl}^3 f_{yl}}{32} = 0$

F&A = Flores and Alcocer (1996); T&K = Tomaževič and Klemenc (1997a); M&C = Marinilli and Castilla (2004); Bzm1 = Bourzam et al. (2008a) (Eq. 6.4a); Bzm2 = Bourzam et al. (2008a) (Eq. 6.4b); Bzm3 = Bourzam et al. (2008a) (Eq. 6.4c); Ria = Riahi et al. (2009); S&R = Singhal and Rai (2016); M&L3 = Marques and Lourenço (2019) (Eq. 6.9b).

The different parameters related to the contribution of tie-columns in the lateral strength prediction of CM walls are: diameter of longitudinal rebars (d_{bl}), concrete compressive strength (f_c), yield strength of longitudinal rebar (f_{yl}), number of longitudinal rebars in a tie-column (n_r), number of total or intermediate tie-columns in a CM wall (n or n_i), geometrical length ratio L_i/L_p, and cross-sectional area of tie-column (A_c) (Table 7.1). It is to be noted here that in Riahi et al. (2009), total wall area (A) parameter is also kept in the second part as it was difficult to separate the tie-columns' contribution from Eq. 6.5a. The percentage contribution of tie-columns in the predicted lateral strength obtained using the existing formulations are given in Table 7.2 for seventy-eight CM wall specimens tested in the past (as given in Chapter 6).

Table 7.2: Lateral load contribution of tie-columns $V_{tc,p}$ (as % of empirically obtained lateral strength $V_{m,p}$) in all the specimens.

Sr	Experimental Study and Model Id	$V_{tc,p}/V_{m,p}$ (in %)								
		M&L3	S&R	Ria	Bzm1	Bzm2	Bzm3	M&C	T&K	F&A
1	Kato et al. (1992) - A	31	53	29	47	37	49	42	23	3
2	Kato et al. (1992) - B	31	53	29	31	23	32	42	23	3
3	Kato et al. (1992) - C	31	53	18	36	27	37	42	7	1
4	Kato et al. (1992) - D	31	53	18	11	8	11	42	7	1
5	Aguilar et al. (1996) - MO	45	53	41	36	31	39	54	15	4
6	Iiba et al. (1996) - IDM	45	53	33	36	32	41	60	31	5
7	Iiba et al. (1996) - IDJ	30	53	23	25	20	26	51	15	2
8	Iiba et al. (1996) - HDJ	30	53	13	6	4	6	51	4	1
9	Yoshimura et al. (1996) - 4-H0V0	31	53	38	18	15	19	47	15	4
10	Yoshimura et al. (1996) - 1-H0V0	29	53	34	16	13	17	45	12	11
11	Tomaževič and Klemenc (1997a) - AH-1	58	53	46	40	35	46	98	35	12
12	Tomaževič and Klemenc (1997a) - AH-3	58	53	46	40	35	46	98	35	12
13	Tomaževič and Klemenc (1997a) - AH-2	58	53	46	40	35	46	98	35	12
14	Yoshimura et al. (2000) - H1-H0V0-HC	23	53	24	15	13	16	38	12	9
15	Yoshimura et al. (2000) - H1-H0V0-LC	29	53	34	16	13	17	45	12	11
16	Yoshimura et al. (2000) - H1-H0V0-T	48	53	63	25	20	26	65	17	21
17	Yoshimura et al. (2000) - L1-H0V0-HC	19	53	21	13	11	14	37	9	7
18	Yoshimura et al. (2000) - L1-H0V0-LC	29	53	34	16	13	17	45	12	11
19	Yoshimura et al. (2000) - L1-H0V0-T	41	53	57	21	16	21	60	14	16
20	Kumazawa and Ohkubo (2000) - ISM	39	53	27	33	28	37	53	23	4
21	Yoshimura et al. (2004) - 2D-H1-H0V0-48-2	27	53	37	12	10	12	41	9	10
22	Yoshimura et al. (2004) - 2D-H1-H0V0-84-2	23	53	30	11	8	11	37	8	8
23	Yoshimura et al. (2004) - 2D-L1-H0V0-48-1	31	53	39	16	13	16	50	12	12
24	Yoshimura et al. (2004) - 2D-L1-H0V0-84-1	29	53	34	15	13	16	46	12	11
25	Yáñez et al. (2004) - Pattern 1-CMU-1	49	53	59	13	10	14	44	10	3
26	Yáñez et al. (2004) - Pattern 1-CMU-2	49	53	59	13	10	14	44	10	3
27	Yáñez et al. (2004) - Pattern 1-Clay Brick-1	47	53	56	12	9	13	42	9	3
28	Yáñez et al. (2004) - Pattern 1-Clay Brick-2	47	53	56	12	9	13	42	9	3
29	Marinilli and Castilla (2004) - M1	38	53	49	49	43	51	38	13	4
30	Zabala et al. (2004) - 1	57	53	48	14	11	15	46	10	3
31	Zabala et al. (2004) - 2	57	53	48	14	11	15	46	10	3
32	Zabala et al. (2004) - 3	51	53	49	26	21	28	40	21	6
33	Zabala et al. (2004) - 4	51	53	49	26	21	28	40	21	6
34	Gouveia and Lourenço (2007) - W2.4	38	53	25	13	11	16	61	11	2
35	Gouveia and Lourenço (2007) - W2.4	38	53	25	13	11	16	61	11	2
36	Bourzam et al. (2008a) - JCM	35	53	33	21	16	23	60	15	3

37	Bourzam et al. (2008b) - CM30J-1	35	53	33	21	16	23	60	15	3
38	Bourzam et al. (2008b) - CM30J-2	27	53	19	31	26	36	51	13	2
39	Kuroki et al. (2010) - CMWO-01	29	53	38	13	11	14	48	11	11
40	Kuroki et al. (2010) - CMWO-07	34	53	42	20	17	22	57	15	14
41	Wijaya et al. (2011) - A	61	53	71	21	15	23	64	15	5
42	Bourzam et al. (2013) - CM60J	29	53	28	16	12	17	53	12	2
43	Matošević et al. (2014) - A1	59	53	41	24	19	29	51	19	4
44	Matošević et al. (2014) - A2	57	53	39	22	18	27	51	18	3
45	Matošević et al. (2014) - A3	54	53	36	20	16	25	51	16	3
46	Gavilán et al. (2015) - ME1	68	53	53	65	54	67	74	54	15
47	Gavilán et al. (2015) - ME2	53	53	46	47	39	49	63	39	8
48	Gavilán et al. (2015) - ME3	45	53	45	35	29	37	56	29	6
49	Gavilán et al. (2015) - ME4	43	53	48	28	23	30	51	23	6
50	Gavilán et al. (2015) - ME5	30	53	45	16	14	17	36	13	3
51	Varela-Rivera et al. (2019) - M1	25	53	26	3	2	3	40	2	2
52	Varela-Rivera et al. (2019) - M2	32	53	26	5	4	6	49	4	3
53	Varela-Rivera et al. (2019) - M3	30	53	22	5	4	6	45	4	3
54	Varela-Rivera et al. (2019) - M4	42	53	26	9	5	9	61	5	4
55	Varela-Rivera et al. (2019) - M5	41	53	23	9	5	10	58	5	4
56	Varela-Rivera et al. (2019) - M6	37	53	19	8	5	9	55	5	4
57	Cruz et al. (2019) - MB0	32	53	54	26	21	29	32	24	8
58	Gavilán (2020) - M1-1	30	53	25	14	12	18	37	12	2
59	Gavilán (2020) - M2-1	18	53	25	27	23	29	32	23	5
60	Present Study - S1	70	53	53	49	38	52	78	23	5
61	Present Study - S2	65	53	53	42	34	45	73	20	4
62	Present Study - S3	57	53	53	25	19	26	64	10	3
63	Wijaya et al. (2011) - C	61	53	71	21	15	23	64	15	5
64	Matošević et al. (2014) - B1	59	53	41	24	19	29	51	19	4
65	Matošević et al. (2014) - B2	57	53	39	22	18	27	51	18	3
66	Matošević et al. (2014) - B3	54	53	36	20	16	25	51	16	3
67	Quiroz et al. (2017) - A1-1	60	53	42	25	19	28	41	13	3
68	Quiroz et al. (2017) - A1-2	60	53	42	25	19	28	41	13	3
69	Quiroz et al. (2017) - A2-1	60	53	35	24	18	27	41	8	2
70	Quiroz et al. (2017) - A2-2	60	53	42	25	19	28	41	13	3
71	Marinilli and Castilla (2004) - M2	64	56	49	59	53	61	49	13	4
72	Marinilli and Castilla (2004) - M3	64	56	49	59	53	61	49	13	4
73	Marinilli and Castilla (2004) - M4	78	59	49	66	60	68	58	13	4
74	Gavilán et al. (2015) - ME6	44	55	46	14	13	15	32	9	2
75	Gavilán et al. (2015) - ME7	57	56	50	16	15	17	33	8	2
76	Singhal and Rai (2014) - SC_{NT}	61	56	68	45	39	46	78	13	4
77	Singhal and Rai (2014) - SC_{CT}	62	56	71	23	19	24	76	13	4
78	Singhal and Rai (2014) - SC_{FT}	61	56	70	22	19	23	76	13	4
		M&L3	S&R	Ria	Bzm1	Bzm2	Bzm3	M&C	T&K	F&A

M&L3 = Marques and Lourenço (2019) (Eq. 6.9b); S&R = Singhal and Rai (2016); Ria = Riahi et al. (2009); Bzm1 = Bourzam et al. (2008a) (Eq. 6.4a); Bzm2 = Bourzam et al. (2008a) (Eq. 6.4b); Bzm3 = Bourzam et al. (2008a) (Eq. 6.4c); M&C = Marinilli and Castilla (2004); T&K = Tomaževič and Klemenc (1997a); F&A = Flores and Alcocer (1996)

Huge variation is observed in the estimated values using different methods for all the specimens. The maximum contribution to lateral strength of single bay CM wall by the tie-columns was observed to vary from 21% to 78% using different empirical formulations and these maximum values were mainly observed with the slender specimen ME1 of Gavilán et al. (2015), slender specimen S1 of present study, specimen C of Wijaya et al. (2011), and H1-H0V0-T specimen of Yoshimura et al. (2000) as given in Table 7.2. It is to be noted here that the contribution of tie-columns was found to be maximum (98%) using the formulation of M&C for the specimens of Tomaževič and Klemenc (1997a). However, the second part of the lateral strength equation proposed by M&C gives a constant minimum additive lateral strength of 82 kN for single bay walls with two tie-columns as a contribution by the tie-elements. This is a very huge number for the one-fifth scaled specimens of Tomaževič and Klemenc (1997a), where the maximum capacity of the walls is not more than 3 kN. Thus, these three specimens were removed from the database of M&C. For the eight multi-bay specimens, the maximum contribution by the tie-columns was observed to vary from 4% to 78% using different empirical formulations. Further, the minimum contribution of tie-columns was found to vary from 1% to 53% for single bay and 2% to 55% for multi-bay specimens using different empirical formulations.

This comparative assessment for the contribution of predicted lateral strength of CM wall coming from masonry wall and tie-columns is also shown in Fig. 7.2. Here, the individual bar diagram shows the mean percentage contribution of masonry wall and tie-columns in the lateral strength obtained using the existing formulations on seventy-eight CM walls, while the error bar shows the standard deviation. The mean values shown in Fig. 7.2 (i.e., 5% to 55% contribution of tie-columns in the lateral strength) show a huge variation in the estimated percentage contribution of the tie-columns in lateral strength of wall using different formulations. It is observed that the mean contribution of the tie-columns at the predicted lateral strength of CM wall is comparatively low when the models developed by F&A, T&K, Bzm1, Bzm2, and Bzm3 are used. However, the four remaining models (M&L, S&R, Ria, and M&C) estimate comparatively higher contribution of the tie-columns in the lateral strength of CM walls. As observed in Fig. 7.2, the highest average contribution of masonry part to lateral strength of CM wall is 95% when the model of F&A was used; whereas the highest mean contribution by the tie-columns was 54% using the model of S&R. S&R provides a constant additive part (i.e., 1.15 times the masonry part or 53%) for single bay CM specimens (as $L_i = 0$ for single bay wall); whereas based on L_i/L_p a small part is added if the wall is multi-bay. Thus, the mean percentage contribution of masonry wall and tie-columns was 46% and 54%, respectively, with very less standard deviation.

Clearly, some studies do not intend to rely on the strength of RC tie-columns (such as F&A, T&K) as these are generally not designed and detailed for seismic resistance. On the other hand, some studies take full utilization of the strength of RC tie-columns as well in the lateral load sharing (such as M&L3, S&R, Ria, M&C used to consider 40% to 55% contribution by the tie-columns in lateral strength of CM wall on an average), thereby reducing the design loads on the masonry walls. As the formulations provide inconsistent distribution of forces, a more refined study is required which can capture the load distribution between different members of a CM wall.

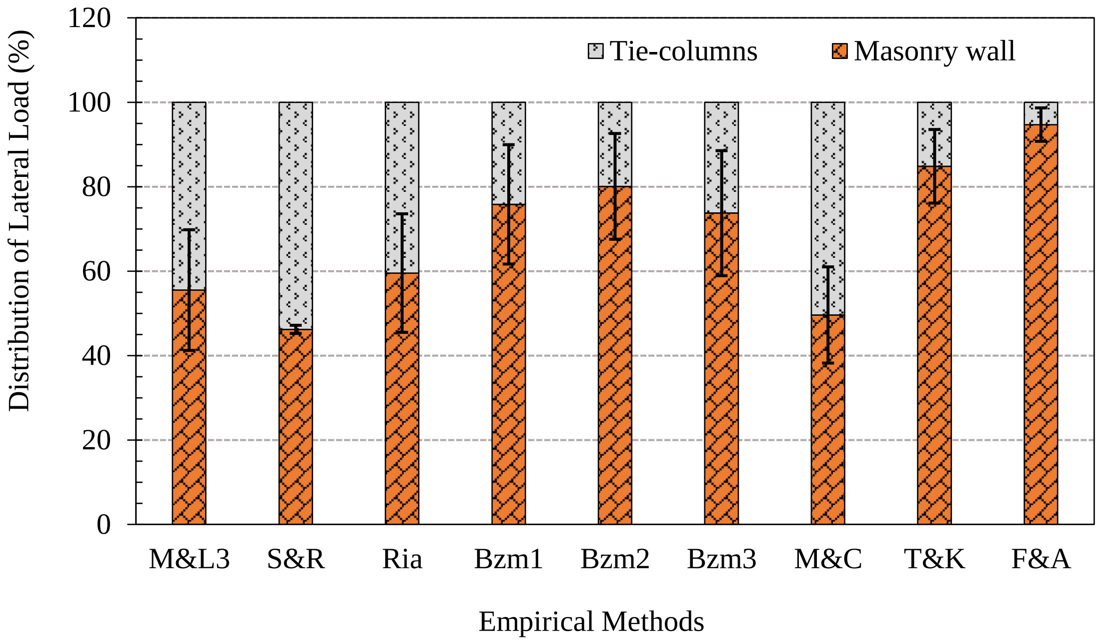

Figure 7.2: Distribution of lateral load at the lateral strength stage in the considered database of CM wall specimens tested in the past obtained using different empirical formulations (individual bar represents mean percentage contribution of masonry wall and tie-columns obtained in seventy-eight specimens, with standard deviation depicted by the error bar).

7.3.2 Distribution of Forces based on FE Analysis

As already discussed in Chapter 6 and also shown in Table 7.1, past studies have evaluated and formulated the lateral load resistance of CM walls as a combined resistance of masonry wall and tie-columns under lateral loading assuming the members, i.e., masonry and ties, work in unison. The individual effect of the members on the lateral strength, or in other words, distribution of lateral forces in masonry wall and the tie-columns has not been studied in detail for confined masonry because of the complexities associated with the analysis of composite structures like CM. Thus, in order to develop better understanding in this aspect, the previously calibrated 3D finite element models of the three tested specimens - S1, S2, and S3 (as discussed in Chapter 3) were again studied here in detail.

Using the FE analyses of the three CM walls, the average nodal forces at different cross-sections along the wall height were extracted for both tie-columns and masonry wall at different lateral displacement levels. A visual representation of extraction of nodal forces at different cross-sections of tie-columns and masonry wall of a typical CM wall are shown in Fig. 7.3. The schematic of the developed FE model showing the elements, interfaces, boundary and loading conditions is shown in Fig. 7.3a, which also show the left and right tie-columns and the masonry wall on which the nodal forces are evaluated. Figs. 7.3b and 7.3c show the developed shear forces at a particular drift level under lateral loading at different cross-sections along the wall height for masonry wall and tie-columns, respectively. The formation of diagonal strut in masonry wall under lateral loading can also be clearly observed from the stress-contours shown in the figure. Similarly, Fig. 7.3d shows the extracted bending moment in tie-columns as well as in masonry walls at a particular drift level under lateral loading at different cross-sections along the wall height. At first, the nodal forces will be evaluated and discussed at two limit states – cracking and lateral strength level, before evaluating them at several other displacement levels.

7.3.2.1 At initial cracking stage

The shear forces (SF) and bending moments (BM) obtained from the cross-sections along the height of the three CM walls S1, S2, and S3 at the initial cracking stage (i.e., at 0.2% drift level) under the combined action of axial and lateral loading are shown in Figs. 7.4 and 7.5, respectively. Here, the forces were extracted from the sections of different elements of wall – left tie-column (LC), masonry wall (MW), and right tie-column (RC). In addition, the SF extracted from the section taken along the whole length of the CM walls (including both the tie-columns and masonry wall) is also shown in the figures (as CM). The y-axis represents the height of the considered section (H_s) in terms of the total height H. It was observed that significant forces (SF and BM) developed at top and bottom sections of the tie-columns in all three specimens. On the other hand, a relatively low SF was observed towards the mid-height of tie-columns, where most of the shear forces were resisted by the masonry wall. The total SF in the entire CM wall was found to be same as the cumulative SF extracted in the CM walls obtained by adding the two components from tie-columns and masonry wall. The maximum BM was obviously observed at both ends of the tie-columns as well as the masonry wall, while very low BM was developed towards the mid-height of tie-columns as well as masonry wall.

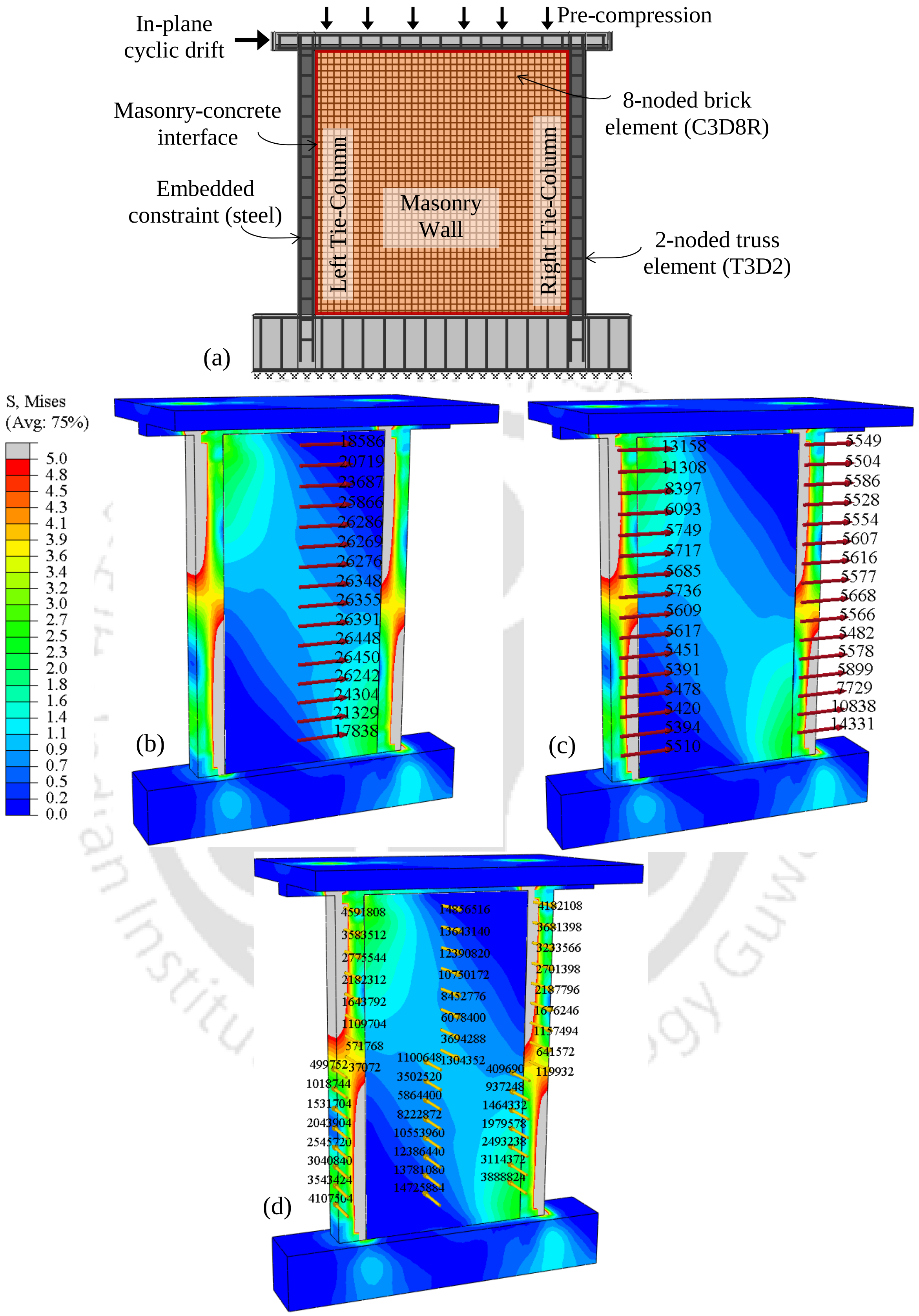

Figure 7.3: Estimation of force resultants in different elements of CM walls using FE analysis: (a) schematic of FE model, (b) SF extraction in masonry wall, (c) SF extraction in tie-columns, and (d) BM extraction in masonry wall as well as tie-columns (all units in N and mm).

The maximum SF developed in the left or right tie-column was about 10 kN, 16 kN and 27 kN for S1, S2, and S3, respectively; whereas the maximum BM was about 3 kNm for all three specimens. In case of masonry wall, the maximum SF developed was 22 kN, 41 kN, and 73 kN at the mid-height of S1, S2, and S3, respectively; whereas the maximum BM was 13 kNm, 23 kNm, and 36 kNm near the end region for the three specimens, respectively. For the complete wall, the maximum SF developed was 29 kN, 49 kN, and 79 kN; whereas the maximum BM was 17 kNm, 33 kNm, and 41 kNm for S1, S2, and S3, respectively. It can be clearly observed from these figures that the force resultants in tie-columns as well as masonry walls consistently increase with increasing aspect ratio of CM walls. Therefore, the commonly adopted design rules for CM walls, in which the design of tie-columns is kept unchanged irrespective of the aspect ratio, need a relook.

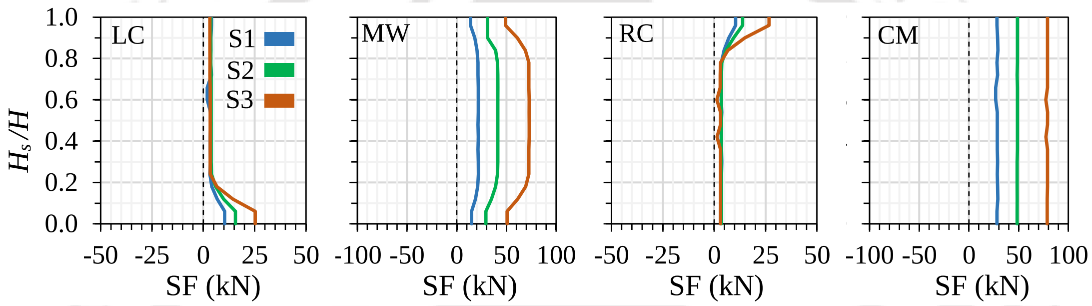

Figure 7.4: Shear force in tie-columns and masonry wall at cracking stage.

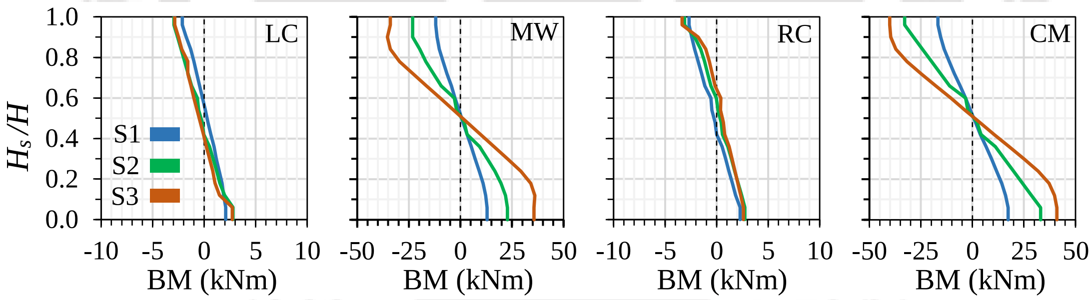

Figure 7.5: Bending moment in tie-columns and masonry wall at cracking stage.

7.3.2.2 At lateral strength stage

From the FE analyses, it was observed that when CM walls reach the lateral strength stage, the masonry wall contributes their highest possible contribution; whereas, the tie-columns attain their maximum contribution at a slightly higher drift level. Figs. 7.6 and 7.7 show the SF and BM developed in masonry wall, tie-columns, and total wall at the lateral strength level for the three specimens. When all three specimens achieved the lateral strength, the shear resistance towards the mid-height of the CM wall was mostly provided by masonry wall only; thus, the maximum forces developed in masonry wall at mid-height became almost equal to the lateral strength of the CM walls. The tie-columns exhibited significant resistance at top and bottom. The maximum SF developed in the left or right tie-column was about 13 kN, 29 kN and 34 kN for S1, S2, and S3, respectively; whereas, the maximum BM developed in the left or right tie-column was 4 kNm, 6 kNm, and 7 kNm near the end region for the three specimens. In case of masonry wall, the maximum SF developed was 24 kN, 52 kN, and 89 kN at the mid-height of S1, S2, and S3, respectively; whereas, the maximum BM was 10 kNm, 20 kNm, and 39 kNm near the end region. For the complete wall, the maximum SF developed was 36 kN, 59 kN, and 93 kN; whereas the maximum BM was 14 kNm, 41 kNm, and 50 kNm for S1, S2, and S3, respectively. The force resultants as well as the lateral strength, obtained numerically or experimentally, for specimen S3 came out to be largest because of the lower AR of the specimen; comparatively squat specimens have been found to resist larger lateral loads due to higher horizontal cross-sectional area of the masonry.

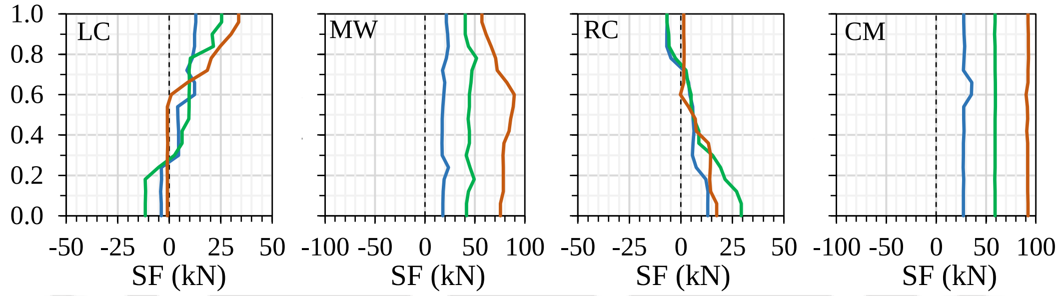

Figure 7.6: Shear force in tie-columns and masonry wall at lateral strength stage.

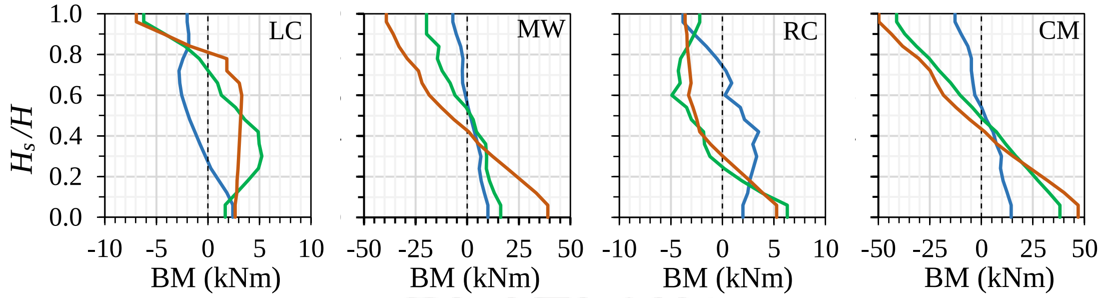

Figure 7.7: Bending moment in tie-columns and masonry wall at lateral strength stage.

7.3.2.3 At all the drift levels

The above discussion on the force resultants extracted at different cross-sections of tie-columns and masonry wall along the height of the specimens provided an understanding on the distribution of forces in members of CM walls under lateral loading. However, so far, the discussion was concentrated on the distribution of the force resultants at only two drift limit states in the entire loading history applied on the CM walls. In order to develop a complete understanding on the issue, the distribution of shear forces in different members (maximum from left or right tie-columns, and masonry wall) along the height of the wall models was also studied for the entire loading or displacement history. For simplification, Fig. 7.8 shows the distribution of SF for the entire loading history in only the left tie-columns of all the CM walls along with the SF in masonry walls. The SF extracted from the section taken along the whole length of the CM walls is also shown in the figures as S1 - CM, S2 - CM, and S3 - CM. The total SF in the entire CM wall was found to be same as the cumulative SF extracted in the CM walls obtained by adding the two components from tie-columns and masonry wall.

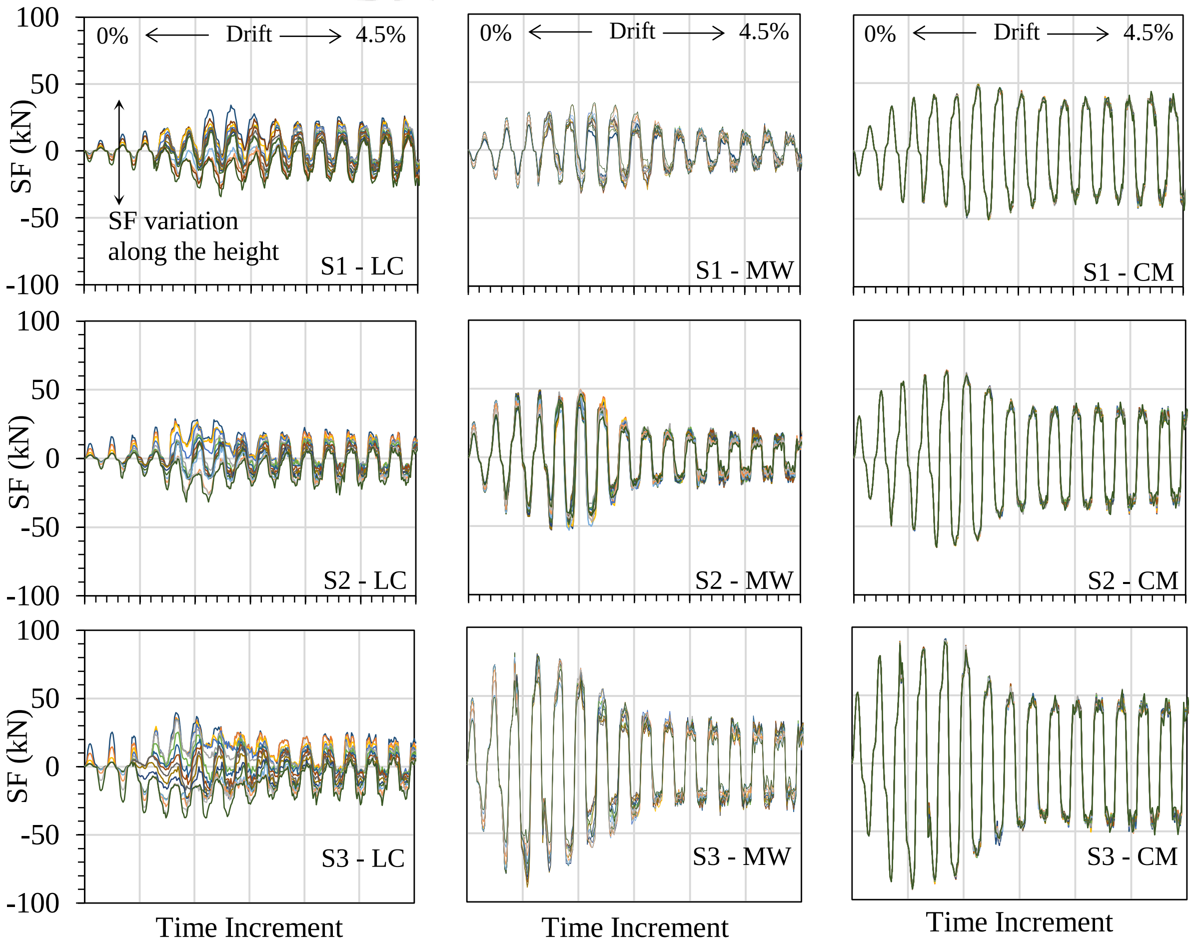

Figure 7.8: Distribution of lateral loads to tie-columns and masonry walls along the height of the wall at different drift levels for specimens S1, S2, and S3 (different curves represent distribution of shear force in different sections taken along the height of the model).

The summary of the force resultants obtained in tie-columns and masonry walls of the three specimens are given in Table 7.3. As already discussed, the maximum SF developed in the tie-columns along the height at first cracking stage was about 11 kN, 16 kN, and 27 kN for S1, S2, and S3, respectively. Thus, the tie-columns of wall S3 experienced almost double SF compared to that of the other walls. This could also be one of the reasons for early failure of tie-columns in wall S3 and its inferior performance. In masonry wall, the generated SF was more than that in the tie-columns in all the specimens. At cracking, the ratio of SF in tie-columns to that in the masonry wall was 0.50, 0.39, and 0.37 for S1, S2, and S3, respectively. On consideration of the maximum possible values, which occurred at the lateral strength stage, the ratio increased to 0.97, 0.64, and 0.45 for S1, S2, and S3, respectively. The observed values of BM were more or less similar in the tie-columns of all three walls (around 3 kNm at cracking, and maximum value of 11 kNm); however, for the three specimens, the BM in masonry wall varied from 13 kNm to 36 kNm and 16 kNm to 43 kNm, respectively at cracking level and at strength level. In all three specimens, tie-columns started resisting considerable amount of SF beyond the lateral drift corresponding to the maximum lateral strength of the wall, where masonry wall attained the maximum resistance. The maximum SF carried by tie-columns was 34 kN, 34 kN, and 40 kN at lateral drift values of 1.4%, 1.0%, and 0.50% for the three specimens, respectively. Evidently, the force resultants obtained in tie-columns and masonry walls depended largely on the aspect ratio of the CM wall. In any case, it is clear that the tie-columns are required to resist a significant amount of SF and BM, and therefore, they must be designed sufficiently to safely withstand these forces.

Table 7.3: Comparison of force resultants and corresponding drifts obtained in the FE analyses of specimens S1, S2, and S3.

Details	S1		S2		S3	
	SF, BM, Drift	*R*	SF, BM, Drift	*R*	SF, BM, Drift	*R*
SF in tie-column at cracking (kN)	11 (0.20%)*	0.50	16 (0.20%)	0.39	27 (0.20%)	0.37
SF in masonry at cracking (kN)	22 (0.20%)		41 (0.20%)		73 (0.20%)	
Maximum SF in tie-column (kN)	34 (1.40%)	0.97	34 (1.00%)	0.64	40 (0.50%)	0.45
Maximum SF in masonry (kN)	35 (1.00%)		53 (0.75%)		89 (0.35%)	
BM in tie-column at cracking (kNm)	3 (0.20%)	0.23	3 (0.20%)	0.13	3 (0.20%)	0.08
BM in masonry at cracking (kNm)	13 (0.20%)		23 (0.20%)		36 (0.20%)	
Maximum BM in tie-column (kNm)	11 (2.20%)	0.69	10 (0.75%)	0.37	11 (0.75%)	0.26
Maximum BM in masonry (kNm)	16 (0.50%)		27 (0.50%)		43 (0.25%)	

* Numbers in the () are the lateral drift values corresponding to the obtained force resultants
R = ratio of the force resultants in tie-columns to masonry wall

As observed in the past, CM walls resist lateral loads primarily in shear mode, thus making the shear as the most common failure mode. Considering this, the distribution of only shear forces in CM walls be discussed in the subsequent discussion; the tie-columns will be assumed to be designed for the minimum required BM. If required, the same method can be applied to extract the BM too in different members.

7.4 PARAMETRIC FE STUDY

In order to develop a generalized method for determining the relative force distribution in masonry walls and individual tie-column in CM walls, a parametric nonlinear FE analyses was carried out in Abaqus by considering the variation in six important parameters related to: material properties ($f_m^{'}$ and f_c), reinforcement detailing (ρ_l), gravity loads (σ), and geometric characteristics (t and AR). These parameters were discussed in Chapter 4 in developing the database of lateral capacity of CM walls of different parametric variations. As already given in Table 4.4, the considered variation in these parameters were: $f_m^{'}$ (in MPa) = 3, 5.5, and 8.5; f_c (in MPa) = 20, 25, 30; ρ_l (in %) = 0.6, 1.0, 1.5, 2; σ (in MPa) = 0.1, 0.3, 0.65; t (in mm) = 100, 200, 250; and AR = 0.75, 1.0, 1.25, 1.5, 1.75. In addition to the five AR considered in Chapter 4, one additional AR of 2.0 was considered in this section to study the influence of very slender CM walls. It is to be noted here that in most CM walls, the thickness of tie-columns (along the direction of the masonry wall thickness) is generally kept equal to the thickness of the masonry wall as a thumb rule. Therefore, in the present study, variation in the thickness of the masonry wall also resulted in variation in the dimensions of the tie-columns, which were square in cross-section. Aspect ratio was varied by varying the length of the wall, while the height of the masonry wall (H_w) was kept constant as 3 m. Varying each of these parameters one at a time while keeping other parameters constant resulted in 1944 (= 3×3×4×3×3×6) models, which were analyzed under gravity and cyclic lateral loads to extract the shear forces in tie-columns and masonry wall. The FE models used here were already validated with the experimental study discussed in Chapter 4.

In order to understand the lateral SF distribution in different members of 1944 CM walls with different parametric variation, the results obtained from the FE analyses were studied in terms of peak lateral strength (V), developed forces in masonry walls in terms of the lateral strength (V_w/V), and developed forces in tie-columns (maximum from left and right tie-columns) in terms of the lateral strength (V_{tc}/V). As obtained in the previous section, the developed forces in tie-columns are maximum either at the top or the bottom. Thus, for brevity, the force distributions for all the walls studied in the parametric study were assessed at the bottom section of the walls. As an example, the results of a CM wall from the parametric study are represented in Fig. 7.9, which verified that the cumulative shear forces developed in different members of the CM wall matched with the base shear of the CM wall under the effect of incremental lateral displacement loading.

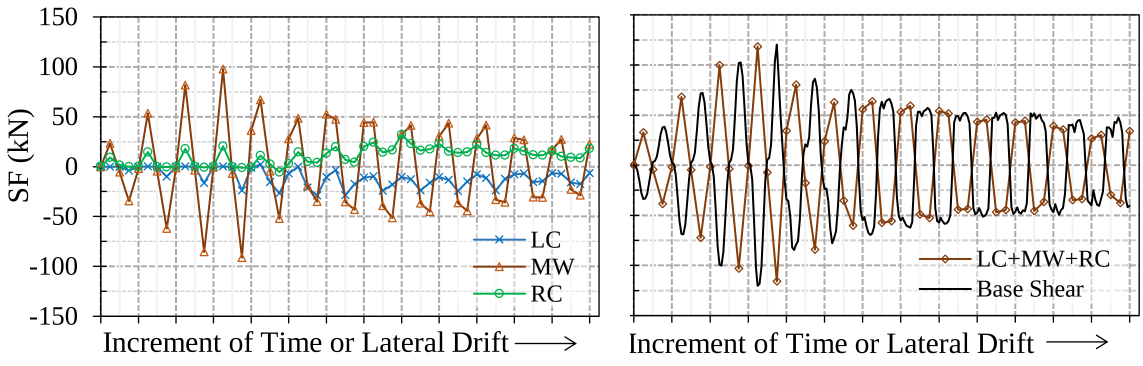

(a) (b)

Figure 7.9: Variation in the lateral shear with lateral drift levels observed in the parametric study: (a) SF in the bottom sections of LC, MW, and RC; (b) Comparison of sum of these shear forces with the base shear of the CM wall. (Model: AR = 2, f'_m = 8.5 MPa, t = 100 mm, σ = 0.1 MPa, f_c = 30 MPa, ρ_l = 1.5%).

Fig. 7.10 shows the variation in lateral strength and its distribution in different members plotted against the corresponding parameters (AR, f'_m, t, σ, f_c, ρ_l) for all the considered CM walls. As observed here, the contribution of tie-columns in lateral strength increased as AR was increased from 1 to 2. It is to be noted here that the variability in the distribution of lateral strength is quite high for the squat specimens with AR = 0.75. The shear forces in tie-columns also increased with the increment in t and ρ_l. When f'_m was increased, the shear forces developed in the masonry wall increased significantly, which is contrary to the observed variation of shear forces in the tie-columns.

The obtained FE results were segregated into two groups corresponding to – half brick thick wall, i.e. CM walls with t = 100 mm, and full brick thick wall, i.e., CM wall with t = 200 mm and 250 mm. Each of the two groups was again subdivided into three sub-groups based on masonry strength corresponding to – weak masonry with f'_m = 3 MPa, intermediate masonry with f'_m = 5.5 MPa, and strong masonry with f'_m = 8.5 MPa. For each of these six groups, the upper and lower bound values of V_{tc}/V are plotted against the wall aspect ratios and shown in Fig. 7.11. Such a representation of the shear force distribution in tie-columns resulted in the formation of distinctive bands for V_{tc}/V distribution. From the figure, it may be concluded that for thick CM walls with similar tie-column configuration, the shear forces developed in tie-columns are significantly high. However, for usual half brick thick CM wall with small sized tie-columns, the developed shear forces in tie-columns are comparatively lower and masonry wall mainly contributes to the lateral strength.

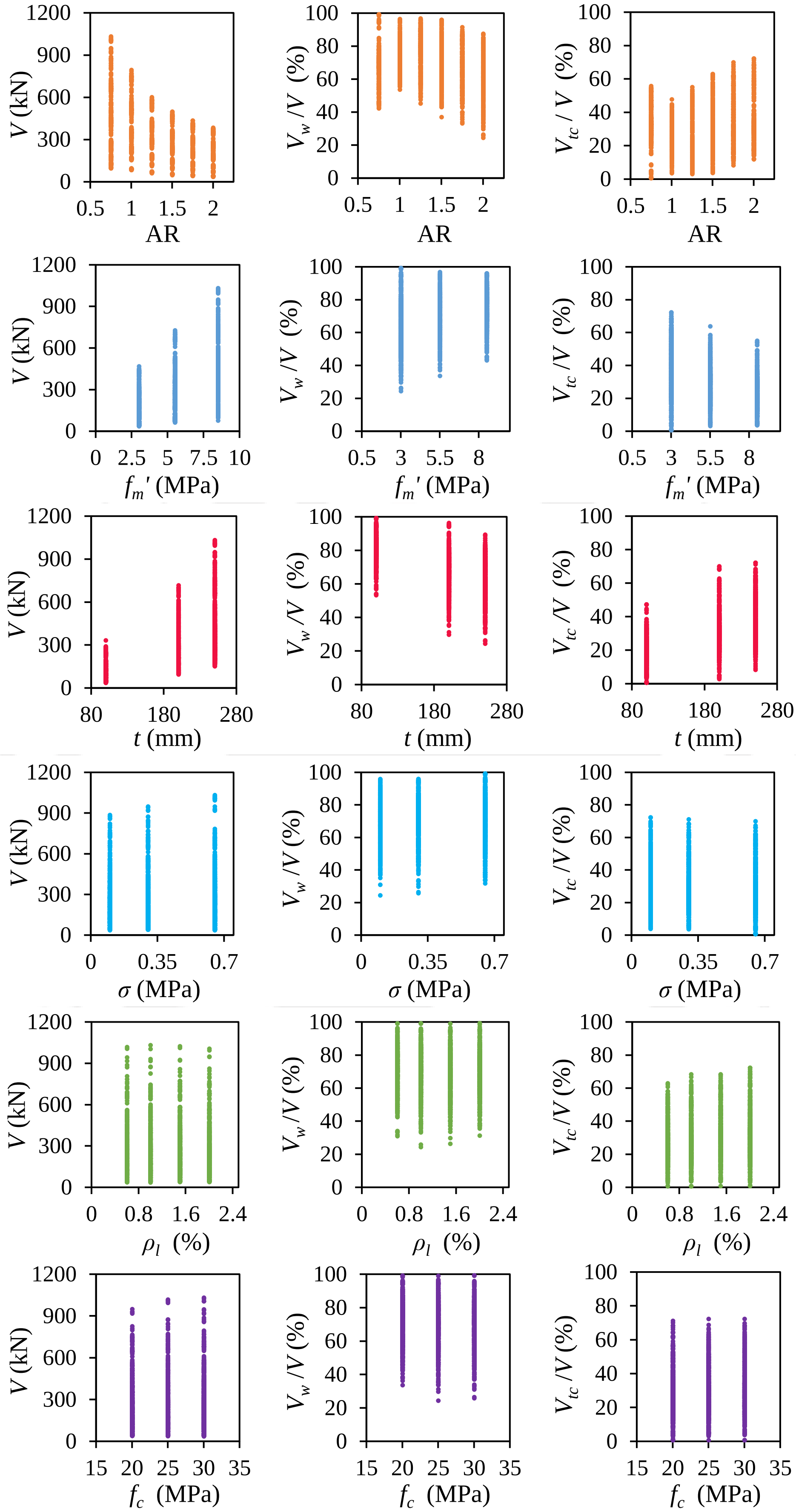

Figure 7.10: Variation in the lateral strength observed in the parametric study and its distribution to masonry wall and tie-columns.

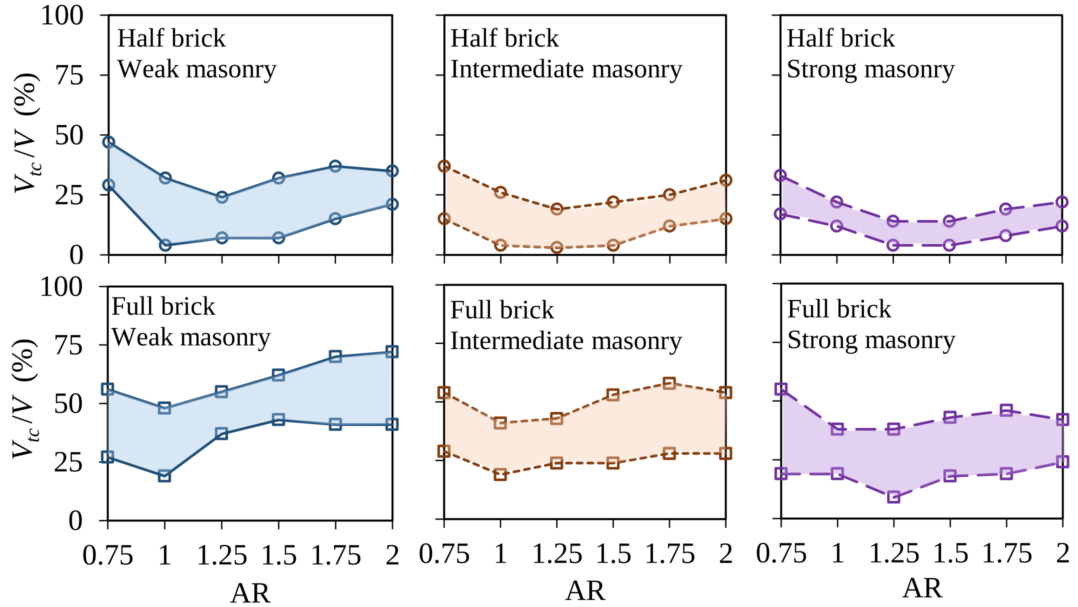

Figure 7.11: Upper and lower bound shear forces in tie-columns shown as banded distribution considering variation in thickness of masonry wall, strength of masonry, and AR.

7.5 RECOMMENDATIONS

It is clear that the shear forces in tie-columns can be very high for CM walls having high aspect ratio, thicker walls, and low compressive strength of masonry. However, as already discussed, the primary role of the tie-columns is not to resist the lateral shear but to provide the stability and confinement to the masonry walls. Therefore, a method was suggested in the present study to limit the distributed lateral shear to the tie-columns. Four distinct points (A, B, C, and D), corresponding to the maximum relative shear force that the tie-columns are required to resist in CM walls having four aspect ratios, are marked on the generalized force distribution curve shown in Table 7.4. Based on the results of the FE study, the maximum normalized shear forces for which the tie-columns are required to be designed are recommended and given in the table. It is suggested that those combinations of aspect ratio, thickness, and masonry strength that result in normalized shear force in individual tie-column higher than 50% should be rejected, and such CM walls should be redesigned with a different combination of the parameters. The recommended shear forces are to be considered for each of the tie-columns. The resulting tie-column design should be able to provide additional deformability, ductility, and stability to CM walls by continued confinement even after reaching the lateral strength. It is also recommended that the masonry walls must be designed to resist the full lateral strength of the CM walls.

Table 7.4: Distribution of shear forces on tie-columns.

Wall Thickness	Masonry Type	Normalized shear force in each tie-column (V_{tc}/V in %) A	B	C	D	Generalized distribution of shear force on tie-columns
Half Brick Thick	Weak Masonry	45	25	30	35	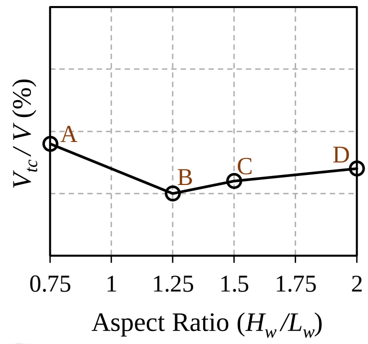
	Intermediate Masonry	35	20	20	30	
	Strong Masonry	30	15	15	20	
Full Brick Thick	Weak Masonry	50	50	50	50	
	Intermediate Masonry	50	40	50	50	
	Strong Masonry	50	35	35	35	

Linear interpolation can be carried out between the four points

7.6 SUMMARY

Influence of RC tie-columns are generally disregarded in seismic design of CM walls. However, based on experimental behavior and performance in past earthquakes, time and again it has been iterated that tie-columns are required to provide sufficient confinement and stability to the masonry walls for improved seismic behavior of CM walls. Therefore, it is felt essential to get an in-depth understanding of the influence of tie-columns on the lateral load behavior of CM walls. This issue is studied in the present chapter in great detail to develop a systematic approach for estimating the design shear forces for tie-columns. Based on the formulations available in the literature, an indirect method was used to segregate the contribution of masonry walls and tie-columns in lateral strength resistance. A huge variation in the range of 5% to 55% was observed in the mean percentage contribution of the tie-columns in lateral strength predicted using different formulations. The study clearly marked that the tie-columns may be subjected to a significant amount of shear forces. However, the available formulations provide an inconsistent distribution of shear forces due to the limited number of experimental studies and parameters considered in developing these formulations.

A finite element study was therefore carried out to understand the load distribution between different members of CM walls under the combined action of gravity and lateral loads. The adopted FE models were used to evaluate the load distribution between different members of CM walls. An extensive parametric FE study was carried out considering the influence of several important parameters on the lateral load distribution. Finally, recommendations were proposed for distribution of lateral loads to the tie-columns. The proposed method recommends that the tie-columns be designed for about 15% to 50% of the total design lateral shear of a CM wall, depending upon the masonry strength, thickness, and aspect ratio. The upper limit of 50% is recommended to ensure that the designed building behaves like a CM building in which the masonry walls are the primary load resisting elements, and the tie-members play a supporting role while providing the residual structural strength even after the failure of masonry walls. The accuracy of the developed method can be further improved by conducting additional experimental and numerical studies.

Chapter 8
SUMMARY AND CONCLUSIONS

CONTENTS

8.1 OVERVIEW

Confined Masonry (CM) buildings have been embraced in many earthquake-prone regions and continuously gaining popularity all over the world. This is primarily because of the better seismic performance exhibited by these buildings, which were made at an affordable cost with simple construction methodology. Several guidelines and design codes have been developed over the years in different countries to provide basic details on CM and promote its construction practice. However, the engineering behavior of this building type has not been established sufficiently due to significant variation in materials used, lack of research in order to understand the complex composite mechanism and lack of development efforts in building sectors. Significant gaps exist in research, especially in reliable method of analysis and design under gravity and seismic loadings. Therefore, an attempt has been made in the present study to assess the behavior of confined masonry walls by carrying out extensive experimental, numerical, and analytical studies. In this chapter, a brief summary of the work carried out in the study is presented, and the major conclusions are drawn. Finally, limitations of the study, and recommendations for possible future work have been suggested.

8.2 SUMMARY

The present study can be broadly summarized into five main parts, which have been discussed elaborately in the previous chapters of the thesis and summarized below.

8.2.1 Experimental Evaluation of Lateral Load Behavior

Experimental study on half-scale specimens of CM walls having three different aspect ratios was carried out considering one slender CM wall (aspect ratio 2.0), one wall with intermediate aspect ratio (aspect ratio 1.5), and one relatively squat wall (aspect ratio 1.0). The properties related to bricks, mortar cubes, concrete cubes, rebars, masonry prisms, masonry triplets and masonry wallettes were evaluated. Then, the CM wall specimens were subjected to quasi-static cyclic lateral loads at the slab level using servo-controlled hydraulic actuators to evaluate their lateral load behaviour. Quasi-static cyclic testing of the specimens exhibited the strong influence of aspect ratio on their lateral load responses. The initiation of damage pattern changed from flexural cracking of tie-columns to shear cracking of masonry when the configuration of the CM wall changed from slender to squat. The uniform lateral deformability of the slender wall along the height drastically altered, and the lateral drift values corresponding to yielding of rebars in tie-columns reduced with decreasing aspect ratio. Again, when the aspect ratio of the wall panel reduced by 50% (i.e., from 2 to 1), initial cyclic stiffness of specimen increased by about 48%, the lateral strength increased by about 70%; whereas, the shear stresses in masonry wall decreased by about 13%, the lateral drift capacity corresponding to the lateral strength reduced by 43%, and the ductility reduced by 59%. A similar trend for cyclic stiffness degradation was observed in all three specimens; whereas, degradation in the post-peak strength increases as aspect ratio decreases. Though the relatively squat wall (S3) achieved the highest lateral strength among all three specimens, the drift level corresponding to the strength was comparatively low, and the strength degradation after the peak was also more due to early damage in its tie-columns; so, the lowest dissipation of energy was observed for the squat wall when compared to others.

8.2.2 Development of a Simplified Numerical Model

From a preliminary study, it was observed that the equivalent diagonal strut model (ESM), which is a reliable modeling technique for masonry infilled RC frames, needs some important modifications for the application in CM buildings. Thus, ESM was modified and a new V-D (Vertical-Diagonal) strut model was developed in which a vertical strut was also modeled in addition to the diagonal strut to simulate realistic tie-beam deflection and tie-column axial forces under gravity loading. In the developed model, thickness of the diagonal struts was taken equal to the masonry panel thickness; width of diagonal strut was considered as one-third of the diagonal length of the strut; width of the vertical strut was taken as 75% of the panel length; and modulus of elasticity of tie-beam was enhanced by 20 times of the original. These modifications provided accurate prediction of displacement of tie-beam in the V-D strut model and ensured realistic vertical load distribution in different elements of the CM wall. Further, nonlinear static analyses showed that the use of masonry prism strength (f'_m) as the compressive strength the diagonal strut overestimates the lateral strength of CM walls because of the unique failure modes of the CM walls. In order to simulate the realistic failure of CM walls, a new term "Effective Shear Strength of Masonry (f_{ss})" was defined that corresponds to the lowest strength of masonry considering all the possible failure modes. f_{ss} was used in place of f'_m for defining the strength of the diagonal strut. As the strength of the strut, corresponding to various failure modes, depends on various parameters, a parametric finite element study was carried out to develop a methodology for the estimation of f_{ss}. Two empirical equations were proposed for the estimation of f_{ss} by carrying out regression analysis of the obtained data. The effectiveness of the empirical equations and V-D strut model was validated using several past experimental studies carried out on CM walls of different configurations. It was observed that the developed V-D strut model is able to suitably capture the linear and nonlinear behavior of CM walls with acceptable accuracy. The developed analysis method that uses the V-D strut model and f_{ss} is extremely simple and effective to use, as it needs only a few easily available input parameters and well-established principles of ESM.

8.2.3 Assessment of Design Provisions

In order to assess the efficacy of the existing codes of practice in safely predicting the design lateral strength of CM walls of different configurations, the existing methods adopted in the design codes of different countries were thoroughly reviewed. Nine design codes provide the design values of shear strength of CM walls; whereas the design flexural strength is provided only in six design codes. The design shear and flexural strengths for three specimens tested in the present study were evaluated using all the formulations. The variation in the weightage given to the input parameters (related to material, geometry and axial loading) along with the safety factors related to materials, loading, and others recommended in the design codes were compared. In addition to the three specimens tested in the present study, nine CM walls (having similar geometrical configurations) tested in past studies were also investigated by estimating the design values of shear and flexural strengths using different seismic codes. Comparison of the design-to-experimental strength ratios unveiled the global safety margins adopted in different codes against shear and flexural failure. A large variation was observed in the estimated global safety margins in different codes against shear failure (ratio of design shear to lateral load at cracking varies from 0.21 to 1.31) as well as flexural failure (ratio of equivalent design shear corresponding to design flexural strength to lateral strength varies from 0.3 to 1.7). Even after considering all the partial safety factors associated with the design shear strength of CM wall, design-to-experimental strength ratios was greater than one for some cases. This highlights the inconsistent estimation of design strength by design codes and limitations of some of the design codes in safe and economical design of CM walls against shear and flexure failure. Such inconsistencies may arise due to limited experimental data and highly uncertain material properties of masonry.

8.2.4 Development of Lateral Load-Displacement Backbone Model

Seismic analysis and performance-based design of confined masonry walls require accurate representation of lateral stiffness, strength, and deformation capacity. The in-plane hysteretic responses of CM walls obtained from experimental investigations have been commonly idealized into trilinear lateral load-deformation envelope curves. Utilizing the idealized envelope curves, formulations were established in the past to predict lateral stiffness, lateral loads, and lateral drift of CM walls at different damage stages. It is necessary to assess the effectiveness of the available methods in estimating the key parameters of CM walls at different damage stages as most of these methods were calibrated for a particular CM wall scheme considering the assumed material properties. First, a database of past experimental studies on seventy-eight (seventy single-bay and eight multi-bay) solid one-story CM walls was prepared. Trilinear backbone curves of the seventy-eight CM walls were then developed using the experimental results, which showed high variability associated with all three critical points. The experimentally obtained backbone parameters were then compared with those estimated analytically using different models to evaluate their effectiveness. From the comparison of the existing models, it was observed that the lateral strength equation recommended by Marques and Lourenço (2013) provides comparatively better prediction. Similarly, Gavilán et al. (2015) provides better prediction of cracking load. As far as the prediction of lateral drifts at different damage stages are concerned, the available two methods (Riahi et al. 2009 and Flores and Alcocer 1996) showed very large variations. This is primarily because of huge variation in the lateral drifts observed in the past experimental studies due to sensitivity of lateral load response of masonry walls to different parameters. Finally, using the past experimental and analytical data and employing engineering judgment, recommendations were provided for a suitable easy-to-use analytical backbone curve model for seismic analysis and design of CM walls.

8.2.5 Design Force Estimation in Different Members

Though masonry walls are the primary load resisting members in CM walls, confining members, particularly the tie-columns, influence the deformation capacity by maintaining structural stability and integrity. Most of the existing design codes as well as past research studies do not clearly provide method for estimation of the design forces for tie-columns and masonry wall of a CM wall. The FE analysis of the three tested CM walls showed that the maximum shear force in masonry wall developed towards the mid-height of wall under the action of lateral loading; whereas significant shear forces developed at the top and bottom of tie-columns. Thus, the tie-columns must have sufficient shear capacity at the top and bottom regions to resist the lateral loads. It was also observed that the bending moments developed in the tie-columns were very less compared to that developed in the masonry walls. A parametric nonlinear FE analyses of CM walls was carried out considering variations in six important parameters related to three different types of masonry as well as concrete, four different axial reinforcement percentage in tie members, three variations in gravity loads, three variations in wall thickness, and six variations in geometric characteristics. From the analyses, it was observed that for usual half-brick thick CM walls with small sized tie-columns, masonry walls mainly contribute to the lateral load resistance and the shear forces developed in tie-columns are comparatively lower. However, for thicker CM walls with similar tie-column configuration, the shear forces developed in the tie-columns are significantly higher.

8.3 CONCLUSIONS

Following major conclusions can be drawn from the exhaustive experimental, numerical, and analytical study:

1. Quasi-static cyclic tests on three specimens demonstrated the significant influence of aspect ratio on the lateral load behavior of confined walls including the damage pattern of tie-columns and masonry walls.
2. The inferior performance of squat wall highlighted that the existing design methodologies for confined masonry walls, especially for tie-columns, are required to be further improved by providing clear influence of aspect ratio and other relevant parameters.
3. A novel numerical method was developed for seismic analysis of confined masonry walls by using a simple V-D strut model that can reliably simulate the gravity load response as well as the nonlinear lateral load response of confined masonry walls with reasonable accuracy.
4. Comparison of the global safety factors associated with design forces (both shear and flexure) for confined masonry walls using all the available seismic design codes showed large variations and inconsistencies in the estimation of design forces. Clearly, additional studies are required to improve the design safety of CM walls.
5. The existing models for strength estimation reasonably predicted the lateral strength and lateral load at cracking of confined masonry walls; however, the prediction of lateral drifts at different limit states show large variations. Thus, a suitable easy-to-use analytical trilinear lateral load-deformation backbone curve model for confined masonry walls was developed. The proposed backbone curve can be used for performance-based design of confined masonry walls.
6. Based on a parametric finite element study, a method was developed to determine relative distribution of shear forces in tie-columns and masonry wall of confined masonry walls. It is recommended that the masonry walls be designed for total shear force corresponding to the lateral strength of the confined masonry walls. The lateral design forces in masonry walls can be estimated from either the V-D strut model or the empirical model developed in the study.
7. The size, configuration, and reinforcement detailing in confined masonry walls should be such that the tie-columns are not required to resist more than 50% of the total lateral shear force resisted by walls; in such cases reconfiguration and redesign of confined masonry walls are recommended.

Though great care was taken to carry out the present experimental, numerical, and analytical studies, the results reported in this study are based on limited data. Therefore, additional supplementary studies are required to be carried out for establishing specific design requirements for confined masonry buildings.

8.4 Recommendations for Future Work

The study can be further extended by removing some of the above-mentioned limitations and the following aspects:

- The current set of experimental investigations was carried out on single bay-single storey half-scale models representing ground floor wall of a two-storeyed CM buildings. The axial load ratio was kept constant in the experimental study. The study may be extended to multi-bay multi-storey for varying axial load ratios.
- In the present study, the influence of openings was not considered. As in CM buildings openings are advised to be confined by tie-elements, it will be interesting to study the influence of various positions of window and door openings with reliable confining schemes on the effectiveness of the V-D strut model as well as on the recommended distribution of the design forces on different members of confined masonry walls.
- The V-D strut model can be further developed for 3D house specimens and can be validated with experimental results.
- A refined methodology may be developed to accurately estimate the forces in different members of a CM wall under gravity and lateral loading by carrying out additional experimental and numerical studies.

REFERENCES

ACI 374 (2005). *Acceptance criteria for moment frames based on structural testing and commentary*. ACI 374.1-05. American Concrete Institute, Farmington Hills, Michigan.

Agnihotri, P., Singhal, V., and Rai, D.C. (2013). "Effect of in-plane damage on out-of-plane strength of unreinforced masonry walls." *Engineering Structures*, 57, 1-11.

Aguilar, G., Meli, R., Diaz, R., and Vázquez-del-Mercado, R. (1996). "Influence of horizontal reinforcement on the behavior of confined masonry walls." *Proceedings of the Eleventh World Conference on Earthquake Engineering*, 23-28 June 1996, Acapulco, Mexico, Elsevier Science Ltd, paper no. 1380.

Ahmad, N., Ali, Q., Ashraf, M., Khan, A. N., and Alam, B. (2012). "Performance assessment of low-rise confined masonry structures for Earthquake induced ground motions." *International Journal of Civil and Structural Engineering*, 2(3), 851-868.

Alcocer, S.M., and Casas, N. (2020). "Response assessment of small-scale confined masonry buildings through shaking table tests." *Proceedings of the 17th World Conference on Earthquake Engineering*, 13-18 September 2020, Sendai, Japan, International Association for Earthquake Engineering and Japan Association for Earthquake Engineering, paper id 2i-0218.

Alcocer, S.M., and Klingner, R.E. (2006). *The Tecomán, México earthquake, January 21, 2003: an EERI and SMIS learning from earthquakes reconnaissance report*. Earthquake Engineering Research Institute, Oakland, California.

Alcocer, S.M., Arias, J.G., and Vázquez, A. (2004). "Response assessment of Mexican confined masonry structures through shaking table test." *Proceedings of the Thirteenth World Conference on Earthquake Engineering*, 1-6 August 2004, Vancouver, British Columbia, Canada, paper no. 2130.

Amouzadeh Tabrizi, M., and Soltani, M. (2017). "In-plane response of unreinforced masonry walls confined by reinforced concrete tie-columns and tie-beams." *Advances in Structural Engineering*, 20(11), 1632-1643.

Arya, A.S., Boen, T., and Ishiyama, Y. (2014). *Guidelines for earthquake resistant non-engineered construction*. United Nations Educational Scientific and Cultural Organization, Paris, France.

Asfura, A.P., and Flores, P. J. (1999). *Quindio, Colombia earthquake, January 25, 1999: Reconnaissance report*. Multidisciplinary Center for Earthquake Engineering Research, State University of New York at Buffalo, Technical Report MCEER-99-0017, Buffalo, NY.

Asteris, P.G., Chronopoulos, M. P., Chrysostomou, C. Z., Varum, H., Plevris, V., Kyriakides, N., and Silva, V. (2014). "Seismic vulnerability assessment of historical masonry structural systems." *Engineering Structures*, 62, 118-134.

ASTM (2010). *Standard test method for diagonal tension (shear) in masonry assemblages*. E 519/E519M-10, West Conshohocken, PA.

ASTM. (2013a). *Standard test methods for sampling and testing brick and structural clay tile*. C67-13, West Conshohocken, PA.

ASTM. (2013b). *Standard test method for compressive strength of hydraulic cement mortars (using 2-in. or [50-mm] cube specimens).* C109/C109M-13, West Conshohocken, PA.

Basha, S.H., Surendran, S., and Kaushik, H.B. (2020). "Empirical models for lateral stiffness and strength of masonry infilled RC Frames considering the influence of openings." *Journal of Structural Engineering*, 146(4), ASCE, 04020021.

Bilek, S.L., Satake, K., and Sieh, K. (2007). "Introduction to the special issue on the 2004 Sumatra–Andaman earthquake and the Indian Ocean tsunami." *Bulletin of the Seismological Society of America*, 97(1A), S1-S5.

BIS (1987). *Indian standard code of practice for structural use of unreinforced masonry*. IS 1905, Third revision, Bureau of Indian Standards, New Delhi, India.

BIS (1992). *Indian standard methods of test of burn clay building bricks—Part 1: Determination of compressive strength.* IS 3495, Third revision, Bureau of Indian Standards, New Delhi, India.

BIS (1995). *Indian standard code of practice for preparation and use of masonry mortar*. IS 2250, Fifth revision, Bureau of Indian Standards; New Delhi, India.

BIS (2000). *Indian standard plain and reinforced concrete-code of practice*. IS 456, Fourth revision, Bureau of Indian Standards, New Delhi.

BIS (2004). *Indian standard methods of tests for strength of concrete*. IS 516-1959, Bureau of Indian Standards, New Delhi, India.

BIS (2013). *Code of practice for earthquake resistant design and construction of buildings*. IS 4326, Third revision, Bureau of Indian Standards, New Delhi, India.

BIS (2018). *Metallic materials - Tensile testing: Part 1 method of test at room temperature*. IS 1608-Part 1, Fourth revision, Bureau of Indian Standards, New Delhi, India.

BIS (2021). *Confined masonry for earthquake resistance - code of practice.* Draft version, Bureau of Indian Standards, New Delhi, India.

Blondet, M. (2005). *Construction and maintenance of masonry houses – For Masons and Craftsmen*. Second edition, Pontificia Universidad Catolica del Peru, Lima, Peru.

Boen, T. (2005). *Sumatra Earthquake 26 Dec 2004*. Earthquake Engineering Research Institute (EERI), Oakland, California.

Boen, T. and associates (2009). *Constructing seismic resistant masonry houses in Indonesia*. Second edition, World Seismic Safety Initiative and United Nations Centre for Regional Development, Disaster Management Planning Hyogo Office, Japan/ Indonesia.

Bolhassani, M., Hamid, A.A., Lau, A.C., and Moon, F., 2015. "Simplified micro modeling of partially grouted masonry assemblages." *Construction and Building Materials*, 83, 159-173.

Borri, A., Castori, G., and Corradi, M. (2013). "Masonry confinement using steel cords." *Journal of Materials in Civil Engineering*, ASCE, 25(12), 1910-1919.

Borri, A., Corradi, M., Castori, G., and Molinari, A. (2019). "Stainless steel strip–A proposed shear reinforcement for masonry wall panels." *Construction and Building Materials*, 211, 594-604.

Bourzam, A., Goto, T., and Miyajima, M. (2008b). "Shear capacity prediction of confined masonry walls subjected to cyclic lateral loading." *Journal of Structural and Earthquake Engineering* (*Doboku Gakkai Ronbunshuu A*), 64(4), 692-704.

Bourzam, A., Ikemoto, T., and Miyajima, M. (2008a). "Lateral resistance of confined brick wall under cyclic quasi-static lateral loading." *Proceedings of the Fourteenth World Conference on Earthquake Engineering*, 12-17 October 2008, Beijing, China, paper id 05-04-0045.

Bourzam, A., Toshikazu, I., Saiji, F., and Masakatsu, M. (2013). "Influence of RC tie-columns due to dowel action on confined masonry panels subjected to in-plane cyclic loading." *International Journal of Engineering Science and Technology*, 5(12), 1924.

Brzev, S. (2007). *Earthquake-resistant confined masonry construction*. First edition, National Information Center of Earthquake Engineering, Indian Institute of Technology Kanpur, India.

Brzev, S. and Mitra, K. (2018). *Earthquake-resistant confined masonry construction*. Third edition, National Information Center for Earthquake Engineering, Indian Institute of Technology Kanpur, India

Brzev, S., and Pérez Gavilán, J.J. (2013). "Seismic design of confined masonry buildings using the Strut-and-Tie Method." *Proceedings: Course on Masonry Structures*, Mexican Society for Structural Engineering, Puebla, Mexico.

Brzev, S., and Pérez Gavilán, J.J. (2016). "Application of strut-and-tie model for seismic design of confined masonry shear walls." *Proceedings: 16th International Brick and Block Masonry Conference*, 26-30 June 2016, Padova, Italy. *Brick and Block Masonry – Trends, Innovations and Challenges*, Editors: C. Modena, F. da Porto & M.R. Valluzzi, CRC Press, First edition, Taylor & Francis Group, London.

Brzev, S., Astroza, M., and Moroni, O. (2010). *Performance of confined masonry buildings in the February 27, 2010 Chile earthquake*. Earthquake Engineering Research Institute, Oakland, California.

Brzev, S., Greene, M., and Murty, C.V.R. (2008). Non-Ductile RC Frames and Alternative Improved Construction Technologies. *Proceedings of the Fourteenth World Conference on Earthquake Engineering*, 12-17 October 2008, Beijing, China, paper id S23-004.

Brzev, S., Reiter, M., Pérez-Gavilán, J.J., Quinn, D., Membreño, M., Hart, T., and Sommer, D. (2019). "Confined masonry: the current design standards." *Thirteenth North American Masonry Conference*, 16-19 June 2019, Salt Lake City, Utah, USA. Editor: Dillon, P. B. et al., The Masonry Society.

BSI (2002). *Methods of test for masonry–Part 3: Determination of initial shear strength*. BS EN 1052-3, British Standard Institution, London.

Carlevaro, N., and Roux-Fouillet, G. (2015). *Guide book for building earthquake-resistant houses in confined masonry* (revised version). Swiss Agency for Development and Cooperation-SDC, Bern, Switzerland and Earthquake Engineering Research Institute – EERI, Oakland, California, USA.

Castellazzi, G., D'Altri, A.M., de Miranda, S., and Ubertini, F. (2017). "An innovative numerical modeling strategy for the structural analysis of historical monumental buildings." *Engineering Structures*, 132, 229-248.

CEN (2005). *Eurocode 6: Design of Masonry Buildings - Part 1-1: Common rules for reinforced and unreinforced masonry structures*. EN 1996-1-1, European Committee for Standardization (CEN), Brussels, Belgium.

Chakra-Varthy, P., and Basu, D. (2021). "Natural period and vertical distribution of base shear in confined masonry buildings using ambient vibration test." *Bulletin of Earthquake Engineering*, 19(4), 1851-1899.

Chopra, A.K. (2017). *Dynamics of structures: theory and applications to earthquake engineering*. Fifth edition, Pearson Education Limited.

Choudhury, T., and Kaushik, H.B. (2021). "Experimental evaluation of full-scale URM buildings strengthened using surface-mounted steel bands." *Journal of Structural Engineering*, ASCE, 147(2), 04020337.

Corradi, M., Borri, A., and Vignoli, A. (2002). "Strengthening techniques tested on masonry structures struck by the Umbria–Marche earthquake of 1997–1998." *Construction and Building Materials*, 16(4), 229-239.

Cruz, O., Perez-Gavilan, E., and Flores, C. (2019). "Experimental study of in-plane shear strength of confined concrete masonry walls with joint reinforcement." *Engineering Structures*, 182, 213-226.

CSCR (2002). *Código sísmico de Costa Rica* (Costa Rica seismic code). Colegio Federado de Ingenieros y de Arquitectos de Costa Rica, Costa Rica [in Spanish].

Decanini, L.D., Payer, A., Serrano, C., and Terzariol, R. (1985). "Experimental research on the seismic behavior of prototypes of masonry walls to natural scale." *XXIII South American Conference on Structural Engineering* [in Spanish].

Dhanasekar, M., and Haider, W. (2011). "Effect of spacing of reinforcement on the behaviour of partially grouted masonry shear walls." *Advances in Structural Engineering*, 14(2), 281-293.

Drysdale, R.G., Hamid, A.A. and Baker, L.R. (1999). *Masonry structures: behaviour and design*. Second edition, The Masonry Society, Boulder Co.

EERI (1999). *The Tehuacan, Mexico, earthquake of June 15, 1999*. EERI Special Earthquake Report. Newsletter, Earthquake Engineering Research Institute, California.

EERI (2001). *Preliminary observations on the El Salvador earthquakes of January 13 and February 13, 2003*. EERI Special Earthquake Report. Newsletter, Earthquake Engineering Research Institute, California.

EERI (2007). *The Pisco, Peru Earthquake of August 15, 2007*. EERI Special Earthquake Report. Newsletter, Earthquake Engineering Research Institute, Oakland, California.

Eshghi, S. and Pourazin, K. (2009). "In-plane behavior of confined masonry walls–with and without opening." *International Journal of Civil Engineering*, 7(1), 49-60.

FEMA 356 (2000). *Prestandard and commentary for the seismic rehabilitation of buildings*. American Society of Civil Engineers and Federal Emergency Management Agency, Washington, DC.

Flores, L.E., and Alcocer, S.M. (1996). "Calculated response of confined masonry structures." *Proceedings of the Eleventh World Conference on Earthquake Engineering*, 23-28 June 1996, Acapulco, Mexico, Elsevier Science Ltd, paper no. 1830.

Flores, L.E., Pérez Gavilán, J.J., and Alcocer, S. (2017). "Displacement capacity of confined masonry structures reinforced with horizontal reinforcement: Shaking Table Tests." *Proceedings of the 16th World Conference on Earthquake Engineering, Resilience – The New Challenge in Earthquake Engineering*, 9-13 January 2017, Santiago, Chile, Chilean Association on Seismology and Earthquake Engineering, paper no. 436.

Furtado, A., Arêde, A., Rodrigues, H., and Varum, H. (2021). "The role of the openings in the out-of-plane behaviour of masonry infill walls." *Engineering Structures*, 244, 112793.

Furtado, A., Rodrigues, H., Arêde, A., and Varum, H. (2021). "A Review of the Performance of Infilled RC Structures in Recent Earthquakes." *Applied Sciences*, 11(13), 5889.

Galvis, F.A., Miranda, E., Heresi, P., Dávalos, H., and Ruiz-García, J. (2020). "Overview of collapsed buildings in Mexico City after the 19 September 2017 (Mw7. 1) earthquake." *Earthquake Spectra*, 36(S2), S83-S109.

Gavilán, Pérez J.J. (2020). "The effect of shear-moment interaction on the shear strength of confined masonry walls." *Construction and Building Materials*, 263, 120087.

Gavilán, Pérez J.J., Flores, L.E., and Alcocer, S.M. (2015). "An experimental study of confined masonry walls with varying aspect ratios." *Earthquake Spectra*, 31(2), 945-968.

GB 50003 (2011). *Code for design of masonry structures*. Ministry of Housing and Urban-Rural Development of the People's Republic of China, Beijing, China [in Chinese].

Ghaisas, K.V., Basu, D., Brzev, S., and Gavilán, Pérez J.J. (2017). "Strut-and-Tie Model for seismic design of confined masonry buildings." *Construction and Building Materials*, 147, 677-700.

Gouveia, J. P., and Lourenço, P. B. (2007). "Masonry shear walls subjected to cyclic loading: Influence of confinement and horizontal reinforcement." *Proceedings: 10th North American Masonry Conference*, 3-6 June 2007, St. Louis, Missouri, The Masonry Society, 838‑848.

Grillanda, N., Valente, M., Milani, G., Chiozzi, A. and Tralli, A. (2020). "Advanced numerical strategies for seismic assessment of historical masonry aggregates." *Engineering Structures*, 212, 110441.

Hashemi, B.H., Alemi, F., and Ashtiany, G. (2003). *Confined brick masonry building with concrete tie-columns and beams*. Iran, Report 27, World Housing Encyclopaedia, Earthquake Engineering Research Institute.

Holmes, M., (1961). “Steel frames with brickwork and concrete infilling.” *Proceedings: Institute of Civil Engineers*, 19 (2), 473-478.

Iiba, M., Mizuno, H., Goto, T., and Kato, H. (1996). “Shaking table test on seismic performance of confined masonry wall.” *Proceedings of the Eleventh World Conference on Earthquake Engineering*, 23-28 June 1996, Acapulco, Mexico, Elsevier Science Ltd, paper no. 659.

INPRES-CIRSOC 103 (2018). *Normas Argentinas para Construcciones Sismorresistentes. Parte III - Construcciones de Mampostería* (Argentinean Code for Seismic-Resistant Construction. Part III - Masonry Construction). Instituto Nacional De Prevención Sísmica (INPRES) and Centro de Investigación de los Reglamentos Nacionales de Seguridad para las Obras Civiles (CIRSOC), Argentina [in Spanish].

Irimies, M.T. (2002) “Confined Masonry Walls: the influence of the tie-column vertical reinforcement ratio on the seismic behaviour.” *Proceedings: 12th European Conference on Earthquake Engineering*, 9-13 September 2002, London, 241 Pages.

Ishibashi, K., Meli, R., Alcocer, S.M., Leon, F. and Sanchez, T.A. (1992) “Experimental study on earthquake-resistant design of confined masonry structures.” *Proceedings of the Tenth World Conference on Earthquake Engineering*, 19-24 July 1992, Madrid, Spain, A.A. Balkema, Rotterdam / Brookfield, 3469-3474.

Iyer, K., Kulkarni, S.M., Subramaniam, S., Murty, C.V.R., Goswami, R., and Vijayanarayanan, A.R. (2012). *Build A Safe House with Confined Masonry*. Gujarat State Disaster Management Authority, Government of Gujarat, Gandhinagar, India.

Jain, S.K., Basu, D., Ghosh, I., Rai, D.C., Brzev, S., and Bhargava, L. K. (2014). “Application of confined masonry in a major project in India.” *Proceedings: 10th National Conference on Earthquake Engineering*, 21-25 July 2014, Anchorage, Alaska, USA, Earthquake Engineering Research Institute.

Jain, S.K., Lettis, W. R., Murty, C.V.R., and Bardet, J.P., ed., (2002). “Bhuj, India Earthquake of January 26, 2001 Reconnaissance Report.” *Earthquake Spectra*, Supplement A to Vol. 18, July, Earthquake Engineering Research Institute (EERI), USA.

Janaraj, T., and Dhanasekar, M. (2014). “Finite element analysis of the in-plane shear behavior of masonry panels confined with reinforced grouted cores.” *Construction and Building Materials*, 65, 495-506.

Jimenez, J. I., Villarreal, J. I., Centeno, M. R., Gonzalez, B. G., Correa, J. J. G., Acevedo, C. R., and Salazar, I. S. (1999). *Tehuacan, Mexico, Earthquake of June 15, 1999*. Seismological Research Letters, 70(6), 698-704.

Joshi, V., and Kaushik, H.B., (2017). “Historic Earthquake Resilient Structures in Nepal and other Himalayan Regions and Their Seismic Restoration.” *Earthquake Spectra*, Vol 33(S1), EERI, USA, S299-S319.

Kappos, A.J., Penelis, G.G., and Drakopoulos, C.G. (2002). “Evaluation of simplified models for lateral load analysis of unreinforced masonry buildings.” *Journal of Structural Engineering*, 128(7), 890-897.

Kato, H., Goto, T., Mizuno, H., and Iiba, M. (1992). "Cyclic loading tests of confined masonry wall elements for structural design development of apartment houses in the third world." *Proceedings of the Tenth World Conference on Earthquake Engineering*, 19-24 July 1992, Madrid, Spain, A.A. Balkema, Rotterdam / Brookfield, 3539-3544.

Kaushik, H.B., and Dasgupta, K. (2013). "Assessment of Seismic Vulnerability of Structures in Sikkim, India, based on Damage Observation during Two Recent Earthquakes." *Journal of Performance of Constructed Facilities*, 27(6), ASCE, 697-720.

Kaushik, H.B., and Jain, S.K. (2007). "Impact of great December 26, 2004 Sumatra earthquake and tsunami on structures in Port Blair." *Journal of Performance of Constructed Facilities*, 21(2), ASCE, 128-142.

Kaushik, H.B., and Sanganee, D.A. (2010). "Analytical investigations of confined masonry constructions." *Proceedings of the 3rd International Earthquake Symposium*, 5-6 March 2010, Dhaka, Bangladesh, Bangladesh Earthquake Society and Civil Engineering Department of Bangladesh University of Engineering and Technology, 223-230.

Kaushik, H.B., Rai, D.C., and Jain, S.K. (2006), "Code approaches to seismic design of masonry infilled reinforced concrete frames: A state-of-the-art review", *Earthquake Spectra*, 22(4), EERI, USA, 961-983.

Kaushik, H.B., Rai, D.C., and Jain, S.K. (2007). "Stress-Strain Characteristics of Clay Brick Masonry under Uniaxial Compression." *Journal of Materials in Civil Engineering*, 19 (9), 728-739.

Kaushik, H.B., Rai, D.C., and Jain, S.K. (2008). "A rational approach to analytical modeling of masonry infills in reinforced concrete frame buildings." *Proceedings of the Fourteenth World Conference on Earthquake Engineering*, 12-17 October 2008, Beijing, China, paper id 05-01-0317.

Kaushik, H.B., Rai, D.C., and Jain, S.K. (2009), "Effectiveness of some strengthening options for masonry-infilled RC frames with open first story." *Journal of Structural Engineering*, ASCE, 135(8), 925-937.

Kent, D.C., and Park, R. (1971). "Flexural members with confined concrete." *Journal of Structural Division*, 97(7), 1969-1990.

Kumazawa, F., and Ohkubo, M. (2000). "Nonlinear characteristics of confined masonry wall with lateral reinforcement in mortar joints." *Proceedings of the Twelfth World Conference on Earthquake Engineering*, 30 January-4 February 2000, Auckland, New Zealand, Upper Hutt, N.Z.: New Zealand Society for Earthquake Engineering, paper no. 0743.

Kuroki, M., Kikuchi, K., and Nonaka, H. (2010). "Experimental study on reinforcing methods for window openings in confined masonry walls." *Proceedings of the 35th conference on our world in concrete and structures*, 25-27 August 2010, Singapore, vol XXIX, CI-Premier PTE LTD, Singapore.

Kuroki, M., Kikuchi, K., Nonaka, H., and Shimosako, M. (2012). "Experimental Study on Reinforcing Methods Using Extra RC Elements for Confined Masonry Walls with Openings." *Proceedings of the Fifthteenth World Conference on Earthquake*

Engineering, 24-28 September 2012, Lisbon, Portugal, Sociedade Portuguesa de Engenharia Sismica (SPES), paper no. 4967.

Lagomarsino, S., Penna, A., Galasco, A., and Cattari, S. (2013). "TREMURI program: an equivalent frame model for the nonlinear seismic analysis of masonry buildings." *Engineering Structures*, 56, 1787-1799..

Lang, A.F., Crisafulli, F.J., and Torrisi, G.S. (2014). "Overview and assessment of analysis techniques for confined masonry buildings". *Proceedings: 10th National Conference on Earthquake Engineering*, 21-25 July 2014, Anchorage, Alaska, USA, Earthquake Engineering Research Institute.

Lee, J., and Fenves, G. L. (1998). "Plastic-damage model for cyclic loading of concrete structures." *Journal of Engineering Mechanics*, 124(8), 892-900.

Liberatore, L., Noto, F., Mollaioli, F. and Franchin, P. (2017). "Comparative assessment of strut models for the modelling of in-plane seismic response of infill walls." *Proceedings: COMPDYN 2017-6th International Conference on Computational Methods in Structural Dynamics and Earthquake Engineering*, 15-17 June 2017, Rhodes Island, Greece, Eccomas Proceedia.

Lourenço, P.B., Rots, J.G. and Blaauwendraad, J. (1995). "Two approaches for the analysis of masonry structures: micro and macro-modeling." HERON, 40 (4).

Lubliner, J., Oliver, J., Oller, S., and Oñate, E. (1989). "A plastic-damage model for concrete." *International Journal of solids and structures*, 25(3), 299-326.

Mander, J. B., Priestley, M. J., and Park, R. (1988). "Theoretical stress-strain model for confined concrete." *Journal of Structural Engineering*, ASCE, 114 (8), 1804-1826.

Marinilli, A., and Castilla, E. (2004). "Experimental evaluation of confined masonry walls with several confining-columns." *Proceedings of the Thirteenth World Conference on Earthquake Engineering*, 1-6 August 2004, Vancouver, British Columbia, Canada, paper no 2129.

Marques, R., and Lourenço, P. B. (2013). "A model for pushover analysis of confined masonry structures: implementation and validation." *Bulletin of Earthquake Engineering*, 11(6), 2133-2150.

Marques, R., and Lourenço, P. B. (2014). "Unreinforced and confined masonry buildings in seismic regions: Validation of macro-element models and cost analysis." *Engineering Structures*, 64, 52-67.

Marques, R., and Lourenço, P. B. (2019). "Structural behaviour and design rules of confined masonry walls: Review and proposals." *Construction and Building Materials*, 217, 137-155.

Matošević, Đ., Sigmund, V., and Guljaš, I. (2015). "Cyclic testing of single bay confined masonry walls with various connection details." *Bulletin of earthquake engineering*, 13(2), 565-586.

Matthews, T., Riahi, Z., Centeno, J., Charlet, A., Garcia, H. J., Hoffman, C., Safaie, S., and Elwood, K. (2007). *Evaluation of Confined Masonry Guidelines for Earthquake-Resistant Housing*. UBC EERI.

Medeiros, P., Vasconcelos, G., Lourenço, P. B., and Gouveia, J. (2013). "Numerical modeling of non-confined and confined masonry walls." *Construction and Building Materials*., 41, 968-976.

Meisl, C.S., Safaie, S., Elwood, K. J., Gupta, R., and Kowsari, R. (2006). "Housing reconstruction in northern Sumatra after the December 2004 great Sumatra earthquake and tsunami." *Earthquake Spectra*, 22(S3), S777-S802.

Meli, R., Brzev, S., Astroza, M., Boen, T., Crisafulli, F., Dai, J., Farsi, M., Hart, T., Mebarki, A., Moghadam, A. S., and Quinn, D. (2011). *Seismic design guide for low-rise confined masonry buildings*. Publication WHE – 2011 – 02, World Housing Encyclopedia, Earthquake Engineering Research Institute, Oakland, California.

Michał, S., and Andrzej, W. (2015). "Calibration of the CDP model parameters in Abaqus." *World Congress on Advances in Structural Engineering and Mechanics* (ASEM15), 25-29 August 2015, Songdo Convensia in Incheon, Korea.

Moreno-Herrera, J., Varela-Rivera, J., and Fernandez-Baqueiro, L. (2016). "Out-of-plane design procedure for confined masonry walls." *Journal of Structural Engineering*, ASCE, 142(2), 04015126.

Moroni, M.O., Astroza, M., and Acevedo, C. (2004). "Performance and seismic vulnerability of masonry housing types used in Chile." *Journal of performance of constructed facilities*, ASCE, 18(3), 173-179.

Moroni, O., Gomez, C., and Astroza, M. (2002). *Housing Report Confined block masonry building*. An initiative of Earthquake Engineering Research Institute and International Association for Earthquake Engineering, World Housing Encyclopedia.

MSJC (2011). *Building code requirements for masonry structures*. Masonry Standards Joint Committee, American Concrete Institute, Farmington Hills, MI.

Murty, C.V.R., Brzev, S., Faison, H., Comartin, C. D., Irfanoglu, A. (2006a). *At Risk: The seismic performance of reinforced concrete frame buildings with masonry infill walls*. A tutorial developed by a committee of the World Housing Encyclopaedia, a project of the Earthquake Engineering Research Institute and the International Association for Earthquake Engineering. Publication Number WHE-2006-03.

Murty, C.V.R., Rai, D.C., Jain, S.K., Kaushik, H.B., Mondal, G., and Dash, S.R. (2006b). "Performance of structures in the Andaman and Nicobar Islands (India) during the December 2004 Great Sumatra earthquake and Indian Ocean tsunami." *Earthquake Spectra*, 22(S3), EERI, USA, S321-S354.

Navarrete-Macias, D., Varela-Rivera, J., and Fernandez-Baqueiro, L. (2016). "Out-of-plane behavior of confined masonry walls subjected to concentrated loads (one-way bending)." *Earthquake Spectra*, 32(4), 2317-2335.

NCh2123 (2003). *Albañilería Confinada – Requisitos para el diseño y cálculo* (Confined Masonry – Requirements for Structural Design). Instituto Nacional de Normalizacion (INN), Chile [in Spanish].

NSR-98 (2010). *Normas Colombianas de Diseño y Construcción. Sismo Resistente. Titulo D - Mampostería structural* (Colombian Design and Construction Standards. Earthquake

Resistant. Title D - Structural masonry). Asociación Colombiana de Ingeniería Sísmica (AIS), Colombia [in Spanish].

NT E.070 (2019). *Propuesta de Norma E.070 Albañilería* (Proposal of Standard E.070 Masonry). Servicio Nacional de Capacitación para la Industria de la Construcción (SENCICO), Peru [in Spanish].

NTC-M (2004). *Complementary Technical Norms for Design and Construction of Masonry Structures*. Mexico City Building Code, Gaceta Oficial del Distrito Federal, Mexico.

NTC-M (2017). *Normas Técnicas Complementarias para Diseño y Construcción de Estructuras de Mampostería*. (Technical Norms for Design and Construction of Masonry Structures) Mexico D.F. [in Spanish].

Okail, H., Abdelrahman, A., Abdelkhalik, A., and Metwaly, M. (2016). "Experimental and analytical investigation of the lateral load response of confined masonry walls." *HBRC journal*, 12(1), 33-46.

Park, Y.J., Reinhorn, A.M., and Kunnath, S.K. (1987). *IDARC: Inelastic damage analysis of reinforced concrete frame-shear-wall structures*. National Center for Earthquake Engineering Research, Buffalo, New York.

Paulay, T., and Priestley, M. J. N. (1992). *Seismic design of reinforced concrete and masonry buildings*. Wiley-Interscience, New York.

Polyakov, S.V., (1956). *Masonry in framed buildings: An investigation into the strength and stiffness of masonry infilling*. Published by Gosudarstvennoe izdatel'stvo literatury po stroitel'stvu i arkhitekture, Moscow (Translation into English by G. L. Cairns).

Quiroz, L.G., Maruyama, Y., and Zavala, C. (2017). "Experimental assessment of the cyclic behavior of Peruvian confined masonry walls and numerical modeling using genetic algorithms." *Proceedings of the 16th World Conference on Earthquake Engineering, Resilience – The New Challenge in Earthquake Engineering*, 9-13 January 2017, Santiago, Chile, Chilean Association on Seismology and Earthquake Engineering, paper no. 642.

Rai, D.C., Singhal, V., and Kaushik, H.B. (2017). "M6.7 January 4, 2016 Imphal Earthquake: Dismal Performance of Publicly-Funded Buildings." *Current Science*, 113(12), Indian Academy of Sciences, Bangalore, India, 2341-2350.

Rai, D.C., Singhal, V., Paikara, S., and Mukherjee, D. (2014). "Sub-paneling of Masonry Walls using Pre-Cast RC Elements for Earthquake Resistance." *Earthquake Spectra*, 30(2), 913-937.

Rangwani, K., and Brzev, S. (2017). "Seismic analysis of confined masonry shear walls using the wide column model." *Applied Mechanics and Materials*, 857, 212-218, Trans Tech Publications Ltd.

Ranjbaran, F., Hosseini, M., and Soltani, M. (2012). "Simplified formulation for modeling the nonlinear behavior of confined masonry walls in seismic analysis." *International Journal of Architectural Heritage*, 6(3), 259-289.

Rankawat, N., Brzev, S., Jain, S. K., and Gavilan, J. J. P. (2021). "Nonlinear seismic evaluation of confined masonry structures using equivalent truss model." *Engineering Structures*, 248, 113114.

Riahi, Z., Elwood, K. J., and Alcocer, S. M. (2009). "Backbone model for confined masonry walls for performance-based seismic design." *Journal of Structural Engineering*, ASCE, 135(6), 644-654.

Rodrigues, H., Varum, H., and Costa, A. (2010). "Simplified macro-model for infill masonry panels." *Journal of Earthquake Engineering*, 14(3), 390-416.

San Bartolomé, A., Quiun, D., and Torrealva, D. (1992). "Seismic behaviour of a three-story half scale confined masonry structure." *Proceedings of the Tenth World Conference on Earthquake Engineering*, 19-24 July 1992, Madrid, Spain, A.A. Balkema, Rotterdam / Brookfield, 3527-3531.

Scaletti, H., Chariarse, V., Cuadras, C., Cuadros G. and Tsugawa T. (1992) "Pseudo dynamic tests of confined masonry buildings." *Proceedings of the Tenth World Conference on Earthquake Engineering*, 19-24 July 1992, Madrid, Spain, A.A. Balkema, Rotterdam / Brookfield, 3493-3497.

Schacher, T. (2009). *Confined Masonry for One and Two Storey Buildings in Low-tech Environments-A Guidebook for Technicians and Artisans*. National Information Centre of Earthquake Engineering, Kanpur, India.

Schacher, T., and Hart, T. (2015). *Construction guide for low-rise confined masonry buildings*. Publication WHE – 2015 – 01, World Housing Encyclopedia, Earthquake Engineering Research Institute, Oakland, California.

Schlaich, J., Schäfer, K., and Jennewein, M. (1987). "Toward a consistent design of structural concrete." *PCI journal*, 32(3), 74-150.

Schultz, A. E. (1994). "Performance of masonry structures during extreme lateral loading events." Masonry in the Americas, *ACI Publication*, SP 147-4, American Concrete Institute, Detroit, 85-126.

Simulia (2016). *ABAQUS analysis user's manual* (Version 6.16). Hibbitt, Karlsson, and Sorenson, Pawtucket, R.I.

Singhal, V. (2014). *Effect of Toothing and Openings on Bi-Directional Seismic Behaviour of Confined Masonry Walls*. A thesis submitted in partial fulfillment of the requirements for the degree of doctor of philosophy, IIT Kanpur.

Singhal, V., and Rai, D. C. (2014). "Role of toothing on in-plane and out-of-plane behavior of confined masonry walls." *Journal of Structural Engineering*, ASCE, 140(9), 04014053.

Singhal, V., and Rai, D.C. (2016). "In-plane and out-of-plane behavior of confined masonry walls for various toothing and openings details and prediction of their strength and stiffness." *Earthquake Engineering and Structural Dynamics*, 45(15), 2551-2569.

Smoljanović, H., Živaljić, N., Nikolić, Ž., and Munjiza, A. (2017). "Numerical model for confined masonry structures based on finite discrete element method." *International Journal for Engineering Modeling*, 30(1-4), 19-35.

Sucuoğlu, H., and McNiven, H.D. (1991). "Seismic shear capacity of reinforced masonry piers." *Journal of Structural Engineering*, ASCE, 117(7), 2166-2185.

Terán-Gilmore, A., Zuñiga-Cuevas, O., and Ruiz-García, J. (2009). "Displacement-based seismic assessment of low-height confined masonry buildings." *Earthquake Spectra*, 25(2), 439-464.

Tomaževič, M. (1999). *Earthquake-resistant design of masonry buildings*. Series on Innovation in structures and Construction -Vol. 1, Imperial College press, World Scientific.

Tomaževič, M., and Klemenc, I. (1997a). "Seismic behaviour of confined masonry walls." *Earthquake Engineering and Structural Dynamics*, 26(10), 1059-1071.

Tomaževič, M., and Klemenc, I. (1997b). "Verification of seismic resistance of confined masonry buildings." *Earthquake Engineering and Structural Dynamics*, 26(10), 1073-1088.

Torrisi, G. and Crisafulli, F. (2017). "Computational implementation of an improved masonry panel element." *Proceedings of the 16th World Conference on Earthquake Engineering, Resilience – The New Challenge in Earthquake Engineering*, 9-13 January 2017, Santiago, Chile, Chilean Association on Seismology and Earthquake Engineering, paper no. 501.

Torrisi, G.S., Crisafulli, F.J. and Pavese, A. (2012). "An innovative model for the in-plane nonlinear analysis of confined masonry and infilled frame structures." *Proceedings of the Fifthteenth World Conference on Earthquake Engineering*, 24-28 September 2012, Lisbon, Portugal, Sociedade Portuguesa de Engenharia Sismica (SPES), 24-28.

Totten, C. (2010). *Confined Masonry Workshop Handbook. The Construction and Maintenance of Masonry Building in Haiti*. Third edition, AIDG (Appropriate Infrastructure Development Group), Architects Without Borders - Oregon (AWB) and HaitiRewired.

Tripathy, D., and Singhal, V. (2019). "Estimation of in-plane shear capacity of confined masonry walls with and without openings using strut-and-tie analysis." *Engineering Structures*, 188, 290-304.

Tu, Y. H., Chuang, T. H., Liu, P. M., and Yang, Y. S. (2010). "Out-of-plane shaking table tests on unreinforced masonry panels in RC frames." *Engineering Structures*, 32(12), 3925-3935.

Turnšek, V. and Čačovič, F. (1971). "Some experimental results on the strength of brick masonry walls." *Proceedings: 2nd International Brick Masonry Conference*, 12-15 April 1970, Stoke-on-Trent, England, British Ceramic Research Association, 149-156.

Valente, M., and Milani, G. (2016). "Non-linear dynamic and static analyses on eight historical masonry towers in the North-East of Italy." *Engineering Structures*, 114, 241-270.

Varela-Rivera, J., Fernandez-Baqueiro, L., Gamboa-Villegas, J., Prieto-Coyoc, A., and Moreno-Herrera, J. (2019). "Flexural behavior of confined Masonry walls subjected to in-plane lateral loads." *Earthquake Spectra*, 35(1), 405-422.

Varela-Rivera, J., Moreno-Herrera, J., Lopez-Gutierrez, I., and Fernandez-Baqueiro, L. (2012). "Out-of-plane strength of confined masonry walls." *Journal of Structural Engineering*, ASCE, 138(11), 1331-1341.

Varela-Rivera, J.L., Navarrete-Macias, D., Fernandez-Baqueiro, L. E., and Moreno, E. I. (2011). "Out-of-plane behaviour of confined masonry walls." *Engineering Structures*, 33(5), 1734-1741.

Wahalathantri, B.L., Thambiratnam, D.P., Chan, T. H. T., and Fawzia, S. (2011). "A material model for flexural crack simulation in reinforced concrete elements using Abaqus." Cowled, C. J. L. (Ed.), *Proceedings of the First International Postgraduate Conference on Engineering, Designing and Developing the Built Environment for Sustainable Wellbeing*, Queensland University of Technology, Australia, 260-264.

Wang, Y. (2008). "Lessons learned from the "5.12" Wenchuan Earthquake: evaluation of earthquake performance objectives and the importance of seismic conceptual design principles." *Earthquake Engineering and Engineering Vibration*, 7(3), 255-262.

Wight, J.K., and MacGregor, J.G. (2005). *Reinforced concrete: Mechanics and design*. Fifth Edition, Upper Saddle River, NJ: Prentice Hall.

Wijaya, W., Kusumastuti, D., Suarjana, M., and Pribadi, K. (2011). "Experimental study on wall-frame connection of confined masonry wall." *Procedia engineering*, *14*, 2094-2102.

Yacila, J., Camata, G., Salsavilca, J., and Tarque, N. (2019). "Pushover analysis of confined masonry walls using a 3D macro-modelling approach." *Engineering Structures*, 201, 109731.

Yáñez, F., Astorza, M., Holmberg, A., and Ogaz, O. (2004). "Behavior of confined masonry shear walls with large openings." *Proceedings of the Thirteenth World Conference of Earthquake Engineering*, 1-6 August 2004, Vancouver, British Columbia, Canada, paper no. 3438.

Yang, W., and Jian, Z. (1988). "Functions of tied concrete columns in brick walls." *Proceedings of the Ninth World Conference on Earthquake Engineering*, 2-9 August 1988, Tokyo-Kyoto, Japan, Japan Association for Earthquake Disaster Prevention, 1989, VI, 139-144.

Yekrangnia, M., Bakhshi, A., and Ghannad, M. A. (2017). "Force-displacement model for solid confined masonry walls with shear-dominated failure mode." *Earthquake Engineering and Structural Dynamics*, 46(13), 2209-2234.

Yoshimura, K., Kikuchi, K., Kuroki, M., Liu, L., and Ma, L. (2000). "Effect of wall reinforcement, applied lateral forces and vertical axial loads on seismic behavior of confined concrete masonry walls." *Proceedings of the Twelfth World Conference on Earthquake Engineering*, 30 January-4 February 2000, Auckland, New Zealand, Upper Hutt, N.Z.: New Zealand Society for Earthquake Engineering, paper no. 0984.

Yoshimura, K., Kikuchi, K., Kuroki, M., Nonaka, H., Kim, K. T., Wangdi, R., and Oshikata, A. (2004a). "Experimental study on effects of height of lateral forces, column reinforcement and wall reinforcements on seismic behavior of confined masonry walls."

Proceedings of the Thirteenth World Conference on Earthquake Engineering, 1-6 August 2004, Vancouver, British Columbia, Canada, paper no. 1870.

Yoshimura, K., Kikuchi, K., Kuroki, M., Nonaka, H., Kim, K. T., Wangdi, R., and Oshikata, A. (2004b). "Experimental study for developing higher seismic performance of brick masonry walls." *Proceedings of the Thirteenth World Conference on Earthquake Engineering*, 1-6 August 2004, Vancouver, British Columbia, Canada, paper no. 1597.

Yoshimura, K., Kikuchi, K., Okamoto, T., and Sanchez, T. (1996). "Effect of vertical and horizontal wall reinforcement on seismic behavior of confined masonry walls." *Proceedings: 11th World Conference of Earthquake Engineering*, Acapulco, Mexico, June 23-28, 1996, paper no. 191, Pergamon, Oxford.

Yoshimura. K., and K. Kikuchi. (1995). "Experimental study on seismic behaviour of masonry walls confined by R/C frames." *Proceedings: Pacific Conference on Earthquake Engineering*, 20-22 November 1995, Melbourne, Australia, Australian Earthquake Engineering Society, 3, 97-106.

Zabala, F., Bustos, J.L., Masanet, A., and Santalucia, J. (2004). "Experimental behaviour of masonry structural walls used in Argentina." *Proceedings of the Thirteenth World Conference on Earthquake Engineering*, 1-6 August 2004, Vancouver, British Columbia, Canada, paper no. 1093.

LIST OF PUBLICATIONS

Refereed Journals

1. Borah, B., Kaushik, H.B., and Singhal, V. (under review). "Seismic Force Distribution in Members of Confined Masonry Buildings." *Engineering Structures*, Elsevier.
2. Borah, B., Kaushik, H.B., and Singhal, V. (under review). "Evaluation of Modeling Strategies for Seismic Analysis of Confined Masonry Structures." *Bulletin of Earthquake Engineering*, Springer Nature B.V.
3. Borah, B., Kaushik, H.B., and Singhal, V. (2022). "Lateral Load-Deformation Models for Seismic Analysis and Performance-Based Design of Confined Masonry Walls." *Journal of Building Engineering*, Elsevier, 48, 103978. https://doi.org/10.1016/j.jobe.2021.103978
4. Borah, B., Singhal, V., and Kaushik, H.B. (2021). "Assessment of Seismic Design Provisions for Confined Masonry using Experimental and Numerical Approaches." *Engineering Structures*, Elsevier, 245, 112864. https://doi.org/10.1016/j.engstruct.2021.112864
5. Borah, B., Kaushik, H.B., and Singhal, V. (2021). "Development of a Novel V-D Strut Model for Seismic Analysis of Confined Masonry Buildings." *Journal of Structural Engineering*, ASCE, 147(3), 04021001. https://doi.org/10.1061/(ASCE)ST.1943-541X.0002941
6. Borah, B., Singhal, V., and Kaushik, H.B. (2019). "Sustainable Housing using Confined Masonry Buildings." *SN Applied Sciences*, Springer Nature, 1, 983. https://doi.org/10.1007/s42452-019-1020-4

Conferences

7. Borah, B., Kaushik, H.B., and Singhal, V. (2022). "Application of V-D Strut Model for Analysis and Design of Multi-Story Confined Masonry Buildings." *2nd International Conference on Materials, Mechanics and Structures (ICMMS2022)*, 10-12 March 2022, National Institute of Technology Calicut, India, paper id CMS058.
8. Borah, B., Kaushik, H.B., and Singhal, V. (2020). "Effectiveness of Code Approaches in Seismic Design of Confined Masonry Walls." *Proceedings of the 17th World Conference on Earthquake Engineering (17WCEE)*, 13-18 September 2020, Sendai, Japan, International Association for Earthquake Engineering and Japan Association for Earthquake Engineering, paper id 2c-0268.

9. Borah, B., Kaushik, H.B., and Singhal, V. (2020). "Finite Element Modelling of Confined Masonry Wall under In-plane Cyclic Load." *Proceedings: International Conference on Materials, Mechanics and Structures 2020 (ICMMS2020)*, 14-15 July 2020, National Institute of Technology Calicut, India, paper id CMS045. Also, in: *IOP Conf. Series: Materials Science and Engineering* IOP Publishing, 936, 012020. https://doi.org/10.1088/1757-899X/936/1/012020
10. Borah, B., Singhal, V., and Kaushik, H.B. (2019). "Assessment of Important Parameters for Seismic Analysis and Design of Confined Masonry Buildings." *Proceedings: National Conference on Advances in Structural Technologies (CoAST2019)*, 1-3 Feb 2019, NIT Silchar, India, paper no. 138. Also, in: Adhikari, S., Dutta A., and Choudhury, S. (eds) *Advances in Structural Technologies. Lecture Notes in Civil Engineering*, Springer, Singapore, 81. https://doi.org/10.1007/978-981-15-5235-9_20
11. Borah, B., Singhal, V., and Kaushik, H.B. (2018). "A Simplified Approach to Analytical Modeling of Confined Masonry Buildings." *Proceedings: 16th Symposium on Earthquake Engineering (16SEE)*, 20-22 Dec 2018, IIT Roorkee, India, paper no. 247.
12. Borah, B., Singhal, V., and Kaushik, H.B. (2018). "Sustainable Housing using Confined Masonry Buildings." *Proceedings: 2nd International Conf on Civil Engineering for Sustainable Development-Opportunities & Challenges (CESDOC 2018)*, 18-19 Dec 2018, Assam Engineering College, Guwahati, India, paper id SRD0103.